

**AN EXPERIMENTAL STUDY INTO IMPACT WAVE PROPAGATION IN  
CROSS PLY COMPOSITE PLATES**

Thesis submitted for degree of  
Doctor of Philosophy  
at the University of Leicester

by

Mark Bernhardt James Walters  
Department of Engineering  
University of Leicester

October 1994

UMI Number: U068850

All rights reserved

INFORMATION TO ALL USERS

The quality of this reproduction is dependent upon the quality of the copy submitted.

In the unlikely event that the author did not send a complete manuscript and there are missing pages, these will be noted. Also, if material had to be removed, a note will indicate the deletion.



UMI U068850

Published by ProQuest LLC 2015. Copyright in the Dissertation held by the Author.  
Microform Edition © ProQuest LLC.

All rights reserved. This work is protected against  
unauthorized copying under Title 17, United States Code.



ProQuest LLC  
789 East Eisenhower Parkway  
P.O. Box 1346  
Ann Arbor, MI 48106-1346



---

## An Experimental Study Into Impact Wave Propagation in Cross Ply Composite Plates

By

Mark B.J. Walters

### Abstract

To gain insight into the problem of impact on to composite materials this work has examined experimentally the characteristics of stress waves propagating through a multi layered plate due to a surface impact. Theoretical and numerical techniques have been developed for an impulsive line load acting on the upper surface of a four layer cross ply plate. These resolve the surface and inter lamina disturbances caused by the passing stress waves due to a normal line impulse onto a plate.

The objective of this work was to examine the wave propagation in a cross ply plate with experimental techniques and compare the wave characteristics with the analytical predictions.

To detect the passing of the stress waves on the surfaces and at the ply interfaces a piezo electric sensor was developed using polarized homopolymer of vinylidene fluoride (PVDF) film. The responses collected from surfaces and mid plane of the impacted plate were dominated by the low frequency contribution of the impact, so the high frequency shear wave responses were extracted with digital filters.

The experimental results presented show that when the limiting wave velocity in the plate was that of a Rayleigh type surface wave the largest disturbance in the plate occurred on the upper surface of the plate, and that when the limiting wave velocity in the plate was that in an internal shear wave and the largest disturbance occurred at the mid plane of the plate.

These results demonstrated that the presence or absence of shear waves could be resolved experimentally at the surfaces and ply interfaces of a multi layered material. A good correlation was seen between the experimental results and the analytical results which provided some verification for the analysis method.

---

---

## Contents

### Chapter 1 Introduction

- 1.1 Theoretical Background
- 1.1 Experimental Background
- 1.2 Outline of Research

### Chapter 2 Theoretical Model of a 4 Ply Composite Plate

- 2.1 Material Model
- 2.2 4 Ply Plate
- 2.3 Theoretical Solution
- 2.4 Numerical Procedure
- 2.5 Numerical Solution
- 2.6 Limiting Wave Velocities
- 2.7 Wave Propagation Through a Cross Ply Composite Plate

### Chapter 3 Design of Stress Wave Propagation and Detection System

- 3.1 Plate Excitation
- 3.2 Plane Wave Propagation
- 3.3 Detailed Design of Stress Wave Propagation System
- 3.4 Data Recording System
- 3.5 System Evaluation Test

### Chapter 4 Stress Wave Sensors

- 4.1 Review of Stress Wave Sensor Methods
- 4.2 Strain Gauge Measurement System
- 4.3 Investigation into the use of Piezo-electric Film sensors as dynamic strain gauges
- 4.4 Design and Manufacture of a Piezo-electric Film Sensor
- 4.4 Experimental Verification of Sensor Design

---

<b>Chapter 5</b>	<b>Materials</b>
5.1	ICI Plytron
5.2	Advanced Composite Group LTM22/T700
5.3	Elastic Wave Speeds
<b>Chapter 6</b>	<b>Surface Wave Propagation in a Cross Ply Composite Plate</b>
6.1	Analytical Solution to Dispersion Equation
6.2	Experimental Study
6.3	Analytical Results
6.4	Experimental Results
6.5	Comparison of Experimental and Analytical Results
<b>Chapter 7</b>	<b>Internal Wave Propagation in a 4-Ply Laminated Plate</b>
7.1	Analytical Solution to Dispersion Equation
7.2	Experimental Study
7.3	Analytical Results
7.4	Experimental Results
7.5	Quality of Results
<b>Chapter 8</b>	<b>Conclusions</b>
<b>Chapter 9</b>	<b>References</b>

#### Appendices

- Appendix 1: Analytical Analysis Computer Programs.
- Appendix 2: PVDF Piezo Electric Film Properties
- Appendix 3: Material Tests of AGC LTM22/T700 Composite Material.
- Appendix 4: Published Work.

## Chapter 1: Introduction

Over the last 20 years there has been a rapid expansion in the use of fibre reinforced materials for a wide range of engineering applications. These composite materials of reinforcement fibres mixed with a matrix material offer distinct advantages over more conventional engineering metallic alloys. They generally offer higher specific stiffness and superior corrosion resistance and in some situations can provide lower cost with the production of complex load bearing structures in single operation, Chou, McCullough and Pipes [1]. With this increase in the application of composite materials there has been a large expansion in the research effort into the understanding of all aspects of their mechanical behaviour in particular examining the material strengths and weakness.

One perceived weakness of fibre reinforced polymer material is its response to localised impact, where the material's low ductility can result in extensive damage from relatively low energy impacts. This is becoming increasingly important with the trend in the aerospace industry in the use of fibre reinforced polymers as replacements for aluminium on the outside skin of aeroplanes, Ratwani [2]. The outside skin of aircrafts is vulnerable to impact from a range of sources such as a dropped tool during maintenance, runway debris during takeoff and landing and airborne foreign objects such as birds during flight. In recent years there have been many research programs undertaken in attempts to understand better the impact response of fibre reinforced materials. The majority have studied the continuous fibre high performance composites which have been used in civil and military aircraft where the consequences of extensive impact damage could be serious. A review article by Cantwell and Morton [3] has described much of the previous work in this field.

The manner in which composite materials dissipate the kinetic energy from a projectile impact loading is very different to that of metals. When metals are impacted by low and

intermediate incident energy projectiles the energy is absorbed by elastic and then plastic deformation, which can cause permanent deformation to the materials, but the reduction in the components load bearing capability is usually small. High incident impacts can result in target penetration with the impactor passing through the material, this often causes the degradation to the loading bearing capacity of the material but this can usually be predicted with fracture mechanics principles.

In fibre reinforced polymers the plastic deformation capacity is limited depending on the fibres and polymers in the material. This results in the energy from the impact being absorbed into the material creating a large area of fracture which results in the loss of strength and stiffness in the material. The nature of composite materials with a multi layered construction makes the prediction of post fracture load bearing capacity of a damaged composite structure difficult due to the complex nature of the damage zone. These effects are described in Mortimer, Chou and Carleone [4], Schonberg [5], Ujihashi et al [6] and Kumar, Rai [7]. This problem can also be compounded with difficulty in detecting the post impact damage where the fracture occurs as a delamination of the material layers with little or no surface deformation. The research work concerned with impact assessment of multi layered composite materials has concentrated on the evaluation of damage caused on a variety of material constructions with various impactors and energies and the resulting post impact material strength, Cantwell and Morton [8], Park [9] and Qian et al [10].

A second area of impact research has also developed into the way stress waves propagate away from an impact on a material. An impact on to a material causes the propagation of elastic waves known as stress waves from the point of impact. This phenomena was first investigated by Lord Rayleigh [11] who examined the waves travelling in solid isotropic materials. Lord Rayleigh gave his name to a particular high frequency surface wave known as the Rayleigh wave. As mathematical and experimental techniques developed Kolsky [12] continued the investigation into the wave propagation in solid materials and

describes it in detail . With the development of fibre reinforced materials into anisotropic laminated plates there was the requirement to investigate the wave propagation in this material to aid the better understanding of the response due to stress waves propagated from impacts, Green [13] and Kolsky [14]

The aim of this research work was to investigate the stress wave propagation in multi layered anisotropic plates due to surface impacts. The area of particular interest was the interaction between the direction of propagation and the wave characteristics at the different layers in the plate. This was achieved with the examination of the correlation between experimental and analytical data.

The theoretical study of wave motion in laminated plates has been extensively researched in recent years and the developments are presented in the review articles by Mikliwitz [15], and Ting [16]. These accounts show that the methods of analysing the problem can be classified into essentially three groups. One group involves the use of assumptions about the stress or displacement variations through the thickness of the laminate. This method is the usual engineering mechanics approach to plate theory and the integration through the thickness reduced the number of spatial variables from three to two.

Examples of the use of this technique to study impact problems are contained in the papers by Chow [17], Moon [18] and Sun [19]. There is a hybrid numerical method described by Lui et al [20] which can also be regarded as an example of this method. This method involves the use of a finite element formalism which expresses the through thickness displacement on a number of planes which therefore reduces the equations of motion to involving two spatial dimensions on each plane.

The second group of methods involves a pure numerical approach to solving the problem and an example is furnished in the paper by Lee et al [21]. This evaluates the transient stresses in a composite due to an impact with a finite element numerical technique.

Solution methods which belong in either of the two groups described above will of necessity lead only to approximate results, since by their nature they are incapable of reproducing the details of the stress variation throughout the laminate thickness. For low frequency vibrations, or for transient motion due to low velocity impact, where the wavelength of the disturbance is large in comparison with the overall plate thickness, these methods could be expected to provide good results. High velocity impacts and internal impulsive events such as delamination or cracking, on the other hand, will give rise to transient motion involving a wide range of frequencies (and wavelengths). For these, the stress variation through the laminate thickness may well differ significantly from that assumed in the approximate theories and it becomes necessary to analyse these problems using the full three dimensional equations of elasticity. It is a method which make use of these full elasticity equations which constitute the third group of solution techniques. Examples are provided in the work of Baylis and Green [22,23,24], these methods generate the exact analytic solutions using transform techniques. With these solutions it becomes possible to evaluate stress and displacement components at any location within or on the surfaces of the plate with the only approximation being that arising from the procedure for numerical computation of the analytic solution, Baylis and Green [25], Green and Green [26]. It is this three dimensional approach that has been adopted in this work.

The details of the stress variation throughout the laminate have a practical significance in a paper by Stone and Chatterjee [66] dealing with the effect of several impacts on laminated plates. These authors showed that the directional focusing of waves arising from the first impact could cause reduction in the strength of the inter-ply bonds at regions away from the immediate impact site, with the weakened regions suffering delamination as a result of subsequent impacts. In the work reported here it is assumed that the plate maintains its structural integrity during and after the impact process and in consequence the results are not valid in the immediate impact region where the magnitude of the event is such as to cause fracture or delamination of the material.

In addition to their immediate relevance to the problem of impact, these results are important in the quantitative non-destructive evaluation (QNDE) process. The QNDE technique of acoustic emission employs the stress waves generated of internal cracks or delamination under applied loads as a means of determining the location and extent of internal flaws within structural members. The interruption of acoustic emission events monitored on the surface relies on a detailed knowledge of the mode of transmission of the stress waves through the structure which the theoretical model presented in this work can provide, Green [27, 28].

In carrying out the analysis of a 4-ply laminated plate it was assumed that the plies were perfectly bonded to each other so the displacements and tractions were continuous across each interface. The material forming each of the plies has been modelled as transversely isotropic homogeneous elastic continuum. The elastic properties of a transversely isotropic material involve five independent elastic constants which were measured from the material used in the experimental testing. In adopting the homogeneous continuum model for the fibre composite it was assumed that the wavelengths of the disturbances were large in comparison with the fibre diameter and inter fibre spacing. For typical prepreg-ply containing some 60% by volume of fibre, the fibre diameter and inter fibre spacing is of the order of  $6\mu\text{m}$  with the ply thickness being approximately  $210\mu\text{m}$ . The assumption of homogeneity might be expected to be valid in such a material for wavelengths of the order  $1/3$  the ply thickness or greater. On the other hand, for wavelengths of order  $1/10$  the ply thickness or less, the waves would suffer diffraction and scattering by the individual fibres and the homogeneous continuum model would no longer hold.

The analytical solutions have been derived for impulsive loads which were represented mathematically by a Dirac delta function of time. An impulse of this kind has a constant spectrum, indicating that all frequencies from zero to infinity occur with equal amplitude.

While such a function is physically unrealistic the response generated by it constitutes the fundamental (Green's function) solution.

All the work carried out in this project relates to a line load impulse acting on the upper plate surface which provides the basic solution to the surface impact problem. The laminated plates have been assumed to have infinite lateral extent so that the results relate to waves propagating outwards from the impulse location. In the realistic situation, the results remain valid at any point up to the time of arrival of disturbances reflected from the plate edges. The impulse employed to generate these solutions were assumed to act along a line of infinite length and to be of uniform strength along the line. An impulse of this kind would set up a disturbance travelling away from the line through the laminate in such a way that the solution would be identical in every plane perpendicular to the impulse line. The analytical solutions are consequently independent of position along the line and are functions of two space variables and time only. For isotropic materials the displacement would be confined to lie in the planes perpendicular to the impulse line but this is not the case for the anisotropic materials which have been studied here. The solutions involve all three components of displacement and all six components of stress, despite the fact that these are all functions of two space variables only. A line load impulse was used in this analysis as the first steps towards the determining of the response to a point load.

The basic method of solution as detailed in Green [29] was to take the Laplace Transforms with respect to time and the Fourier Transforms with respect to one of the spatial variables. This reduced the governing equations to a coupled system of linear ordinary differential and algebraic equations for the transforms of the displacement components and the stress components in terms of the variable measuring distance through the laminate. These equations have different forms within each of the plies and the solution within each ply has been derived in terms of the propagator matrix for that ply. Continuity of displacement and traction components between each ply leads to the solution for the stress and displacement transforms in terms of an overall propagator

matrix for the laminate as a whole and the transform of the impulse load. In order to recover the solution as functions of position and time, it is necessary to invert the transforms and this process was performed numerically.

The solutions were recovered as a time history of the disturbances at the surfaces and ply interfaces at a fixed location away from the point of impact. This provided comparable results with the experimental data which came from a sensor mounted on a plate, which recorded the disturbances in the plate after a surface impact.

### 1.1 Experimental Background.

The experimental work concerned with stress waves propagation in fibre composites due to impact has employed three main experimental techniques. They have involved the use of optical techniques to measure the out of plane displacements of a surface, strain gauges to measure surface strain and acoustic emission sensors to detect the vibration caused by the passing stress waves.

The optical techniques employed light refraction methodology to measure the out of plane displacement of an impacted plate, Degrieck and Dechaenes [30] used a high speed streak photography combined with a shadow moiré technique to measure the back wall out of plane deflections of a composite plate. Fallstrom et al [31] employed hologram interferometry to investigate the transient bending waves in anisotropic plates. Both these techniques provided pictures at discrete time points after the impact of the overall deformation of the plates.

The second technique was to use strain gauges to measure strains in the plate at points away from the impact. Kolsky [14] and Sayir [32] both investigated the response of unidirectional composite plates with strain gauges. Daniel and Wooh [33] embedded strain gauges into composite plates to study the transient deformations and dynamic fractures of composite plates under impact. This work showed the strain responses of the plate at various locations remote to the impact but the monitoring of the strain gauge

outputs was limited to a sampling interval of  $10\mu s$ , which provided a frequency limit of 25 kHz for random data, and therefore investigated the low frequency response of the plates and not the higher frequency stress waves propagated from the impact. Similar work was completed by Takeda et al [34] and Khan and Hsiao [35] who used electrical resistance foil strain gauges to study plastic waves in solids. This involved the impacting a bar of material and recording the waves passing through the bar by applying a 30V-dc to the strain gauges for a short period of time.

Both these techniques provided information on the gross deformation of the plates when impacted but failed to resolve the detailed picture of specific stress waves propagating from the point of impact due to frequency response limitations of the measurement systems.

The third area of experimental research which relates to this work is the non destructive evaluation (NDE) of materials. The NDE of materials involves the detection and evaluation of damage and flaws in materials caused by material processing of subsequent material damage. The traditional methods employed on composite materials either employ X-rays or ultrasonic C-scanning, Cantwell and Morton [68]. Ultrasonic C-scanning involves the placement of a transmitter on one side of the material and the ultrasonic waves propagate through the material and are detected by a receiver on the other side. The waves travelling through the material are disrupted by any flaws in the material, this is detected to provide an indication of the structural integrity through the thickness of the material. The recent developments in ultrasonics have been discussed by Sachse et al [69] on the quantitative ultrasonic detection for the specific location of flaws and defects in composite materials. Veidt and Sachse [70] describe the use of an ultrasonic point source and point receiver to characterise the elastic wave field in a material. Barcohen, Mal and Lit [71] have described the use of ultrasonic oblique insonification in the NDE of composites. Ultrasonic wave propagation is also employed in the investigation of material

properties by the measurement of the wave speeds travelling through a material, Hsu and Hughes [72], Whooh and Daniel [39].

The use of anisotropic wave propagation in the NDE of composites has been described by Wu and Ho [73]. This has included the use of acoustic emission (AE) sources such as pencil lead break and laser sources with AE detectors to characterise the wave propagation through composite materials, Mal et al [74]. This technique has been used to measure the elastic properties of the material, Mal et al [38] or to examine the location of flaws in the material, Guo and Crawley [37], Gorman [36].

The combination of the use of acoustic emission sources and ultrasonic detectors, described as acousto-ultrasonics, has been discussed by Guo and Crawley [77], and Prosser and Gorman [75] and [78].

Gorman [36] has reported the use of plate wave acoustic emissions (AE) in composites. This work describes the acoustic emissions which are produced by impulsive sources such as matrix cracking and fibre breakage. Transverse matrix cracking which is the first failure mode was induced into cross ply (0/90)s graphite/epoxy plates by loading in tension along the zero degree direction. The resulting acoustic emission was monitored using wide band transducers and a digital oscilloscope and the fundamental flexural and extensional modes were observed which developed understanding in the distinguishing of AE sources in plates and thin walled structures.

Guo and Cawley [76] have reported the use of Lamb waves which can propagate over distances in the order of 1m as a potential long range non destructive inspection method. The work reports the detection of the reflection and scattering effects on the propagating Lamb waves due to their interaction with delamination in the composite materials.

Hutchins [40] describes the use of pulsed lasers for quantitative ultrasonic NDE and describes its mechanisms of operating and the typical surface wave responses produced in aluminium plate. Scudder, Hutchins and Mottram [41] describe the use of pulsed lasers

on unidirectional carbon fibre laminates to characterise the ultrasonic propagation resulting from an impulsive force on the surface from a pulsed laser. The material responses were detected using a broad band capacitance transducer mounted on the surface of the material and therefore only displayed the surface responses.

In relation to this work the NDE methods described are capable of detecting the individual waves propagated through the material, but the sensors used to detect the disturbances caused by the passing of the waves were broad band capacitance devices mounted on the surface of the material and therefore only responded to the out of plane surface disturbances and would not distinguish the ply interface disturbances.

The most relevant aspect of NDE to this project was the development of the piezo film sensor which had been applied in the field of NDE, Brown and Brown [42]. This film sensor was manufactured from lightweight thin plastic piezo electric which resulted in sensors of 52 $\mu$ m thickness which provided the capability of embedding the sensors into a composite plate at the ply interfaces.

## 1.2 Outline of Research

In the work completed by Green [29] and the references within, it is described how theoretical and numerical techniques were developed for the analysis of the wave propagation through a laminated plate consisting of a periodically repeating configuration of a unit cell subjected to a surface impact. The solutions reported were for a 4-ply plate of cross ply symmetric construction (0/90)s and presented the scaled displacements through the thickness of the plate as a function of the distance from the impact site. Included in the report was the variation in the plate displacements due to the variation in the angle  $\gamma$ , where  $\gamma$  is the angle between the direction of propagation and the direction of the fibres at the mid plane of the plate. The results from this work showed that when the angle  $\gamma=30^\circ$  there was a very large amplitude present on the upper surface which was not transmitted to any of the lower levels, which was typical of a surface wave.

When the angle  $\gamma=60^\circ$  the very large amplitude was absent. It had been previously shown by Green [43] that the limiting wave velocity of both the antisymmetric and symmetric fundamental modes is the smaller of two wave speeds, a Rayleigh type surface wave speed in the upper layer  $V_R$  or that of a shear wave speed in the inner layers  $V_S$ . These speeds are material dependent and are equal for angle  $\gamma = 47.6^\circ$  for the material properties used in [29]. When  $\gamma < 47.6^\circ$   $V_R < V_S$  and when  $\gamma > 47.6^\circ$   $V_R > V_S$ . As the disturbances in the plate are dominated by the behaviour of the fundamental mode the surface wave was expected at  $\gamma=30^\circ$  but not at  $\gamma=60^\circ$ .

A limitation of the theoretical model and numerical analysis techniques developed by Green was the shortage of experimental correlation with the theoretical analysis of a 4-ply plate subjected to a surface impact. There was some experimental evidence of the presence of large surface waves on the impact surface from NDE work, Wu and Ho [44], but evidence of the internal shear waves and the variation of the limiting wave velocity in the plate did not have any experimental validity.

The aim of this work was to build on the work by Green [43] by studying the wave propagation due to a surface impact through a 4-ply composite plate by experimental investigation for a range of wave propagation directions. The main requirement of the experimental program was to detect and record the disturbances at the surfaces and ply interfaces separately caused by the stress wave propagation and examine behaviour for different values of the angle of wave propagation  $\gamma$ .

This required the design and construction of an experimental test facility which would provide a line loading onto a 4-ply plate to propagate a plane wave front through the plate. It was also necessary to develop a sensor system which could detect and record the stress wave disturbances at the plate surfaces and ply interfaces.

There were two main components of the experimental facility designed to produce and detect stress waves propagating through a 4 ply composite plate. These were an impulse

system to generate the stress waves and the equipment to detect and record the stress waves passing a point on the plate. The main requirement of the impulse system was to produce a line load on to the plate to propagate a plane wave front through the material. A plane wave front was required as the theoretical model and analytical solution considered a plane wave travelling through an infinite plate, and the angle of propagation  $\gamma$  with a plane wave front could be specified. For the experimental aspect of this project a point load would have been simpler to generate, but the required analytical solution to the point load on a composite plate is more complex and is currently under development, Mal [45].

To produce the impact onto the surface of the material a variety of plate excitation methods were considered including a drop weight, ballistic, explosive, piezoelectric crystals and an electromechanical shaker. The use of an ultrasonic line impulse from a laser was considered but not followed due to resources that would have been required for this method. As this work's objective was to examine the elastic stress waves from the point of impact it was desirable not to damage the plate during the impact so many tests could be conducted on the same material samples, and no additional information would have been obtained from a plate if it was damaged during the impact. This provided an energy constraint on the impact system of a maximum energy in the region of 0.5J as there was evidence that some materials could be damaged with impact energies as low as 1J Cantwell and Morton [8]. Of the considered energy sources a ballistic gas gun source was selected with a fast lightweight projectile to provide a controllable energy level. The problem with the ballistic energy source was that the projectile from the gas gun could only provide a point load onto the plate, so a bar striker was placed in front of the plate. This bar striker was accelerated by the gas gun projectile and impacted the plate to provide a line load impact with a speed in the region of  $5\text{ms}^{-1}$  and a maximum energy of 0.5J.

The second aspect of the experimental system was the detecting and recording of the stress waves generated from the surface impact. The initial intent of the project was to use semiconductor strain gauges placed on the surfaces and ply interfaces on the plate to detect the stress waves. Previous work [33] had shown that the fundamental wave modes could be detected by strain gauges but had not examined the higher frequency wave components. Kim and Sachse [79] has described the use of strain gauges for the generation of line sources in thin metal films. The resistance strain gauges were attached to the material and an electrical pulse was applied to the gauge. The effect of this pulse was to cause a temperature rise in the gauge which thermal expanded which caused a thermal dilatation in the film to generate a ultrasonic pulse.

It has been shown by Green [43] that the channelling effects caused by the limiting wave velocities in a composite plate are associated with stress waves whose wavelengths are of the order of five times the single ply thickness or less, corresponding to a frequency of the order  $c/5h$  or greater, where  $c$  is a typical shear wave speed and  $h$  is the ply thickness. For a typical carbon fibre pre preg material with a shear wave speed  $c$  of approximately 1000m/s and a ply thickness of the order of 125 $\mu$ m, the channelling effects would be associated with frequencies of the order of 1MHz or greater. This frequency could be reduced by increasing the thickness of each ply to the order of 1mm which would reduce the channelling effects associated to the order of 200kHz and greater. This indicated that the measurement system would require a frequency response of a minimum of 200kHz and ideally going into the low MHz region.

This frequency requirement presented problems with the original intention of using strain gauges to monitor the strains in the plate as described by Hofstotter [46] and used by Kahn and Hsiao [35]. The frequency range required the use of broad band high gain amplifiers to amplify the strain gauge outputs and no commercial amplifiers could be found with sufficient gain and frequency response to meet this requirement. Following further investigation into possible sensors the PVDF piezo film sensors were investigated

into their possible use. These sensors manufactured from thin piezo electric film had a frequency response ranging from low frequency up to the GHz region, the sensor response to low level disturbances was relatively high so no further amplification was required. As the desire of the sensors was to measure the response at a point location on the plate the ideal sensor size would have been less than half the shortest wave length to be measured, but the very short wave lengths being measured resulted in this being physically impossible. It was necessary to design the PVDF sensors with the smallest sensing area possible which resulted in a sensor size of 1mm x 0.5mm, this small size limited the sensor's low frequency response to 20kHz but this was not a problem as only the frequencies above 200kHz were of interest.

These sensors resulted in the only frequency limit on the measurement system was the equipment used to record the PVDF sensors response. To record this response a digital recording system was selected with a sampling frequency of 20MHz and 64Kbytes of memory storage. This would provide a good frequency response of 4MHz for random signals and provide 1ms of recording time. Eight channels of data recording were obtained in the form of two 4 channel Yokogawa DL1200 oscilloscopes. Once the sensor responses were captured on the oscilloscopes the data was down loaded to a PC computer where it could be post processed with PAFEC spiders digital signal processing package.

The main limitation of the PVDF film sensors was that their survival temperature was 90°C. This presented problems with the placing of sensors at the ply interfaces during the lay up of the plate as the majority of epoxy based fibre reinforced materials are cured at 120°C and above. This resulted in two experimental investigations being conducted, the first investigated the surface wave propagation in the ICI material Plytron which was a glass fibre polypropylene composite which cured at 170°C, this material was donated by ICI. For this investigation the plates were manufactured and the sensors bonded onto the surface after the plate was cured.

Following an investigation into the fibre reinforced materials available on the commercial market a low temperature resin cure material was found manufactured by the Advanced Composite Group called LTM22, this resin could be cured at 50°C and supplied with a range of fibre reinforcement. This material provided the capability to place sensors at the ply interfaces during the construction of the plate and survive the cure process. The material combination selected was a LTM22 epoxy resin reinforced with T700 carbon fibres.

There were two experimental investigations completed within this project, the first was the study of the surface wave responses of the Plytron material due to the line load surface impact. These first set of results showed that the PVDF film sensors were capable of detecting the disturbances caused by the passing of the stress waves propagating from the point of impact. The responses recorded showed the same form as the responses from the previous work involving the use of strain gauges in the measurement of stress waves, [33].

The work by Green [47,48] had shown that the response of the plate was dependent on the duration of the impact loading with the longer the impulse the more dominant the low frequency contribution of the response becomes. Therefore to examine the high frequency waves which were associated with the channelling effects under investigation this low frequency contribution required removal from the recorded response. This was achieved with the use of the digital filtering capability of the PAFEC spiders post processing software, where band pass filters were employed to remove low frequency response and very high frequency interference from the recorded responses. A typical filter used on the Plytron results was a 10th order Butterworth band pass filter between 0.2MHz and 3MHz.

The results presented for Plytron show the upper and lower surface responses for the two cases of  $\gamma = 0^\circ$  and  $\gamma=90^\circ$ , both the experimental and analytical results are presented. The graphs show the plate responses at a distance of 15mm (15h, where h=ply thickness) away from the point of impact. These results show quite clearly the presence of a high

frequency Rayleigh type surface wave on the upper surface when  $\gamma = 0^\circ$  which was absent from the lower surface and was also absent from both surfaces when  $\gamma = 90^\circ$ .

The second set of results presented are the surface and mid plane responses of the LTM22/T700 material in a cross ply 4 layered plate. As with the Plytron results the recorded responses from the sensors were subjected to filtering to remove the low frequency contribution of the impact. In this case the sensors were placed 32mm (40h) away from the point of impact, and again showed the presence of a Rayleigh type surface wave when  $\gamma = 0^\circ$  on the upper surface which was absent when  $\gamma = 90^\circ$ . The mid plane responses showed a larger disturbance when  $\gamma = 90^\circ$  than when  $\gamma = 0^\circ$ .

The meaning of these results and the conclusions drawn from them are discussed in chapters 7, 8 and 9 of this work. Chapter 2 contains the theoretical model and analytical solution employed for the numerical analysis associated with the experimental test conditions. Chapters 3 and 4 contain details of the experimental system and sensors which were developed to experimental propagate and detect the surface and internal stress waves in a multi layered material, and chapter 5 contains full details of the materials studied.

## Chapter 2: Theoretical Model of a 4 Ply Composite Plate

The theoretical model presented is for a laminated plate constructed from four layers of unidirectional fibre composite material into a symmetric cross ply plate. Each layer of material consisted of a single family of straight, parallel, strong fibres embedded in an isotropic matrix. A typical material is formed from carbon fibres embedded into a thermoplastic resin, with a layer thickness of  $125\mu\text{m}$  and an inter fibre spacing of the order of  $6\mu\text{m}$ . The modulus in the fibre direction is of the order of 25 times that at right angles to the fibres. The model does not consider the individual fibres on a micro scale but considers the whole material as a homogenous continuum of transversely isotropic elastic material with the axis of transverse isotropy parallel to the fibre direction.

The use of this model in the study of wave propagation through a material is only valid for wavelengths which are an order of magnitude greater than the fibre diameter and the inter fibre spacing. Wavelengths that are less than this are effected directly by the presence of the fibres which leads to diffraction and scattering of the waves. For a typical carbon reinforced plastic containing 60% by volume of fibres the fibre diameter and inter fibre spacing is in the order of  $6\mu\text{m}$ , therefore the assumption of homogeneity is only valid for wavelengths greater than  $60\mu\text{m}$ . This implies that the non-dimensional wave number  $kh=2\pi h/\lambda$  varies between 0 and approximately 13. ( $\lambda$  is the wavelength and  $h$  is the ply thickness).

### 2.1 Single Layer of Material

A Cartesian co-ordinate system is established on the material with its origin at the centre. The  $x_1$ -axis is normal to the plane of the fibres with the  $x_2$ -axis perpendicular to the fibres and the  $x_3$ -axis is thus parallel to the fibres. The material has a unit thickness of  $h$ . A plane wave front is propagated from a normal surface impact through the material in the direction  $x$  at the angle  $\gamma$  to the  $x_3$ -axis, figure 2.1.

### Governing Equations

To define the disturbances in a material the displacement at any point can be defined by  $u_i(x_1, x_2, x_3)$ , ( $i=1,2,3$ ). The strain components  $e_{ij}(x_1, x_2, x_3, t)$  can be described in terms of displacement by the usual expressions

$$e_{ij} = \frac{1}{2} \left( \frac{\partial u_i}{\partial x_j} + \frac{\partial u_j}{\partial x_i} \right) \quad [2.1]$$

Here and throughout this chapter the summation convention is used to describe sets of equations.

The constitutive equation relating to the Cauchy stress tensor  $t_{ij}(x_k, t)$  to the strain components  $e_{lm}(x_p, t)$  was defined by Spencer [49] for a transversely isotropic materials with the fibres in the  $x_2, x_3$  plane at an angle  $\phi$  to the  $x_3$  axis

$$t_{ij} = \lambda e_{kk} \delta_{ij} + 2\mu_T e_{ij} + 2(\mu_L - \mu_T)(a_i a_k e_{kj} + a_j a_k e_{ik}) + \alpha(a_i a_j e_{kk} + a_k a_l e_{kl} \delta_{ij}) + \beta(a_i a_j a_k a_l e_{kl}) \quad [2.2]$$

where  $\delta_{ij}$  is the kronecker delta,  $\lambda, \mu_T, \mu_L, \alpha, \beta$  are the anisotropy Lamé material constants,  $a_1=0$ ,  $a_2=\sin\phi$ , and  $a_3=\cos\phi$ . These constants can be related to the components of the symmetric (6x6) stiffness matrix  $c_{pq}$ , defined by Musgrave [50], through the expressions

$$\begin{aligned} c_{11} &= \lambda + 2\mu_T = c_{22} & c_{33} &= \lambda + 4\mu_L - 2\mu_T + 2\alpha + \beta \\ c_{44} &= \mu_L = c_{55} & c_{66} &= 1/2(c_{11} - c_{12}) = \mu_T \\ c_{12} &= \lambda & c_{13} &= \lambda + \alpha = c_{23} \end{aligned} \quad [2.3]$$

The five elastic constants together with the density  $\rho$  gives a complete description of the material, but they are not the most convenient when investigating a dynamic response in a material. It is more natural to work with the density  $\rho$  and the five squared wave speeds,  $c_1^2, c_2^2, c_3^2, c_4^2$  and  $c_5^2$  where

$$\begin{aligned} \rho c_1^2 &= \lambda + 2\mu_T & \rho c_2^2 &= \mu_T \\ \rho c_3^2 &= \mu_L & \rho c_4^2 &= \lambda + \alpha \\ \rho c_5^2 &= \lambda + 4\mu_L - 2\mu_T + 2\alpha + \beta \end{aligned} \quad [2.4]$$

To study the disturbances caused by the propagation of waves through a material it is necessary to solve the equations of motions for the material in terms of displacement or stress. The equations of motion are defined as

$$\frac{\partial t_{ij}}{\partial x_j} = \rho \ddot{u}_i \quad [2.5]$$

where the dots denote the differential with respect to time. To solve these equations it is necessary to combine them with the constitutive equations [2.2]. To reduce the components involved it is assumed that a plane wave is travelling through the material in the direction  $x$  at the angle  $\gamma$  to the  $x_3$ -axis. The displacement components of the motion are therefore defined as

$$u_i(x_1, x_2, x_3, t) = u_i(x_1, x, t) \quad [2.6]$$

and the stress components as

$$t_{ij}(x_1, x_2, x_3, t) = t_{ij}(x_1, x, t) \quad [2.7]$$

where

$$x = x_3 \cos \gamma + x_2 \sin \gamma. \quad [2.8]$$

It is also convenient to take the Laplace transform in time and the Fourier transform with respect to  $x$  of both the displacement and stress components. These can be typified by

$$U_i(x, k, \hat{s}) = \int_{-\infty}^{\infty} \int_0^{\infty} u_i(x_1, x, t) e^{-\hat{s}t} e^{-ikx} dt dx \quad [2.9]$$

and

$$T_{ij}(x, k, \hat{s}) = \int_{-\infty}^{\infty} \int_0^{\infty} t_{ij}(x_1, x, t) e^{-\hat{s}t} e^{-ikx} dt dx \quad [2.10]$$

The transformed displacements and stresses  $U_i$  and  $T_{ij}$  are functions of the normal coordinate  $x$ , and the Laplace transform parameter  $\hat{s}$  and the Fourier parameter  $k$ . Since the Laplace transform has been taken with respect to time and the Fourier transform with respect to the spatial variable  $x$  the governing equations, Equ. [2.1,2.2,2.5], can be reduced to a coupled system of linear ordinary differential equations for the transforms of

the displacement and stress components in terms of the variable measuring distance through the material along the  $x_1$  axis together with three algebraic. These are :

$$\frac{dU_1}{dx_1} = \frac{T_{11}}{\rho c_1^2} - \left(1 - 2\frac{c_2^2}{c_1^2}\right) iks U_2 - \frac{c_4^2}{c_1^2} ikc U_3 \quad [2.11]$$

$$\frac{dU_2}{dx_1} = \frac{T_{12}}{\rho c_2^2} - iks U_1 \quad [2.12]$$

$$\frac{dU_3}{dx_1} = \frac{T_{13}}{\rho c_3^2} - ikc U_1 \quad [2.13]$$

$$\frac{dT_{11}}{dx_1} = \rho U_1 \hat{s}^2 - T_{12} iks - T_{13} ikc \quad [2.14]$$

$$\frac{dT_{12}}{dx_1} = \rho U_2 \left[ \hat{s}^2 + k^2 (c^2 c_3^2 + 4s^2 c_2^2 \left(1 - \frac{c_2^2}{c_1^2}\right)) \right] + \rho U_3 k^2 sc \left[ c_3^2 + \frac{2c_2^2 c_4^2}{c_1^2} \right] - T_{11} iks \left(1 - \frac{2c_2^2}{c_1^2}\right) \quad [2.15]$$

$$\frac{dT_{13}}{dx_1} = \rho U_2 k^2 sc \left( c_3^2 + \frac{2c_4^2 c_3^2}{c_1^2} \right) + \rho U_3 \left( \hat{s}^2 + k^2 \left( s^2 c_3^2 + cc_5^2 - \frac{c^2 c_4^2}{c_1^2} \right) \right) - T_{11} ikc \frac{c_4^2}{c_1^2} \quad [2.16]$$

$$T_{22} = \rho U_2 4iksc_2^2 \left(1 - \frac{c_2^2}{c_1^2}\right) + \rho U_3 2ics \frac{c_2^2 c_4^2}{c_1^2} + T_{11} \left(1 - \frac{2c_2^2}{c_1^2}\right) \quad [2.17]$$

$$T_{23} = \rho ikc_3^2 (cU_2 + sU_3) \quad [2.18]$$

$$T_{33} = \frac{c_2^2 c_4^2}{c_1^2} (\rho U_2 2iks + T_{11}) + \rho U_2 ikc \left( c_5^2 - \frac{c_4^2}{c_1^2} \right) \quad [2.19]$$

Where  $c = \cos\gamma$ , and  $s = \sin\gamma$ .

If this is considered as the  $m^{\text{th}}$  layer in the plate, equations [2.11] to [2.16] can be written in the form

$$\frac{d\mathbb{Y}_m(x_1)}{dx_1} = \mathbb{A}_m \mathbb{Y}_m(x_1) \quad [2.20]$$

where  $\mathbb{Y}_m$  is the transpose of the vector  $(U_1, U_2, U_3, T_{11}, T_{12}, T_{13})$ , and  $\mathbb{A}$  is a 6x6 matrix whose elements are functions of the transpose parameters,  $\hat{s}$ ,  $k$  and the propagation angle  $\gamma$ , and the five material wave speeds.

It is possible to write the general solution for equation [2.20] in the form

$$\mathbb{Y}_m(x_1) = \mathbb{P}_m \mathbb{E}_m(x_1) \mathbb{K}_m \quad [2.21]$$

Where  $\mathbb{P}_m$  is the 6x6 matrix whose columns contain the eigen vectors of the matrix  $\mathbb{A}_m$ ,  $\mathbb{K}_m$  is a constant vector of order 6, and  $\mathbb{E}_m(x_1)$  is a 6x6 diagonal matrix given by

$$\mathbb{E}_m(x_1) = \text{Diag} \{ e^{kp_1(x_1-x_a)}, e^{kp_2(x_1-x_a)}, e^{kp_3(x_1-x_a)}, e^{kp_1(x_b-x_1)}, e^{kp_2(x_b-x_1)}, e^{kp_3(x_b-x_1)} \} \quad [2.22]$$

where  $\pm kp_1, \pm kp_2, \pm kp_3$  are the six eigen values of  $\mathbb{A}_m$  and  $x_a$  and  $x_b$  are the  $x_1$  coordinates of the upper and lower surfaces of the layers respectively. The reason for the choice of the particular matrix  $\mathbb{E}_m$  is so there are no positive exponentials present, even when the eigenvalue  $kp_1$  is real. Hence the numerical instabilities caused by growing exponentials are removed.

The layer of material has a finite thickness  $h$ , and is assumed to be of infinite lateral extent, thus occupies the region of  $x_a < x_1 < x_b$ ,  $-\infty > x_2, x_3 < \infty$ . It is possible to define the general solution Equ. [2.21] for the upper and lower surfaces of the layer of material. For the upper surface, at  $x_1 = x_a$  the matrix  $\mathbb{E}_m(x_1)$  can be written as

$$\mathbb{E}_m(x_a) = \mathbb{E}_m^+ = \text{Diag} \{ 1, 1, 1, e^{-kp_1 h}, e^{-kp_2 h}, e^{-kp_3 h} \} \quad [2.23]$$

and the lower surface, at  $x_1 = x_b$

$$\mathbb{E}_m(x_b) = \mathbb{E}_m^- = \text{diag} \{ e^{-kp_1 h}, e^{-kp_2 h}, e^{-kp_3 h}, 1, 1, 1, \} \quad [2.24]$$

Thus the general solution for the upper surface of a layer of material is expresses as

$$\mathbb{Y}_m^+ = \mathbb{P}_m \mathbb{E}_m^+ \mathbb{K}_m \quad [2.25]$$

and for the lower surface of a layer

$$\mathbb{Y}_m^- = \mathbb{P}_m \mathbb{E}_m^- \mathbb{K}_m \quad [2.26]$$

The application of the relevant boundary and interface conditions for each layers of material can yield a system of equations, which can be solved to find the arbitrary constants  $\mathbb{K}_m$  for each layer. These solutions in turn can then be used to determine the displacement and stresses for any point  $(x_1, x_2, x_3)$  in the layer of material. The detail model of a four layer cross ply plate is described in the next section.

## 2.2 Four Layer Plate

The plate examined here is constructed from four layers of the transversely anisotropy material described in the previous section. The top two layers have their axes of transverse anisotropy at  $90^\circ$  to each other, and the bottom two layers have an orientation that is symmetric about the mid plane of the plate. This configuration of plate is of cross ply orientation and can be denoted by  $(0,90)_s$ . Each layer has a thickness of  $h$  and it is assumed that there is perfect bonding between each layer. A Cartesian co-ordinate system was established on the plate with its origin at the mid plane of the plate. The  $x_1$ -axis is normal to the plate with the  $x_2$ -axis parallel to the fibres in the outer layers and the  $x_3$ -axis is thus parallel to the fibres in the inner layers. The laminated plate is assumed to be of infinite lateral extent and occupies the region  $-2h \leq x_1 \leq 2h$ ,  $-\infty < x_2, x_3 < \infty$  figure 2.2.

A plane wave front is propagated from an impulse line load applied on the upper surface where  $x_1=2h$  on the plate at an angle  $\pi/2 - \gamma$  to the  $x_3$ -axis. The lower surface is traction free, and the upper surface has a stress discontinuity where the line load is applied. The resultant disturbance travels along the plate in a direction  $x$  normal to the line load.

The examination of wave propagation through a multi layered plate requires that the dispersion equation is solved for each layer and then appropriate boundary and interface conditions are applied to find the overall response of the whole plate. To do this it is necessary to derive the matrix  $A_m$  from equation [2.20] for each layer and then produce the associated eigenvector matrix  $P_m$  for equation [2.21].

In this particular case the second and third (inner) layers have the same orientation as in the previous section. The first and fourth (outer) layers are orthogonal to the inner layers therefore the matrix  $A_m$  can be derived by replacing  $\gamma$  by  $90 - \gamma$  in the governing equations for the inner layers.

The elements of  $A_2 = A_3$  are

$$A_2 = \begin{bmatrix} 0 & -ikc(1-2\frac{c_2^2}{c_1^2}) & -ks\frac{c_4^2}{c_1^2} & \frac{1}{\rho c_1^2} & 0 & 0 \\ -iks & 0 & 0 & 0 & \frac{1}{\rho c_2^2} & 0 \\ -ikc & 0 & 0 & 0 & 0 & \frac{1}{\rho c_1^2} \\ \rho \hat{s}^2 & 0 & 0 & 0 & -iks & -ikc \\ 0 & \rho(s+k^2(s^2(c_5^2-\frac{c_4^2}{2})+c^2c_3^2)) & \rho k^2 sc(c_3^2+2\frac{c_2^2c_4^2}{c_1^2}) & -iks(1-2\frac{c_2^2}{c_1^2}) & 0 & 0 \\ 0 & \rho k^2 sc(c_3^2+2\frac{c_2^2c_4^2}{c_1^2}) & s^2+k^2(s^2c_3^2+4c^2(c_2^2-\frac{c_4^2}{2})) & -ikc\frac{c_4^2}{c_1^2} & 0 & 0 \end{bmatrix}$$

[2.27]

Then using eigenvector extraction techniques the matrix  $P_2$  is written as

$$P_2 = \begin{bmatrix} -ip_1c & is & -1p_3c & ip_1c & is & ip_3c \\ sc & -p_2 & sc & sc & p_2 & sc \\ -\alpha & 0 & -\beta & -\alpha & 0 & -\beta \\ i\alpha_1kc & 2iksp_2 & i\beta kc & i\alpha_1kc & -2iksp_2 & i\beta kc \\ 2kscp_1 & -k(s^2+p_2^2) & 2kscp_3 & -2kscp_1 & -k(s^2+p_2^2) & -2kscp_3 \\ (c^2-\alpha)\frac{c_3^2}{c_2^2}kp_1 & \frac{-c_3^2}{c_2^2}ksc & (c^2-\beta)\frac{c_3^2}{c_2^2}kp_3 & (\alpha-c^2)\frac{c_3^2}{c_2^2}kp_1 & \frac{-c_3^2}{c_2^2}ksc & (\beta-c^2)\frac{c_3^2}{c_2^2}kp_3 \end{bmatrix}$$

[2.28]

where  $p_1^2$  and  $p_2^2$  are roots of the equation

$$\left(\frac{\hat{s}^2}{k^2} + s^2c_1^2 + c^2c_3^2 - c_1^2p^2\right)\left(\frac{\hat{s}^2}{k^2} + s^2c_3^2 + c^2c_5^2 - c_3^2p^2\right) + c^2(c_3^2 + c_4^2)^2(p^2 - s^2) = 0$$

[2.29]

and  $p_2^2$  is given by

$$p_2^2 = \frac{1}{c_2^2} \left( \frac{\hat{s}^2}{k^2} + s^2 c_2^2 + c^2 c_3^2 \right) \quad [2.30]$$

$$\alpha = \frac{c_1^2 (s^2 - p_1^2) + c^2 c_3^2 + \hat{s}^2 / k^2}{c_3^2 + c_4^2} \quad [2.31]$$

$$\beta = \frac{c_1^2 (s^2 - p_3^2) + c^2 c_3^2 + \hat{s}^2 / k^2}{c_3^2 + c_4^2} \quad [2.32]$$

$$\alpha_1 = \frac{c_3^2}{c_2^2} \alpha - (p_2^2 + s^2) \quad [2.33]$$

$$\beta_1 = \frac{c_3^2}{c_2^2} \beta - (p_2^2 + s^2) \quad [2.34]$$

### Boundary Conditions

It is assumed that the layers in the plate are perfectly bonded together this means that the stress and displacement components at the interfaces have to satisfy continuity conditions for the interface. When  $x_I = \pm h$  these are given by

$$u_i^1(x_1, x, t) = u_i^2(x_1, x, t) \quad [2.35]$$

and

$$t_{ij}^1(x_1, x, t) = t_{ij}^2(x_1, x, t) \quad [2.36]$$

where the superscripts refers to the layer number.

The traction free boundary condition for the lower surface when  $x_I = -2h$

$$t_{ij}^4(x_1, x, t) = 0 \quad [2.37]$$

On the upper surface there is a stress discontinuity caused by the impact so the upper surface boundary condition is defined as

$$t_{11}^1(x_1, x, t) = f(t) \quad [2.38]$$

$$t_{1j}^1(x_1, x, t) = 0 \quad (j=2,3) \quad [2.39]$$

where  $f(t)$  is the loading on the plate.

By applying these boundary conditions to the general solution of equation [2.20] the constant vector  $\mathbb{K}_m$  from Equ. [2.21] for each layer can be evaluated.

### 2.3 Theoretical Solution

To solve the general solution to equation [2.20] the arbitrary constants vector  $\mathbb{K}_m$  for each layer are resolved. From these arbitrary constants the displacements and stress at any point on a multi layered plate can be calculated by applying inverse Fourier and Laplace transforms. As the plate is symmetric about the mid plane there are two distinct types of motion, flexural (antisymmetric) and longitudinal (symmetric). The arbitrary constants  $\mathbb{K}_m$  is defined as  $\mathbb{K}_m^a$  for the antisymmetric motion and as  $\mathbb{K}_m^s$  for the symmetric motion. The disturbances due to each type of motion are resolved separately and then combined to form the total disturbance.

Throughout the rest of this chapter the transformed displacements  $U_i$  ( $i = 1$  to 3) are denoted as  $U, V, W$  and the transformed stresses  $t_{ij}$  ( $j = 1$  to 3) as  $R, S, T$ .

#### Loading condition

The upper surface of the plate is subjected to line load normal to the plate (-ve  $x_1$  direction). The loading is of a form

$$t_{11}(x_2, x_3, t) = \rho c_2^2 f(t) \delta(x) \quad [2.40]$$

where  $\delta(x)$  is the Dirac delta function, the Laplace transform of  $f(t)$  is denoted by  $F(\hat{s})$ .

#### Antisymmetric Motion

From the boundary conditions, the upper surface of the plate is traction free except for the applied stress from the impact. For layer 1 where  $x_1 = 2h$ ,

$$\mathbb{Y}(2h) = (U, V, W, F(\hat{s}), 0, 0) \quad [2.41]$$

and therefore equation [2.25] and equation [2.41] are combined as

$$\mathbb{Y}(2h) = \mathbb{P} \mathbb{E}^+ \mathbb{K}_1^a = \mathbb{R}_1 \mathbb{K}_1^a = (U, V, W, F(\hat{s}), 0, 0) \quad [2.42]$$

Where the matrix  $\mathbb{R}$  is the combination of the matrices  $\mathbb{P}$  and  $\mathbb{E}$ .

Considering the interface condition of the 1st and 2nd layers, where  $x = h$  equations [2.25], [2.26] and [2.35] can be combined to

$$P_1 E^+ K_1^a = P_2 E^+ K_2^a \quad [2.43]$$

therefore

$$P_1 E^+ K_1^a - P_2 E^+ K_2^a = R_2 K_1^a - R_3 K_2^a = 0. \quad [2.44]$$

Considering the antisymmetric motion at the mid plane it can be shown that

$$V = W = R = 0 \quad [2.45]$$

The motion in the centre of the plate is defined from equations [2.26] and [2.37] as

$$Y(0) = P_2 E^+ K_2^a = R_4 K_2^a = (U, 0, 0, 0, S, T) \quad [2.46]$$

To evaluate the arbitrary constants  $K_m$  it is convenient to combine equations [2.42] [2.44] [2.46] and to write them in the form

$$M^a K^a = L \quad [2.47]$$

The matrix  $M^a = (m_{ij})$  is a 12x12 matrix constructed from the bottom three rows of  $R_1$ , all of  $R_2$  and  $R_3$ , and the second third and fourth rows of  $R_4$ . the matrix  $K_a$  is a 12 vector combining the six elements of  $K_1^a$  and  $K_2^a$  and  $L$  is the 12-vector  $(F(s), 0, 0, 0, 0, 0, 0, 0, 0, 0, 0, 0)$ .

To obtain the twelve arbitrary constants for the antisymmetric motion  $K^a$  equation [3.45] gives

$$K^a = M^+ L \quad [2.48]$$

which implies that

$$k_i = \frac{M_{ij}}{\det M} F(s) \quad [2.49]$$

where  $K^a = k_i$  ( $i = 1, 12$ ) and  $M_{ij}$  is the adjoint of the element  $m_{ij}$

#### Symmetric Motion

The boundary conditions for the antisymmetric and the symmetric motion are the same except for the mid plane conditions.

Considering the symmetric motion at the mid plane it can be shown that

$$U = S = T = 0 \quad [2.50]$$

In the same way as for the antisymmetric motion this provides the second set of 12 arbitrary constants.

Since the transforms of any displacement or stress is given in terms of these arbitrary constants, all that remains is to invert the transforms to obtain the displacement or stresses at any point on the plate after an impact.

#### 2.4 Numerical Procedure

To outline the numerical procedure for resolving the stresses or displacements in a plate a typical quality, the displacement in the  $x_2$ -axis  $u_2(x, x, t)$  at the upper surface of the plate will be described.

The plate was subjected to a line load consisting of a delta function in time, so that

$$f(t) = \delta(t) \quad [2.51]$$

with

$$F(\hat{s}) = 1. \quad [2.52]$$

For simplicity only the antisymmetric motion is described here but the same procedure is used for the symmetric motion.

The double transform of  $u_2(x, x, t)$  is given by  $V(2h, k, \hat{s})$  where

$$V(2h, k, \hat{s}) = \sum_{i=1}^6 m_{2i} k_i = \sum_{i=1}^6 m_{2i} \frac{M_{2i}(k, \hat{s})}{\det M(k, \hat{s})} \quad [2.53]$$

The formal solution on inverting the transforms is

$$u_2(2h, x, t) = \frac{1}{4\pi^2 i} \int_{\gamma-i\infty}^{\gamma+i\infty} \int_{-\infty}^{\infty} \frac{Z(k, \hat{s})}{\det M(k, \hat{s})} e^{\hat{s}t} e^{ikx} d\hat{s} dk \quad [2.54]$$

where 
$$Z(k, \hat{s}) = \sum_{i=1}^6 m_{2i} M_{1i}(k, \hat{s}) \quad [2.55]$$

The integral with respect to  $k$  may be evaluated in terms of the residues of the integrand at zeros of the function  $\det M(k, \hat{s})$  in the left half of the plane. The equation

$$\det M(k, i\omega) = 0 \quad [2.56]$$

is the dispersion equation for the antisymmetric motion of a plane harmonic wave of frequency  $\omega$  travelling at an angle  $\gamma$  to the  $x_3$ -axis under traction free boundary conditions. This equation has an infinite number of pairs of roots,  $k_j = \pm k_j(i\omega)$ , ( $j = 1, 2, \dots$ ), each pair corresponds to forward and backward travelling waves associated with one branch of the dispersion curve. In terms of these solutions, equation [2.54] becomes

$$u_1(2h, x, t) = \frac{1}{2\pi} \int_{\gamma-i\infty}^{\gamma+i\infty} \sum_{j=1}^{\infty} [R_2(k, \hat{s}) e^{ikx} J_{k=\pm k_j(\hat{s})} e^{\hat{s}t} d\hat{s} \quad [2.57]$$

where the sum of the residues are 
$$R_2(k, \hat{s}) = \sum_{i=1}^6 m_{2i} Z_i(k, \hat{s}) \quad [2.58]$$

and 
$$Z_i(k, \hat{s}) = \frac{M_{1i}(k, \hat{s})}{d(\det M(k, \hat{s}))/dk} \quad [2.59]$$

$R_2(k, \hat{s})$  is an odd function of  $k$ , equation [2.57] is written as

$$u_2(2h, x, t) = \frac{1}{2\pi} \int_{\gamma-i\infty}^{\gamma+i\infty} \sum_{j=1}^{\infty} [R_2(k, \hat{s}) e^{ikx} J_{k=\pm k_j(\hat{s})} e^{\hat{s}t} d\hat{s} \quad [2.60]$$

where 
$$R_j(\hat{s}) = \frac{[R_2(k, \hat{s})]_{k=k_j(\hat{s})}}{-[R_2(k, \hat{s})]_{k=-k_j(\hat{s})}} \quad [2.61]$$

$R_j(\hat{s})$  is an even function of  $\hat{s}$ , and there for equation [2.60] can be further simplified to give

$$u_2(2h, x, t) = \frac{2i}{\pi} \int_0^{\infty} \sum_{j=1}^{\infty} R_j(\omega) \sin k_j(\omega)x \cos \omega d\omega \quad [2.62]$$

This expression for the normal displacement consists of a sum of integrals, one along each branch of the dispersion curve.

The equations [2.62] provides the antisymmetric displacements of the plate, the symmetric displacements are resolved in a similar way.

The total displacement of the upper surface of the plate is given by the combination of the antisymmetric motion and symmetric motion of the form

$$u_1 = u_1^a + u_1^s, u_2 = u_2^a + u_2^s, u_3 = u_3^a + u_3^s \quad [2.63]$$

### Strain

As was described earlier the aim of this theoretical work was to produce results that could be easily compared with experimentally collected data. This required the data to be of the same form. The experimental data was in the form of the strain developed in the plane of the plate in the direction of the wave propagation. The strain was measured over a finite length of the plate and recorded for a time duration. It was necessary to transform the displacements in the  $x_2$  and  $x_3$  direction into strain for a finite length of the plate at a fixed distance from the impact.

The strain is defined in terms of position and time as

$$\epsilon_{xx} = \delta u / \delta x \quad [2.64]$$

where the displacement in the x direction is  $u$ .

Since the direction of the wave propagation is defined by equation [2.8]

$$x = x_3 \cos \gamma + x_2 \sin \gamma$$

the displacement  $u(x, t)$  is defined by

$$u(h, x, t) = u_3(h, x, t) \cos \gamma + u_2(h, x, t) \sin \gamma \quad [2.65]$$

equations [2.64] and [2.65] can be combined to provide the strain in the direction of wave propagation over a length  $l_0$ .

$$\epsilon_{xx} = \cos\gamma(u_3(x,t,h)/l_0) + \sin\gamma(u_2(x,t,h)/l_0) \quad [2.66]$$

Therefore the combination of equation [2.66] with the  $u_2$  and  $u_3$  displacements will provide the solution to the dispersion equation [2.35] in the form of strain in the direction of wave propagation.

## 2.5 Numerical Solution

The numerical solution for the dispersion wave equation [2.35] was completed in two parts. The first stage was to calculate the solutions to the form of the dispersion equation, [2.35] for the antisymmetric and symmetric motion separately. A computer program was produced (Appendix 1) which calculated the solution  $k(i\omega)$  to equation [2.56] by fixing a value of  $\Omega$ , where  $\Omega = \omega h/c_1$ , and then starting from  $k = 0$ , the program marching up the  $k$ -axis in steps evaluating the values of  $M$  at each step until the branches of the dispersion curves had been resolved.

The zeros of  $M$  were determined by dividing a step in  $k$  into equal sub intervals, and the value of  $M$  was calculated at each sub interval. If the sign of the value of  $M$  changed for successive intervals there was at a root of the equation in between these values. To verify the number of roots in the step of  $k$  the sub interval between the values was reduced by a factor of 2 and the number of sign changes was checked. This was repeated until the number of sign changes remained constant after four successive sub divisions of the values of  $k$ , when it was judged that all the sign changes, and hence roots of the equation had been found for this step in  $k$ . If the number of sign changes did not become stable after 10 sub divisions of the values of  $k$ , the step values of  $k$  were reduced and the operation repeated. Once the values of  $k$  were known either side of a root of the equation the value of the root was approximated by the secant method. This was repeated until all the root for a particular value of  $\omega$  were found.

The analysis was completed for a range of  $\Omega = 0$  to 14 in steps of 0.02. The maximum value of 14 for  $\Omega$  was selected as this gave an upper frequency limit of between 4.4MHz and 44MHz for layer thickness  $h$  between 0.1mm and 1mm, and a wave speed  $c_T = 2000\text{ms}^{-1}$ .

Once a root of equation [2.56] was found the corresponding value of  $Z_i(k,s)$ , equation [2.39], was evaluated numerically and stored. This operation was repeated separately for the antisymmetric motion and the symmetric motion, and the stored values were recorded in a data file for the second stage of the analysis.

Once the solutions to the dispersion equation were obtained with the corresponding values of  $Z_i(k,s)$ , the second stage of the analysis could be performed. This involved the numerical integration and summations for the inversion of the transforms to resolve the displacements at the required locations of the plate. This was completed separately for each of the surfaces and the mid plane of the plate.

A separate computer program (Appendix 1) was written to resolve the  $x_2$  and  $x_3$  displacements from the surface and the mid plane disturbances in the plate, using numerical integration methods. Once these displacements were resolved the required strain values were calculated with equation [2.81]. This resulted in the strain values at a fixed point on the plate, for a specified time duration, which could be compared with experimental data.

The results from the analysis of a four ply plate are presented in chapters 6 and 7 for the two materials studies in this work.

## 2.6 Limiting Wave Velocities

It has been shown by Green and Baylis [23] that the limiting solution of the dispersion equation [Equ. 2.56] for short wavelengths (high frequency) is the smaller of the Rayleigh type surface velocity  $v_R$  in the outer layer or a shear wave velocity  $v_s$  in the inner core.

The Rayleigh type surface wave velocity in the outer layer is given by

$$v_R^2 = c_3^2 \sin^2 \gamma + c_R^2 \cos^2 \gamma \quad [2.67]$$

and the shear wave velocity in the inner core by

$$v_s^2 = c_3^2 \cos^2 \gamma + c_2^2 \sin^2 \gamma \quad [2.68]$$

In equation [2.67],  $c_R$  is the Rayleigh wave velocity in the direction at right angles to the fibres and is equal to that in an isotropic material for which the longitudinal wave has speed  $c_1$  and shear wave speed  $c_2$ . The Rayleigh wave velocity of an isotropic material was defined by Kolsky [12] as

$$(2c_2^2 - c_R^2)^2 = 4c_2^2 \left(1 - \frac{c_R^2}{c_1^2}\right) \left(1 - \frac{c_R^2}{c_2^2}\right). \quad [2.69]$$

The surface wave velocity  $v_R$  in the outer layer becomes equal to the shear wave velocity  $v_s$  in the core at a critical value of  $\gamma_c$ , which can be determined from

$$v_R^2 = c_3^2 \cos^2 \gamma_c + c_2^2 \sin^2 \gamma_c. \quad [2.70]$$

For the values of  $\gamma < \gamma_c$  the limiting speed at short wavelengths is  $v_R$  and for values of  $\gamma > \gamma_c$  the limit is  $v_s$ .

## 2.7 Wave Propagation Through a Cross Ply Composite Plate

The transmission of stress waves through a plate is described by the dispersion equation [Equ. 2.35] the roots of which generate a series of dispersion curves. There exists an infinite number of these curves which correspond to the harmonics of the dispersion equation. Each harmonic of the plate will contribute to the transient motion of the plate with the bulk of disturbance normally associated with the fundamental mode. The

disturbances associated with the fundamental modes are called the Lamb waves. It has been described by Green and Balysis [24] that the speed of propagation of these Lamb waves is considerably less than the speed of waves travelling through an infinite medium whereas it is known that the first arrivals in a plate travel with this speed. To account for this motion the high harmonics are required to describe the motion of the plate after an impact.

The motion in the plate due to the long wavelength (low frequency) limit, wavelength is long in comparison with the plate thickness, is the Lamb waves which generate a linear variation in the stress distribution in the plate which is associated with pure bending. The fundamental flexural Lamb mode is almost non dispersive which indicates that it can propagate over a long distance without significant change in the shape of the propagating waveform. The motion due to the higher harmonics up to the short wavelength limit, wavelength is short in comparison to plate thickness, is associated with rapid variation in the shear stress of the plate, Green [23]. This motion is highly dispersive and so will change its waveform as it propagates through the plate. It is therefore this short wavelength limit with the associated rapid variation in shear stresses which are of interest in this work.

In the examination of the short wavelength (high frequency) wave propagation in a cross ply plate of anisotropic layers the main consideration is the relationship between the direction of wave propagation and the direction of anisotropy of a particular layer. For an infinite anisotropic material the five wave speeds defined in section 2.1 can be described in terms of longitudinal wave ( $v_L$ ) and shear waves ( $v_S$ ) and the axis of anisotropy of the material. If the 1 direction is parallel to the axis of anisotropy, the 2 direction perpendicular to the direction of anisotropy (i.e., normal to the fibre length in a unidirectional material) and the 3 direction is normal to the 1-2 plane the five material wave speed can be described as  $c_1=v_{L2}$ ,  $c_2=v_{S23}$ ,  $c_3=v_{S31}$ ,  $c_4=v_{L1}$  and  $c_5=v_{S12}$ , where the

subscripts define the direction. It can be seen that the wave speeds  $c_1$  and  $c_2$  are associated with a wave propagating perpendicular to the direction of anisotropy, wave speeds  $c_4$  and  $c_5$  are associated with the waves propagating in the direction of anisotropy and  $c_3$  with a shear wave travelling through the thickness of the layer.

Considering a plate impacted on the upper surface with the angle of propagation  $\gamma=0^\circ$ , the direction of the wave propagation would be parallel the direction of anisotropy in the inner core and perpendicular to it in the outer layer. In the outer layers the direction of wave propagation would be perpendicular to the direction of anisotropy, therefore the waves would be travelling in a quasi-isotropic material. This would result in longitudinal and shear waves travelling through the upper surface of the layer as if it was an quasi-isotropic plate. This would result in symmetric and anti-symmetric motion occurring on the upper surface which would generate a Rayleigh type surface wave. At the interface between the upper layer and the core of the plate the motion would be constrained by the anisotropy of the inner core, this would result in the motion decaying rapidly from the surface to the interface with the core. In the core of the plate the waves would be propagating in the direction of anisotropy but would generate lower amplitude in this layer due to its greater stiffness than the outer layers. On the lower surface the waves would be propagating through a quasi-isotropic material again.

Considering a second condition of  $\gamma=90^\circ$ , the direction of wave propagation is parallel to the axis of anisotropy in the outer layers and perpendicular to it in the inner core. In this condition the effect of the anisotropic material would be on the outer layers of the plate and the waves propagating through the inner core passing through a quasi-isotropic material. The longitudinal motion of the inner core would be constrained by the anisotropic outer layers which would result in the shear wave propagating through the centre of the plate generating the largest motion in the plate.

The overall effect of the short wavelength limit will be to channel the largest motion in the plate due the propagation of the stress waves into the most flexible layers of material in the direction of the propagating wavefronts.

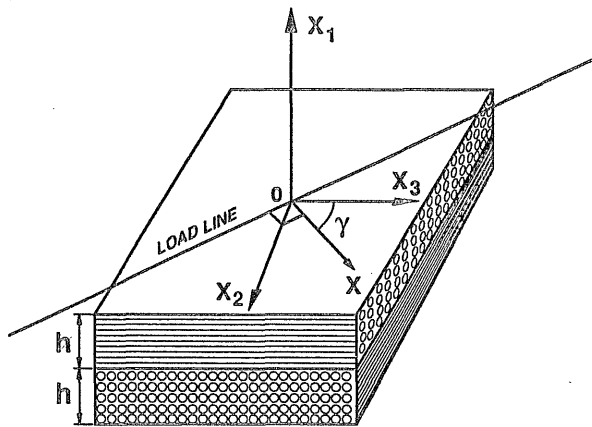


Figure 2.1: Lower Half of Four Layer Plate with Axis System

### Chapter 3: Design of Stress Wave Propagation and Detection System

In Chapter 2 a theoretical model was presented which predicted the elastic response of a multi layered plate when subjected to a normal surface impact. The solution resolved the in plane strain responses of the plate due to a stress wave propagating following a normal surface line impact. The plate construction examined was a symmetric cross-ply assembly of four layers of a uni-directional composite material.

The objective of the experimental study was to examine the disturbances caused by the stress waves and to examine for correlation between the results of the numerical solution of the theoretical model and experimental data. Therefore the aim of the experimentation was to propagate and detect the stress wave passage at the surfaces and the internal ply interfaces for a four ply laminated plate. To achieve this an experimental system was required to excite a plate with a normal surface line load and also to detect and record the passing of the stress waves at locations on and in the plate away from the point of impact.

The three main requirements of the experimental system were:

- i) A system which would excite the plate with a normal surface line load.
- ii) Sensors that could detect the passing of the stress waves on the surface and at the ply interfaces of the plate.
- iii) The collection and processing of the sensor signals.

Parts (i) and (iii) of the experimental system are discussed in this chapter while the sensor requirement and design are described in detail in Chapter 4.

#### 3.1 Plate Excitation

In the analytical solution the plate model was excited by a numerical delta function impulse, whose characteristics were an infinite magnitude over zero time. This style of

ideal impulse could not be physically produced in an experimental environment as any impulse would possess a finite magnitude and duration over which it was applied to the plate. Previous work by Green [47,48] had shown that the length of the impulse applied affected the plate response. For an impulse of long duration the low frequency bending responses dominate the high frequency shear responses in a plate. This indicated that if an impulse of finite duration was used which resulted in a dominating low frequency response, the high frequency shear wave component responses would have to be separated to permit their examination.

A requirement for the plate excitation system was that the responses produced were within the plate were elastic. The reason for this was that the analytical solution only resolved the elastic disturbances caused by the passing stress waves. A second consideration was that if the plate response was elastic no damage would occur to the plate and therefore it could be used for successive tests.

Cantwell and Morton [8] have examined the effects of low and high velocity impacts on the damage threshold of composite materials. It was reported that for low velocity impacts surface fibre failures were observed with an impact energy of 1.0J and for high velocity (short duration) impacts damage could occur at 0.5J. This was for a material of Grafil XA-s fibres in a Ciba - Geigy BSL91LL epoxy resin in a  $((\pm 45^\circ)_4)_s$  configuration. This provided an initial estimate that an impulse energy in the region of 0.1J to 0.5J was required to provide an elastic response dependent on the material under examination.

#### Energy sources

A variety of impact systems have been used in the study of the impact response of fibre reinforced plates. These have been extensively reviewed by Cantwell and Morton [3]. The majority of this work was concerned with the plastic deformation and damage of the

material in relation to its post impact strength, Park [9], Falabella et al [51], Mortimer [4]. Those studies concerned with an elastic response have mainly been of quasi static loading conditions involving servo hydraulic machines, Kakarala and Roche [52].

There was no quantified impulse duration requirements for the energy source except that the shorter the duration the easier it would be to isolate individual characteristics in the general response, such as surface waves. The use of filtering of the responses could remove the low frequency bending waves to provide more a detailed picture of the shear waves responses. There were five primary energy sources were considered to provide the energy impulse into the plate.

#### Electromechanical

This involved the use of an electro magnetic coil which would induce movement into a steel bar when a current is applied to the coil. This method was used in a preliminary study by Awang [52] where a single square wave pulse was applied to an electric shaker. This system provided an impact of velocity of  $2ms^{-1}$  and an impulse duration of  $150\mu s$ . This response was the fastest possible due to the limitation with this electro mechanical device caused by the inertia of the steel bar and the time for the electro magnetic field to be produced. These limitations provided little capability for variation in the characteristics of the impulse applied to the plate.

Chetwynd and Sachse [81] have developed a micro hammer as a broad band ultrasonic source for point source / point receiver applications. The principle of the design was that a small projectile is attached to a larger carrier. This carrier is accelerated towards the test material but is rapidly decelerated just before the surface which releases the projectile to impact the material. The device used an electromagnet armature as a carrier with small 16mg and 1mg point masses as the projectiles, these were attached to the armature with a thin metal strip. This device produced an impact velocity in the region of  $1ms^{-1}$  which

resulted in impact energies of 8mJ for the 16mg projectile and 0.5mJ for the 1mg projectile. This device produced a point load onto the plate with an impulse duration in the region of 2 $\mu$ s.

#### Piezoelectric Crystal

The application of an electrical charge to a piezo electric material causes the deformation of the material structure. The direction of the material deformation can be controlled in piezo electric crystals depending on their structure. If a crystal was placed in contact with a plate the deformation of the crystal could be used to provide an impulse into the plate. This method could result in a very short duration impulse depending on the response of the crystal, and the frequency of the applied electrical charge. Piezo electric crystals have been used extensively in acoustic emitters for quantitative non destructive evaluation (QNDE) of materials where radial waves are used to detect flaws in materials, Gorman [36]. A limitation of this technique was that very small displacement would be applied to the plate and therefore produce small responses which could be difficult to detect at the ply interfaces.

#### Explosive

Several methods of producing line impulses using explosives are discussed in [53]. This appeared to be a simple way of applying a line impulse, but problems would occur with the control of the energy levels and the location of the test site which would have to be in a safe environment. A second problem would be that an explosive force could generate a large amount heat to be dissipated which would result in damage to the composite plates.

#### Ballistic

There are two basic types of ballistic impact systems currently employed in the investigation into impact response of materials. The first involves the low speed techniques where the projectile is accelerated by gravity i.e. drop weight machine Gause and Buckley [54]. The second is where the projectile is accelerated by an external energy

such as compressed gas or explosive charge Cantwell and Morton [8]. The main limitation with the ballistic systems for the requirements of this work was that they generally used spherical projectiles which result in a point impulse when impacting on a material. To produce a plane wave from a point loading the impulse would require translating into a line impulse with some form of load spreader or striker. The two basic types of ballistic impact systems are described in detail below.

#### Drop Weight Machine

The drop weight machine has been a popular method of examining the damage caused in composite plates by impact, Gause and Buckley [54]. The advantage of this type of machine is that they are simple to manufacture and operate, as the energy is supplied by gravity. The impact energy can be varied as it is proportional to the drop height of the projectile. If the projectile does not cause penetration of the plate during the impact event the rebound of the projectile can provide the opportunity for it to be caught to prevent multiple impact occurring. The velocity of the projectile can be measured using an optical speed measurement device before impact. A problem with the use of drop weight system with low energy impacts is that a small rebound of the projectile could provide difficulties in the prevention of multiple plate impacts. A second effect that could occur was that the projectile could not rebound at all and remain on the plate which could alter its response characteristics.

#### Gas Gun

The gas gun has been used to study the response of strain gauges to plastic waves in solids Khan [35], and the hyper velocity impact response of composites, Schonberg [5]. It has also been used by Cantwell and Morton [8] to compare the impact response of carbon-fibre reinforced plastic at low and high velocities. There is also reported work by Takeda et. al. [55] where a variety of projectile nose shapes and masses were used in the study of the delamination of composite plates. Another form of Ballistic impact is the

pneumatic impact device where a piston is accelerated to a high velocity. This then strikes the striker which in turn impacts the test specimen. This type of device was used to simulate the front of a car hitting an object Nusholtz et al [56]. A similar design was used to investigate intermediate velocity impact of fibre reinforced composites Derieck J. and Dechaene R. [30] where the shear wave surface disturbances from a delamination were examined using high speed streak photography.

#### Pulsed Laser

The use of a pulsed laser for quantitative ultrasonic NDE is described by Hutchins [40]. There are three basic mechanisms by which a laser can produce stress waves in a material, the first is by heating the material which leads to rapid thermal expansion of the material which radiates the elastic waves. The second mechanism is the removal of a coating from the material by evaporation, which produces a pulse due to the material leaving the surface. A third mechanism which was recently identified was the effect of plasma formation close to the surface but not in contact with it. The reflected energy and incident pulse combine to produce the breakdown of the air close to the surface of the plate and so provide the impulse into the plate.

The main advantage of this system was that very short duration impulses could be produced which would reduce the dominance of the low frequency bending wave response of the plate. A second consideration was that although a laser would provide an impulse at point location on the plate there was the capability to scan the laser across the plate which would provide the required line impulse. The primary concern with the use of the laser system was whether the plate responses produced by the propagated waves be of sufficient magnitude to be detected by the sensors embedded at the ply interfaces.

After consideration of all the proposed energy sources a gas gun energy source seemed to provide the best initial impulse source. The impulse energy could be controlled by altering

the projectile speed, and the gas gun could be mounted horizontally and therefore prevent the projectile from resting on the plate after the impact. There were also suitable gas guns available on the open market in the form of commercial pneumatic air rifles that could be modified to meet the energy requirements.

### 3.2 Plane Wave Propagation

There were two basic ideas that were considered to translate the impulse of a point load from a gas gun projectile in to a line impulse applied on a plate. The first was to use a load spreader which would be in contact with the plate at one end and the projectile would strike the other end. The load would be transferred from the projectile through the spreader onto the plate in a line form, figure 3.1. A second method was to mount a line striker in-between the plate and the projectile. The striker would be impacted by the projectile and would then accelerate to impact the plate, figure 3.2.

#### Load Spreader or Striker

##### Load spreader

The principal function of the load spreader was to distribute the load from a point source into a line source across the plate. This was to be achieved by fixing a shaped piece of material such as steel in contact with the plate. This was struck at one end by the projectile from the gas gun and the stress waves would propagate through the spreader into a line load onto the plate. The load spreader would be supported horizontally to avoid the addition of extra weight to the plate. There were two initial designs for load spreaders figures 3.3 and 3.4, but after consideration of the designs it was resolved that a consistent force would not be produced along the bottom edge as the stress waves travelling through the spreader would reach the centre of the spreader before the outside edges. There was also the concern that the spreader remaining in contact with the plate would affect the response of the plate by providing an extra constraint on the movement of

the plate after the initial impulse.

#### Striker

The principle of using a striker was to provide a second projectile in-between the gas gun projectile and the plate. This second projectile would be impacted by the gas gun projectile and then accelerate to impact the plate. The major consideration was the loss of energy due to the projectile hitting the striker and then the striker hitting the plate.

#### Striker Design

The basic design for a striker was a triangular section bar of material supported by two flat spring steel strips from a suitable structure, Figure 3.5. The most important criterion for the striker was to produce a maximum impact energy of 0.5J onto the plate from a 1g pellet travelling with a speed range of 80ms<sup>-1</sup> to 150ms<sup>-1</sup>. The first requirement was to calculate the mass limit of the striker to provide the required impact energy.

Preliminary tests with the gas gun indicated that 1g soft lead pellets deformed on impact with a steel bar and produced no rebound. This led to the assumption that the impact between the striker and gas gun pellet was virtually plastic and therefore the majority of the momentum would be transferred from the pellet to the striker.

Therefore the momentum equation can be written as

$$m_p V_p = m_s V_s \quad [3.1]$$

where  $m_p$  = mass of pellet,  $V_p$  = velocity of pellet before impact

$m_s$  = mass of striker,  $V_s$  = velocity of striker after impact.

If the maximum required striker energy was 0.5J,

from the definition of kinetic energy, K.E. =  $1/2 mV^2$  the striker velocity is

$$V_s^2 = 1/m_s \quad [3.2]$$

substituting the striker velocity into the momentum equation Equ [3.1] for a maximum

impact energy of 0.5J

$$m_s = (m_p V_p)^2$$

therefore

Maximum pellet velocity =  $150\text{ms}^{-1}$       Maximum striker mass = 22.5g

Minimum pellet velocity =  $80\text{ms}^{-1}$       Minimum striker mass = 6.4g

This provides the requirement of a maximum striker mass of 22.5g, with an impact velocity of  $V_s = 6.6\text{mS}^{-1}$ .

In the design of a striker a second consideration was the stiffness along the length. If the striker deformed under the point loading in its centre a line load would not be produced on the plate. An initial design was to use a triangular section of short fibre reinforced plastic, but this was found to have insufficient strength across the striker width and fractured under impact with the plate.

A striker was then designed from steel which was to be case hardened to prevent local deformation during impact. The striker was 100mm long to provide a broad impact across the plate, and the back face required a minimum depth of 5mm to provide sufficient area for the pellet to impact. To produce a striker of 20g the total volume of material was  $2.54\text{cm}^3$ . This resulted in a striker dimensions shown in figure 3.5.

#### Finite Element Analysis of Striker Design

To evaluate the performance of the striker and suspension system a forced response finite element analysis of the structure was completed. This analysis examined the response of the striker due to an impulse applied at its centre considering its first four modes of vibration. The analysis involved the construction of a simple finite element mesh, figure 3.6 which was subjected to a vibration analysis to find the first four vibration modes. Once the displacement of the striker was known for each vibration mode Guyan reduction

techniques were applied to the mesh to reduce the analysis to 35 degrees of freedom. The impulse was applied to one of the degrees of freedom at the centre of the striker for a duration of 10ms and the forced response vibration displacement of the 35 degrees of freedom was calculated. The impulse applied was equivalent to a 1g projectile impacting the striker at  $120 \text{ ms}^{-1}$ . The results of the analysis, figure 3.7, shows the duration of time a section of the leading edge of the striker takes to travel 0.5mm. These results show clearly that centre 15mm section of the striker would impact the plate with in  $1\mu\text{s}$  of the initial contact between the striker and a plate mounted 0.5mm away from the initial striker location. Since the width of the sensors that were used to detect the disturbance in the plate was 0.5mm, it was considered that the sensors would be subjected to a plane wave front across their sensing area due the ratio of the sensor width and the width of the load striker.

### 3.3 Detailed Design of Stress Wave Propagation System

The general arrangement of the design for the stress wave propagation system can be seen in Figure 3.8. There were the three main parts of the system, the gas gun to provide the initial energy input into the system, the load striker assembly to produce the line load onto the plate and the plate and the structure to hold the plate into position.

#### Gas Gun

One of the considerations in selection of a gas gun as the primary energy source was the availability of commercial air rifles which could produce a 1g projectile with a maximum energy of 12 J. This provided an advantage that time and money was saved compared with the manufacture of a one off design. A second reason for the selection of a commercial air rifle was that a high standard projectiles were available which produced a plastic impact between the air rifle pellet and the load striker.

The type of air rifle selected functioned by filling a chamber under the barrel with compressed gas. This gas was then released through a mechanical valve operated by the trigger into the gun barrel which accelerated the projectile down the gun barrel. This method of operation produced very little recoil in the gun and provided the capability to control the pressure in the chamber which in turn controlled the exit velocity of the pellet. The gun was modified to directly pressurise the chamber with an external gas supply controlled with a Druck pressure controller. This provided accurate control on the exit velocity of the pellet and thence the initial energy into the impact system.

It was necessary to measure the initial energy going into the impact system to ensure consistency between tests. For this purpose an optical velocity measurement device was designed and built using fast response optical emitters and detectors, figure 3.9.

An extension was designed for the end of the gun barrel which contained three pairs of optical emitters and detectors. These optical emitters and detectors were mounted opposite each other and with a distance of 30mm between each pair. When the detectors were receiving the light from the emitters they produced a voltage which could be measured. The pellet passed through the light beams which resulted in a change in the output levels of the detector which was recorded on a storage oscilloscope. This change in the output of the detectors resulted the determination of the time of travel between two light beams and so the velocity of the pellet was known.

Using the optical velocity measurement device a pressure/velocity calibration was carried out on the air gun Figure 3.10, which showed the gun could produce a range of impact velocities..

The air rifle with the optical measurement device attached to the end of the barrel were mounted in a V block onto a solid table. The gun mounting onto the table provided

vertical and horizontal movement to provide alignment with the striker. A remote trigger system was also mounted onto the gun mounting to release the air from the pressure chamber to propel the pellet with the minimal disturbance of the gun.

#### Striker Mounting

A suspension frame was designed and built, with the striker mounted on it. Micrometer heads were used to adjust the distance between the striker and the plate. To detect the exact point in time when the striker first made contact with the plate a small electrical potential was applied between the striker and the plate from a 9V battery. When the striker contacted the plate there was a drop in the potential which was detected and provide the exact instant of the striker impact.

#### Plate Mounting

The analytical analysis of the stress waves in a multi layered plate presented in Chapter 2 was based on the assumption of an infinite plate with no edge restraints. In the experimental system to minimise the edge effects on the plate it was simply supported at the two edges parallel to the load striker with the other two sides left free.

### 3.4 Data Recording System

#### Requirements

The data recording system was required to record the disturbance caused by the passing of the stress wave propagated from the line impulse normal to the plate. A typical carbon fibre reinforced laminated material with a ply thickness of  $125\mu\text{m}$  has a typical shear wave speed is  $1000\text{ms}^{-1}$ , and an associated frequency in the order of 1MHz. This provided the initial requirements that the data recording system required a frequency response into the low MHz region.

The recording system needed the capability to record the output of at least 5 signals simultaneously, one for a sensor at each interface of a four ply laminated plate and one for each of the surfaces. The high frequency nature of the signals collected required the system to store the data while it was collected and then download it to a computer for permanent storage.

Once the data was stored onto the computer there was the requirement to post process the data to extract the shear wave responses from the lower frequency bending plate response.

The main requirements for the data recording system were:

- i) Upper frequency response limit in the low MHz region.
- ii) Signal storage and recovery facilities
- iii) Post processing facilities, including digital filtering.

The data recording system consisted of two parts, the first part recording the signals from the sensors and a second part for post processing and storing the signals after the test.

The data was to be stored during capture and then transferred onto a computer for post processed and storage. This required the sensor signals to be converted from time analogue into digital for storage. The recording units were required to contain sufficient memory to record the data for a minimum recording time of  $40\mu\text{s}$  for a sensor mounted 40mm away from the impact for a typical wave speed of  $1000\text{ms}^{-1}$ .

The data recorders selected were Yokogawa digital oscilloscopes, these oscilloscopes contained four channels with 32Kbytes of data storage on each channel and an analogue to digital sampling frequency of 20MHz.

This recording system provided 1ms of recording time on each channel and therefore it was important to synchronise the data recording with the impact event. To achieve this a PVDF sensor was mounted on the striker. When the striker was impacted by the

projectile from the gun, the local deformation of the striker caused a response in the PVDF sensor which could be used as a trigger to the data recording system.

#### Post processing

After the sensor signals had been recorded and stored on the oscilloscopes the data was then transferred to a computer (Dell 386) for processing via a IEEE communication card. The post processing of the signals was then completed using the PAFEC Spiders digital signal processing software. This software provided the facilities to window in on particular areas of data, apply fast Fourier transforms to the data and to use digital filters on the data. The digital filters were important as the theoretical work had shown that as the impulse duration became longer the lower frequency bending waves dominated the high frequency shear waves and the high frequency component was not visible. To recover the high frequency component of the signals, digital filters were used to remove the low frequency components.

### 3.5 System Evaluation Test

To complete an initial evaluation of the stress wave propagation and detection system some preliminary tests were completed with a steel plate. The principal objective of the tests was to verify that the impact system produced stress waves travelling through a material, that the sensors could detect the stress wave disturbances and that the data capture system could record and extract the required stress waves from the sensor signals.

Steel was selected as the initial evaluation material since it is an isotropic material and therefore only two waves (longitudinal and flexural) are propagated through the material from a surface impact. Thus evaluating the data would be simpler as would the understanding of plate response. An effect particularly under investigation was the Rayleigh surface wave which should be present on the surface subjected to the impact but

would be absent from the lower surface. If these wave disturbances could be detected for a steel plate subjected to an impact it could be concluded that the stress wave propagation and detection system fulfil the requirements and would be capable of detecting the stress wave disturbances in multi layered plates of anisotropic materials.

The sensors used to detect the stress wave disturbances were the PVDF piezo electric film sensors which are discussed in detail in Chapter 4.

The steel tested was 4mm gauge plate which was selected as the thickness was comparable to the proposed thickness of the composite plates to be tested. The plate dimensions were 200mm by 300mm with the impact occurring 100mm away from the bottom edge of the plate, and the sensors mounted 15mm away from the striker impact. The layout of the plate can be seen on figure 3.11.

To mount the sensors on the plate the Micro Measurement M610 adhesive was used which provided a minimal adhesive layer between the plate and the sensor and provided insulation between the electrical contacts on the sensor and the plate.

The plate test was completed with the gun pressure set at 40 bar. This pressure provided an initial projectile velocity of  $120\text{ms}^{-1}$ . This projectile speed resulted in an impact energy of the striker onto the plate of 0.42J. This was the magnitude of impact energy that was required to impact the composite plates with outdamage.

#### System Evaluation Test Results

Figure 3.12 shows the raw responses from the sensors mounted on the surfaces of the plate impacted by the striker, for a duration of  $50\mu\text{s}$ . Figure 3.13a is the upper impact surface at a distance of 15 mm from impact, figure 3.12b shows the lower surface response 15mm from the impact and figure 3.13c shows the upper surface response 30mm

from the point of impact. The responses recorded show similar low frequency characteristics to the responses recorded by Daniel and Wooh [33], Mortimer et al [4] and Takeda et al [34] with strain gauges on impacted composite plates. This indicated that the sensors were detecting similar responses to the strain gauges used in the previous impact wave propagation work. This indicated that the responses produced from the impact were of the same nature as from other ballistic impact systems.

Following the test the raw responses collected were subjected to post processing with the PAFEC spiders digital signal processing package. The objective of this was to extract the high frequency shear wave component disturbances caused by the passing of the shear waves.

The raw data responses were filtered with a 10th order Butterworth filter with a lower frequency filter of 400kHz and an upper frequency filter limit of 4MHz. The lower frequency limit was set to remove the plate bending effects, and the upper frequency limit was to remove any high frequency noise and aliasing effects from the digital conversion. The filtered responses can be seen in Figure 3.13.

To compare with the experimental results an analytical analysis was also completed for a steel plate using the methods described in Chapter 2. The results of this analysis can be seen in Figure 3.14. To ensure compatibility between the analytical and experimental results the same filters were applied to both sets of results.

The analytical results of the upper surface [Fig 3.14a] show the clear presence of two waves, the first occurs  $2.5\mu\text{s}$  after the impact and is therefore travelling at  $6\text{mm}\mu\text{s}^{-1}$ . The second response occurs after  $4.9\mu\text{s}$  and is travelling at a speed of  $2.9\text{mm}\mu\text{s}^{-1}$ . The lower surface response [Fig 3.14b] also shows two responses the first occurring at  $2.8\mu\text{s}$  after impact and the second at  $5.4\mu\text{s}$  after impact. The propagation speed of this response

matches the longitudinal wave speed for steel, table 3.1. The delay between the upper surface response and the lower surface response is due to the time the wave takes to propagate from the upper surface impact to the lower surface.

The second response detected on the upper surface is a large magnitude response whose propagation speed matches the Rayleigh wave speed for this material, table 3.1. The magnitude of this response and the absence of a similar response on the lower surface are the characteristics of a Rayleigh wave. The second response on the lower surface is propagating at a speed of  $2.9\text{mm}\mu\text{s}^{-1}$  and is identified as the response due to the flexural (shear) wave propagating through the plate and generates symmetric motion on the upper and lower surface of the plate. The effect of this wave cannot be seen on the upper surface due to the presence of the larger Rayleigh wave and the small difference in speed between the flexural and Rayleigh wave speeds in steel, table 3.1.

The experimental results [Fig 3.13] show the sensor responses for a period of  $30\mu\text{s}$  with the point of impact indicated. There are the responses of three sensors shown, the upper and lower disturbances at 15 mm from the point of impact and the upper surface disturbance at 30mm from the point of impact. At the point 15mm from the impact the upper surface response [Fig 3.13a] shows a greater disturbance occurring than appears on the lower surface [Fig 3.13b] which is consistent with the presence of a Rayleigh surface wave but the individual waves present are not distinguishable. The most likely cause of the poor resolution of the individual waves was that the sensors were mounted 15mm away from the impact point which was only 3.75 times the thickness of the steel plate, and the sensors would be subjected to the wave reflection occurring between the plate surfaces, and that there would be little time for the separation of the waves due to their different wave speeds to occur. On the upper surface 30mm away from the impact [Fig 3.13c] there are two distinguishable waves, the first wave (1) is the faster of the waves and is travelling at  $6\text{mm}\mu\text{s}^{-1}$  and the second waves (2) appeared to be travelling at

$3\text{mm}\mu\text{s}^{-1}$ . These wave speeds are comparable with the theoretical longitudinal wave speed ( $c_l$ ) and the Rayleigh surface wave speed ( $v_R$ ) in Table 3.1, which indicated that these were the waves that were detected by the sensors on the plate.

In conclusion to the system evaluation test the initial raw responses of the sensors recorded similar characteristics in the plate response to previous ballistic testing [39],[4],[34] of material in plate form. The higher frequency stress wave disturbances were detected with the digital filtering of the sensor responses but the individual waves could only be resolved with a sufficient distance from the impact relative to the plate thickness to avoid interference from the internal reflections of the waves between the upper and lower surfaces. This testing showed that the stress wave propagation and detection systems were capable of propagating stress waves through a plate, which caused disturbances which could be detected by the sensors and recorded by the data capture system.

Wave	Speed ( $\text{mm}\mu\text{s}^{-1}$ )
Longitudinal ( $c_l$ )	5.95
Flexural ( $c_f$ )	3.18
Rayleigh ( $v_R$ )	2.95

Table 3.1: Shear Wave Speed for Steel

Wave speeds calculated from equations in Kolsky [12].

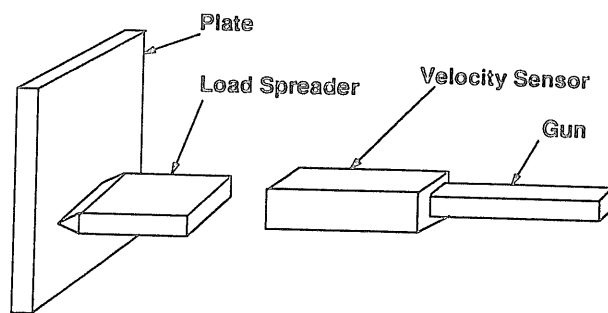


Figure 3.1: Load Spreader Arrangement

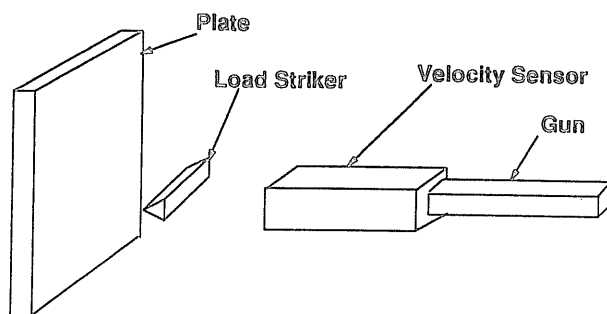


Figure 3.2: Load Striker Arrangement

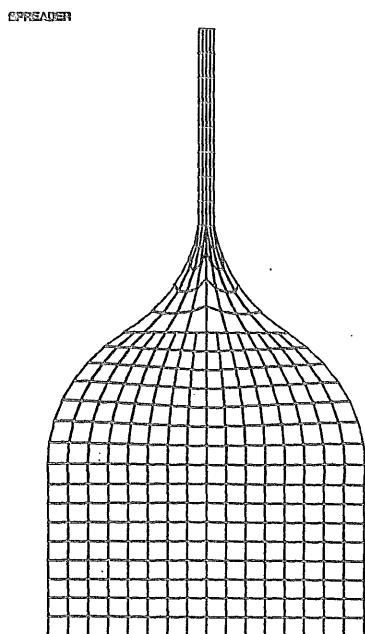


Figure 3.3: Load Spreader, Design 1

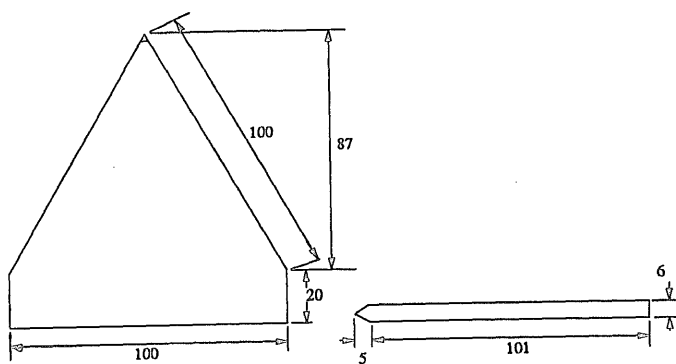


Figure 3.4: Load Spreader, Design 2

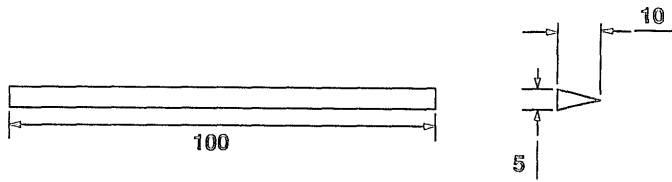


Figure 3.5: Load Striker Design

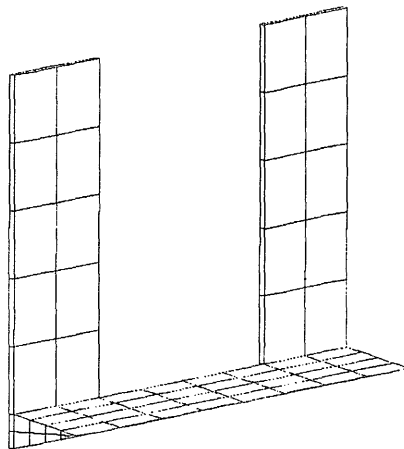


Figure 3.6: Finite Element Mesh of Striker and Suspension System

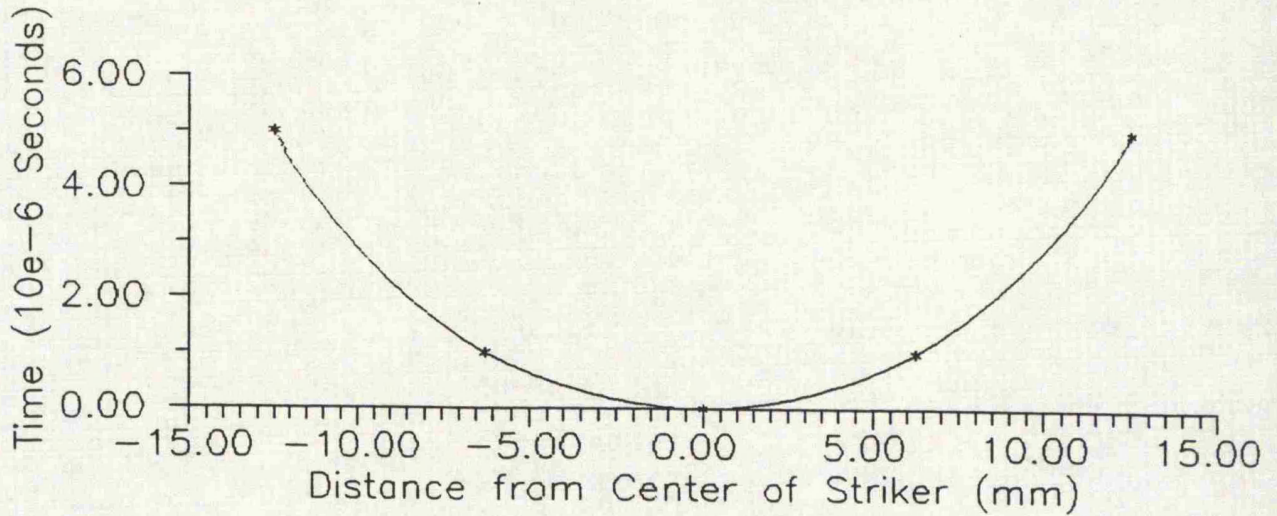


Figure 3.7: Graph Showing the Time the Leading Edge of the Striker Takes to Travels 0.5mm due to an impact of a 1g Projectile Travelling at 120ms-1.

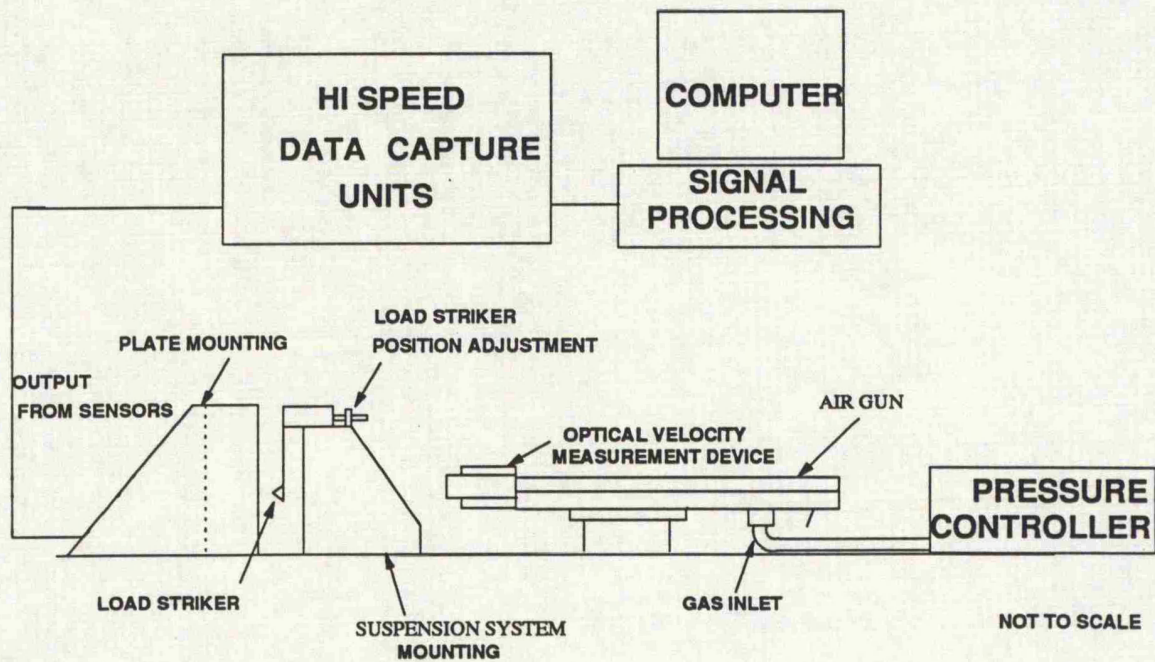


Figure 3.8: General Arrangement of Experimental System

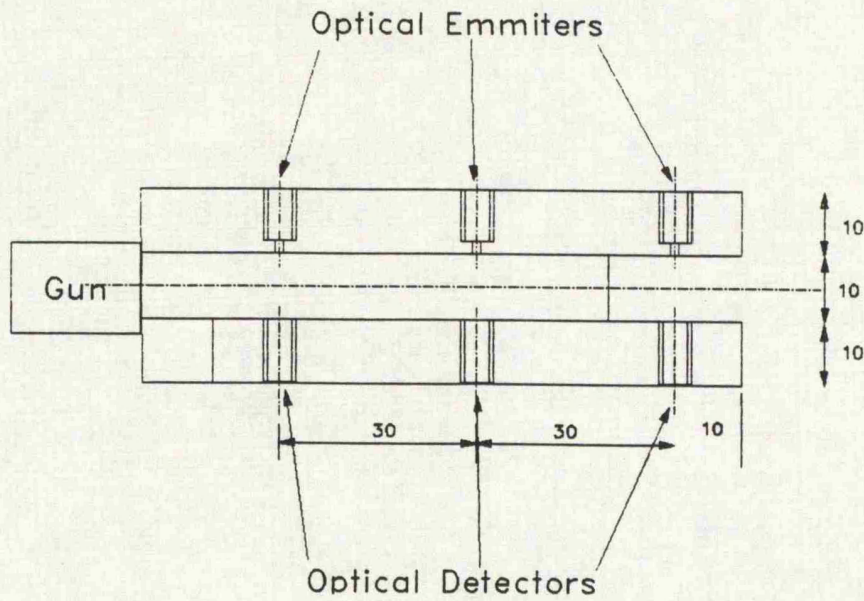


Figure 3.9: Optical Speed Measurement Device

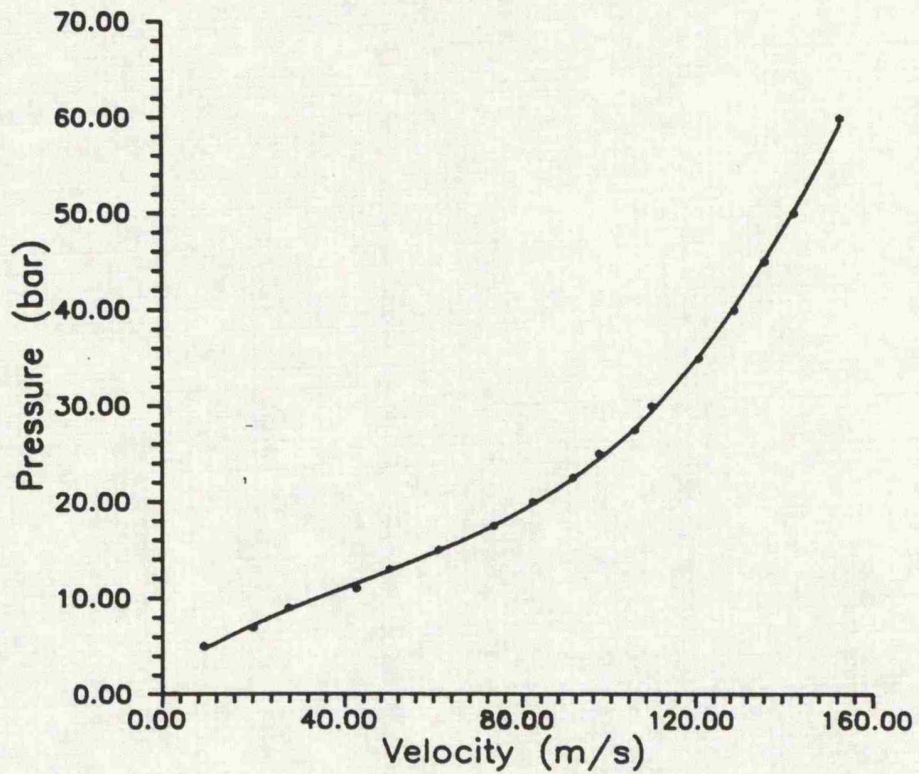


Figure 3.10: Graph of Gas Gun Pressure versus Projectile Velocity

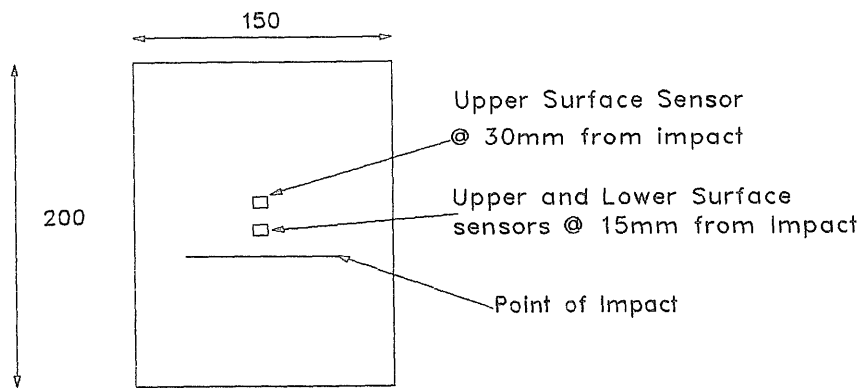


Figure 3.11: 4mm Steel Test Plate Configuration

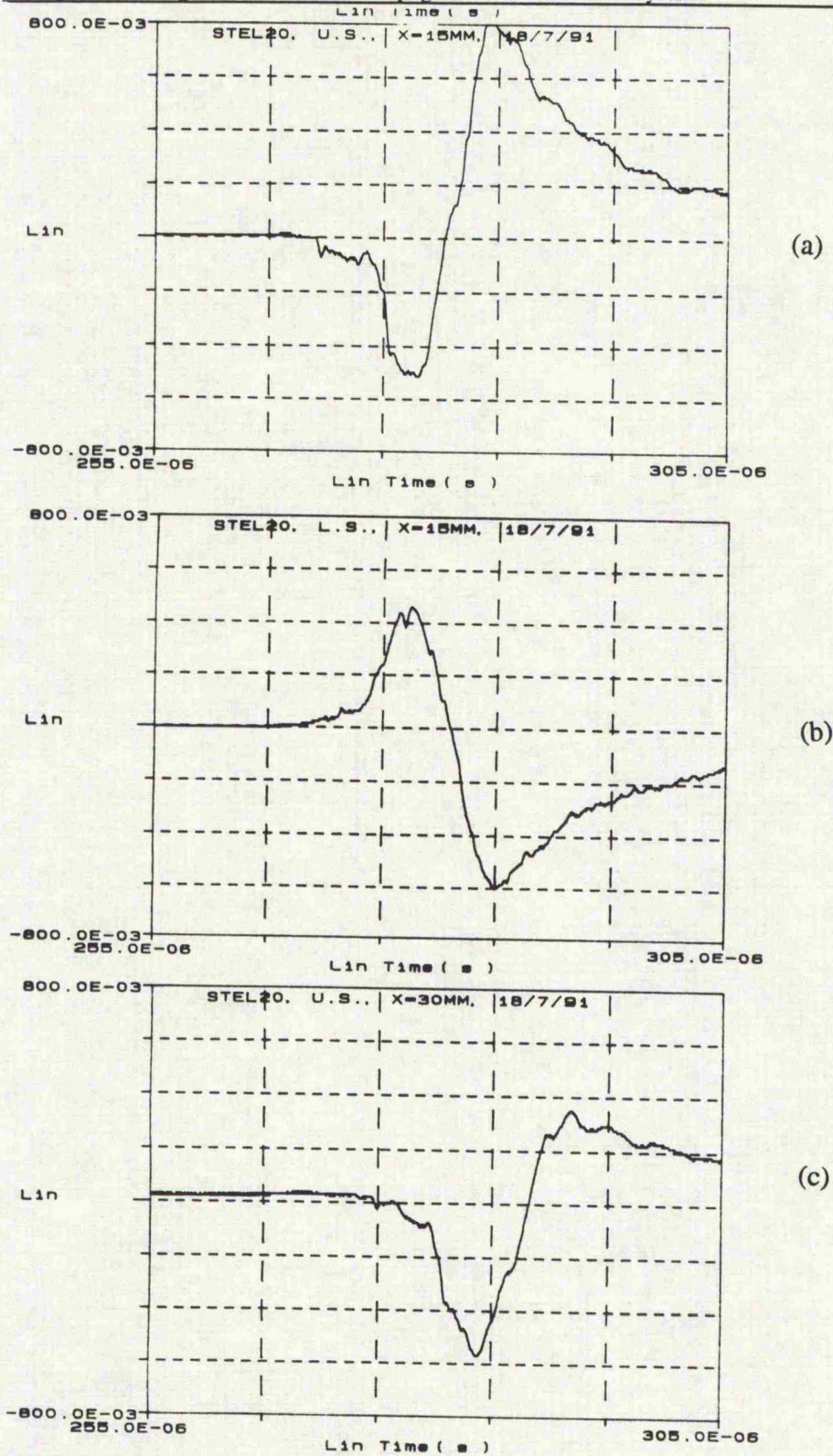


Figure 3.12: Steel Plate Sensor Response  
a) Upper Surface 15mm from Impact  
b) Lower Surface 15mm from Impact  
c) Upper Surface 30mm from Impact

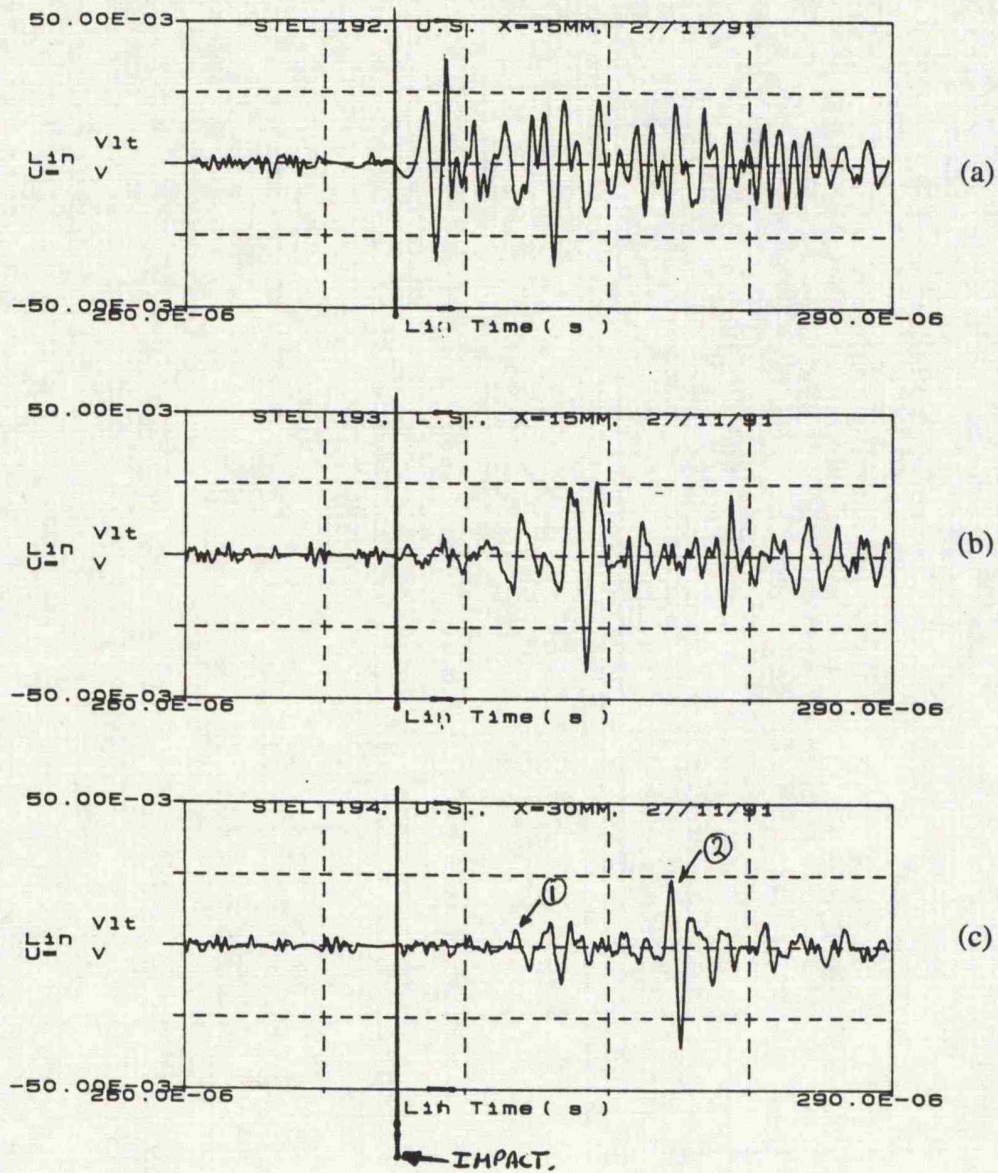
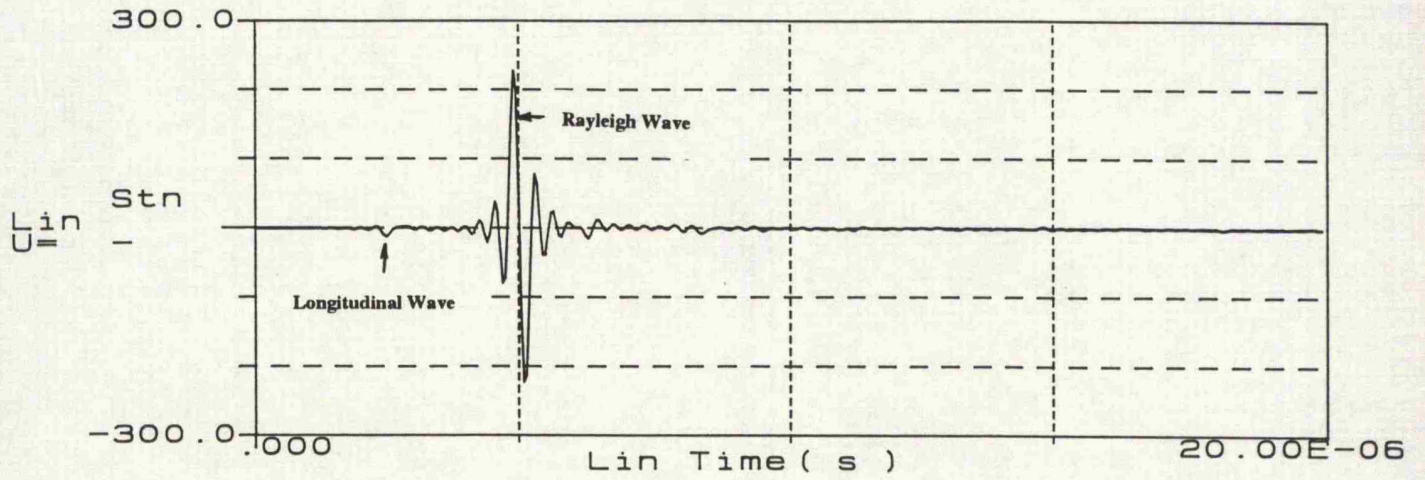
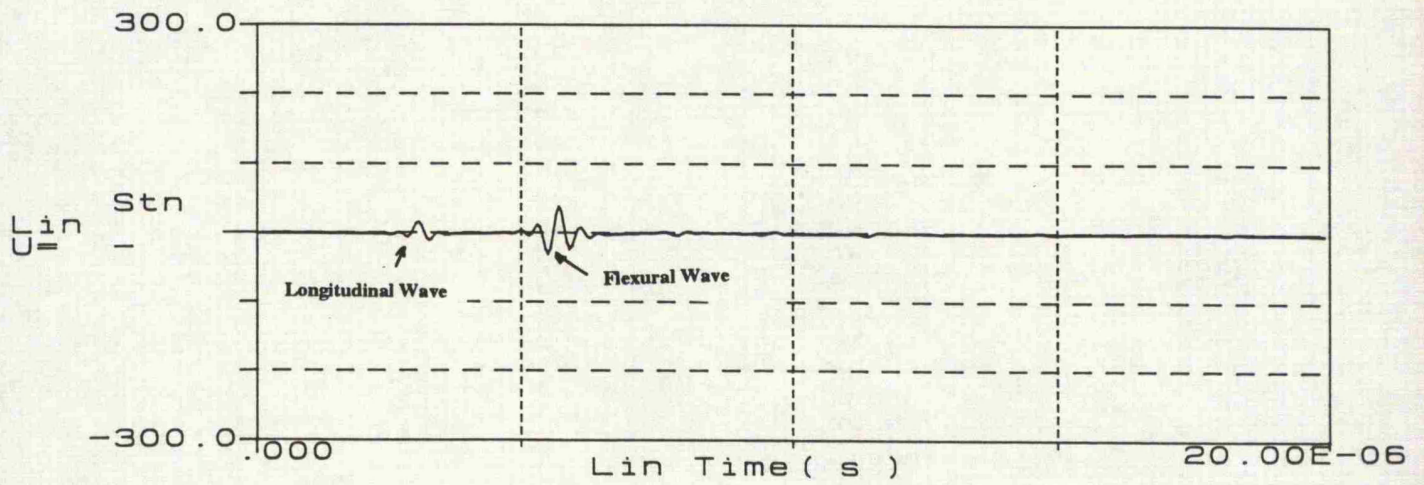


Figure 3.13: Steel Plate Sensor Response,  
 Band Pass Filtered, 0.4MHz-4MHz  
 a) Upper Surface 15mm from Impact  
 b) Lower Surface 15mm from Impact  
 c) Upper Surface 30mm from Impact



(a)



(b)

Figure 3.14: Analytical Steel Plate Response  
a) Upper Surface 15mm from Impact  
b) Lower Surface 15mm from Impact

## Chapter 4: Stress Wave Sensors

A key objective of this work was to develop a method for examining experimentally the disturbances in a laminated plate, caused by the passing of stress waves propagated from a surface impact. The data collected from the experimental work had to be comparable to the analytical solution to the problem, to enable a reasonable comparison between the experimental and theoretical data. The analytical solution enabled the displacements, stresses or strains at any point on a plate caused by the passing of the stress waves to be calculated. This allowed for a wide consideration in the types of sensors that could be used.

There were several important requirements for the stress wave sensor dictated by both the analytical work and physical constraints. To achieve a reasonable comparison between the analytical and experimental work the frequency range of the sensor would have to match the upper frequency limit used in the analytical solution. The upper frequency limit was defined by  $\omega = 14c_l/h$ , in Section 2.5, where  $c_l$  was a wave speed of the material and  $h$  the thickness of one material layer. For the main material used in this study LTM22/T700 the upper frequency limit was  $f = 4.9$  MHz with a layer thickness of 1 mm.

It was desired to examine the stress wave disturbances at the surfaces and the mid plane of a plate. The sensor would have to be capable of detecting the mid plane disturbances which would most probably involve embedding part of the sensor into the plate. It was therefore necessary to consider how the embedding could take place and how much disruption would be caused to the structural integrity of the plate.

A third consideration was to know exactly what the sensor was measuring. Ideally the sensor would detect the normal displacement at a point on the plate, as this was

the form of the early analytical results. However it would have proved to be very difficult to measure the internal responses of a plate in this way. The favoured method to detect the disturbances was to measure the strains developed in the direction of wave travel caused by the passing of the stress waves. A sensor of this type would have a finite length that could be longer than the wavelengths of the waves to be examined, which would lead to an integration of the waves as they passed the sensor. It was decided that this could be acceptable if necessary as the analytical results could be modified to show the responses of the plate over a finite length of plate, provided the sensor was as small as physically possible.

The disturbance caused by the passage of the stress waves was to be of an elastic nature in this study and therefore very small. The sensors would have to be very sensitive to measure the physical disturbances caused by the passing of the stress waves.

The main requirements of the stress wave sensor system are summarised below.

- i) Detection of disturbances over a small area to minimise the wave integration.
- ii) To detect the internal disturbances of the plate with the minimise disturbance to the plate structure.
- iii) The frequency response of the system must be in the MHz region.
- iv) High Sensitivity

#### 4.1 Review of Stress Wave Sensor Methods

There were five main types of sensors considered, that met some of the requirements above. These sensors were fibre optic systems, non contact displacement/stress

systems, non destructive evaluation techniques, strain gauges and piezo - electric transducers.

Fibre optic systems.

Optical Fibres have a number of advantages when used as sensors in fibre reinforced materials. Their material properties are not dissimilar to carbon fibres, and their size is only one order of magnitude larger. These facts mean that they are very attractive as embedded sensors for fibre reinforced plates. They have been embedded into carbon fibre reinforced plates and used as a damage assessment system or as a strain measurement system. Damage assessment systems are described by Hofer [57] and Crane and Maccander[58] where the fibre optics are laid in a mesh in a laminated plate. When the strains in the composite exceed a critical point and failure within the composite occurs, the fibre optic will also fail and so provide a means of detection. This system is improved in Waite et al [59] where the fibre optics are deliberately weakened so that they will fail at certain strain values to indicate when a structure has been subjected to critical strains. This damage assessment system was not of particular interest for this work as it detects the damage of the material rather than the elastic response, but it did show the viability of embedding optical fibres in fibre reinforced materials.

The optical fibre strain measurement systems were initially of more interest as they would not produce large discontinuities within the laminated plates. The basic theory as described by Butter [60] is that the elastic response of the optical fibre produces a delay in the time it takes for the light to travel down the fibre which can be measured when compared to a reference fibre. This system has been used to measure the strains in a laminate plate during processing, Reddy et. al. [61], and work is being carried out into developing it into a usable strain gauge Uttam et. al [62]. The main drawback with the system is that it is only capable of measuring the strain across

the entire length of the fibre optic and not at specific points. This would make it particularly difficult to measure the strains developed in the mid plane due to the whole length of the fibre optic being embedded in the plate.

#### Non contact measurement systems

Non contact measurement systems fall into two main types, eddy current systems which detect the normal displacements by the reflections of eddy currents from a conductive material and laser displacement systems which detect normal displacement from the reflection of a laser from a surface using the Doppler effect.

#### Eddy current systems.

These systems were advantageous as they measured normal displacement, but the surface of the material had to be conductive to effect the electro magnetic field which was produced by the sensor. This would have meant that for a non conductive composite reflective material would have had to be placed on the material, introducing a second material into the plate. The sensing area also was relative large, the smallest sensor found required an area 6mm in diameter. The frequency response of the systems examined up to 2KHz which was too low for the requirements. The final problem was that it would have been difficult to examine the mid plane disturbances as the sensors have to be normal to the surface and could not be embedded into the plate for internal disturbance measurement. Holes could have been cut into the plate but was not practical due to the large discontinues that would have been created.

#### Laser displacement systems

The laser displacement systems detected the phase change of the reflected light from a moving surface. This system also measured the normal displacement of the surface of a material, but could measure the displacement over an area of 1-2 mm diameter. The disadvantage of the systems was again the frequency limits which were in the region

of 5-10kHz . The mid plane disturbances would also have been difficult to measure and a hole would again have had to be cut in the plate, but it would have been smaller than for the eddy current sensor.

#### Acoustic Emission Techniques

One method for the non destructive evaluation of materials has used elastic wave propagation as a method to detect flaws in materials, this involves the use of acoustic emission sensors which detect the presence of elastic waves travelling through a material. Work was carried out by Gorman [36] examine the acoustic emission in composite plates from waves propagated due to a lead break on the surface of the a plate.

The AE sensors work by detecting the disturbances of the passing of the waves under the sensor. The primary function for acoustic emission sensors has usually been the measurement of time it takes particular types of waves to travel between two points and then calculating the location of flaws or cracks. This type of sensor have been developed to detect the high frequency waves had typical frequency responses in the order of 250kHz to 5MHz.

The smallest available sensor was the point like transducer which was 3mm in diameter, which was comparable with the smallest available strain gauge. The sensors were also the most sensitive of all the sensors examined and could detect the waves propagated from a simple pencil lead break on the surface of the material.

The disadvantage was that they could only be used effectively on the surface of the plate due the physical size. To detect internal waves a sensor would have to again be cut into the plate to place the sensor in physical contact with the mid plane layers of material. A second problem was that the sensors could only detect the passing

waves, and there did not appear to be any direct correlation back to the actual displacement on the surface of the plate.

#### Strain Gauges

The use of strain gauges initially looked very promising as a method of detecting the stress wave disturbances. There was the major advantage of being established technology, and therefore requiring little development work.

The two types of strain gauges under consideration were resistance foil and semiconductor. The resistance foil gauges had gauge factors around 2 and the smallest size of  $2\text{mm}^2$  whereas the semiconductor gauge factor was in the region of 155 and a smallest size of  $0.5\text{mm}^2$ . Both types of gauges survive high temperatures up to  $350^\circ\text{C}$  which was inside the cure temperature of most epoxy based fibre reinforced plastics, which typically cured at  $200^\circ\text{C} - 250^\circ\text{C}$ .

The main problem with strain gauges was the signal conditioning that was required. To meet the requirements the strain gauge amplifiers would need a response in the MHz region. There were large bandwidth amplifiers available but as the gain increased by a order of magnitude the bandwidth of the amplifiers was proportionally reduced. This was considered a possible problem area but since at the early stages of the work it was unclear the strain levels that would be expected some experimental investigation was required.

#### Piezoelectric Transducers

Piezoelectric transducers work on the principle that when certain materials are deformed an electrical charge is produced. The most common material to display this effect is quartz crystal, which is used in many washer style force transducers. Other materials which have been developed and which also exhibit this effect are ceramics

and polyvinylidene fluoride (PVDF). These materials are often used as the sensing element for acoustic emission sensors. Cambel et. al. [80] has reported the use of this material as a multi purpose sensor on composite laminates.

The material that was the most interesting was PVDF film, it exhibited several of the physical characteristics of strain gauges. It was thin (~ 52 $\mu$ m) and could easily be applied to the surface and embedded into a multi layered material, and exhibited a very high sensitivity and had a resonance frequency of 20MHz. Preliminary tests indicated that the response of the film could be detected directly and no further amplification was required.

The overall impression was that the PVDF film could directly be used as a stress wave sensor but further investigation was required.

#### Sensor Selection

After consideration of all the sensing systems considered the two that looked the most suitable were the strain gauges and the PVDF film. The strain gauges looked promising as they were established technology and had been used for laminated materials, but had the problem of frequency bandwidth of the strain gauge amplifiers. The PVDF film had a very good frequency response but there was limited information on them as dynamic strain gauges.

Further investigations were carried out into the use of strain gauges and piezoelectric sensors, and are reported in the following sections. Experimental evaluations were carried out on both sensor systems before the final sensor selection was made.

## 4.2 Strain Gauge Measurement System

As outlined above the main concern in using conventional strain gauges was the gain bandwidth product of the strain gauge amplifiers. This defined the ratio between the gain of the amplifiers and the frequency bandwidth. Since the stress waves travelling through a material only produce low level high frequency responses a high gain and frequency bandwidth measurement system was required. Two types of strain gauges, resistance foil and semiconductor and a high frequency bandwidth strain gauge amplifier were evaluated to see if a suitable stress wave detection system could be developed.

### Strain Gauges

The considerations in the choice of strain gauges were the physical size, gauge factor and the survival temperature. The physical size had to be as small as physically possible to produce the minimum disruption to the plate and have the lowest possible integration of the waves as they passed the gauge. The gauge factor was important as the higher it was the more sensitive the gauge was and therefore the higher output that could be obtained. A good survival temperature was required to enable the gauges to be embedded into the laminated plated during manufacture.

### Resistance foil gauges

The most suitable resistance foil gauge that was found was manufactured by Tinsley, gauge number 002/350/PC. The physical size was 2mm \* 1mm and possessed a survival temperature of 350°C. Due to their small size the maximum excitation voltage that could be applied was 0.75V.

### Semiconductor gauges

The best semiconductor strain gauge was manufactured by Entran, gauge number ESB-020-500, figure 4.1. The gauge size was 1mm x 0.5mm, gauge factor 155 and survival temperature 315°C. The excitation voltage was recommended at 3.5V for long term use but a maximum of 5V could be used for short duration's.

The size and construction of the gauges meant that they could only be handled by the lead out wires and could not be pressed on to the plate during bonding. They were also not encapsulated so insulation layer was required between the gauge and any conductive surface. The fine gold lead out wires were attached normal to the gauge with a relatively large area of solder which led to concern about disruption to the waves for the internal gauges.

Overall the semiconductor strain gauges were more suitable than the resistance foil strain gauges due to their smaller size and higher sensitivity. To evaluate their ability to detect the passing of stress waves it was decided to conduct an experimental evaluation of their performance with the strain gauge amplifiers.

### Bonding semiconductor strain gauges

To evaluate the performance of the semiconductor strain gauges three gauges were bonded onto an aluminium plate with Micro Measurement M310 strain gauge adhesive. Initially an insulating layer of adhesive was applied to the plate and cured at 50°C for 5 hours. A second layer of adhesive was applied to the plate and the gauge placed on the adhesive and held in place with a special jig which clamped the lead wires and then cured at 50°C again. The gauges proved difficult to mount due to the brittle semiconductor material which fractured if it was handled too heavily. Once

the adhesive was cured the fine gold leads were attached to connection tabs which also proved difficult as the leads were prone to breaking.

On the first attempt there was a high mortality rate for the gauges, due to both the gauges breaking during bonding and lead failure after bonding, 3 out of 10 survived. This would have improved with practice but it did raise the question as to whether the gauges would be tough enough to survive the processing of the laminated material for the internal gauges.

#### Strain Gauge Amplifiers

To detect the strain gauge response suitable strain gauge amplifiers were required. These amplifiers were required to respond to stress waves frequencies up to 4MHz to provide realistic comparison with the analytical results. After investigation into commercial products a suitable amplifier was found manufactured by CIL in the form of their SGA1103 board. This board was based around the SGA403 instrumentation amplifier. This amplifier claimed a unity gain bandwidth of 30MHz, and would therefore have a bandwidth of 3MHz at a gain of 10. This was in the upper frequency limits that was required but it was unclear whether a gain of 10 would be sufficient to produce a clear signal. It was decided that a verification of the gain and frequency response of the amplifiers should be carried out since they were to be used at the upper limit of the manufacture's specifications.

To investigate the responses of the amplifiers a sweep function generator was used to provide an input signal varying from 10kHz to 5MHz. The amplifier was set on a gain of 10 as this the minimum gain that would be required for the stress wave signals. The output was recorded on the data collection system described in section 3.5, recording with a 20MHz sampling frequency. A fast fourier transform was used and

the data plotted as frequency against gain. The response of SGA1103 board and just the SGA403 amplifier can be seen in figure 4.2.

The gain of an amplifier is defined as

$$\text{Gain (dB)} = 20\log (V_o/V_i) \quad [4.1]$$

Where,  $V_o$  = output voltage,  $V_i$  = input voltage.

The test showed that the SGA403 amplifier on the board had a response of 20dB up to 3MHz but it was not particularly linear, the overall response of the whole board was 32dB but only up to 2kHz. After consultation with the manufactures it was found that the discrepancy between the SGA403 amplifier and the overall board response was due to a second operational amplifier on the output of the SGA403 which was used to improve the gain and produce a linear response across the frequency range, but introduced a smaller bandwidth. To improve the situation several modifications were made to the board by changing the second stage amplifier to one with a higher bandwidth specification. The results can be seen in figure 4.3

The different output amplifiers did improve the situation but none of them increased the bandwidth limit above 1MHz, which was lower than required. It was decided that the best solution was to by pass the second stage amplifier and accept the non linearity of the SGA403 output with a gain of 20db and a frequency limit of 3MHz. It was therefore necessary to establish if a gain of 20dB would be sufficient to detect the stress waves passing through a material.

#### Evaluation of strain gauge measurement system.

The objective of this test was to evaluate the performance of the semiconductor strain gauges and amplifiers at detecting stress waves passing through an aluminium plate.

A strain gauges was successfully mounted on each surface of a 12.5mm thick aluminium plate. The plate was placed in the wave propagation rig as described in section 3.4, the plate was impacted to propagate stress waves from the point of impact. To produce any response from the strain gauges the excitation of the strain gauges had to be set to the maximum of 5 V. This excitation voltage produced an electrical breakdown in the insulating layer between the gauge and the plate and the gauges started to short to earth. The only successful response can be seen in figure 4.4. The response of the strain gauge showed that the gain of the amplifiers was much too low as the response can only just be seen above the background noise of the amplifiers, and any details of the response were swamped by the noise.

The conclusions from this assessment were that a much larger gain was required from the strain gauge amplifiers to produce a clear response. The problem was that suitable amplifiers could not be found that had a large bandwidth at a high gain.

The other two responses shown in figure 4.4 were from two PVDF film transducers with a gauge length of 2mm. These devices produced a much better response than the strain gauges and are described in the next section.

#### 4.3 Investigation into the use of Piezo-Electric Film Sensors as Dynamic Strain Gauges.

##### Principles of Piezoelectric Material

It was discovered more than a hundred years ago, by Jacques and Pierre Curie, that if a quartz crystal was subjected to pressure an electrical charge was generated.

Similarly if an electrical charge was applied to a quartz crystal it changed in dimension. This effect became known as piezo-electricity from the Greek for pressure electricity. The piezo-electric effect has been used for many different applications

including quartz watches, cigarette lighters and a whole variety of transducers. The most common transducer is the force cell, which contains a layer of crystal for each active axis, and produces a charge when the cell is compressed in an active axis. In the early 1960's studies were carried out on the piezo-electric effect of organic materials, and Kawai [63] found that polarised homopolymer of vinylidene fluoride had greater piezo-electric response than any other synthetic or natural polymer.

When a deformation is applied to a piezoelectric material the charge that develops within its crystalline structure will diminish with time. The deformation of the crystalline structure results in a net change in the charge density of the material. If there are electrical contacts applied to the material there will be a flow of electrons to produce a charge balance within the material. This flow of electrons can be monitored and can be shown to be proportional to the deformation of the material. This effect is enhanced by the doping of the material to increase the number of aligned charge dipoles in a particular direction..

The piezoelectric material under consideration here is manufactured from the polymer polyvinylidene fluoride (PVDF). A film of the material is stretched to produce a polymeric structure as shown in figure 4.5. The charge dipoles within the material are aligned by heating it to the Curie temperature (just below the melting temperature) and applying a strong electric field, . This process is known as poling and the structure of the material is shown in figure 4.6. When the material is below the Curie temperature and a mechanical strain is applied to the film the material develops a variation in charge density which makes an effective sensor. This also produces an upper temperature limit of 120<sup>0</sup>C for the PVDF film. If conductive layers are applied to both sides of the film a capacitance of the film is produced. The capacitance of the film is small, and any measurement device can cause drift, and

therefore the film is most effective when used in dynamic situations. A full description of the characteristic of PVDF sensors is provided in [64].

There are several advantages of piezoelectric film over other piezoelectric materials such as crystal and ceramics. They can easily be cut to any size and therefore fit complex geometry, and due to their low sharpness of resonance ( $Q$ ) they have a bandwidth of 20MHz. This is as opposed to piezo crystals which are only applicable over a narrow bandwidth. As the film is relatively compliant and can absorb more energy than crystals, it acts as good receiver but does not perform as well as Piezo crystals as an emitter or actuator.

Piezo film is a flexible lightweight tough plastic film which is available in a variety of thicknesses. It has a wide frequency range (0 to  $10^9$  Hz) and a large dynamic range ( $10^{-8}$  to  $10^6$  psi). The elastic compliance is high and therefore faithfully reproducing the input forces, and a good mechanical strength ( $10^9$ - $10^{10}$  Pascal modules).

#### Directionality

The polling of the film results in the piezoelectric properties of the material being anisotropic, and the electrical and mechanical properties differ depending on the axis of applied stress or strain. Figure 4.7 shows how axes are defined. To define the properties two subscripts are used. The first defines the axis of electrical field and the second refers to the axis of applied or induced stress or strain. For the film manufactured by the Pennwalt company the polarization axis is always the thickness or 3-axis. Applied loading can take place in all three directions.

#### Frequency dependence

One of the major considerations with piezoelectric film is that it is inherently capacitive, and therefore means that the signal generated by the film will change with

time. The flat response over such a large frequency range is partly due to the polymer softness as oppose to hard ceramics. The basic half wave length resonance of 28  $\mu\text{m}$  piezo film is about 40MHz.

#### Mechanical impedance

Transducers made of PVDF film are thin and flexible, are of low density and excellent sensitivity but still mechanically tough. The compliance of piezo film is 10 times greater then that of ceramic. They can be directly attached to structures with out disturbing the mechanical motion of the structure.

#### Initial evaluation of PVDF film as a strain sensor.

The initial evaluation of the PVDF film was to establish that the film could detect the response of a material when it was impacted. Two standard gauges of size 15mm x 30mm were reduced in length to 15mm x 2mm, to produce a sensor length comparable with the semiconductor strain gauges. The gauges were mounted directly on to the same plate as the semi conductor strain gauges to provide a direct comparison between strain gauge and the PVDF film performance. The output of the PVDF film was directly connected to the data recording equipement with no further amplification. The results can be seen in figure 4.4. The responses from the PVDF film were an improvement compared to the strain gauge results. This showed that the PVDF film could be used as a stress wave sensor, but further investigation was required into the design and manufacture of a sutiable sensor size.

#### 4.4 Design and Manufacture of a Piezoelectric PVDF Film Sensor

The active area of a piece of piezo-electric film is defined by the area of the film where there is a conductive surface on both sides. The requirements for the sensor was that it had to be as small as physically possible to simulate a point on the plate. In the design of the size of the sensor the main concern was the reduction of capacitance of the sensor. The lower cut off frequency of the sensor is defined by the sensor capacitance and the capacitance and resistance of the output device. The lower frequency cut off value ( $f_c$ ) was defined by

$$f_c = 1/2\pi R_i(C_f+C_i) \quad [4.2]$$

where  $R_i$ = input resistance,  $C_i$ = input capacitance and  $C_f$ = film capacitance.

A second consideration in the size of the sensor is the effect of non active parts of the sensor. The non active parts also add capacitance to the output voltage which can reduce the signal. Therefore the optimum size of sensor is one that is small enough so the whole sensor is excited at the same time, but large enough for the lower cut off frequency to be a suitable level. A sensor size of 1mm in length and 1/2mm in width and 52um thickness, would result in a lower cut off frequency of 2KHz. The material data for the PVDF film is presented in appendix 2.

##### Manufacture of PVDF sensor

One of the problems with the piezo-electric film is the form in which the material is available. Commercially it can be purchased in made up gauges the smallest size of which is 15mm\*30mm or it can be purchased in sheet form. The material is available with two different coatings, either a printed silver ink or a thin vacuum deposited metallization. The question was how to produce the sensor design that was required.

Several different techniques were attempted, the first was to remove some of the silver ink from the larger gauges using an organic solvent. This method produced limited success as gauges were produced but the active areas of the gauges varied between  $2\text{mm}^2$  and  $6\text{mm}^2$ , and therefore a better technique was required as a consistent active area could not be achieved. The second technique that was attempted was to use a sheet of the metalised surface film and to etch off the unwanted metal to produce sensor design, using the same techniques as printed circuit board production. The main concern with this system was that the film could not be heated above  $100^\circ\text{C}$  and therefore the standard method of laminating a board with a photo resist material at  $200^\circ\text{C}$  could not be used. A room temperature spray photo resist was found but this did not seem to adhere properly to the smooth metalised surface. The second problem was that the standard metalised surface was a Nickel/Aluminium mixture and it was not possible to find any etchants that would remove both these materials at the same rate. This method would have worked but it required time in the developing of the correct procedures and materials required.

The best solution to the production of the design of sensor was to get ActoChem the film manufactures to screen print the design on to the film during manufacture. This was done and after four prototype gauges were evaluated two hundred gauges were produced. The design of the sensors can be seen in figure 4.8.

#### Experimental verification of sensor design

The first experiment to evaluate the proposed sensor design was a simple comparison between three piezoelectric gauges. This was to study the effects of length of the gauges on their output to look at the difference of the integration of the waves along the active area. Also a comparison was carried out between the polymer film gauges and a ceramic based piezoelectric sensor. The ceramic based piezoelectric sensor was

included for a comparison with the PVDF sensors but was not considered as a viable sensor due to its 1mm thickness.

Gauges used:

- 1) Ceramic sensor length = 10mm
- 2) Prototype of proposed piezoelectric film sensor design, length = 0.5mm
- 3) Standard piezoelectric film sensor, length = 30mm.

Test conditions

The gauges were mounted in a line next to each other at a distance of 15mm from the impact, the impact energy was 0.3J. All the data was recorded on the oscilloscope and stored on the computer. The responses from the sensors can be seen in fig 4.9.

The results show that the smaller custom sensor produced a low level high frequency response of 1.7  $\mu$ s duration, The ceramic sensor also showed a high frequency response but it lasted for 23  $\mu$ s as the waves travelled along the length of the sensor. The standard sensor showed high level response but no detail of the high frequency components.

This result showed that the custom design of PVDF film sensor could provide data on the high frequency response of a plate due to the passing of stress waves. The size of the sensor was comparable with the smallest available strain gauge and was acceptable for this project. The details of the evaluation of the whole impact system including the sensors was described in the previous chapter.

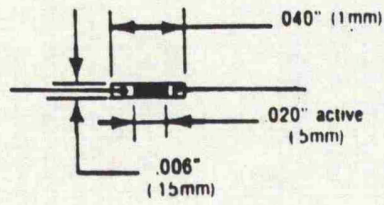


Figure 4.1: Entran ESB-020-500 Semi Conductor Strain Gauge

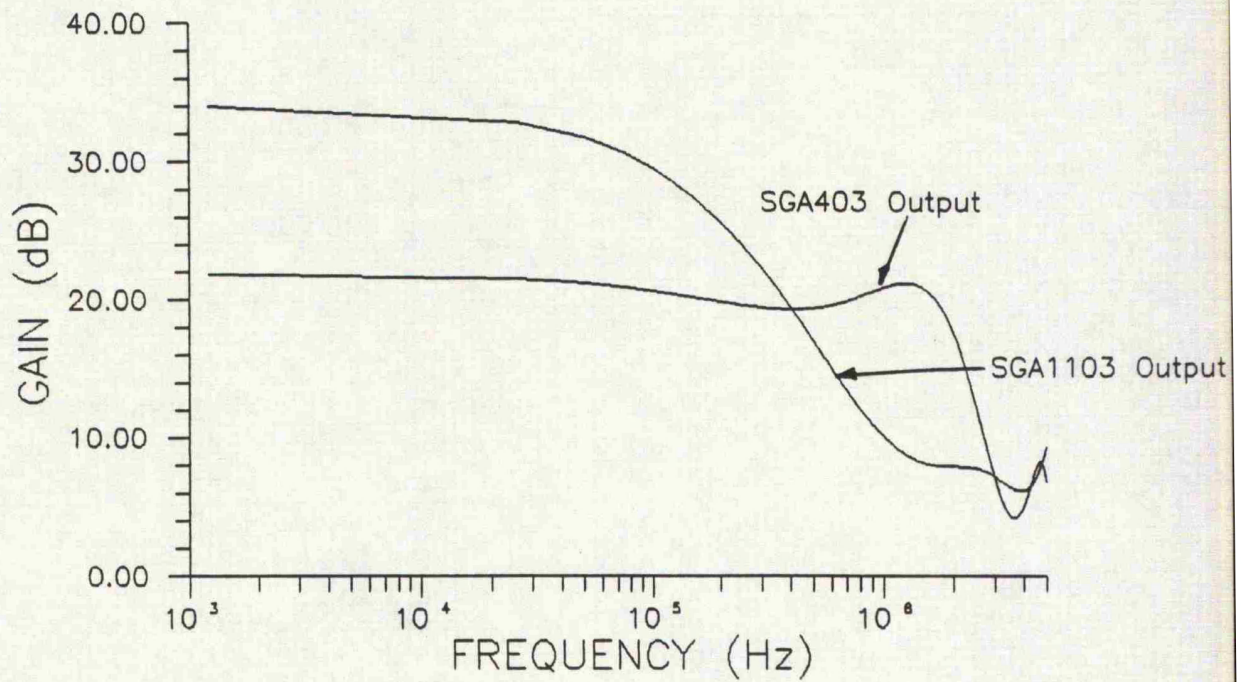


Figure 4.2: Frequency Response of CIL SGA403 Instrumentation Amplifier and CIL SGA1103 Strain Gauge Amplification Board.

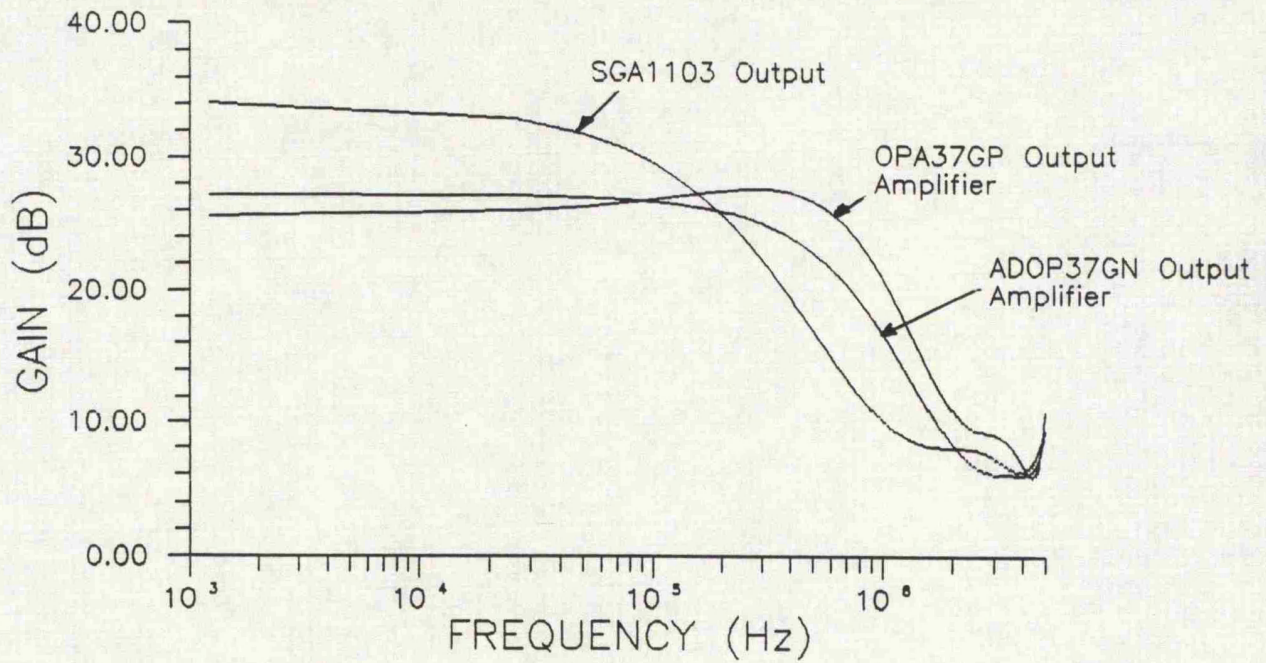


Figure 4.3: Frequency Response of CIL SGA1103 Strain Gauge Amplification Board with Different Output Amplifiers

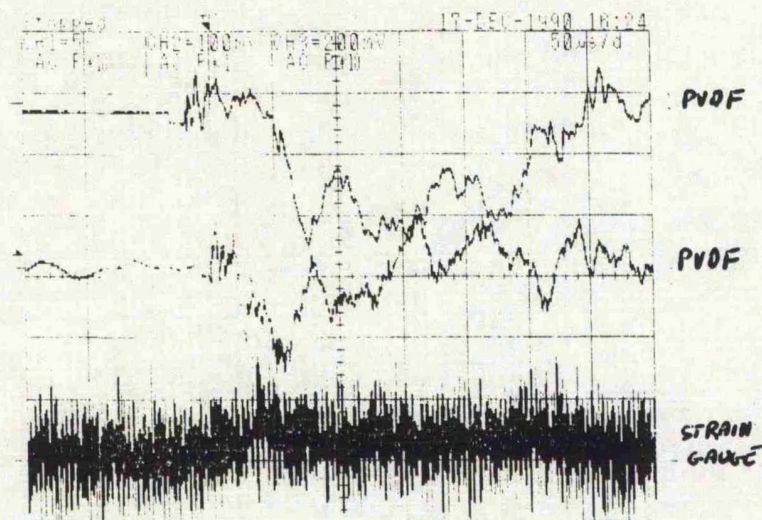


Figure 4.4: Strain Gauge and PVDF Sensor Surface Response from a 12mm Aluminium Plate Subjected to an Impact.

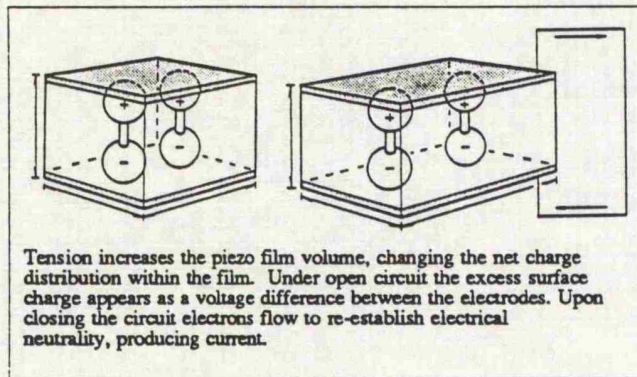


Figure 4.5: PVDF Film Structure, Ref. [69]

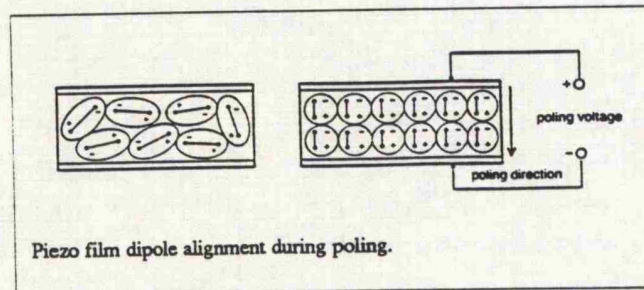


Figure 4.6: PVDF Film Poling, Ref. [69].

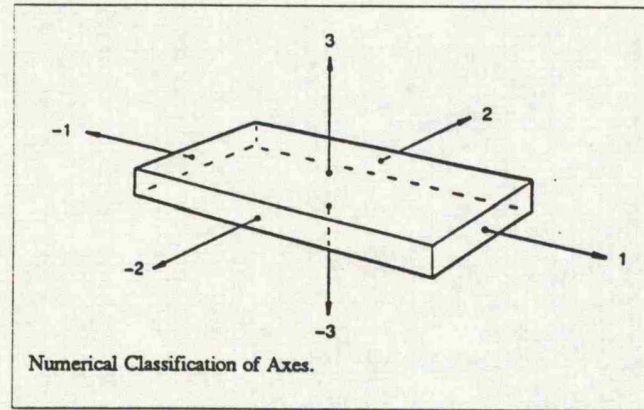


Figure 4.7: PVDF Film Axes

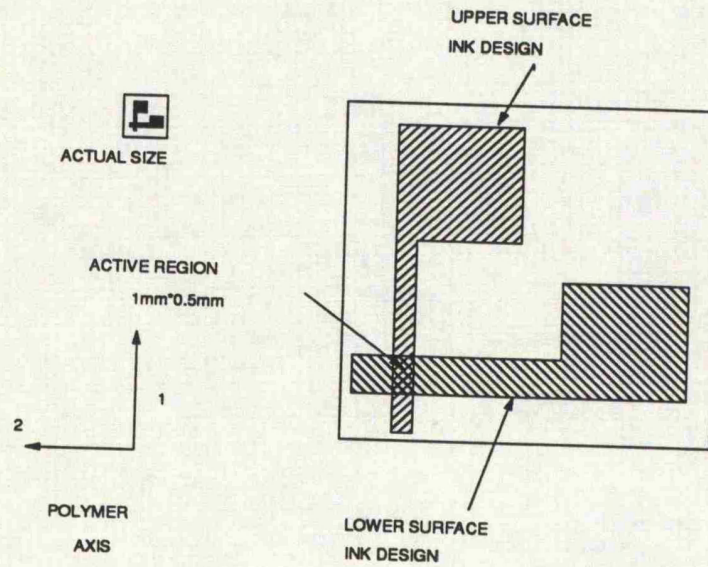


Figure 4.8: PVDF Film Sensor Design.

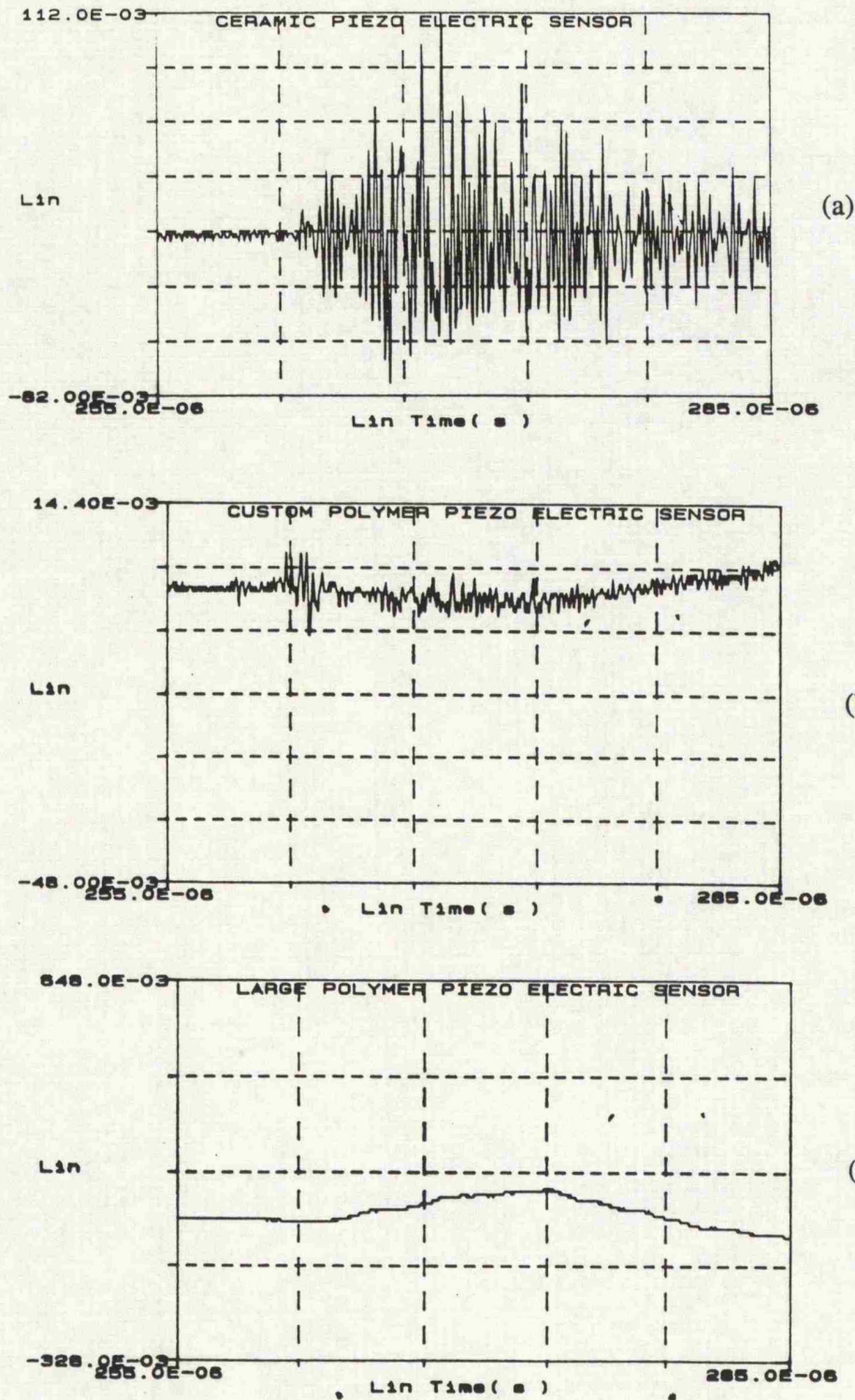


Figure 4.9: Piezo Electric Evaluation Test  
a) Ceramic Piezo Electric Sensor  
b) Prototype PVDF Film Sensor  
c) Standard 30mm PVDF Film Sensor

## Chapter 5: Materials

The main objective of this work was to study experimentally the stress waves propagated through a multi layered plate from a line surface impact. There were two transversely isotropic materials that were used to construct the multi layered plate, the first was a polypropylene polymer reinforced with glass fibre called Plytron manufactured by ICI. The second material was an epoxy resin called LTM22 which was reinforced with T700 carbon fibres, manufactured by Advanced Composite Group (AGC). This chapter details the processing techniques involved in the production of test plates in each material, including the placement of the PVDF sensors on and in the plates.

The model and analytical solution presented in Chapter 2 was for the wave propagation in a 4-ply laminated plate, with the laminate constructed from layers of transversely isotropic material. The material constant input required for analytical solution were the five elastic material wave speeds associated with the transversely isotropic material under investigation. Since any unidirectional composite material could be analysed there was no restriction on the selection of material used to manufacture the 4-ply laminate plates for the comparison between collected experimental data and analytical solution results. This resulted in the main considerations for the selection of the materials being cost, material conductivity and cure temperature.

The material conductivity was important as the PVDF film used as sensors was printed with silver ink on both sides to form the sensor, if the material was conductive insulation would be require to prevent conduction between the sensors and the plate. The cure temperature of the material was important due to the desire to investigate the responses at the laminate interfaces. The sensors were to be placed between the plate layers before the material was cured, this limited the cure temperature of the composite material to 90°C which was the survival temperature of the PVDF film.

The first material that was investigated was Plytron, it fulfilled the requirement of non conductive but possessed a cure temperature of 200°C. The material was donated free of charge by ICI and was used to investigate the surface waves propagating from the line impact. The cure temperature prevented the investigation into the internal shear waves with in the material.

The second experiment investigation was on LTM22/T700. This material possessed a cure cycle of 50°C held for 16 hours. This provided the capability for the placing of the PVDF sensors inbetween the layets of material to investigate the internal shear wave response of the plate. The disadvantage of the material was that the LTM22 toughened epoxy resin was reinforced with carbon fibres which were conductive, which required the PVDF sensors to be insulated to prevented conduction between the fibres and the silver ink and therefore increased the overall thickness of the sensors.

The two materials were manufactured into the cross ply plates containing four layers of the material in a (0/90)<sub>s</sub> configuration.

### 5.1 ICI Plytron

This material was based around a polypropylene matrix with nylon, glass and graphic fibre reinforcement available. The material supplied by ICI was a polypropylene/glass fibre material which apparently possessed similar properties to the ICI thermoset based material APC-2 whose material properties had been used in previous theoretical studies [29]. The material was supplied as a prepreg tape 240mm wide, ply thickness of 0.47mm and a glass content of 35%.

The examination of the short wavelength limiting wave velocities, section 2.7, required that the overall thickness of the plate was sufficient to permit the recording of the high frequency, short wavelength waves propagating from the impact source. The upper

frequency of the plate harmonics in the analytical analysis was defined as  $\omega h/c_l=14$ , where  $\omega$  was the frequency,  $h$  the ply thickness and  $c_l$  is a elastic wave speed calculated as  $c_l = 2040 \text{ ms}^{-1}$ . (The method for calculating the elastic wave speeds is described in section 5.4).. The upper limit of the experimental data capture system was 4MHz, so the layer thickness had to be sufficient so that  $2\pi\omega = 4\text{MHz}$ . This resulted in a layer thickness for the four layer plate in the order of 1mm was required. Since material was supplied with a ply thickness of 0.47mm a eight ply plate was constructed with a ply orientation of (0/0/90/90)<sub>s</sub>. This plate orientation simulated the required a four layer cross-ply plate of (0/90)<sub>s</sub> orientation with the required ply thickness of 0.94mm and an overall thickness of 3.8mm.

#### Plate Manufacture

Plytron required a processing cycle of 30 minutes at 200°C with a 250psi applied pressure, to achieve this a hydraulic press with heated platens was used. To manufacture a plate the eight layers of pre prep were placed in-between steel plates coated in PTFE mould release agent. This sandwich of pre prep and steel was then placed inside a steel window which constrained the edges of the material. There was a clearance of 1/8" between the pre prep and the window to avoid fibre buckling and minimise the resin loss during processing to maintain the fibre volume ratio of the supplied pre prep which had been optimised for strength.

Once the material had cured in the hydraulic press for 30 minutes at 200°C it was cooled with cooling water passing through the platens until the plate could be removed from the mould and trimmed to remove the excess resin. The details of the hydraulic press moulding arrangement can be seen in figure 5.1

#### Sensor Attachment.

The main advantage of using a glass/polypropylene fibre mix was that it was non conductive so the sensors did not require any insulation between themselves and the

plate. To bond the sensors onto the plate a cyanoacrylate adhesive was used as this would produce a thin adhesive layer between the sensor and the plate to minimise any attenuation of the plate response due to the adhesive. The problem with this method was that polypropylene is a difficult material to bond due to its low surface energy, so the plate surfaces were first treated with corona discharge which increased the surface energy to help the adhesive bond. The sensors were connected to the data capture system via ribbon wire which was attached to the sensor with silver paint.

## 5.2 Advance Composite Group LTM22/T700

This material was manufactured by the Advanced composite Group from their toughened epoxy resin LTM22 with T700 carbon fibre reinforcement. This material was selected for its low cure temperature of 50°C which provided the capability of placing the sensors into the plate prior to curing to enable the investigation into the internal shear wave effects. The supplied pre prep contained a fibre content of 58% w/w and with thickness of 0.2mm. To provide the material layers of the required thickness to investigate the short wavelength limiting wave velocities a 16-ply plate was constructed of orientation (0/0/0/0/90/90/90/90)<sub>s</sub>. This plate construction simulated the required four layer plate of cross ply orientation (0/90)<sub>s</sub> with a layer thickness of 0.8mm and a total plate thickness of 3.2mm. A layer thickness of 0.8mm provided an upper frequency limit to the analytical solution ( $\omega h/c_l=14$ ) of  $2\pi\omega=6.15\text{MHz}$  where  $c_l=2209\text{ms}^{-1}$ . This frequency limit was slightly higher than the upper frequency limit of the data capture system but would be compensated for in the post processing of the analytical solution data.

The hot press system that had been used to manufacture the Plytron plates could not be used in the manufacture of this material as the temperature controllers could not provide a stable temperature at 50°C, and the same level of pressure was not required. One recommended manufacturing method was a vacuum bag / oven technique. This method

involved the placing of the assembled prepreg into a vacuum bag where the air between the layers was removed with a vacume and then the bag with the prepreg was placed in an oven to cure. The capability to conduct this form of composite moulding was not available so the necessary materials and skills were developed.

The unidirectional properties of this material were not directly available from the supplier, so once a suitable moulding technique was developed a series of material tests were conducted to evaluate the five elastic constants required for the analytical analysis.

#### Plate Manufacture

There were two suggested manufacturing methods for this material, the first was a vacuum bag / oven cure and the second was a vacuum pressure cure in an autoclave. The initial production trials were completed using the vacuum bag / oven method, figure 5.2. This consisted of a mould base plate with a vacuum outlet on it, a piece of PTFE glass cloth was placed on the base plate with the laid up pre prep on top. Above the prepreg a layer of perforated PTFE bleed film was placed to allow the entrapped air and volatile gases to be extracted from the plate, above this a caul plate was placed to provide a flat upper surface to the plate. Over the whole assembly a piece of breather material was placed to provide a path for the air being removed from the plate, then a piece of vacuum film was placed which was sealed to the mould base. The diagram of the vacuum bag arrangement figure 5.2 shows the specific materials used which were supplied by AeroVac. Once the pre prep was sealed in the bag a vacuum was applied and it was placed in an oven for 16 hours at 50 °C to cure.

The plates produced by this method appeared to have a good surface finish on the bottom, but the surface next to the perforated film contained dimples from the perforations in the release film. When the plate was sectioned after curing it was found to contain a large number of voids due to insufficient air removal during the cure which was unacceptable. After consultation with AGC it was concluded that due to the low

temperature cure of this material it was in a very 'tacky' state at room temperature when the plates were constructed. This resulted in a large amount of entrapped air which the vacuum bag technique was not removing. It was decided that to remove all the entrapped air a vacuum/pressure cure was required, where a positive pressure is applied to the vacuum bag to squeeze out any remaining air.

A simple autoclave was designed and manufactured which contained heating elements in the base and could withstand a pressure of 90psi. The cross section of the autoclave can be seen in figure 5.3 along with the vacuum bag material. A change was made to the initial vacuum bag lay up with the introduction of a second piece of PTFE glass cloth between the caul plate and the upper surface of the pre preg. This was to provide a better surface finish on the upper surface but restricted the bleeding of the air from the plate to along the edges only. The use of the positive pressure on the plate improved the plates, which were found to be void free when sectioned after manufacture.

Once this manufacturing technique was established a set of uni directional plates was manufactured to measure the elastic properties of the material. Details of this are presented in Appendix 3.

#### Embedding Sensors into the Plate

The capability of embedding these sensors into the plate also presented the problem of how to insulate the sensors from the conductive carbon reinforcement fibres. The sensors required an insulation film between themselves and the plate. The main consideration for the insulation was the effect of increasing the thickness of the sensor, which would lead to greater disruption of the plate. A second consideration was that the lead out wires from the sensors would also have to be insulated and be as small as possible.

The first attempt at insulating the sensors was to apply an epoxy resin coating to the sensors, the resin used was Araldite 820 resin system. The resin was mixed to a ratio of

1:1 by weight of PZ820 resin and HZ820 hardener along with 1 part Toluene which acted as a solvent to assist with application. The resin was brushed onto the gauges and allowed to cure of 1 hour at 60°C.

Leads were made for the sensors from 36 SWG enamel coated copper wire with one end of the wire coiled and stripped of the enamel and flattened, this was then joined to the tabs on the sensor with silver paint before the sensors were coated.

This method was not successful for two reasons. The connection between the leads and the sensors was mechanically very weak and sometimes came apart when the sensors were handled. The second problem was that when trials were conducted with embedding the sensors into a plate, the carbon fibres managed to break through the resin coating and contacting the sensors.

A second method of insulating the sensors was with the use of a high temperature polymer tape called 'Mylar' tape, which could survive up to 200°C. The tape was applied to both sides of the sensor, including the connection tabs to provide extra mechanical strength to the lead connection. This application of the insulating tape resulted in a sensor with an overall thickness of 300µm. Figures 5.4 and 5.5 show a cross section through a plate with sensors embedded at the mid plane of the plate and on one surface. The sensor at the mid plane of the plate provides an increase of 18.75% in each of the two mid plane material layers, where the original thickness of each layer was 0.8mm. This increase has provided the visible disturbance in the layer fibres but this disturbance appears to be a gradual deflection in the fibres rather than a sudden discontinuity in the material layer. The sensor on the surface provides a 37% increase in the layer thickness and again provides a visible disturbance to the fibres in the outer layers, but as a gradual change in the fibre direction. The overall effect of a two sensors placed in a plate would be a total addition of 18.75% extra material in the cross section of the plate through the sensors. The total effect of three sensors would be an extra 28.1% material.

The processing of the plate with the prepreg material sandwich between the mould base and the caul plate combined with the application of positive pressure resulted in there being no overall change in thickness where the sensors were placed in the plate. It was therefore concluded that in the layers above and below the sensors the resin was displaced to provide a higher fibre volume ratio. In order to minimise this effect in the plates the number of sensors placed on or in a plate was restricted to two, which could provide comparisons between the upper and lower surface responses of the plate or between the upper surface and the mid plane plate responses.

### 5.3 Elastic Wave Speeds

For the analytical solution of the dispersion equation [Chapter 2] the five anisotropic elastic constants are required for the uni directional material. The analytical solution requires the elastic constants in the form of the elastic wave speeds  $c_1, c_2, c_3, c_4, c_5$ . These elastic wave speeds equate to the anisotropic elastic constants  $E_{11}, E_{22}, \nu_{12}, \nu_{23}$  and  $G_{12}$ , where the 1 direction is along the fibres and the 2 and 3 directions are perpendicular to the fibres.

In Section 2.2 the elastic wave speeds were defined in terms of the Lamé constants and material density which were related to the components of the symmetric 6x6 stiffness matrix  $C_{pq}$ , equation [2.4].

$$\begin{aligned}
 C_{11} &= C_{22} = \lambda + 2\mu_T = \rho c_1^2 \\
 C_{33} &= \lambda + 4\mu_L - 2\mu_T + 2\alpha + \beta = \rho c_5^2 \\
 C_{44} &= C_{55} = \mu_L = \rho c_3^2 \\
 C_{66} &= \frac{1}{2}(C_{11} - C_{12}) = \mu_T = \rho c_2^2 \\
 C_{12} &= \lambda \\
 C_{13} &= \lambda + \alpha = \rho c_4^2
 \end{aligned}$$

In the same way the components of the 6x6 stiffness matrix  $C_{pq}$  can be defined in terms of the engineering elastic constants

$$\begin{aligned}
 C_{11} &= C_{22} = \frac{E_{22}}{(1 - \nu_{12}\nu_{21})} = \rho c_1^2 \\
 C_{33} &= \frac{E_{11}}{(1 - \nu_{21}\nu_{12})} = \rho c_5^2 \\
 C_{44} &= C_{55} = G_{12} = \rho c_3^2 \\
 C_{66} &= G_{23} = \rho c_2^2 \\
 C_{13} &= \frac{\nu_{12}E_{11}}{(1 - \nu_{12}\nu_{21})} = \rho c_4^2
 \end{aligned} \tag{5.1}$$

Since

$$\begin{aligned}
 \frac{\nu_{12}}{\nu_{21}} &= \frac{E_{11}}{E_{22}} \\
 G_{23} &= \frac{E_{22}}{2(1 + \nu_{23})}
 \end{aligned} \tag{5.2}$$

the five elastic wave speeds could be derived from the the five engineering constants  $E_{11}$ ,  $E_{22}$ ,  $\nu_{12}$ ,  $\nu_{23}$  and  $G_{12}$  which could easily be measured from specimen testing of the material.

For the Plytron material the material properties were supplied by ICI and were verified by Soutis and Turkman [65] and are recorded in Table 5.1.

The ACG LTM22/T700 material was not provided with the relevant data for the specific material mix so a testing program was completed to measure the elastic properties, full details in appendix 2. The measured material properties are recorded in Table 5.1 along with the calculated wave speeds.

#### Limiting Wave Velocities

The limiting wave velocity in a cross ply plate was the slower of the two wave speeds, the Rayleigh type surface wave speed ( $v_R$ ) and an internal shear wave speed ( $v_S$ ) which were dependent on the angle of wave propagation  $\gamma$ . In section 2.6 it was shown that for a critical angle of propagation  $\gamma_c$ , when  $\gamma < \gamma_c$  the limiting wave velocity would be  $v_R$  and for values of  $\gamma > \gamma_c$  the limiting wave velocity would be  $v_S$ . The speeds of these waves can be derived from equations [2.67, 2.68, 2.69] and the critical angle of propagation  $\gamma_c$  from equation [2.70].

The calculated wave speeds for each material and condition are recorded in tables 5.1 and 5.3. The values of the critical angle  $\gamma_c$  are recorded in table 5.4.

	Elastic Constants					Elastic Wave Speeds ( $\text{mm}\mu\text{s}^{-1}$ )				
	$E_{11}$ (GPa)	$E_{22}$ (GPa)	$\nu_{12}$	$\nu_{23}$	$G_{12}$ (GPa)	$c_1$	$c_2$	$c_3$	$c_4$	$c_5$
Plytron	28	3.4	0.4	0.63	1.39	2.043	0.839	0.969	1.665	4.590
LTM22/ T700	88.9	3.8	0.29	0.67	4.32	2.210	0.889	1.726	1.546	7.919

Table 5.1: Material Constants

	Density ( $\text{Kg}\text{m}^{-3}$ )
Plytron	$1.48 \times 10^3$
LTM22/T700	$1.45 \times 10^3$

Table 5.2: Material Density

	$v_R$ when $\gamma = 0^\circ$ ( $\text{mm}\mu\text{s}^{-1}$ )
Plytron	0.792
LTM22/T700	0.838

Table 5.3: Material Rayleigh Type Surface Wave Speeds.

	$\gamma_c$
Plytron	$46.14^\circ$
LTM22/T700	$46.16^\circ$

Table 5.4: Critical Angle of Wave Propagation

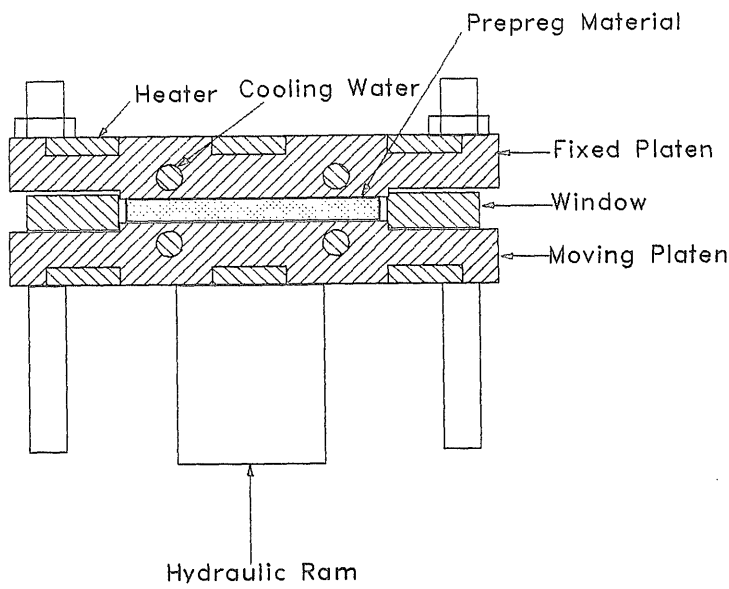
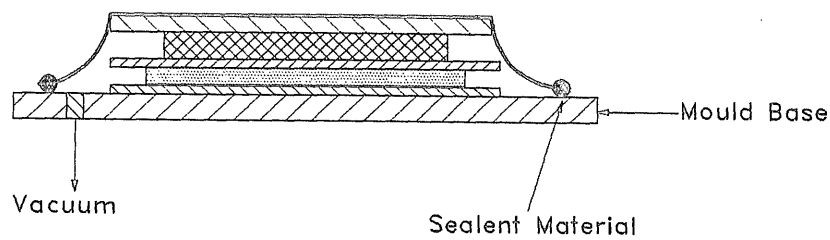


Figure 5.1: Hydraulic Press Arrangement for ICI Plytron Manufacture

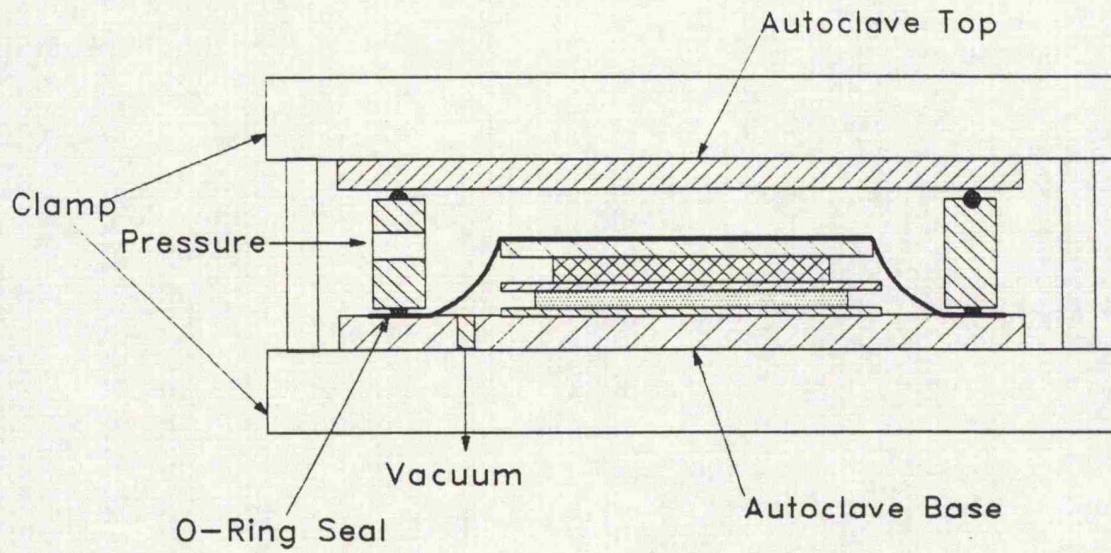


Vacuum Bag Material Key

-  Vacuum Film
-  Breather Cloth
-  Steel Caul Plate
-  P3 Release Film
-  Prepreg Material
-  PTFE Glass Cloth
-  Sealant

- AeroVac Reference
- CAPRAN 996
- AIRBLEED 10
- A5000 FEP
- FF/06/A
- SM5 126-2

Figure 5.2: Vacuum Bag Arrangement for AGC LTM22/T700 Manufacture



Vacuum bag materials are the same as in figure 5.2

Figure 5.3: Autoclave Arrangement for AGC LTM22/T700 Manufacture

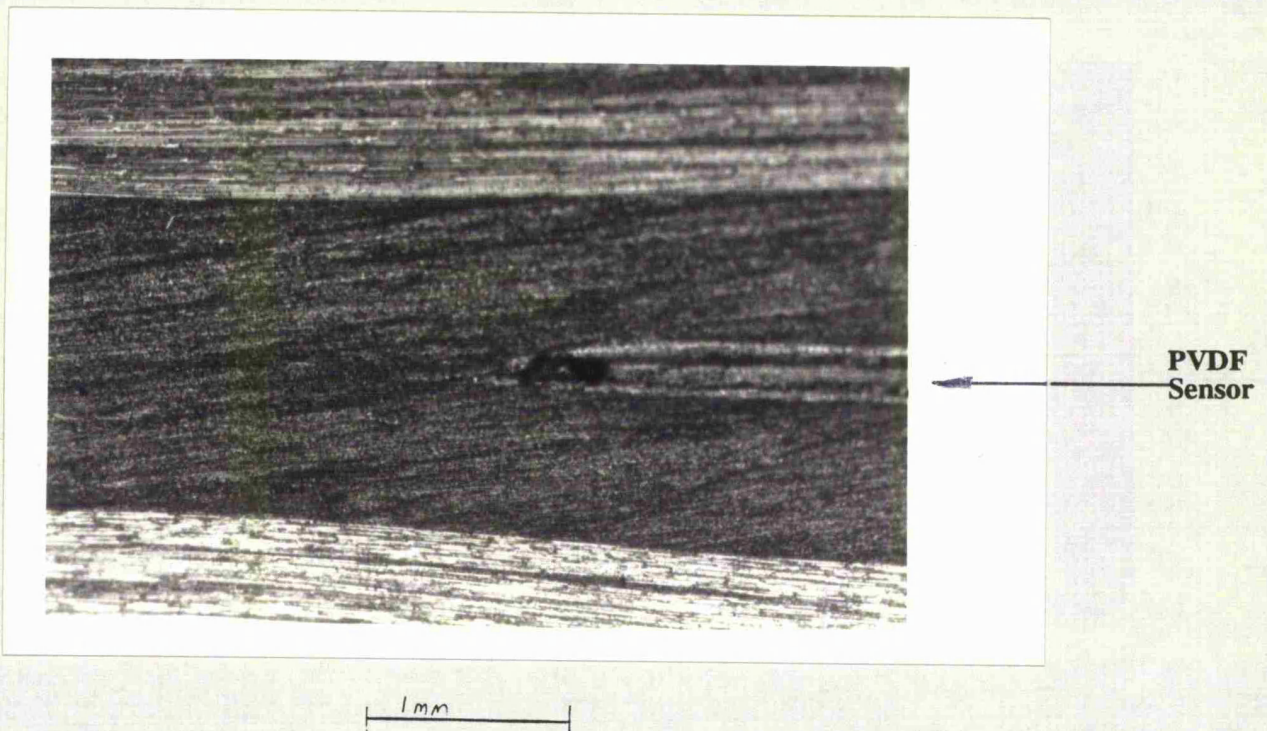


Figure 5.4: Mid Plane Sensor in LTM22/T700 Material

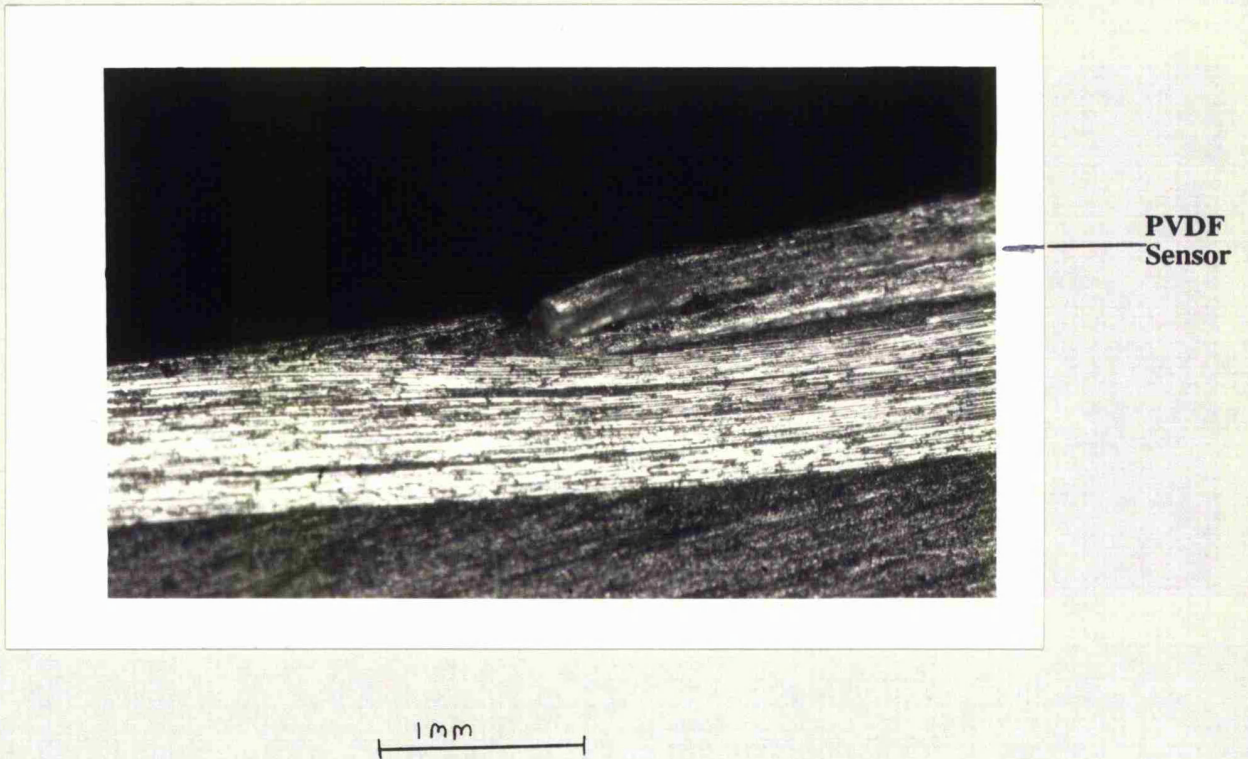


Figure 5.5: Surface Sensor in LTM22/T700 Material

## Chapter 6: Surface Wave Propagation in a Cross Ply Composite Plate

The initial investigation into wave propagation in a multi layered plate was conducted on the Polypropylene/glass fibre material Plytron which was donated by ICI. The details of this material were described in the previous chapter. This investigation was restricted to the study of surface wave propagation. Since the PVDF sensors cannot withstand the 200°C Plytron cure temperature, it was not possible to place any sensors at the laminate interfaces. However an advantage of using Plytron was that it was a composite of non conductive materials so no further insulation of the sensors was required.

The experimental study was to investigate the effect of the angle of wave propagation ( $\gamma$ ) on the surface responses of the plate. There were two conditions that were investigated, the first was when  $\gamma = 0^\circ$ , the direction of wave propagation was parallel to the fibre direction in the inner layers. The second was when  $\gamma = 90^\circ$ , the direction of wave propagation was perpendicular to the fibres in the inner layer.

The analytical solution presented in chapter 2 had shown that the limiting wave velocity was the smaller velocity of two waves, the Rayleigh type surface wave in the upper layer  $v_R$  and a internal shear wave  $v_S$ . It was calculated from equations [2.70] in chapter 2 that the speeds of these waves were equal for Plytron when the angle of propagation  $\gamma = 46.14^\circ$ . Therefore when  $\gamma < 46.14^\circ$  the limiting wave velocity would be the Rayleigh type surface wave velocity ( $v_R$ ) in the upper layer and when  $\gamma > 46.14^\circ$  the limiting wave velocity would be the internal shear wave velocity ( $v_S$ ).

For the condition  $\gamma = 0^\circ$  the lowest wave speed would be  $v_R$ , the Rayleigh type surface wave speed which would be present on the upper surface of the plate. For the second condition of  $\gamma = 90^\circ$  the limiting wave speed would be  $v_S$  the internal shear wave speed. In this case the greatest disturbances should be at the mid plane of the plate with a smaller upper surface response than the  $\gamma = 0^\circ$  case.

A full list of the theoretical wave speeds can be seen in Table 6.1. The details of the derivation of the wave speeds from the engineering material constants was reported in chapter 5.

In the comparison between the analytical and experimental results there were two main features for consideration.

- i) The presence of a Rayleigh type surface wave on the upper impact surface when  $\gamma = 0^\circ$  and the absence of any similar disturbances when  $\gamma=90^\circ$ .
- ii) If a Rayleigh type surface wave is present the speed of this wave should match the theoretically derived wave speed in Table 6.1.

### 6.1 Analytical Solution to Dispersion Equation

Using the techniques described in Chapter 2 the symmetric and antisymmetric forms of the dispersion equation [Equ. 2.56] were solved up to a value  $\omega h/c_1 = 14$ . This equation was solved for the two conditions under consideration of  $\gamma = 0^\circ$  and  $\gamma = 90^\circ$ .

Figure 6.1a shows the dispersion curves for antisymmetric motion for  $\gamma=0^\circ$  and figure 6.1b shows the corresponding curves for the symmetric motion. Similarly, figures 6.2a and 6.2b show the dispersion curves when  $\gamma=90^\circ$  for the antisymmetric and symmetric motion respectively.

The dispersion curves for both values of angle  $\gamma$  examined have the striking feature of three distinct ghost lines brought about by the osculation of the branches which are related to the material wave speeds. As the dispersion curves approach the first ghost line from the left they exhibit the plateau and step phenomenon which has been described by Redwood [67]. Along the plateau the curves are parallel to the ghost line, with a constant phase velocity at the value given by the slope of the ghost line. On the steps the phase velocity exhibits a small but sudden drop either ending up on the next plateau, if to the left

of the ghost line, or passing through and moving rapidly to the next ghost line. On crossing the last ghost line they tend to the lowest stress wave velocity  $c_2$  (shear) which in the  $\gamma=90^\circ$  case is the limiting wave velocity of the fundamental mode. In the  $\gamma=0^\circ$  case the fundamental mode matched a Rayleigh type surface wave velocity. This curve diverges from the direction the curves tend to which is the lowest stress wave velocity  $c_2$  (shear) for this case.

As explained in section 2.4, the analytical solution derived the plane strains caused by the passing of the stress waves at a point remote from the point of impact. For comparison with the experimental results the solution was calculated for a distance of  $15h$  away from the point of impact, where  $h$  is a ply thickness.

The derived strains are presented and discussed in section 6.3 along with the experimental results.

## 6.2 Experimental Study

To examine the conditions  $\gamma = 0^\circ$  and  $\gamma = 90^\circ$ , there were two separate plates manufactured and the PVDF sensors were bonded onto the plate surfaces at a distance of 15mm away from the point of impact.

The testing procedure was previously described in chapter 3. The plates were set up with a distance between the plate and the striker of 0.5mm, with a gun pressure of 45bar which provided a pellet velocity of  $120 \text{ ms}^{-1}$ . This provided an impact energy onto the plate of 0.4J. To verify that this impact energy did not cause damage to the material a dummy plate with no sensors was impacted and X-rayed to examine for internal damage. There was no damage detected with the X-ray so it was assumed that the plate was only experiencing elastic response and could be used for successive tests.

For each test the speed of the pellet was monitored to verify consistent impact energy on the plate. The data recording system was triggered by a PVDF sensor which was mounted on the striker so the sensor response was measured from a time before the plate was impacted for a total duration of 1ms. The data was collected at a sampling frequency of 20MHz and was stored on the computer for further post processing with PAFEC Spiders digital signal processing software. Each test was repeated three times to examine the consistency of results.

Figure 6.3 shows the raw data response from a  $\gamma=0^\circ$  plate at a distance 15mm away from the point of impact. The plot shows the measured potential change of the sensor against a time duration of 50 $\mu$ s from the point of impact. This plot shows dominant low frequency response of the plate and is of a similar shape to the responses detected by Daniel and Wooh [1.47], Mortimer et al [1.4] and Takeda et al [1.41] from surface mounted strain gauges on impacted composite plates. This showed that the responses detected by the PVDF sensors on the composite plate were of the same nature as had been detected by strain gauges in previous work, but that filtering was required to extract the specific stress wave responses of the plate.

#### Analysis of Experimental Results

In section 2.4 the analytical solution had shown that the duration of the impact affected the overall response of the plate. Green [47] has shown that the longer the impulse duration the more dominant the low frequency part of the impulse spectra becomes. This was in agreement with the system evaluation tests conducted of steel in Section 3.6, where the filtering out of the low frequency response from the experimental data resulted in the higher frequency stress wave disturbances becoming more visible.

The same filtering techniques were applied to this experimental data to extract the high frequency stress wave disturbances from the experimental data for comparison to the analytical results. The effect of this filtering was to examine the motion associated with

the short wavelength waves travelling through the plate but remove and long wavelength waves (Lamb waves) from the response. In the application of filters to the raw data care was required since the Rayleigh type surface wave is a result of the interaction of the stress waves travelling through the material. It was important that a broad band filter was used to remove the low frequency components of the response but to retain the high frequency components in the data.

The filter applied to the data was a 10th order rectangular Butterworth band pass filter with a lower frequency limit  $f_l = 200\text{kHz}$  and an upper frequency limit of  $f_u = 3\text{MHz}$ , Fig. 6.4. The application of this filter was completed on the raw test data using the PAFEC spiders digital signal processing package. The filter was applied in the frequency domain by transforming the raw time domain data into the frequency domain via a Fast Fourier Transform (FFT). The filter was applied to remove the spectra above and below the limits and then an inverse FFT was applied to return the data to the time domain. The theoretical form of the filter is presented in appendix 4.

To provide a valid comparison between the analytical results and the experimental results the analytical results were subjected to the same filters as the experimental results. This was to demonstrate that the use of these filters had no adverse affect on the characteristics of the analytical response data and therefore would not remove important information from the experimental data.

### 6.3 Analytical Results

#### Case 1, $\gamma = 0^\circ$

Figure 6.5 shows the analytical results for the upper and lower surface responses at a distance of 15mm from the point of impact. Figure 6.5a shows the plane strain response in the direction of wave propagation for the upper surface of the plate. This shows clearly a

large response with a peak to peak magnitude of 500 on the plate occurring 19  $\mu\text{s}$  after the impact onto the plate. The velocity of this wave is  $0.79\text{mm}\mu\text{s}^{-1}$ . Figure 6.5b shows the comparable lower surface response from which any large response is absent. The presence of the large disturbance on the upper surface which is absent from the lower surface indicated that this upper surface response is a Rayleigh type surface wave. The velocity of this disturbance matches the calculated Rayleigh wave velocity in Table 6.1. This agrees with the theory that the limiting wave velocity when the angle of wave propagation  $\gamma=0^\circ$  would be the velocity of a Rayleigh type surface wave.

#### Case 2, $\gamma = 90^\circ$

Figure 6.6 shows the analytical results for the upper and lower responses of a plate at a distance of 15mm from the point of a delta function impact. Figure 6.6a shows the upper surface plane strain in the direction of the wave propagation, and Figure 6.6b shows the comparable lower surface response. The surface responses for this condition show the complete absence of any large response when compared with the  $\gamma=0^\circ$  condition, with only very small responses occurring at  $10\mu\text{s}^{-1}$  after the impact. This again agrees with the theory that when  $\gamma > 46.14^\circ$  the limiting wave velocity would be that of the  $c_2$  (shear) wave occurring at the mid plane of the plate.

#### 6.4 Experimental Results

Figure 6.7 shows the surface responses of the PVDF sensors mounted on a  $\gamma = 0^\circ$  plate at a distance of 15mm from the point of impact, for an impact energy of 0.4J. The figures show the change of the potential of the sensor detected by data capture system plotted against time starting from the point of impact. In figure 6.7a, which shows the upper surface response, a visible large response is occurring inbetween 18 $\mu\text{s}$  and 20 $\mu\text{s}$  from the striker impact. The average velocity of these responses can be measured at  $v=8.0\text{mm}\mu\text{s}^{-1}$ . The lower surface responses in figure 6.7b shows a complete absence of responses which are comparable with the magnitude of the upper surface response.

Figure 6.8, shows the surface responses of a second plate when  $\gamma = 90^\circ$  at a distance of 15mm from the point of impact, for a impact energy of 0.4J. The upper and lower surfaces show a complete absence of significant disturbances when compared with the previous tests of  $\gamma=0^\circ$ .

#### 6.5 Comparison of Experimental and Analytical Results

The analytical results in figure 6.5 for the  $\gamma = 0^\circ$  condition show clearly the presence of a Rayleigh type surface wave based on the velocity of the detected response and the absence of a comparable lower surface response. The equivalent experimental results in figures 6.7-6.9 show a very similar result with a large upper surface response travelling at  $0.8\text{mm}\mu\text{s}^{-1}$ , which is absent from the lower surface. This resemblance between the analytical results and the experimental lead to two important conclusions at this stage of the work. The first conclusion was that the responses detected in the experimental testing were Rayleigh type surface waves due to their wave velocities and presence only on the upper surface. This showed that the experimental system that had been developed was capable of detecting the presence or absence of the responses in a composite plate which were caused by the passage of stress waves in the plate. This also demonstrated that the results from the experimental impact system with the use of digital filtering could be directly compared with the analytical results from an ideal delta function line impulse on a plate. The second conclusion was that this provided initial experimental evidence to validate the theory which predicted that when  $\gamma < 46.14^\circ$  is the limiting wave velocity for this plate was the velocity of a Rayleigh type surface wave.

The second case examined of  $\gamma = 90^\circ$  showed agreement between the analytical and experimental results in that there was no particularly significant responses compared with the  $\gamma = 0^\circ$  case. This again agreed with the theory which predicted that when  $\gamma > 46.14^\circ$  the

limiting wave velocity would that of an internal shear wave, so there would not be a large Rayleigh type of surface wave present on the upper surface.

These results clearly showed the presence or absence of a Rayleigh type surface wave and showed very good agreement between the analytical results and the experimentally recorded data. They did not present any clear resolution of the individual stress waves which are associated with the ghost lines present in the dispersion curves. It was concluded that this was partly due to the responses being measured at a distance of only  $15h$  where  $h$  is the layer thickness away from the point of interest, which was only 4.25 times the total plate thickness. This did not provide sufficient distance for the different waves to separate due to their separate speeds which prevented observation of the separate shear wave. A second limitation to the resolution of the separate waves in the experimental results could be due to the attenuation of the plate response due to the presence of a layer of adhesive between the sensors and the surfaces of the plates.

In order to validate further the theoretical model, it was necessary to examine the internal response when  $\gamma > 46.14^\circ$ . According to the theory, the core layers should show a larger disturbance than the surfaces due to the limiting wave velocity being an internal shear wave speed. As mentioned earlier this could not be considered for the Plytron material, but a second material, LTM22/T700, was chosen with a low curing temperature to permit the placing of sensors in the core layers. The results for this material are reported in the next chapter.

Elastic Waves	Wave Speed ( $\text{mm}\mu\text{s}^{-1}$ )	Time travel to 15mm ( $\mu\text{s}$ )
$c_1$	2.04	7.34
$c_2$	0.84	17.87
$c_3$	0.97	15.48
$c_4$	1.66	9.0
$c_5$	4.59	3.26
$v_R$ ( $\gamma = 0^\circ$ )	0.792	18.94

Table 6.1: Theoretical wave Speeds For ICI Plytron Material.

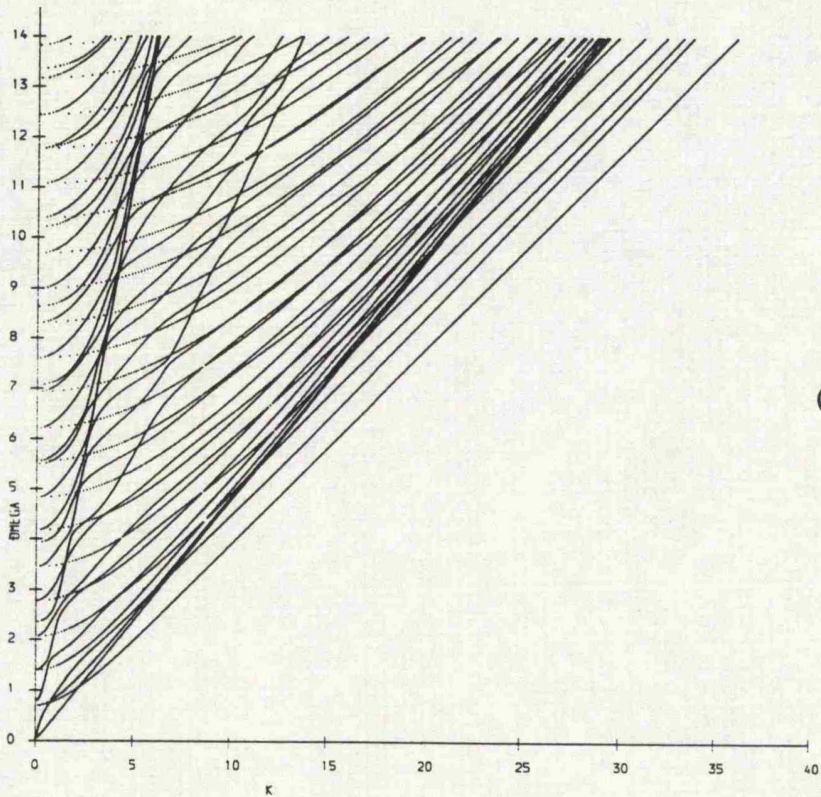
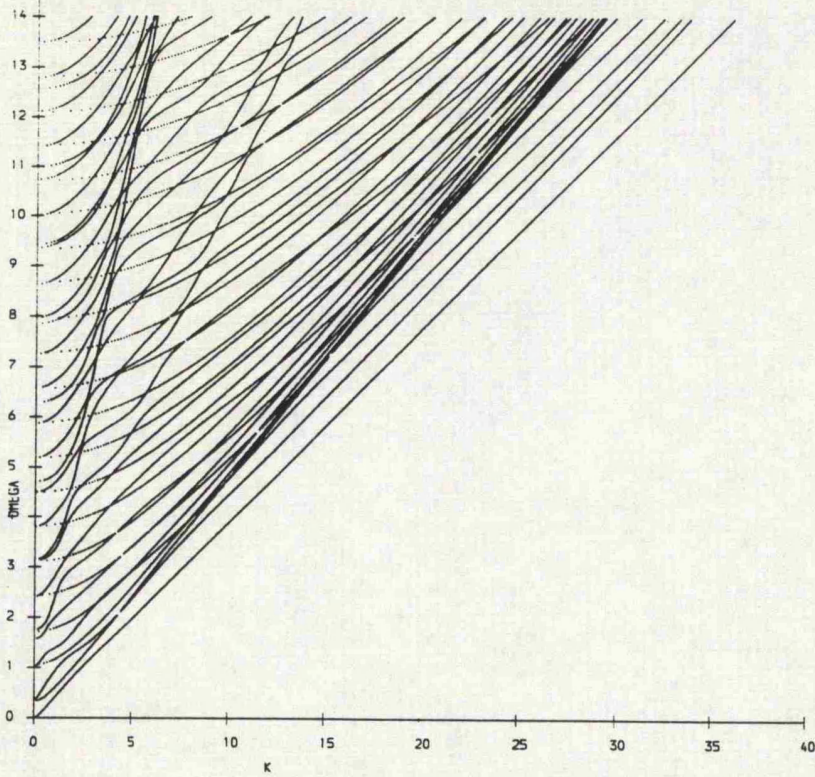


Figure 6.1: ICI Plytron Cross Ply Plate  
Dispersion curves  $\gamma=0^\circ$   
a) Antisymmetric Motion  
b) Symmetric Motion

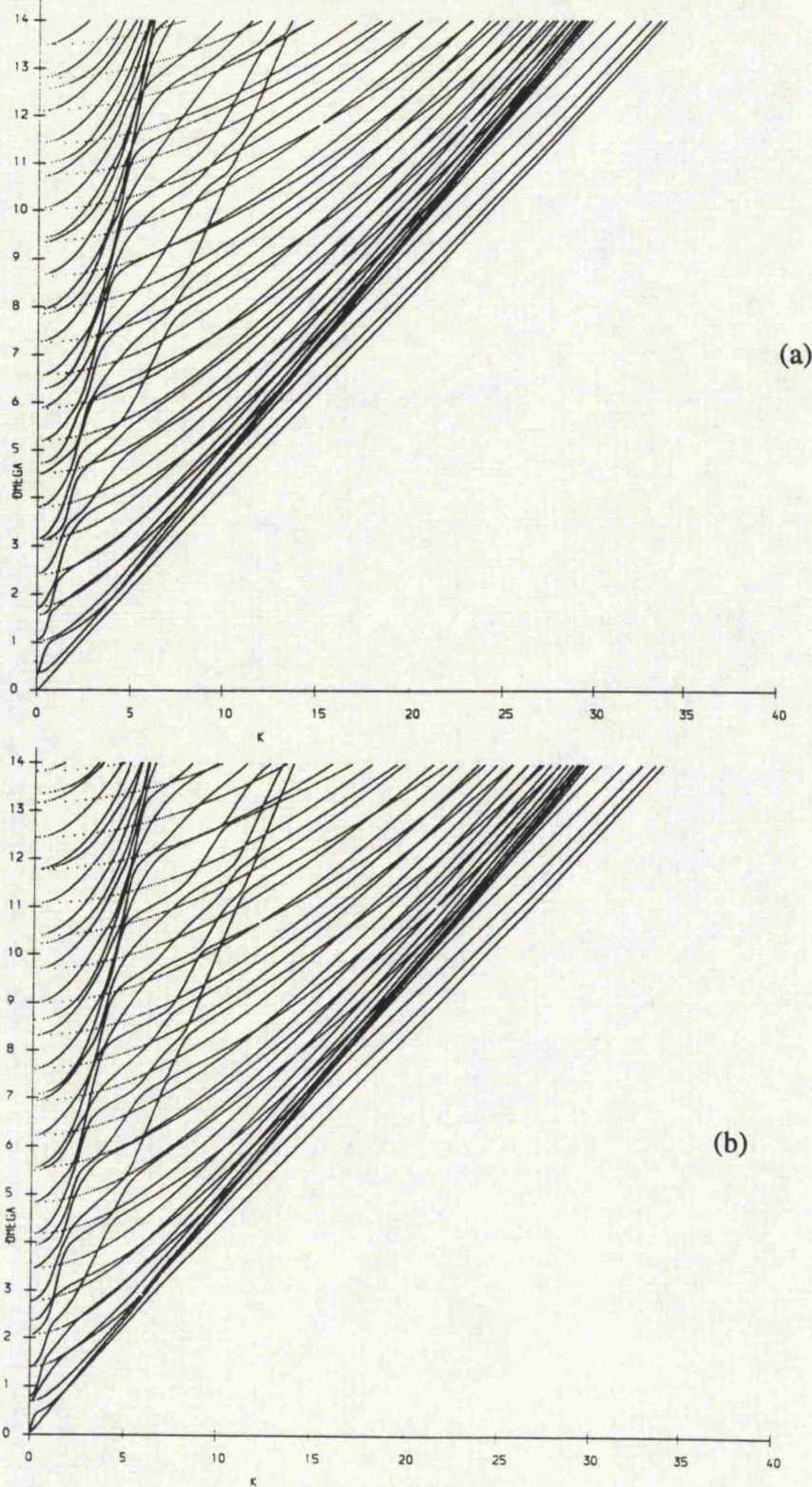


Figure 6.2: ICI Plytron Cross Ply Plate  
Dispersion curves  $\gamma=90^\circ$   
a) Antisymmetric Motion  
b) Symmetric Motion

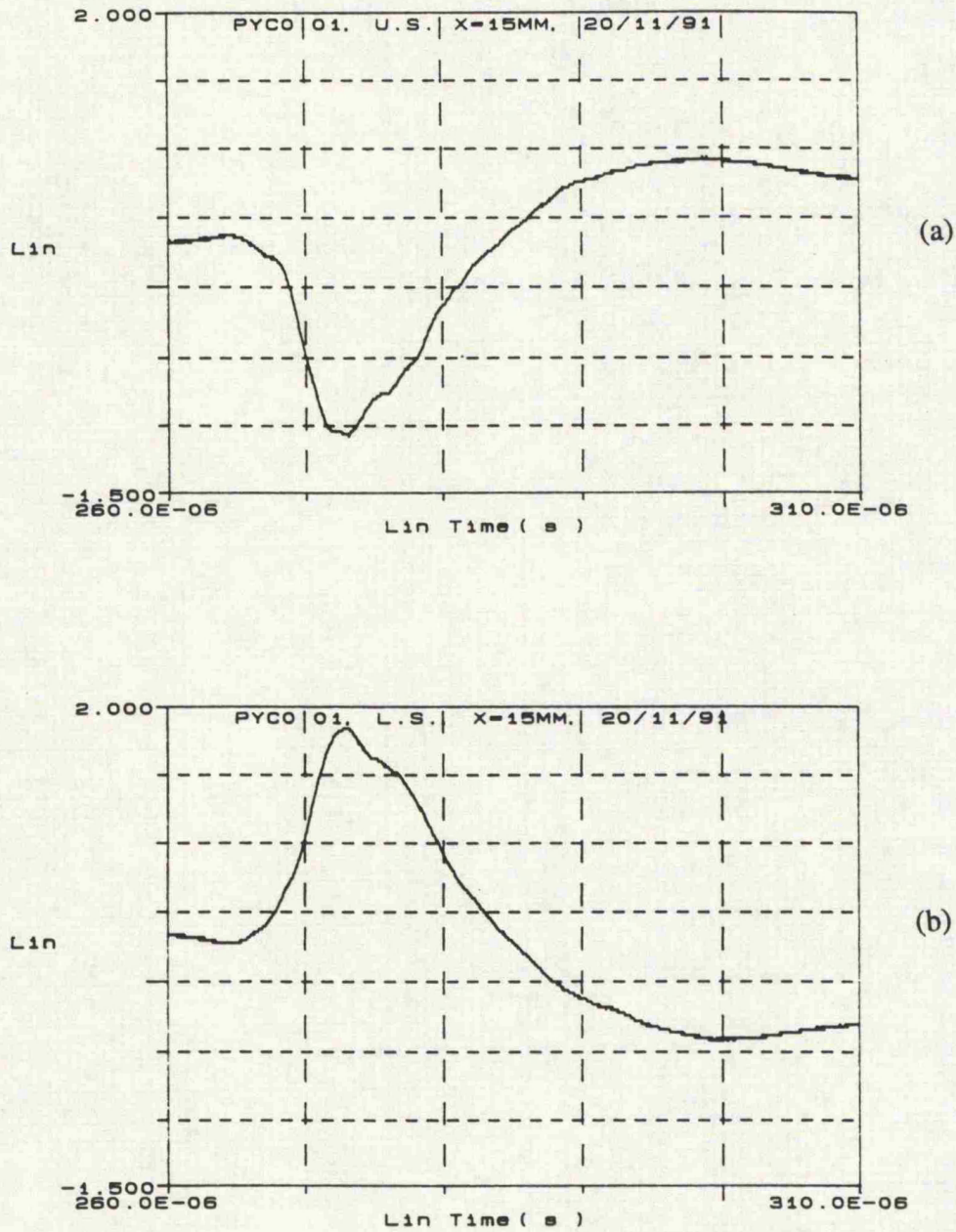


Figure 6.3: ICI Plytron Cross Ply Plate,  $\gamma=0^\circ$   
Experimental Response to Surface Line Impact  
a) Upper surface, 15mm from Impact  
b) Lower surface, 15mm from Impact

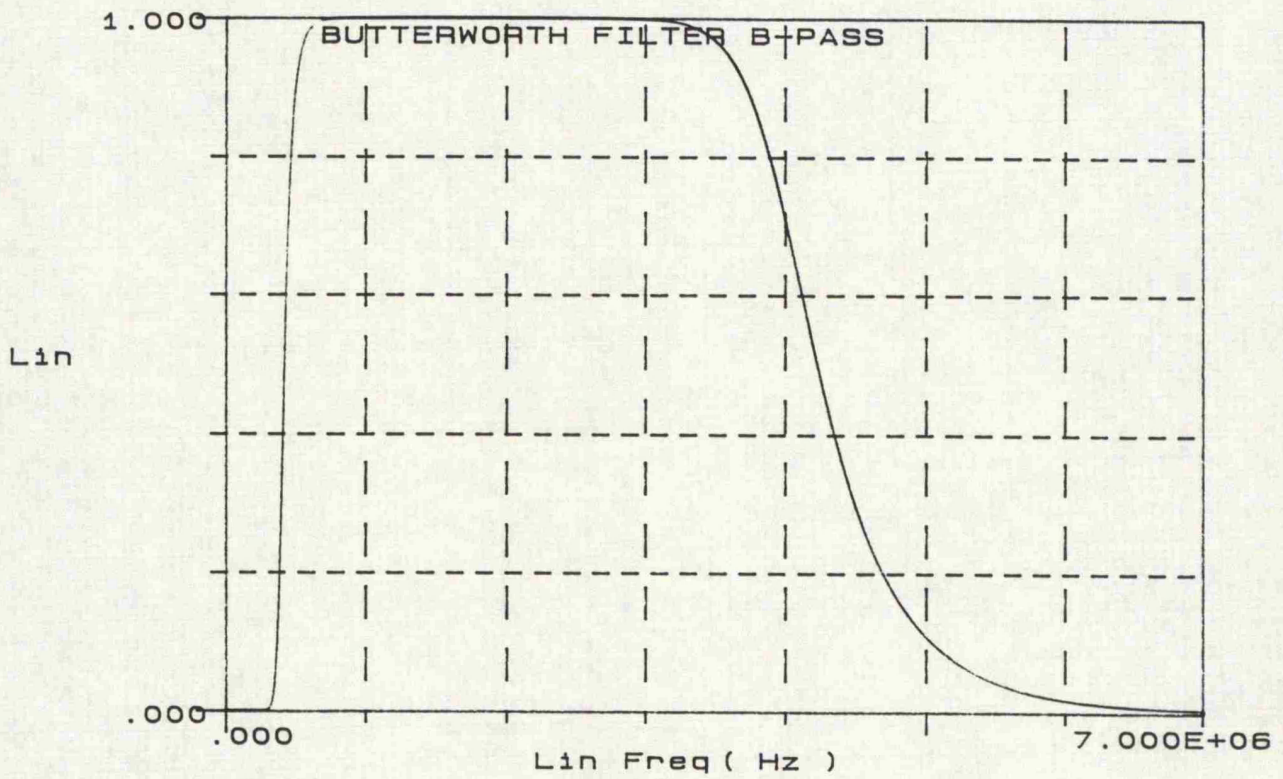


Figure 6.4: 10th Order Butterworth Bandpass Filter  
0.2MHz-4MHz

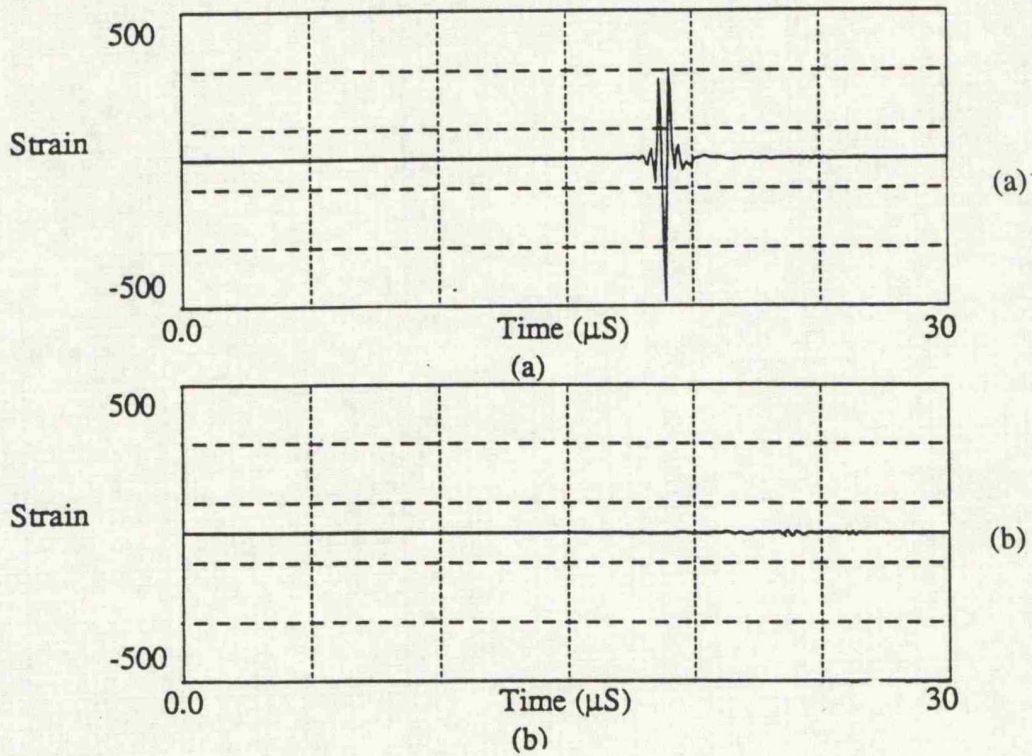


Figure 6.5: ICI Plytron Cross Ply Plate,  $\gamma=0^\circ$   
 Filtered Analytical Response to Surface Line Impact  
 a) Upper surface, 15mm from Impact  
 b) Lower surface, 15mm from Impact

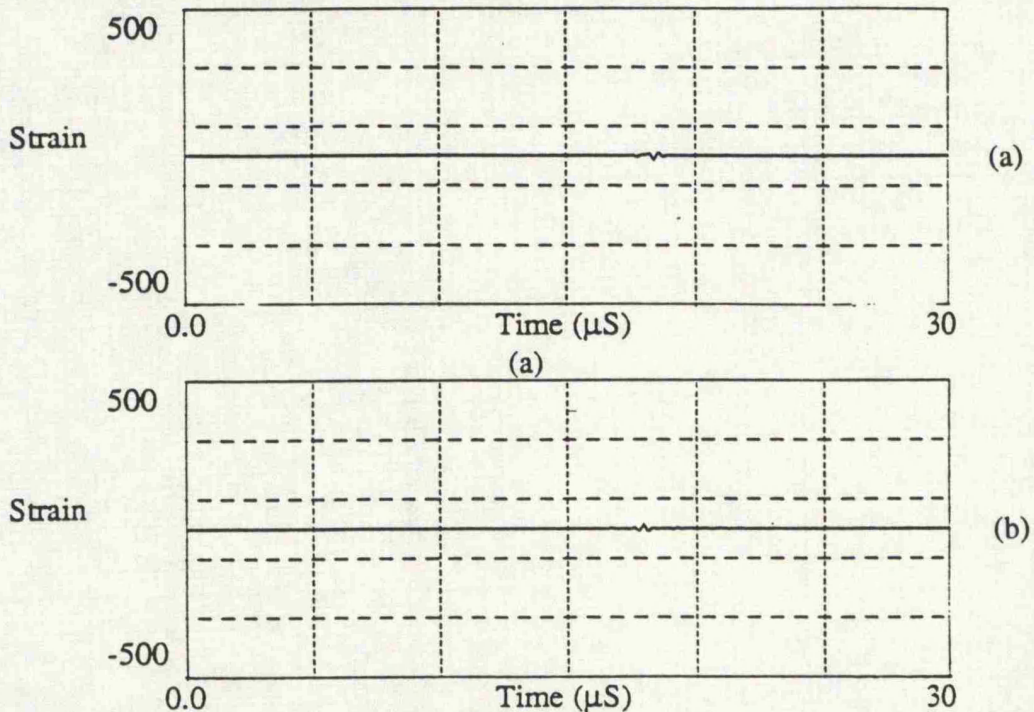


Figure 6.6: ICI Plytron Cross Ply Plate,  $\gamma=90^\circ$   
 Filtered Analytical Response to Surface Line Impact  
 a) Upper surface, 15mm from Impact  
 b) Lower surface, 15mm from Impact

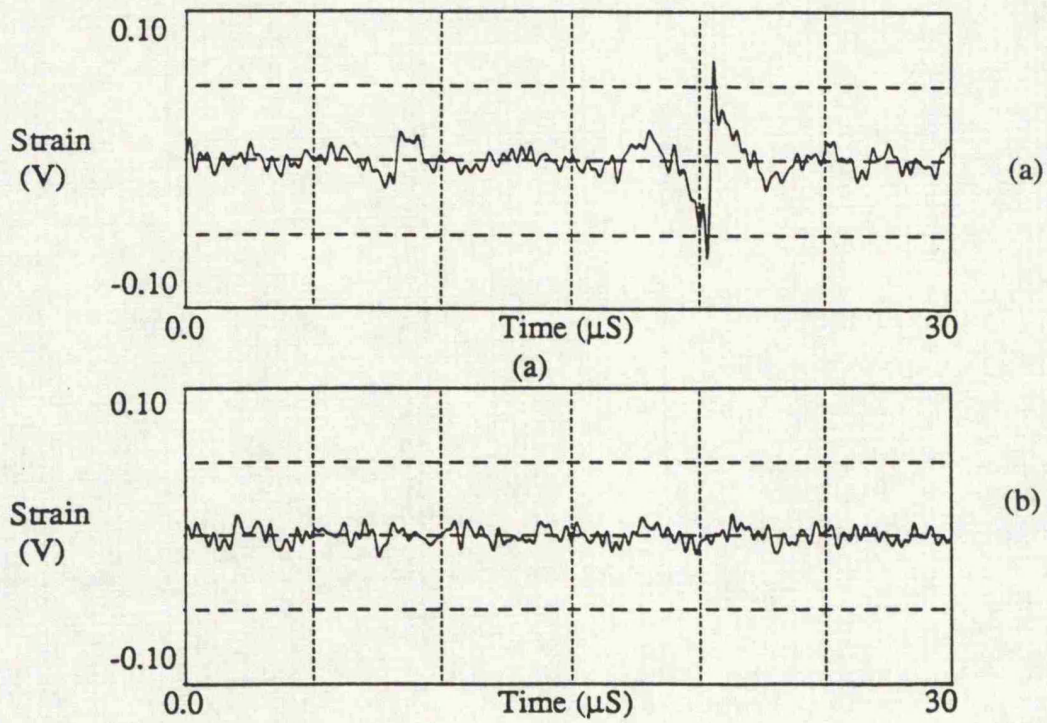


Figure 6.7: ICI Plytron Cross Ply Plate,  $\gamma=0^\circ$   
Filtered Experimental Response to Surface Line Impact  
a) Upper surface, 15mm from Impact  
b) Lower surface, 15mm from Impact

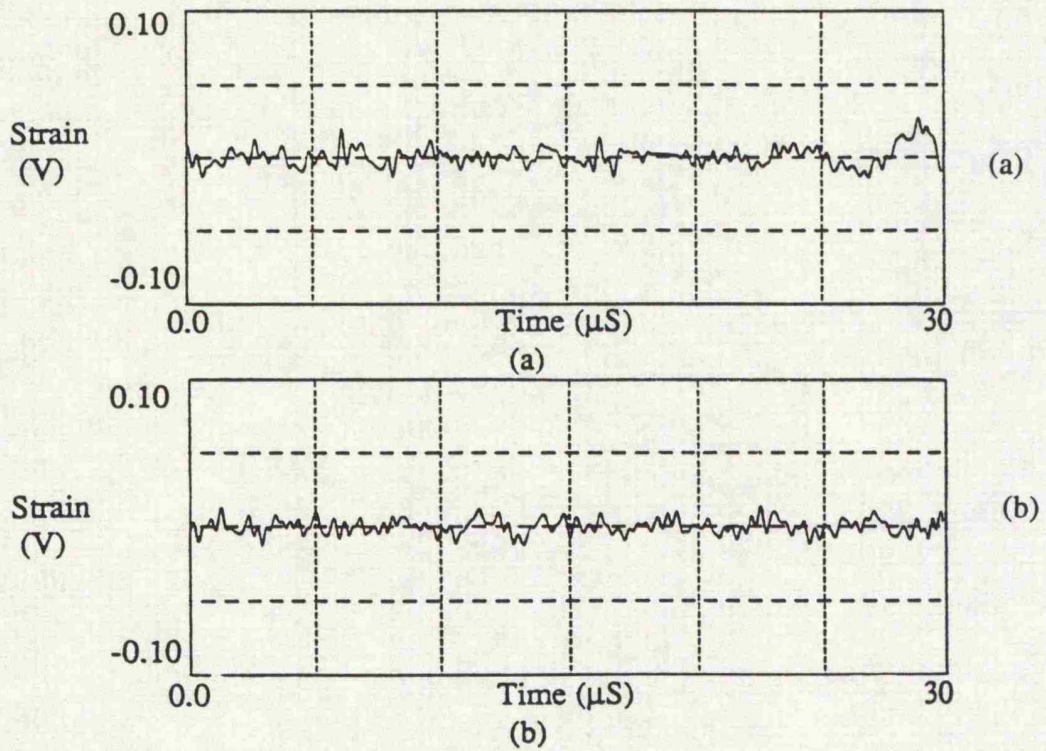


Figure 6.8: ICI Plytron Cross Ply Plate,  $\gamma=90^\circ$   
Filtered Experimental Response to Surface Line Impact  
a) Upper surface, 15mm from Impact  
b) Lower surface, 15mm from Impact

### Chapter 7: Internal Wave Propagation in a 4-Ply Laminated Plate

In the previous chapter the investigation into surface wave propagation of a 4-ply laminated plate was described. The material used in that investigation was ICI Plytron, but the cure temperature of this material prevented the placing of the PVDF sensors at the laminate interfaces to investigate the internal waves. Following an investigation into other fibre reinforced materials available a suitable low temperature material was selected which would provide the capability for the placing sensors inside the plate. The material was produced by Advanced Composite Materials and consisted of their LTM22 resin with T700 carbon fibre reinforcement. This material had a recommended cure cycle of 55°C for 16 hours which was at a lower temperature than the survival temperature of the PVDF sensors of 70°C. This material provided the ability to manufacture plates of material with sensors as an integral part. The full details of the material and processing techniques were presented in chapter 5. Using this material the investigation into the internal stress waves of a 4-ply plate could be conducted.

The major disadvantage of this material was the conductivity of the carbon reinforcement fibres. This required the PVDF sensors and lead out wires to be insulated which resulted in an increase in the overall thickness of the sensors. The conductivity of the plates also resulted in an increase in the electro magnetic interference on the sensor responses. This provided a variation in the quality of the tests and difficulties with the filtering of the sensor outputs due to the lower signal to noise ratio on the sensor responses. The aim of the filtering was to remove the low frequency contribution of the impact and any high frequency noise. The problem arising in removing the noise from the signal was the danger of removing the high frequency component of the stress waves which were under investigation. This resulted in some of the processed data having less clarity than was desirable.

In section 5.4 it was shown that for a four layer cross ply composite plate the angle of wave propagation  $\gamma$  when the wave velocities of an internal shear wave and a Rayleigh type surface wave are equal could be calculated from the material wave speeds, equation [2.70]. For a four layer cross ply composite plate manufactures from LTM22/T700 material with a layer thickness of 0.8mm, the equal wave velocities occurs when the angle between the direction of propagation and the fibres at the mid plane of the plate,  $\gamma = 46.30^\circ$ .

This experimental investigation was completed for the same two cases that had been examined for Plytron in the previous chapter,  $\gamma = 0^\circ$  and  $\gamma = 90^\circ$ . As in the previous study the analytical solution had suggested that when  $\gamma = 0^\circ$  the limiting wave velocity would be the velocity of a Rayleigh type surface wave, and that when  $\gamma = 90^\circ$  the limiting wave velocity would be the velocity of an internal shear wave.

For each case there were three sets of tests completed, the first tests repeated the previous tests on Plytron, and examined the responses of the outer surfaces from an impact. The objective of these tests were to show that the same wave propagation characteristics were observed in the LTM22/T700 material as had been observed in Plytron.

The second set involved plates which had sensors placed on the upper surface and at the mid plane. These tests were particularly to investigate the internal wave characteristics when  $\gamma = 90^\circ$ . The theoretical model had predicted that at this condition the mid plane responses would be of a larger magnitude than the surface responses.

The third set also involved the investigation of the upper surface and mid plane responses but to examine the responses over a range of impact energies. These tests were particularly aimed to study the variation in experimental conditions on the plate responses compared to the analytical delta function responses.

### 7.1 Analytical Solution To Dispersion Equation.

The procedure to solve the symmetric and anti symmetric forms of the dispersion equation [Equ. 2.56] were the same as for the previous material Plytron, but with the relevant material elastic wave speeds. The dispersion equation was solved up to a value of  $\omega h/C_1 = 14$  for the two conditions under investigation  $\gamma = 0^\circ$  and  $\gamma = 90^\circ$ .

Figure 7.1a shows the dispersion curves for the antisymmetric motion for  $\gamma = 0^\circ$  and figure 7.1b shows the corresponding curves for the symmetric motion. Similarly 7.2a and 7.2b shows dispersion curves when  $\gamma = 90^\circ$  for the antisymmetric and symmetric motion respectively.

The dispersion curves for the LTM22/T700 material show the same characteristics as has been previously described for the Plytron material. For the  $\gamma = 90^\circ$  symmetric and antisymmetric case there are two visible ghost lines, which relate to the material elastic wave speeds, brought about by the osculation of the branches. As the curves approach the ghost lines they exhibit the same plateau and step phenomenon described earlier. Once the curves have passed through the left hand ghost line they tend towards the limiting wave velocity of the fundamental mode. For the  $\gamma = 0^\circ$  symmetric and antisymmetric case the same ghost lines are present and as with the Plytron material the curves tend to the lowest stress wave velocity. In this case the lowest stress wave velocity is not the limiting wave velocity and the fundamental mode which equates to a Rayleigh type surface wave speed is diverging from the other curves.

The analytical solution to the theoretical model derived the strains from the dispersion curves for the surfaces and mid plane of the plate. For the comparison with the experimental results the strains were calculated at a point  $40h$  from the impact, where  $h$  is the ply thickness. A larger distance between the impact and the point of examination was selected compared with the previous Plytron results to provide a greater separation between the individual stress waves which would then be detectable experimentally. The

derived strains are presented and discussed in section 7.4 along with the experimental results.

### 7.2 Experimental Study.

This study was aimed at examining the upper, lower surface and mid plane responses of a 4-ply laminated plate. For this investigation surface and mid plane sensors were embedded into the plate during manufacture. This was to make the sensors a more integral part of the plate than in the Plytron investigation, to reduce the attenuation of the plate response due to adhesive layers between the sensors and the plate surfaces.

A problem that occurred with the internal sensors was their location relative to the surface sensors. After each plate was manufactured it was X-rayed [Fig. 7.3] which showed any misalignment between the surface gauge and the mid plane sensor due to poor location of the sensors during plate manufacture and movement of the sensors during the plate cure. This difference in the sensor locations had to be taken into account in the wave speed calculations from the experimental results.

The third stage of this study was an initial investigation into the effect of the variation of the impact energy on the plate responses.

The testing procedure was the same as in the previous tests with the striker displacement set at 0.5mm, and the gun pressure set at 40bar for the first two stages. This provided an impact energy of 0.42J. The same filtering techniques were applied to the data to remove the unwanted low and very high frequency components. The filter used was a Butterworth band pass filter between 250kHz and 4MHz.

### 7.3 Analytical Results

Case 1  $\gamma = 0^\circ$

Figure 7.4 shows each surface and mid plane responses of a plate subjected to a delta function line impulse. The upper surface response in figure 7.4a shows a clear upper surface response of magnitude 12 pk-pk occurring at  $38\mu\text{s}$  after the impulse onto the plate. This response is therefore travelling at  $0.84\text{mm}\mu\text{s}^{-1}$ . This response is of the same type that was observed in the analytical results for Plytron in figure 6.5a. Figure 7.4b shows the mid plane response where the maximum response is 0.2 pk-pk which is insignificant when compared with the upper surface response. Figure 7.4c shows the lower surface response, this surface shows a larger response than at the mid plane with a maximum magnitude of 1.6pk-pk. As with the mid plane response there was no significant response present on the lower surface which could be associated with the large response present on the upper surface.

The large response on the upper surface can be associated with a wave travelling along the upper surface which is absent from the mid plane and lower surface of the plate, and has a velocity of  $0.84\text{mm}\mu\text{s}^{-1}$ . This wave has all the characteristics of a Rayleigh type surface wave, and the velocity matches a theoretical Rayleigh type surface wave velocity in table 7.1. This also matches the theory that the limiting wave velocity at  $\gamma < 46.16^\circ$  is a Rayleigh type surface wave.

#### Case 2, $\gamma = 90^\circ$

Figure 7.5 presents the analytical strain responses for  $\gamma = 90^\circ$  at each surface and mid plane of a plate for a delta function line impulse applied to an infinite plate. Figure 7.5a presents the upper surface responses in which the maximum response occurs between  $18\mu\text{s}$  and  $20\mu\text{s}$ , with a magnitude of 0.8pk-pk. Figure 7.5b of the mid plane response has a magnitude of 1.2pk-pk with large responses occurring at  $20\mu\text{s}$  and  $40\mu\text{s}$ . The lower surface response in figure 7.5c shows a similar response to the upper surface with a maximum magnitude of 0.6pk-pk occurring at  $20\mu\text{s}$ .

These results show that the maximum response occurring for this case is at the mid plane of a plate with the upper surface response significantly lower than the upper surface response of the previous condition when  $\gamma = 0^\circ$ . The mid plane response is larger than both the surface responses and the mid plane response of the  $\gamma = 0^\circ$  case. This shows that in this case that the limiting wave velocity was an internal shear wave occurring at the mid plane of the plate rather than the Rayleigh type surface wave velocity of the  $\gamma = 0^\circ$  case. This agrees with the theoretical predication that when  $\gamma > 46.14$  the limiting wave velocity would be that of an internal shear wave velocity ( $c_2$ ).

#### 7.4 Experimental Results

As described in section 7.3 there were three sets of experimental tests completed, the surfaces only responses, the upper surface and mid plane response, and the upper surface and mid plane response for different impact energies. The results presented are plots of the detected potential change (Volts) of the sensors which is related to the strain in the direction of wave propagation, for a time duration of  $80\mu\text{s}$  after the impact of the striker onto the plate. The point of impact was detected from a sensor mounted onto the striker.

##### Upper and Lower Surfaces Response.

The responses in Figure 7.6 show the upper and lower surface responses 32 mm from the impact, for  $\gamma = 0^\circ$  due to a 0.4J impact. Figure 7.6a shows the upper surface response where two noticeable increases in the signal magnitude can be seen. The first one occurred at  $15\mu\text{s}$  after the point of impact with a magnitude of 25.9mV pk-pk, the second occurs at  $38\mu\text{s}$  with a magnitude of 57mV pk-pk. Following the largest peak the response decays away to the background noise level. The wave speed of the first response is  $2.1\text{ mm}\mu\text{s}^{-1}$  which is close to the  $c_1$  (longitudinal) stress wave speed of the material, table 7.1. The second large response is caused by a wave travelling at  $0.84\text{ mm}\mu\text{s}^{-1}$  which is the same as the wave speed of the Rayleigh type surface wave when  $\gamma = 0^\circ$ .

Figure 7.6b shows the lower surface response and the first noticeable response occurs at  $20\mu\text{s}$  with a magnitude of  $22\text{mV}$ . In the region between  $30\mu\text{s}$  and  $40\text{ms}$  there is a peak response of  $28\text{mV}$ . The first response correlates with the  $c_3$  (shear) response on the upper surface, but the second response is of a smaller magnitude than on the upper surface and can be matched to the  $c_2$  (shear) wave speed.

The responses in Figure 7.7 show the upper and lower surfaces responses for  $\gamma = 90^\circ$  for a  $0.42\text{J}$  impact. Figure 7.7a shows the upper surface response with the first response of the sensor occurring  $13.5\mu\text{s}$  with a magnitude of  $37.6\text{mV}$  after the impact. There is no noticeable response occurring at  $40\mu\text{s}$  after the impact as had been the case on the upper surface when  $\gamma = 0^\circ$ . Figure 7.7b shows the lower surface response with the largest response occurring at  $41\mu\text{s}$  after impact with a magnitude of  $32\text{mV}$ . The time duration between these responses and the point of impact indicate that they can be attributed to the  $c_1$  (longitudinal) and  $c_2$  (shear) waves respectively.

These results for the responses of the upper and lower surfaces have shown the same characteristics as the results for Plytron in the previous chapter. On the upper surface when  $\gamma = 0^\circ$  a large wave is present whose speed matches the speed of a Rayleigh type surface wave, a similar disturbance is noticeably absent from the lower surface. This provides further verification for the predication that the limiting wave velocity when  $\gamma < 46.14^\circ$  is the velocity of a Rayleigh type surface wave, which is only present on the upper surface.

The absence of a similar large upper surface response in the second case of  $\gamma = 90^\circ$  matches the predication that under this condition the limiting wave velocity would be that of an internal shear wave velocity. To fully investigate this prediction the comparison of the upper surface and mid plane responses is required.

### Surface and Mid plane Results

The second set of tests investigated the difference between the upper surface and mid plane responses from the same surface impact conditions as the previous surface wave tests.

For  $\gamma = 0^\circ$  figure 7.8a shows the upper surface response. The surface waves for this test are not as clear as for the previous tests due to a large amount of interference that occurred during this test, and the specific waves cannot be easily separated from the background noise. Figure 7.8b shows the mid plane response in which the overall maximum response is 20mV pk-pk. This level is lower than the responses seen in both the upper surface response in figure 7.8a and in the upper surface response from the previous test figure 7.6a. There are not any large responses present at the mid plane which can be associated with a Rayleigh type surface wave present on the upper surface.

The upper surface and mid plane response when  $\gamma = 90^\circ$  are presented in Figure 7.9. Figure 7.9a shows the upper surface response which is similar in characteristics to the previous surface response [Fig. 7.7a] for this case. This response shows evidence of the individual stress waves between 20 $\mu$ s and 40 $\mu$ s but no Rayleigh type surface wave.

The mid plane response in figure 7.9b shows distinct response occurring 39 $\mu$ s after the impact onto the plate. This response has a magnitude of 33mV and a wave velocity of 0.85mm $\mu$ s<sup>-1</sup>. This velocity correlates with the slowest stress wave velocity of the  $c_2$  (shear) wave in table 7.1.

These responses at the mid plane of a plate have shown that when  $\gamma = 0^\circ$  the dominant response of the plate is at the upper surface. When  $\gamma = 90^\circ$  the dominant response is at the mid plane of the plate, with a velocity closest the  $c_2$  (shear) stress wave velocity. This provides the final verification to the theoretical predictions that when  $\gamma > 46.16^\circ$  the limiting wave velocity will be that of the slowest internal shear wave velocity.

### Surface and Mid plane Response at Different Impact Energies

This third set of tests investigated the effects of different impact energies on the surface and mid plane responses. Figures 7.10 and 7.11 show the upper surface and mid plane responses for  $\gamma = 0^\circ$ , from a time of  $20\mu\text{s}$  after the impact for a duration of  $80\mu\text{s}$ . Figure 7.10a is the upper surface response from a  $0.36\text{J}$  impact and has the same large surface response as the previous tests with a maximum response of  $50.7\text{mV}$ . Similarly figure 7.11a shows the upper surface response for a  $0.49\text{J}$  impact, with a maximum response of  $53.3\text{mV}$ . The velocities of both these responses match the Raleigh type surface wave velocity. The mid plane responses figures 7.10b 7.11b both show little response compared with the upper surface.

Figures 7.12 and 7.13 show the upper surface and mid plane responses for  $\gamma = 90^\circ$ , for impact energies of  $0.36\text{J}$  and  $0.49\text{J}$  respectively. Figures 7.12a and 7.13a are the upper surface responses and show little disturbance as in the previous tests of this condition. Figure 7.12b is the mid plane response with a maximum magnitude of  $31.3\text{mV}$  pk-pk, and figure 7.13b has a maximum magnitude of  $30.7\text{mV}$  pk-pk. The velocities of the mid plane responses match the  $c_2$  (shear) stress wave speed. Figures 7.13a and 7.13b show an electrical interference occurring  $77\mu\text{s}$  after the impact.

Both sets of results show the same characteristics as the previous tests in that when  $\gamma = 0^\circ$  the largest disturbance is at the upper surface and when  $\gamma = 90^\circ$  the largest disturbance is at the mid plane of the plate and shows that there is little variation in the responses of the plates for the different impact energies.

The cause for the lack of variation in the responses due to the different impact energies can be explained by the filtering that was applied to the sensor responses. It was the objective of the filtering to remove the low frequency contribution of the impact from the sensor response caused by the impact duration [Ref. 48]. This reduction of the low frequency contribution also reduced the energy contribution to the magnitude of the signal

responses, which resulted in there being little effect of the different impact energies on the plate responses due to the stress waves propagating through the plate. This provides evidence of the validity in the comparison between the experimental results from a real impact and the analytical results for an ideal delta function impact as the magnitude of the real impact had little effect on the filtered experimental results.

### 7.5 Quality of Results

A comment is required on the quality of these results in relation to the amount of noise present on the results. The PVDF sensors were very sensitive to the responses of the plate in such a way that no further amplification was required to the sensor response. It was this high sensitivity that made them ideal for detecting the stress wave responses, but it was also this high sensitive that resulted in their high sensitivity to electro magnetic interference. This problem was compounded due to the conductivity of the carbon fibres in the plates which also received the interference which resulted in more noise of the sensor responses. This interference resulted in the quality of some of the results being poor which presents difficulty in the resolution in the stress wave responses. There is further work that is required in the development of the sensors and in the signal processing of the results to produce clear and concise data on the stress wave responses of composite plate, but the data presented in this chapter has shown clearly that the characteristics of the stress waves due a surface impact may be resolved.

Stress Wave	Wave Speed ( $\text{mm}\mu\text{s}^{-1}$ )	Time to Travel 32mm ( $\mu\text{s}$ )
$c_1$	2.210	14.48
$c_2$	0.889	36.00
$c_3$	1.726	18.54
$c_4$	1.546	20.70
$c_5$	7.919	4.04
$v_R (\gamma = 0^\circ)$	0.838	38.19

Table 7.1: Theoretical Wave Speeds for LTM22/T700 Material

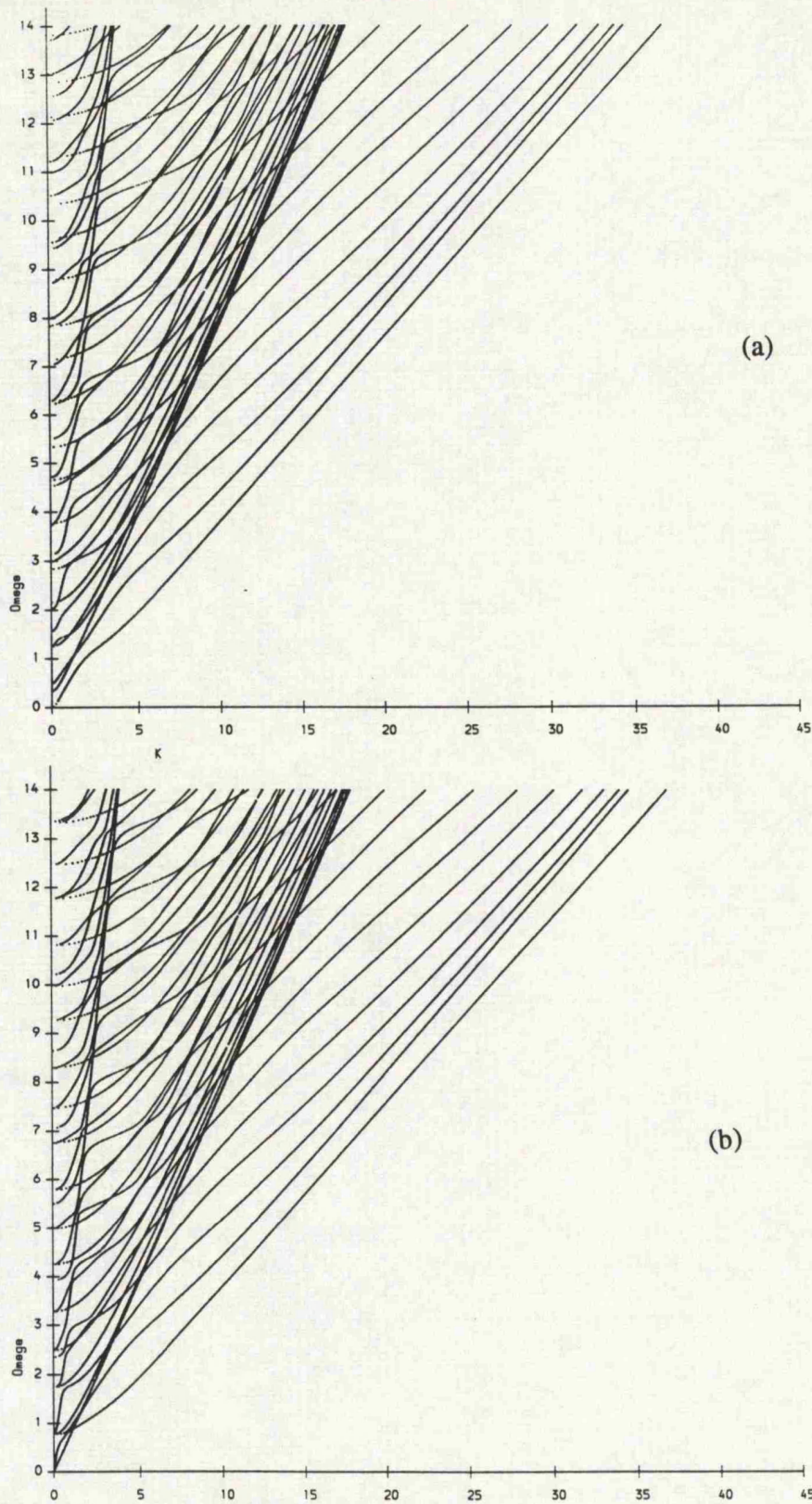


Figure 7.1: LTM22/T700 Cross Ply Plate  
Dispersion curves  $\gamma=0^\circ$   
a) Antisymmetric Motion  
b) Symmetric Motion

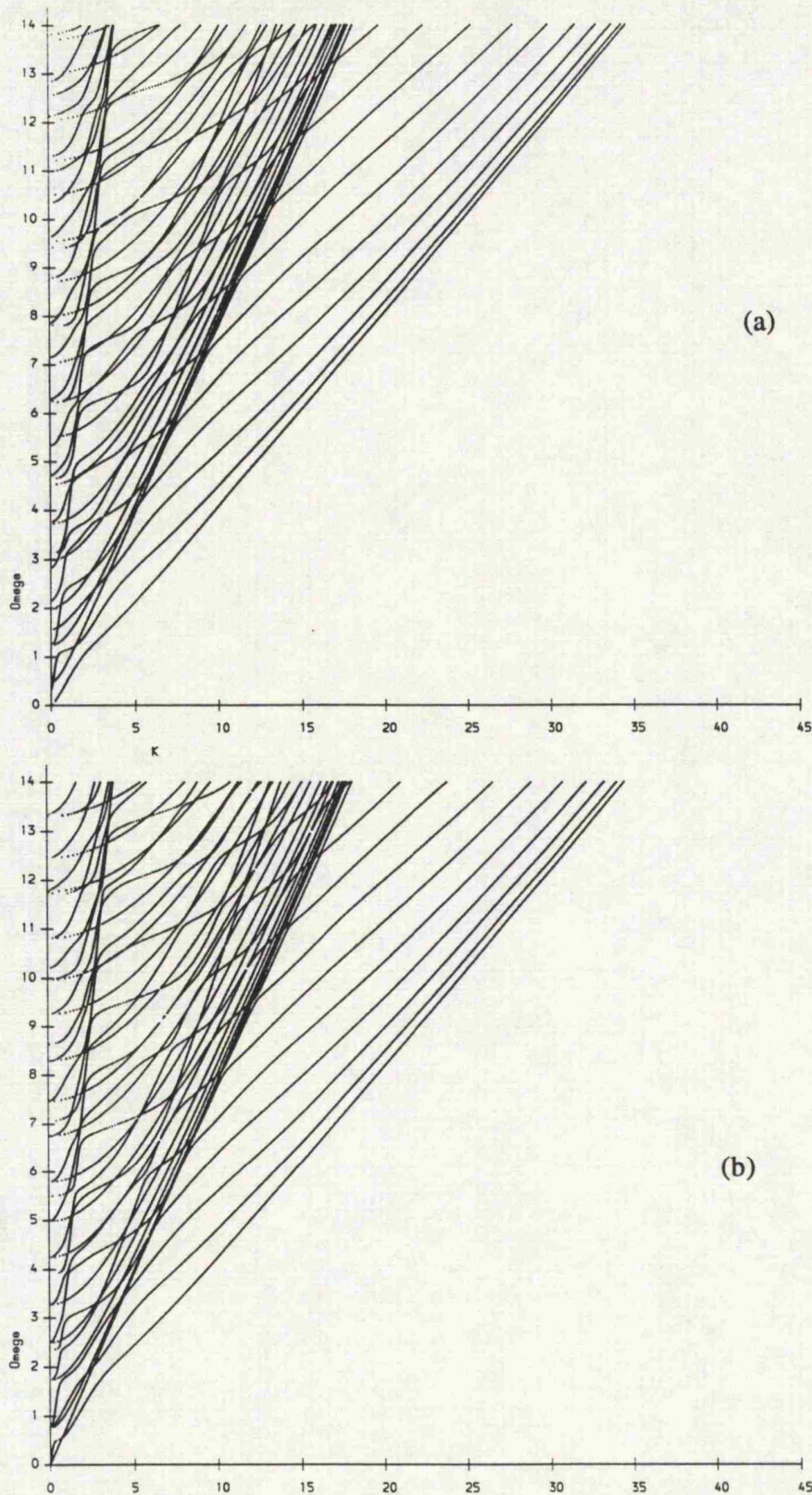


Figure 7.2: LTM22/T700 Cross Ply Plate  
Dispersion curves  $\gamma=90^\circ$   
a) Antisymmetric Motion  
b) Symmetric Motion

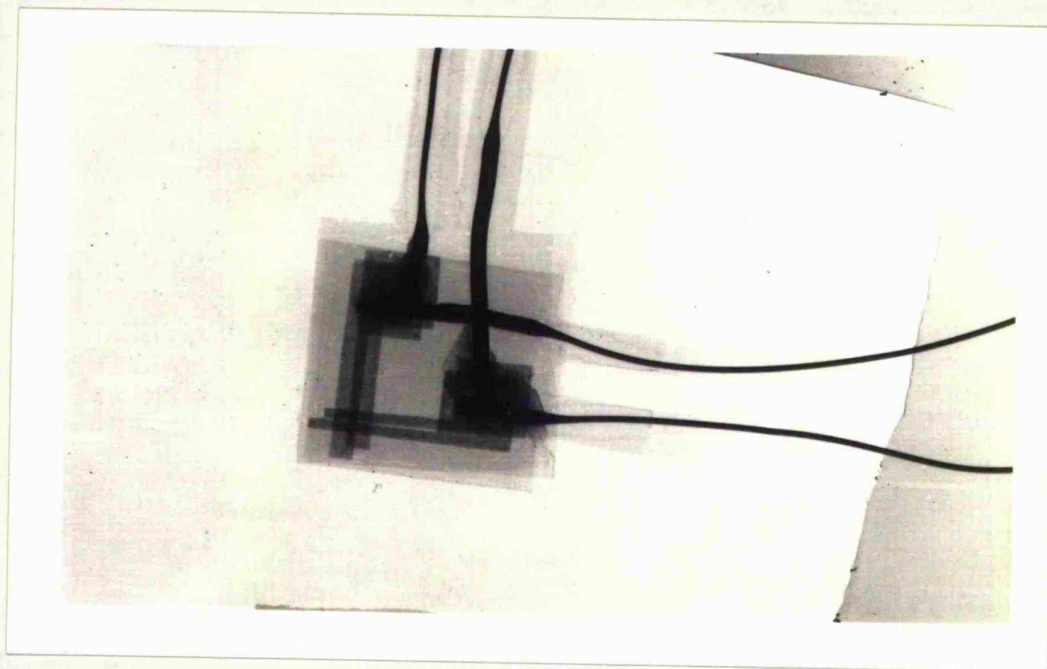


Figure 7.3: X-Ray of LTM22/T700 Cross Ply Plate Showing Sensor Location

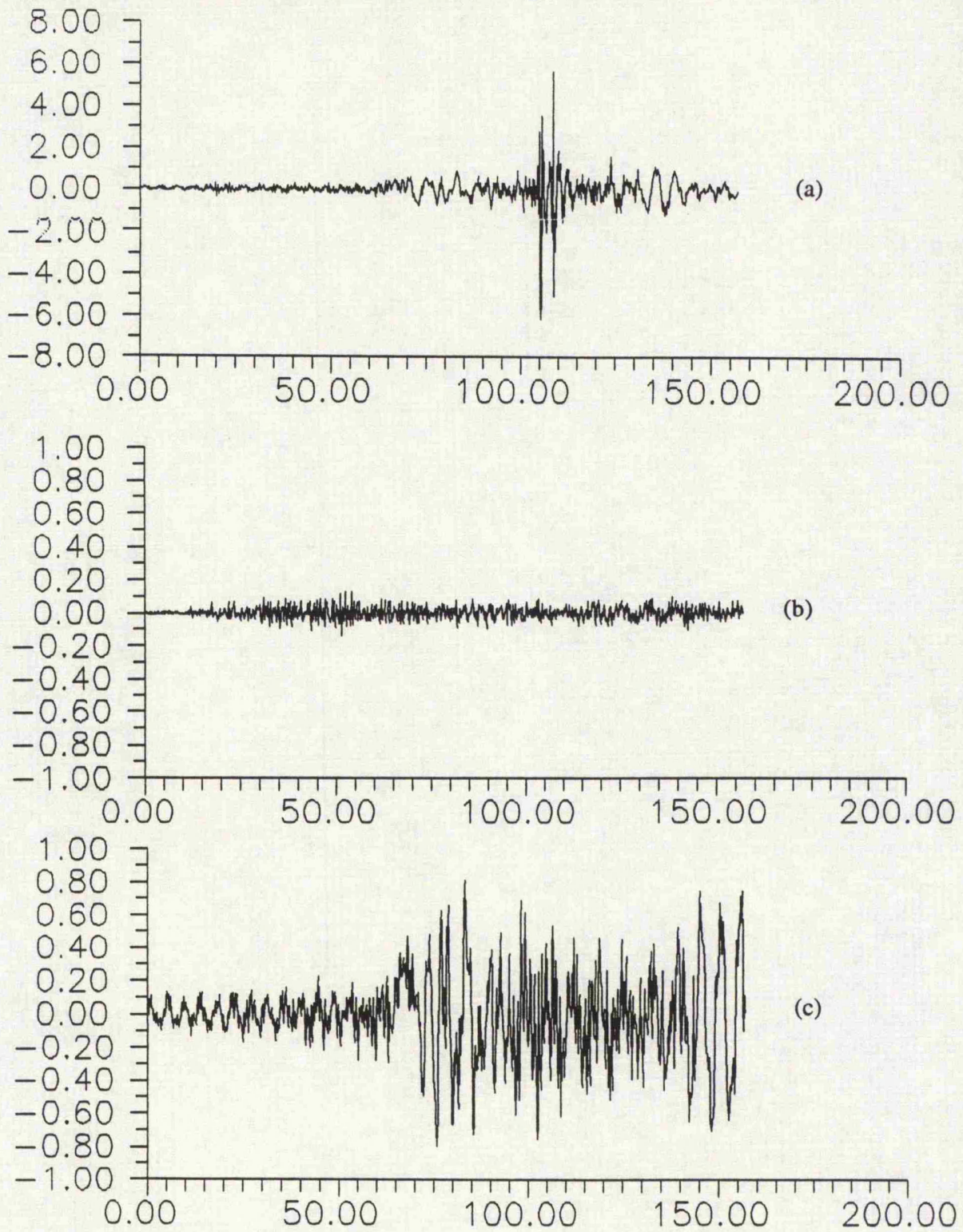


Figure 7.4: LTM22/T700 Cross Ply Plate,  $\gamma=0^\circ$   
Analytical Response to Surface Line Impact  
a) Upper surface, 32mm from Impact  
b) Mid plane, 32mm from Impact  
b) Lower surface, 32mm from Impact

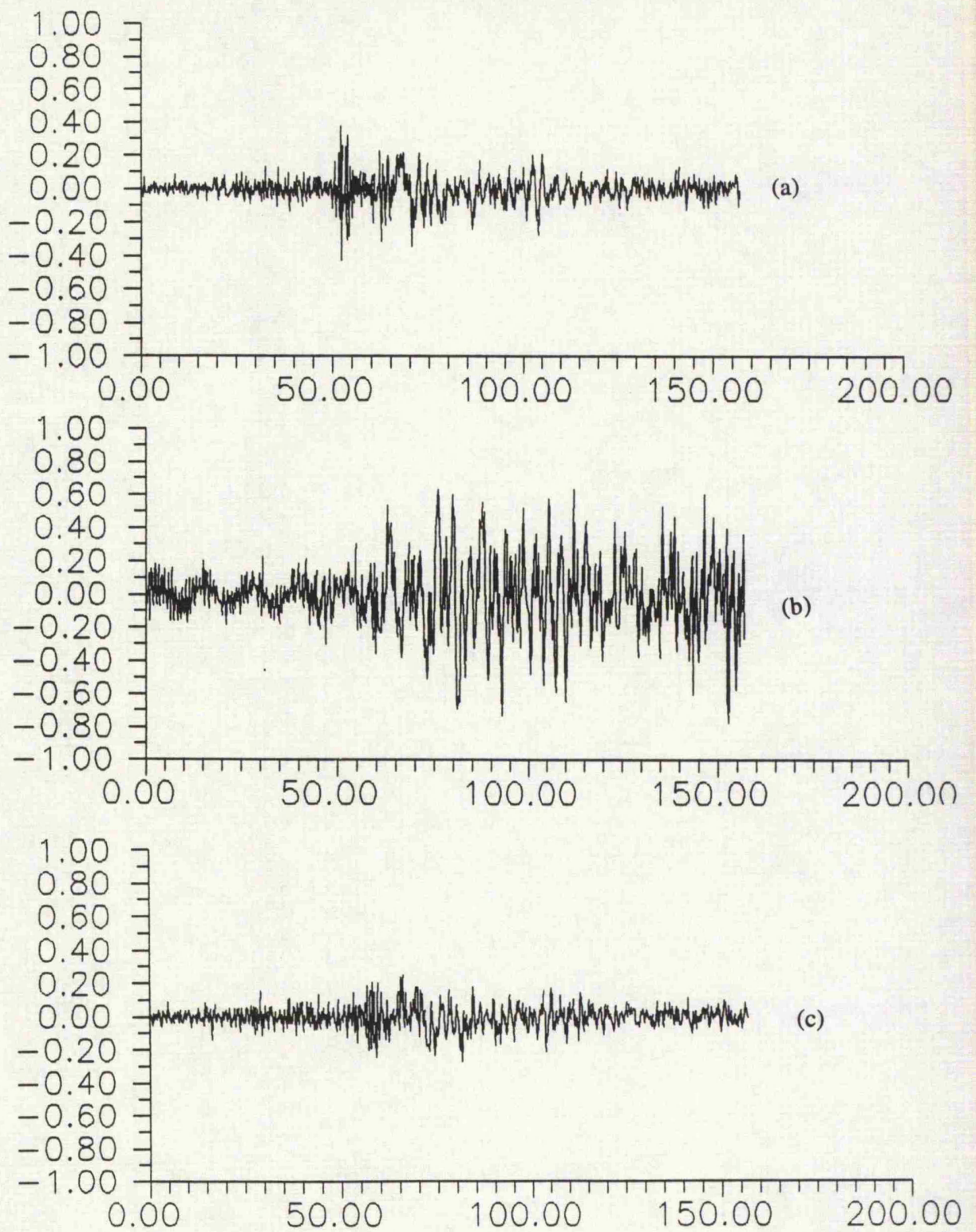


Figure 7.5: LTM22/T700 Cross Ply Plate,  $\gamma=90^\circ$   
Analytical Response to Surface Line Impact  
a) Upper surface, 32mm from Impact  
b) Mid plane, 32mm from Impact  
b) Lower surface, 32mm from Impact

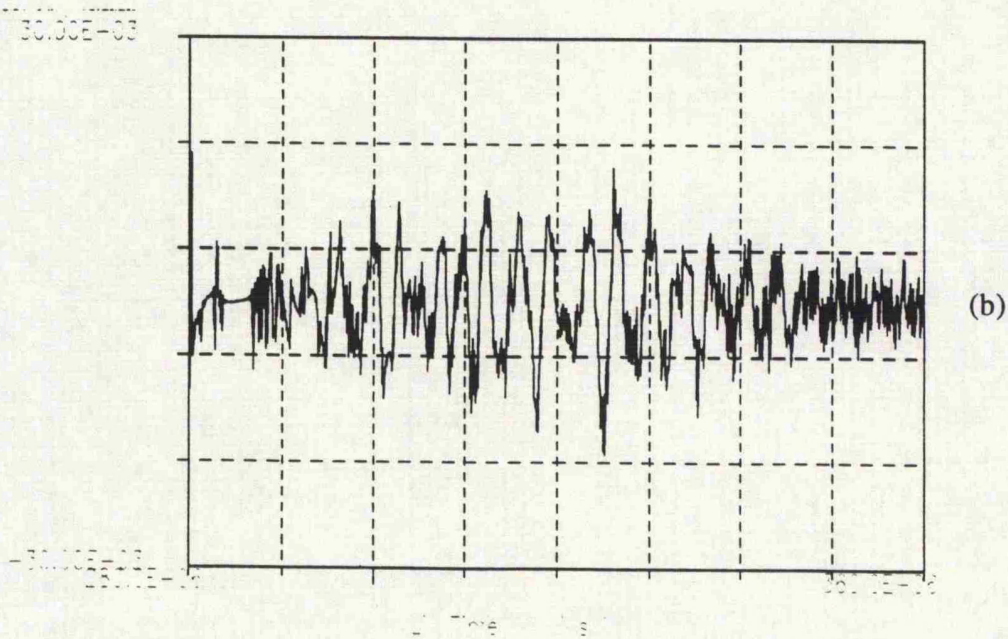
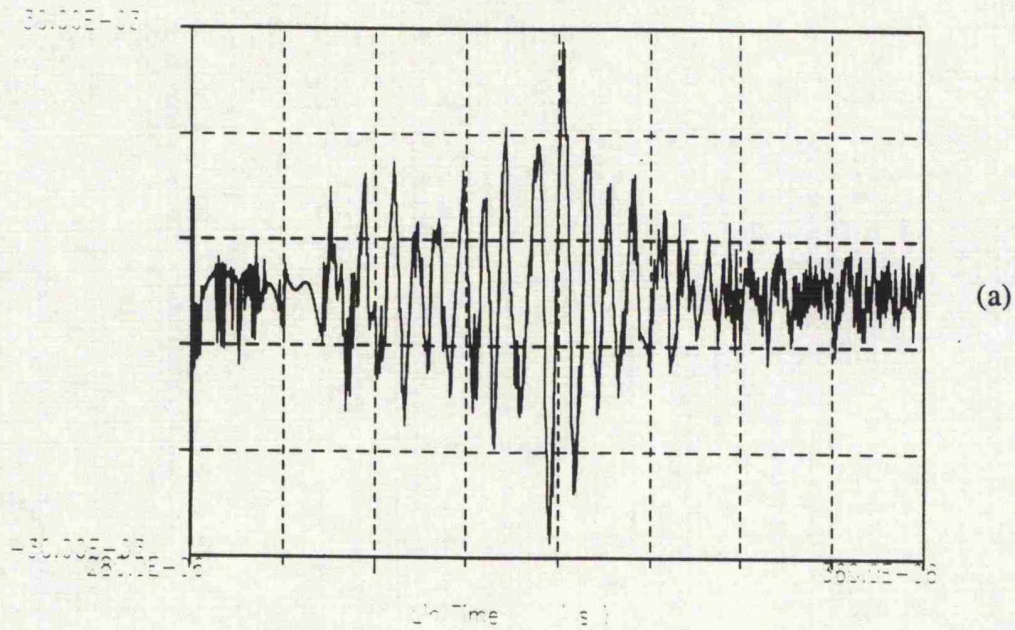


Figure 7.6: LTM22/T700 Cross Ply Plate,  $\gamma=0^\circ$   
Filtered Experimental Response to Surface Line Impact  
a) Upper surface, 32mm from Impact  
b) Lower surface, 32mm from Impact

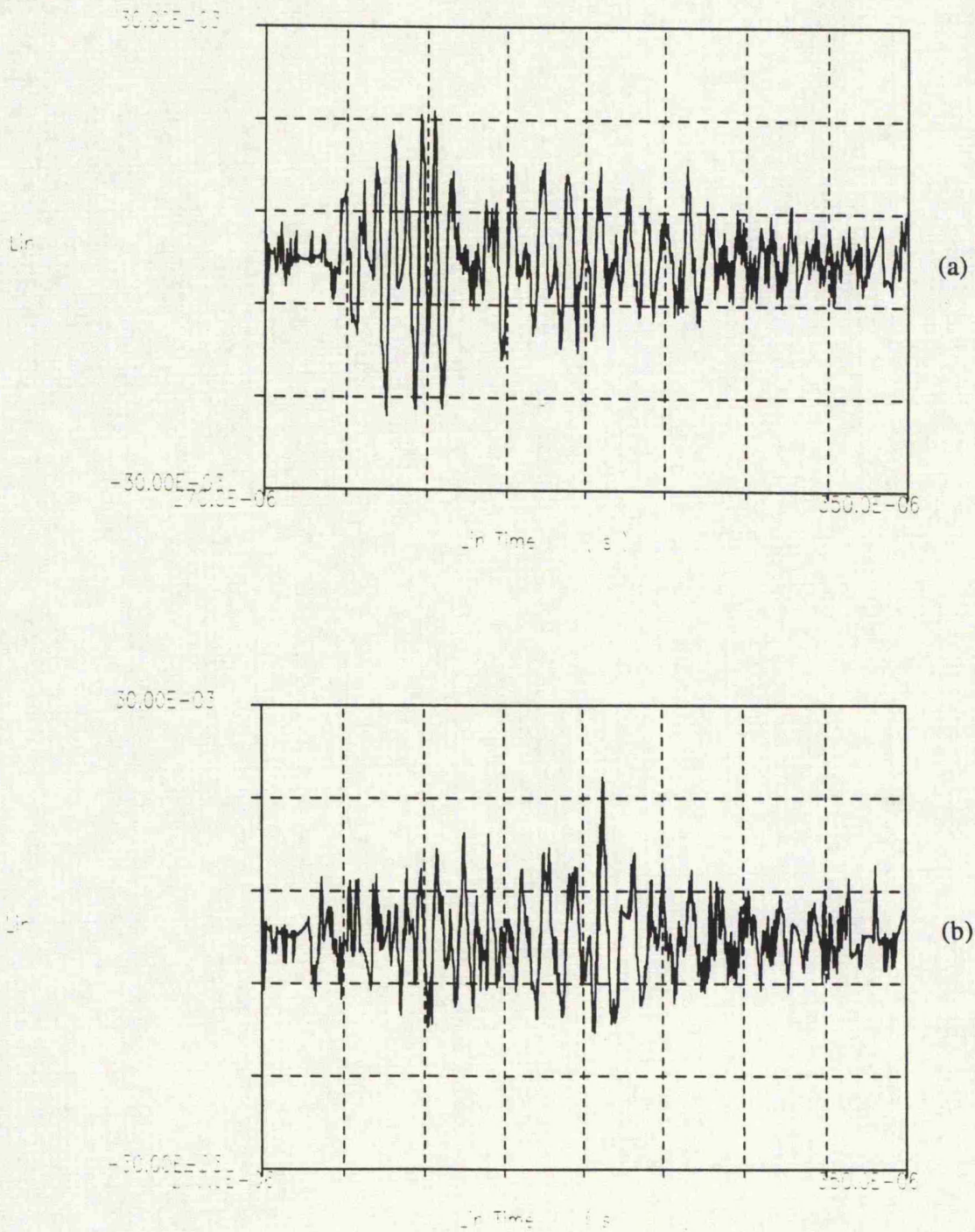


Figure 7.7: LTM22/T700 Cross Ply Plate,  $\gamma=90^\circ$   
Filtered Experimental Response to Surface Line Impact  
a) Upper surface, 32mm from Impact  
b) Lower surface, 32mm from Impact

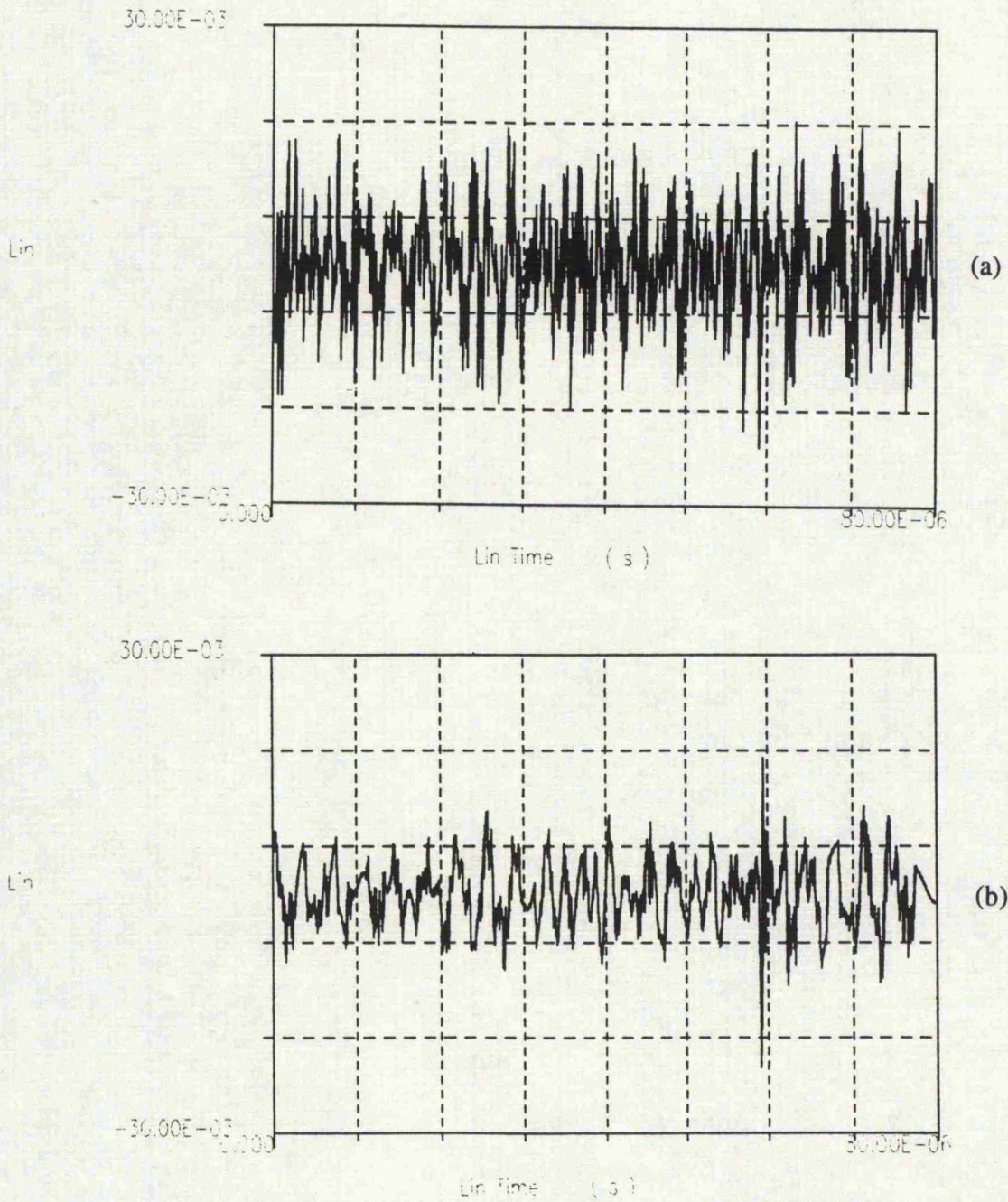


Figure 7.8: LTM22/T700 Cross Ply Plate,  $\gamma=0^\circ$   
Filtered Experimental Response to Surface Line Impact  
a) Upper surface, 32mm from Impact  
b) Mid Plane, 32mm from Impact

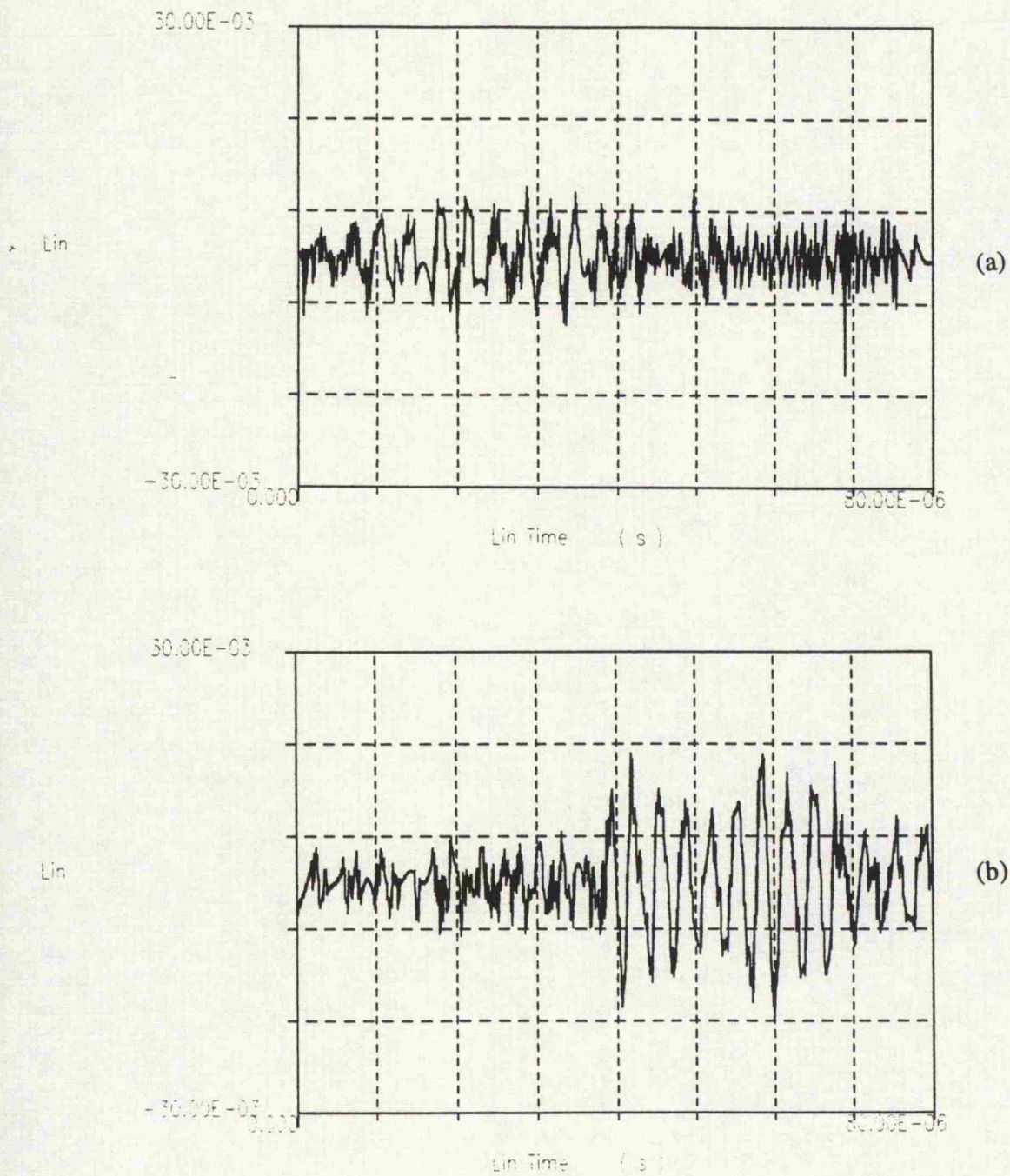


Figure 7.9: LTM22/T700 Cross Ply Plate,  $\gamma=90^\circ$   
Filtered Experimental Response to Surface Line Impact  
a) Upper surface, 32mm from Impact  
b) Mid Plane, 32mm from Impact

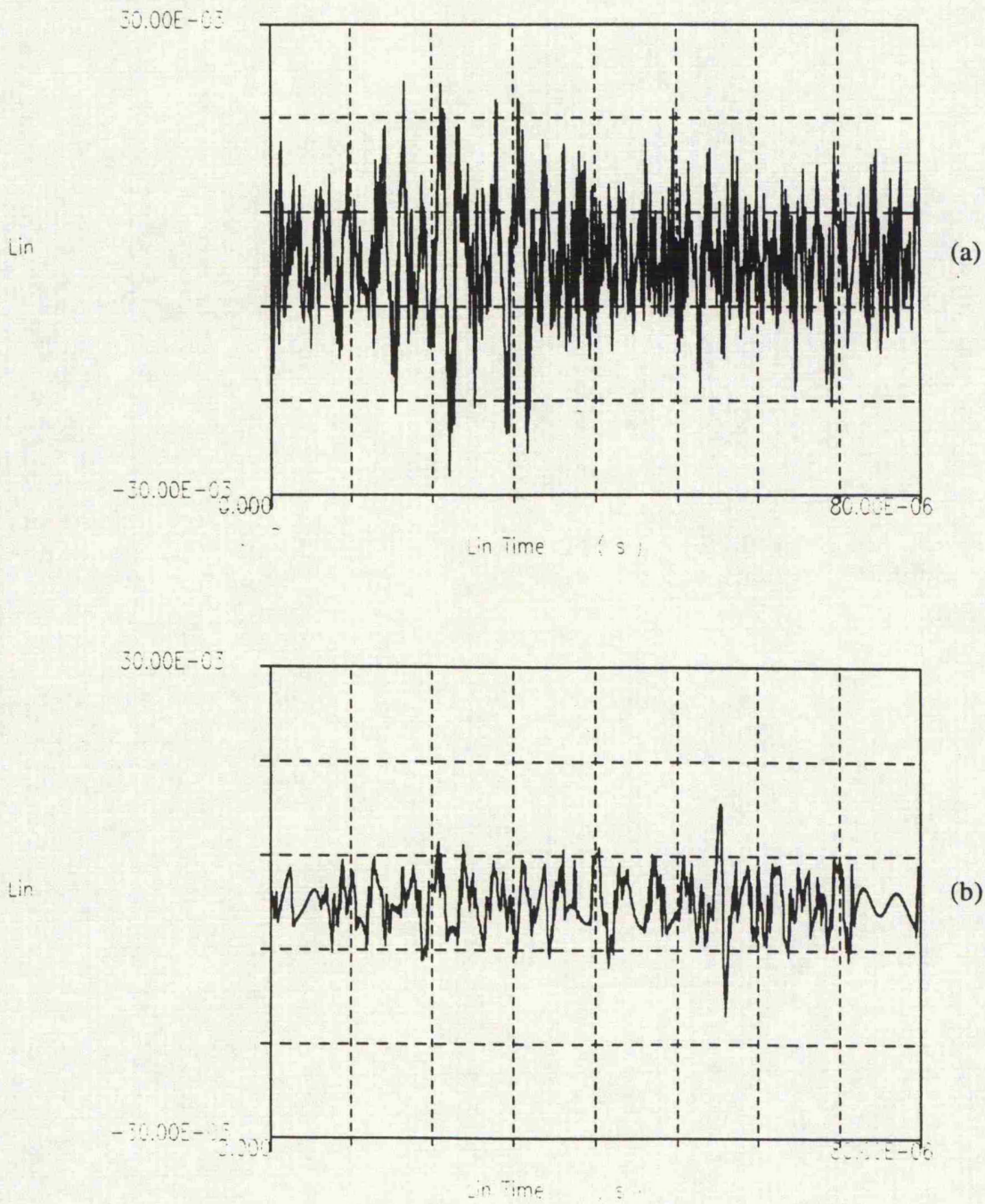


Figure 7.10: LTM22/T700 Cross Ply Plate,  $\gamma=0^\circ$   
Filtered Experimental Response to Surface Line 0.36J Impact,  
a) Upper surface, 32mm from Impact  
b) Mid Plane, 32mm from Impact

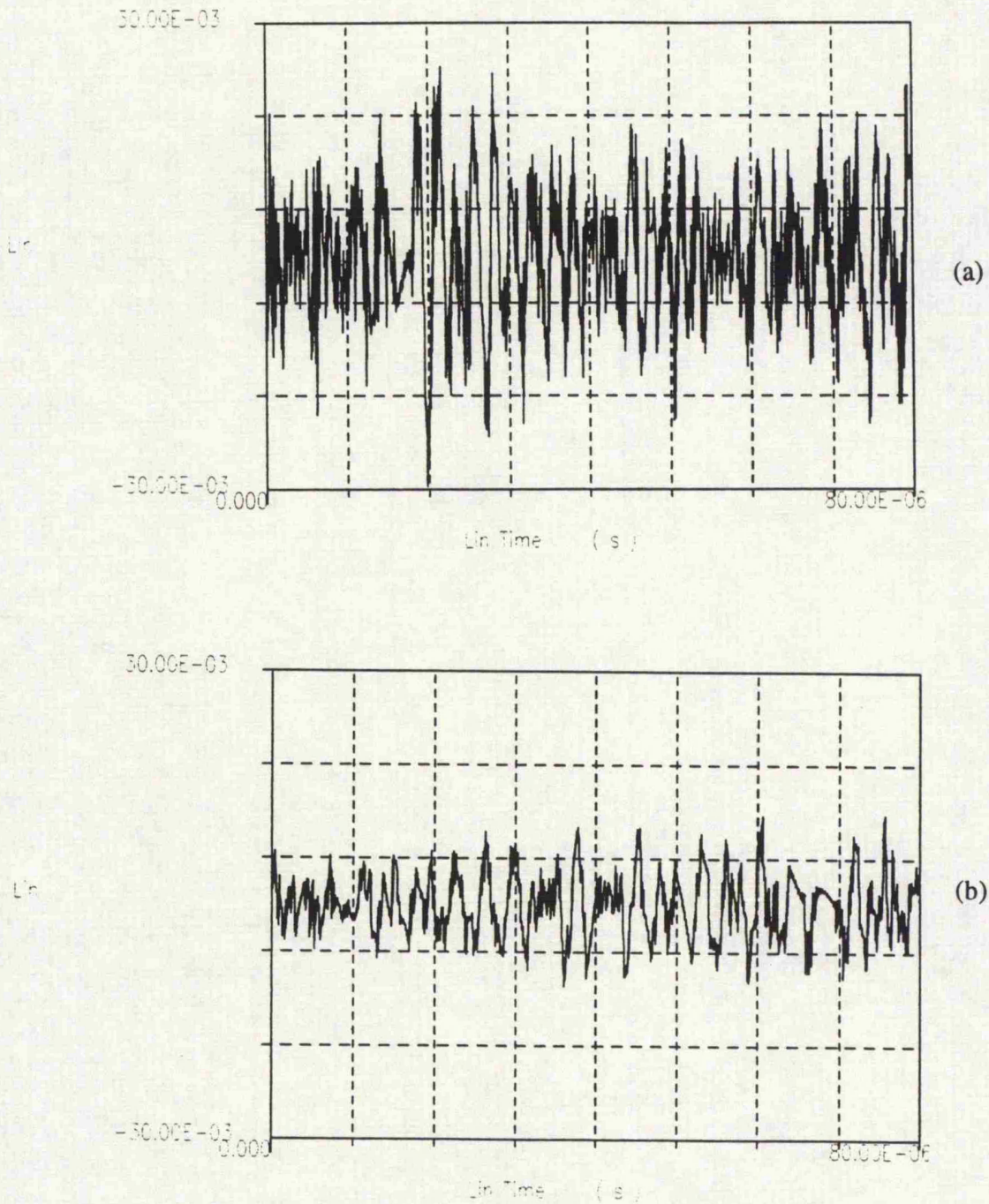


Figure 7.11: LTM22/T700 Cross Ply Plate,  $\gamma=0^\circ$   
Filtered Experimental Response to Surface Line 0.49J Impact,  
a) Upper surface, 32mm from Impact  
b) Mid Plane, 32mm from Impact

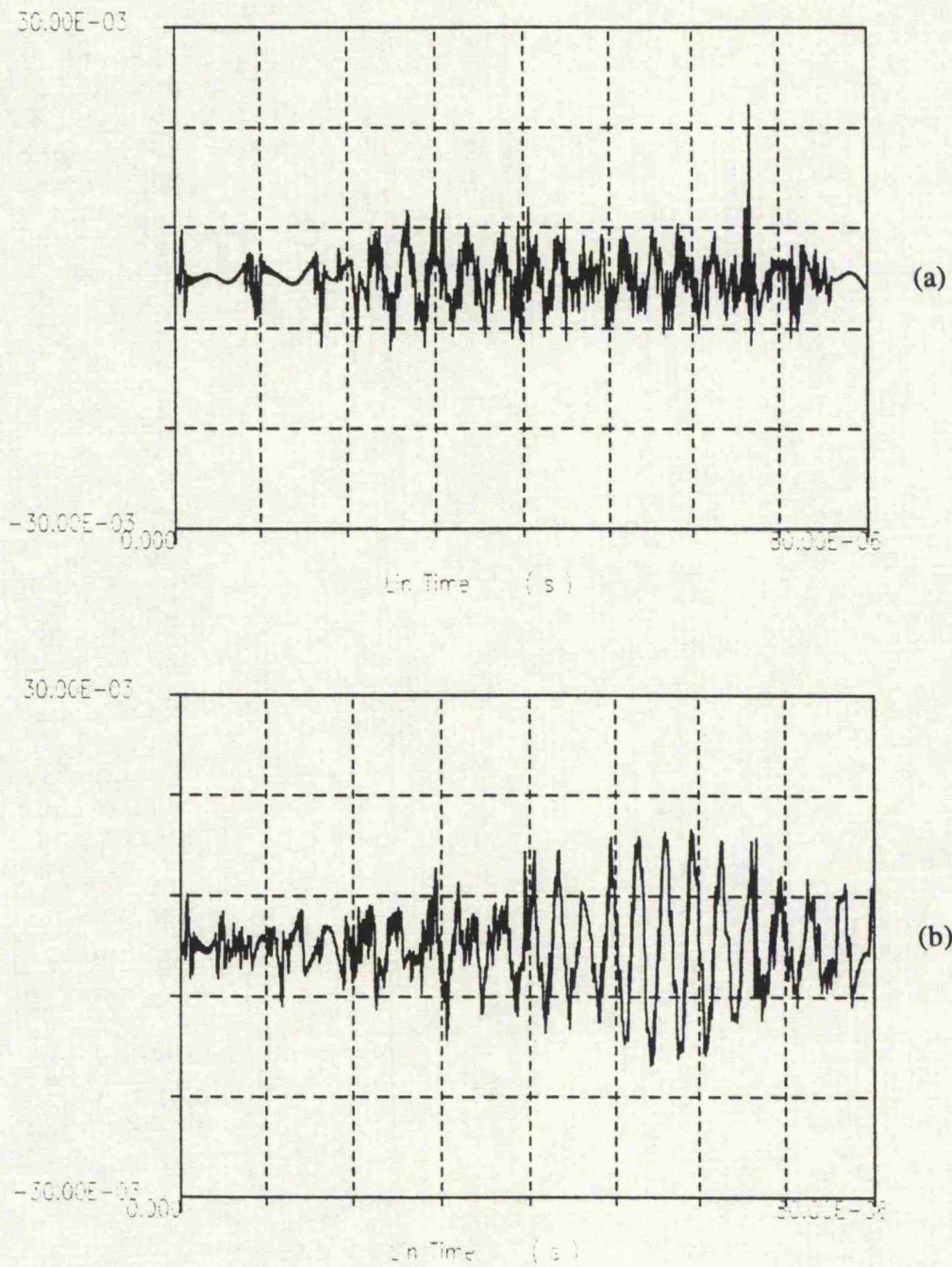


Figure 7.12: LTM22/T700 Cross Ply Plate,  $\gamma=90^\circ$   
Filtered Experimental Response to Surface Line 0.36J Impact,  
a) Upper surface, 32mm from Impact  
b) Mid Plane, 32mm from Impact

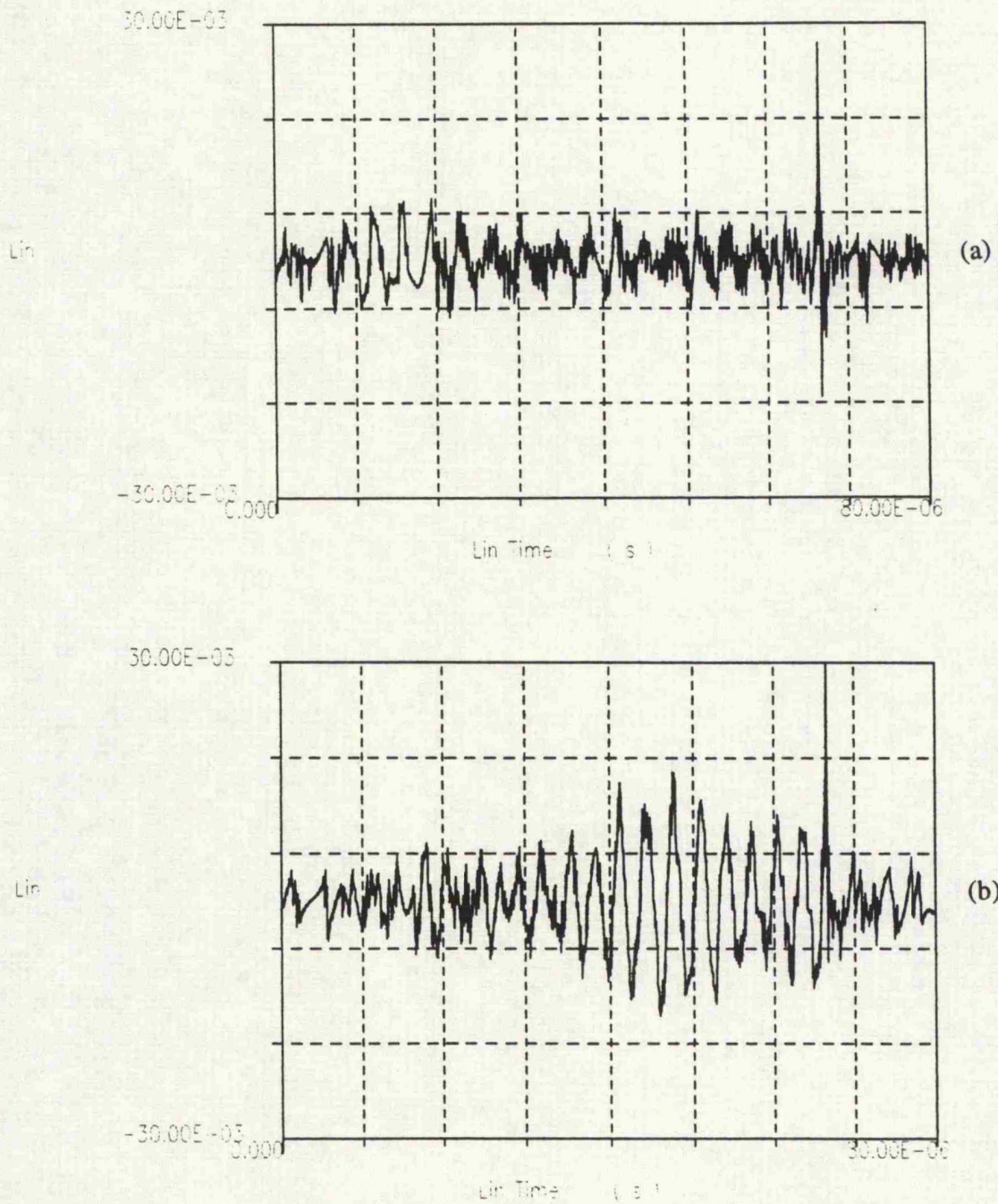


Figure 7.13: LTM22/T700 Cross Ply Plate,  $\gamma=90^\circ$   
Filtered Experimental Response to Surface Line 0.49J Impact,  
a) Upper surface, 32mm from Impact  
b) Mid Plane, 32mm from Impact

## Chapter 8: Conclusions

The original aim of this work was to study impact wave propagation in cross ply composite plates by experimental investigation. The previous work by Green [27] had modelled a cross ply composite plate and produced an analytical solution to the wave dispersion equation which predicted the response at the surfaces and ply interfaces at a point in time of a cross ply composite plate due to a surface impulse. This previous work had shown the characteristics of stress waves propagated from a surface impulse were dependent of the angle of wave propagation between a plane wave front and the direction of the fibres in the inner core of the plate.

The requirements of this project was to detect and examine the stress waves generated from a surface impact at the surfaces and internal ply interfaces and to compare the results to analytical predictions to provide verification for the analytical solution of the material model.

The disturbances caused by the passing of stress waves in the plate were recorded by the piezo electric PVDF sensors. This sensor has shown advantages over more the convent measurement systems of strain gauges due to its frequency response into the GHz region and the high response removing the need for further amplification. The sensor also had an advantage over acoustic emission transducers due to its thickness which permitted the placement of the sensors inside the material during manufacture which enabled the study of the internal shear wave disturbances. The results presented in chapters 6 and 7 have shown good correlation between the measured speeds of disturbances travelling though the material and the calculated material wave speeds from the measured elastic properties.

The filtering of the sensor signals removed the low frequency component of the response due to the finite duration of the impact. This enabled the extraction of the higher frequency responses due to the disturbances caused by the passing of the stress waves.

The results from chapter 7 for the tests with different impact energies showed little difference in the responses, this showed that the filtering was removing the impact influence. This provided evidence that the comparison between the experimental data for a real impact and the analytical data which was for an ideal delta function impact was valid as the effects of the real impact had been removed from the experimental results.

It was reported by Balyis and Green [23] that the limiting wave velocity of the shear waves propagating through a cross ply composite plate was dependent of the lower of two wave speeds, the Rayleigh type surface wave speed ( $v_R$ ) and an internal shear wave speed ( $v_s$ ). It was been demonstrated analytical that the limiting wave velocity is dependent on the angle  $\gamma$  between the direction of wave propagation and the fibre direction at the mid plane of the plate, and that  $v_R = v_s$  at a critical angle  $\gamma_c$ .

The experimental results presented for the two cases examined of  $\gamma = 0^\circ$  and  $\gamma = 90^\circ$  showed the same wave propagation characteristics that when  $\gamma = 0^\circ$  which was less than the critical angle  $\gamma_c$  the slowest disturbance present was a large response on the upper surface whose speed matched that of a Rayleigh type surface wave. When  $\gamma = 90^\circ$  which was greater than the critical angle  $\gamma_c$  the slowest disturbance present occurred at the mid plane of the plate whose speed matched that of the  $c_2$  material wave speed. This showed that when  $\gamma = 0^\circ$  the limiting wave velocity was that of a Rayleigh type surface wave and that when  $\gamma = 90^\circ$  the limiting wave velocity was that of an internal shear wave. This provided some validity to the analytical solution as the same wave propagation characterises of the limiting wave velocities that had been observed from the analytical work were observed in the experimental study into impact wave propagation in cross ply composite plates.

Further Work.

There are several directions in which this work could be extended, the first is to examine the limiting wave velocities of a radial wave propagating out from a point load on a composite material. A radial wave travelling through a multi layered material provides a complex problem to the theoretical modelling of wave propagation as the wave front is moving in two dimensions as compared to the single direction propagation of a plane wave front. The complexity of the problem means that an experimental investigation into the surface and ply interface responses could easily provide insight into the characteristics of a radial wave propagating throughout a cross ply plate, in particular the examination of the internal ply interfaces.

A second area of work would be to increase the magnitude of the impacts to an extent that damage occurred. This would permit the examination of the internal wave propagation characteristics of a multi layered plate before and while the damage is generated. This would permit the examination into a relationship between the limiting wave velocity and the extent and direction of the ply delamination which occurs when a multi layered material is damaged by an impact.

### Chapter 9: References

- [1] Tsu-Wei Chou, McCullough L. and Byron Pipes R., '*Composites*' .
- [2] Ratwani M.M., '*Impact of Composite Materials on Advances Fighters*'. SAMPE Quarterly, Vol. 17, No. 2, January 1986, pp19-24.
- [3] Cantwell W.J and Morton J. '*The Impact Resistance of Composite Materials*'. Composites, Vol 2, No. 5, September 1991.
- [4] Mortimer R.W, Chou P.C. and Carleone J., '*Behavior of Laminated Composite Plates Subjected to Impact*', Forgen Object Impact Damage to Composites, ASTM STP 568, American Society for Testing and Materials, 1975, pp 173-182.
- [5] Schonberg W.P., '*Hypervelocity Impact Response of Spaced Composite Material Structures*'. Int. J. Impact Energy, Vol. 10, 1990, pp509-523.
- [6] Ujihashi S., Sakanoue K., Adachi T., Matsumoto H., '*Experimental Measurement of the Mechanical Properties of Fibre Reinforced Plastics Under Impact Loading*'. Fibre Reinforced Composites 90, C400/052, Proc. Inst. M.Eng, ISBN 085298 7161, 1990, pp157-162.
- [7] Kumar P. and Rai B. '*Impact Damage on Single Interface GFRP Laminates- An Experimental Study*'. Composite Structures Vol. 18, No. 1, 1991.
- [8] Cantwell W.J and Morton J. '*Comparison of the Low and High Velocity Impact Responses of CFRP*'. Composites, Vol 20, No. 6, November 1990
- [9] Park N., '*The Impact Response of Composites under Stress*'. Fibre Reinforced Composites 90, C400/019, Proc. Inst. M.Eng, ISBN 085298 7161, 1990, pp137-142.

Chapter 9: References

---

- [10] Qian Y., Swanson S.R., Nuismer R.J. and Bucinell R.B., '*An Experimental Study of Scaling Rules for Impact Damage in Fiber Composites*', J. of Composite materials, Vol. 24, May 1990.
- [11] Rayleigh, London Mathematical Soc. Proc. 17, 1887.
- [12] Kolsky H., '*Stress Waves in Solids*', Clarendon Press Oxford, 1953 (Dover reprint 1963)
- [13] Green W. A., '*Bending Waves in Strongly Anisotropic Elastic Plates*', J. Mech. appl. Maths., Vol XXXV, Pt. 4, 1982.
- [14] Kolsky H. and Mosquera J.M., '*Dynamic Loading of Fiber Reinforced Beams*', Mechanics of Behavior, Dvorak G.J. and Sheild R.T. Eds, Elsevier Science Publishers 1984.
- [15] Milkliwitz J., '*Modern problems in Elastic Wave Propagation*', Wiley, New York, 1978.
- [16] Ting T.C.T, Applied Mechanics Reviews, 33, pp1629-1635, 1980.
- [17] Chou T.S., J. Composite Materials, 5, pp306-319, 1971
- [18] Moon F.C., J. composite Materials, 6, pp62-79, 1972
- [19] Sun C.T., J. Composite Materials, 7, pp.366-382, 1973
- [20] Lui G.R., Tani J., Ohyoshi T. and Wantanabe, K., ASME Jour. of Vibration and Acoustics, pp230-238, 1991.
- [21] Lee J.D., Du S. and Liebowitz M., Computers and Structures, 19, pp807-812, 1984.

- [22] Balysis E.R. and Green W.A., '*Flexural Waves in Fibre-Reinforced Laminated Plates*', J. of Sound and Vibration Vol 110(1), pp1-26, 1986.
- [23] Balysis E.R. and Green W.A., '*Flexural Waves in Fibre-Reinforced Laminated Plates, Part II*', J. of Sound and Vibration Vol 111(2), pp181-190, 1986.
- [24] Green W.A. and Balysis E.R., '*The Contribution of High Harmonics to Transient Waves in Plates and Laminates*', Recent Advances in Structural Dynamics, Proc. of Third International Conference, ISBN 0-85432-2298
- [25] Green W.A. and Balysis E.R., '*Impact Stress Waves in Fibre-Reinforced Laminated plates*', Recent Advances in Structural Dynamics, Proc. of Third International Conference, ISBN 0-85432-2298.
- [26] Green W.A. and Green E.R., '*Stress Variation due to an Impact Line Load on a Four Ply Fibre Composite Plate*', Int. J. Solids Structures, Vol 25, No. 5, pp567-594, 1991.
- [27] Green E.R., '*Acoustic Emission from Internal Delamination of a Four-Ply Plate*', 1991
- [28] Green E.R. '*Transient Response of a Four-Ply Fiber Composite Laminated to an Internal Line Source*', Review of Progress in Quantitative Nondestructive Evaluation, 1990.
- [29] Green E.R., '*Transient Impact Response of a Fibre Composite Laminate*', Acta Mechanica 86, 1991 pp153-165,
- [30] Derieck J. and DechaeneR. '*Real Time Recording of Transverse Impact Experiments on Composite Laminates*'.

- [31] Fallstrom K.E., Lindgren L.E., Molin N.E. and Wahlin A. , '*Transient Bending Waves in Anisotropic Plates Studied by Hologram Interferometry*', *Experimental Mechanics*, December 1989, pp 409-413.
- [32] Sayir M., '*Flexural Vibrations of Strong Anisotropic Beams*', *Ing. Archiv.*, 49 (1980), pp309-330.
- [33] Daniel I.M. and Wooh S.C., '*Embedded Gauges for Study of Transient Deformations and Dynamic Fracture in Composites*', *Conf. Proc. SEM Fall Conference*, 1985, pp 62-68.
- [34] Takeda N., Sierakowski R.L. and Malvern L.E., '*Wave Propagation On Ballistically Impacted Composite Laminates*', *J. Composite Materials*, Vol 15, March 1981, p 157.
- [35] Khan A.S. and Hsiao C., '*On the Use of Electric Resistance Foil Strain Gauges for Plastic Wave Studies in Solids*', *Experimental Mechanics*, Vol 28, No. 3, September 1988, pp254-258
- [36] Gorman M.R., '*Plate Wave Acoustic Emissions in Composites*', *ibids* 107-134.
- [37] Guo N. and Crawley P., '*Lamb Waves for the NDE of Composite Materials*' *Review of Progress in Quantitative Nondestructive Evaluation*, Thompson D.O., Chimenti D.E. Eds., Vol 11, 1992, pp1443-1450.
- [38] Mal A.K., Gorman M.R. and Prosser W.H., '*Material Characterization of Composite Laminates Using Low-Frequency Plate Wave Dispersion Data*', *Review of Progress in Quantitative Nondestructive Evaluation*, Thompson D.O., Chimenti D.E. Eds., Vol 11, 1992, pp 1451-1458.

- [39] Wooh S.C. and Daniel I.M., '*Nondestructive Determination of Elastic Constants of Composite Materials*', Review of Progress in Quantitative Nondestructive Evaluation, Thompson D.O., Chimenti D.E. Eds., Vol 10B, 1991, pp 1445-1452.
- [40] Hutchins D.A., '*Pulsed Lasers For Quantitative Ultrasonic NDE*', Review of Progress in Quantitative Nondestructive Evaluation, Thompson D.O., Chimenti D.E. Eds., Vol 11, 1992, pp 561-1458.
- [41] Scudder L.P., Hutchins D.A., Mottram J.T., '*The Ultrasonic Impulse Response of Unidirectional Carbon Fibre Laminates*',
- [42] Brown L.F., Brown R.H., '*Permanently Mounted Piezo Film Sensors for Structural Quantitative NDE*', Review of Progress in Quantitative Nondestructive Evaluation, Thompson D.O., Chimenti D.E. Eds., Vol 10A, 1991, pp 853-859.
- [43] Green E.R. '*Propagation of Impact Induced Stress Waves in Composite Plates*', Dept. of Engineering, University of Leicester, Internal Report 92-20, 1992.
- [44] Wu T.T. and Ho Z.H., '*Anisotropic Wave Propagation to NDE of Composite Materials*', Experimental Mechanics, December 1990, pp 313-318.
- [45] Mal A.K. and Lih S.-S., '*Wave Field Produced in a Composite Laminate by a Concentrated Surface Force*', Review of Progress in Quantitative Nondestructive Evaluation, Thompson D.O., Chimenti D.E. Eds., Vol 11, 1992.
- [46] Hofstotter P. '*The Use of Encapsulated High Temperature Strain Gauges at Temperature*', Experimental Techniques, August 1985, pp24-29.
- [47] Green E.R. '*Short Duration Impact Loading on Fibre Composite Laminates*', 92/5 1992

- [48] Green E.R., '*The Effect of Different Impact Time Histories on the Response of a Fibre Composite Plate*' 91-13 1991.
- [49] Spencer A.J.M, '*Deformations of Fibre-Reinforced Materials*', OUP, 1972
- [50] Musgrave M.J.P, '*Crystal Acoustic - Introduction to the Study of Elastic Waves and Vibrations in Crystals*', Holden Day
- [51] Kakarala, S.N and Roche, J.L., 'Experimental Comparasion of Several Impact Test Methods', Intrrumented Impact Testing of Plastics and Composite Materials, ASTM STP 936, S. L. Kessler, G.C. Adams, S.B. Driscoll, and D.R. Ireland, Eds., America Society for Testing and Materials, Philadelphia, 1987, pp144-162.
- [52] Awang, M.N., '*Impact Testing of isotropic and anistropic plates*', Leicester University, Dept. of Engineering, Third Year Report, 1990.
- [53] '*Shock Waves and Hich Strain Rate Phenomena in Metals*', ISBN 0-306-40633-0.
- [54] Gause L.W., Buckley L.J. '*Impact Characterization of New Composite Materials*', Intrrumented Impact Testing of Plastics and Composite Materials, ASTM STP 936, S. L. Kessler, G.C. Adams, S.B. Driscoll, and D.R. Ireland, Eds., America Society for Testing and Materials, Philadelphia, 1987, pp248-261.
- [55] Takeda N., Sierakowski R.L.and Malvern, '*Studies of Impacted Glass fibre Reinforced Composite Laminates*', SAMPE Quarterly, Jan 1981, pp9-17.
- [56] Nusholtz G.S., Kaiker P.S., Lou Z. and Richter S.C., '*Pneumatic Ballistic Impact Device*', Exp. Techniques, July 1987.
- [57] Hofer B., '*Fiber optic damage detection in composite structures*', Proc. Review of Progress in Quantitative N.D.E., San Diego, 1982, pp1419-1430.

- [58] Crane R.N., Macander B.B., '*Fibre Optics for Damage Assessment for Fibre Reinforced Plastic Composite Structures*', Proc. Review of Progress in Quantitative N.D.E., San Diego, 1982, pp1419-1430.
- [59] Waite S.R., Tatam R.P, Jackson A.J., '*Use of Optical Fibre for Damage and Strain Detection in Composite Materials*', Composites, V19, No. 6, Nov 1988, pp435-442.
- [60] Butter C.D., '*Fibre Optic Strain Gauges*', Applied Optics, V17, No.18, Sept. 1987, pp2867-2869
- [61] Reddy M., Bennett K.D., Clause R.O., '*Imbedded Optical Fibre Sensors of Differential Strain in Composites*', Preprint of Review of progress in Quantitative N.D.E. Conf., San Diego, Aug. 1986.
- [62] Uttam D., Culshaw B., Ward J.D., Carter P., '*Interferometric Optical Fibre Strain Measurement*', J. Phys. Elec. Sci. Inst., 18, 1985, pp290-293.
- [63] Kawai H., Japan J. Appl. Phys. 8,975 (1969).
- [64] Penwalt PVDF Design Manual
- [65] Soutis C. and Turkman D., '*High Temperature Effects on the Compressive Strength of Glass Fibre Reinforced Composites*', ICCM 9, Ed. Miravete A., Madrid, Spain, 12-16 July, Vol 6, pp581-587.
- [66] Stone and Chatterjee, A.K. '*Impact Responses and Ultrasonic NDE*', (S.K. Datta, J.D. Achenbach and Y.D.S. Rajapakse, Eds), Elsevier, Amsterdam, pp285-294, 1990.
- [67] Redwood M., Mechanical Wave Guides, New York, Pergamon Press.

- [68] Cantwell W.J. and Morton J. '*Detection of Impact Damage in CRFP Laminates*', Composite Structures 3, pp241-257, 1985.
- [69] Sachse W., Castagnede B., Grabec I., Kim K.Y., Weaver R.L., '*Recent Developments in Quantitative Ultrasonic NDE of Composites*', Ultrasonics, Vol. 28, No 2, pp97-104, 1990.
- [70] Veidt M., Sachse W., '*Ultrasonic Point-source/Point-receiver measurements in Thin Specimens*', Journal of the Acoustical Society of America 1994, Vol. 96, No. 4, pp2318-2326.
- [71] Barcohen Y., Mal A.K., Lih S.S '*NDE of Composite Materials using Ultrasonic Oblique Insonification*', Materials Evaluation 1993, Vol.51, No.11, pp1285-1296
- [72] Hsu D.K., Hughes M.S., '*Simultaneous Ultrasonic Velocity and Sample Thickness Measurement and Application in Composites*', Journal of the Acoustical Society of America 1992, Vol.92, No.2, pp669-675.
- [73] Wu T.T., Ho Z.H., '*Anisotropic Wave Propagation and its Applications to NDE of Composite Materials*', Experimental Mechanics, 1990, Vol. 30 No. 4 pp313-318.
- [74] Mal A.K, Yin C.C., Barcohen Y., '*Analysis of Acoustic Pulses Reflected from Fiber Reinforced Composite Laminates*', J. of Applied Mechanics, Transactions of the ASME 1992, Vol.59, No. 2, pp S 136-S 144.
- [75] Prosser W.H and Gorman M.R., '*Plate Mode Velocities in Graphite/Epoxy Plates*', Journal of the Acoustic Society of America 1994, Vol.96 No.2 pp 902-907.
- [76] Guo N., Cawley P. '*The interaction of Lamb waves with Delaminations in Composite Laminates*', Journal of the Acoustic Society of America 1993, Vol.94, No.4, pp2240-2246.

Chapter 9: References

---

- [77] Guo N., Cawley P. '*Lamb Wave Propagation in Composite Laminates and its Relationship with Acousto-ultrasonics*', NDT & E International 1993, Vol.26, No.2 pp75-84.
- [78] '*Development of ASTM Guide for Acousto-Ultrasonics*', Materials Evaluation 199, Vol.49, No.5 p643.
- [79] Kim K.Y., Sachse W., '*Thin-Film Ultrasonics: Line and Point Sources and the Testing of Thin Metal Films*', Ultrasonics International 89 Conference Proceedings.
- [80] Cambell J.F., Vanderheiden E.G., Martinez L.A., Cairns D.S., Aballah M.G., '*A Multi Purpose Sensor for Composite Laminates Based on a Piezo Electric Film*'. Journal of Composite Materials, Vol.26, No.3 1992.
- [81] Chetwynd D.G. and Sachse W., '*Design of Micro-Hammer for Ultrasonic Source Applications*', Ultrasonics, 1991, Vol 29, Jan, pp 68 - 75

## Appendix 1: Analytical Analysis Computer Programs

### 1.1 Dispersion Equation Solution, Antisymmetric Motion.

```

C FIND ALL VALUES OF K IN 0<K<20 FOR OMEGA = 0 TO 20 STEP 0.02
C WITH GAMMA SQUARED = 4 FOR ANTISYMMETRIC DISPERSION EQUATION
PROGRAM CCOFA
IMPLICIT DOUBLE PRECISION(A-H,K,O-Z)
COMMON C2,C3,C4,C5,OM,SINHE,COSTHE,XI(12,12)
COMMON Q1,Q2,Q3,LQ1,LQ2,LQ3,XQ1,XQ2,XQ3,K1,K2,GB,DB
DIMENSION ROOT(60),DERIV(60),Z(11,11),COFACT(12)
DIMENSION WKSPE(11),UD(12)
C
C THE CALLING TREE OF THIS PROGRAM IS AS FOLLOWS -
C
C COMATW ..FINDR ..ROOTS ..DET
C SET CONSTANTS.
C
C READ IN ALL THE DATA NEEDED TO RUN
C C2,C3,C4,C5
C THETA
C (START OMEGA, FINISH OMEGA, STEP)*100
C ALIM, BLIM, RKLIM
C
C READ (1,*) C2,C3,C4,C5
C READ (1,*) THETA
C READ (1,*) I1,I2,I3
C READ (1,*) SR,FR,TR
C SC=0.0
C DO 250 I=1,50
C ROOT(I)=0.0
250 CONTINUE
C NREQ=20
C DO 20 IK=11,12,13
C PRINT*,IK
C READ(5,*)IK
C DO 20 IK=2,500,2
C OMEGA=IK/100.0D0
C READ(5,*.END=30) RKAY
C WRITE(6,300) OMEGA
C 300 FORMAT(' OMEGA SET TO',1PG14.6)
C PRINT*,FINDR IN
C CALL FINDR(OMEGA,THETA,SR,FR,TR, ROOT,NCOLL)
C PRINT*,FINDR OUT
C PRINT*,NCOLL
C WRITE(6,*) OMEGA,(ROOT(IROOT),IROOT=1,NREQ)
C WRITE(10,*) OMEGA,(ROOT(IROOT),IROOT=1,NREQ)
C 303 FORMAT(6E14.8,6E14.8)
C
C DO 25 ROOT=1,NCOLL
C IF (ROOT(IROOT),NE.0) THEN
C SC=SC+1
C WRITE(10,400) ROOT(IROOT),OMEGA
C 400 FORMAT(2E15.8)
C WRITE(6,125) SC
125 FORMAT(' NUMBER OF PASSES IS ',F5.1)
C ROOT(IROOT)=0.0
C ELSE
C END IF
25 CONTINUE
C
C THE DERIVATIVE IS NOW CALCULATED
C
C DO 233 I=1,60
C DERIV(I)=0.0
233 CONTINUE
C DO 15 I=1,NCOLL
C OP=OMEGA-0.00001
C OI=OMEGA+0.00001
C IF (ROOT(I).GT. OI .AND. ROOT(I).LT. OP) GO TO 15
C DRK=0.01
C DPREV=0.0
C DO 5 IHALF=1,20
C D=(DERIV(ROOT(I))+DRK)-DET(ROOT(I)-DRK)
C D=(2.0*DRK)
C DP=DET(ROOT(I))+DRK
C DM=DET(ROOT(I)-DRK)
C D=(DP-DM)/(2.0*DRK)
C WRITE(6,302) DP,DM,ROOT(I),D
C 302 FORMAT(' DP IS ',G13.5,DM IS ',G13.5,ROOT IS ',G13.5)
C WRITE(6,304) LDRK,D
C 304 FORMAT(' ROOT,I,DRK IS',G13.5,DERIV IS',G13.5)
C IF (ABS(DPREV-D).LT.0.0001*ABS(D)) GO TO 10
C DPREV=D
C DRK=0.5*DRK
5 CONTINUE
C STOP
C PRINT*, 'WARNING DERIVATIVE NOT CONVERGED'
10 DERIV(I)=D

```

## Appendix 1: Analytical Analysis Computer Programs

```

15 CONTINUE
C WRITE(3,301) OMEGA,(DERIV(I),I=1,NCOLL)
301 FORMAT(1P11G12,4)
C
C THE COFACTORS ARE NOW CALCULATED
C
DO 18 IROOT=1,NCOLL
RK=ROOT(IROOT)
IF (DERIV(IROOT).EQ.0.0D0) GOTO 18
D=DET(ROOT(IROOT))
C WRITE(6,*) D,ROOT(IROOT)
C
C RETURN FROM DET WITH D APPROX 0 AND ARRAY X HOLDING
C ELEMENTS OF 12 X 12 DETERMINANT
C
DO 100 L=1,12
DO 90 I=1,11
DO 80 J=1,11
J1=J-L
IF(J1.LT.13) GOTO 75
J1=J-12
75 Z(LJ)=X(I+(J1))
80 CONTINUE
90 CONTINUE
IA=11
N=11
IFAIL=1
CALL F03AAR(Z,IA,N,DT,WKSPCE,IFAIL)
C
C WHEN RK<1 DIFFERENT COFACTOR EQU USED TO COMPENSATE FOR
C THE SCALING OF RK IN DET TO AVOID ERROR
C
IF (RK.LT.1.0) THEN
COFACT(L)=-1**((L+1)*DT)*RK*DERIV(IROOT)
ELSE
COFACT(L)=-1**((L+1)*DT)/(DERIV(IROOT)*RK)
END IF
100 CONTINUE
IF (RK.LT.1.0) THEN
C FURTHER ADJUSTEMENT FOR SMALL RK
COFACT(2)=COFACT(2)/RK
COFACT(5)=COFACT(5)/RK
COFACT(8)=COFACT(8)/RK
COFACT(11)=COFACT(11)/RK
END IF
WRITE(11,400) OMEGA,ROOT(IROOT),(COFACT(L),L=1,12)
400 FORMAT(14G12,4)
18 CONTINUE
WRITE(6,410) OMEGA
410 FORMAT('FINISHED FOR OMEGA IS ',F10.2)
20 CONTINUE
30 STOP
END
SUBROUTINE FINDR(OMEGA,THETA,SR,FR,TR, ROOT,NCOLL)
IMPLICIT DOUBLE PRECISION(A-H,K,G-Z)
COMMON C2,C3,C4,C5,OM,SIN THE,COSTHE,XI(12,12)
DIMENSION ROOT(60),X(60)
EXTERNAL DET
C
C THIS SUBROUTINE RETURNS THE FIRST NREQ POSITIVE ROOTS OF THE
C EQUATION
C
C DET(RK) = 0
C
C IN THE ARRAY ROOT. THE SUBROUTINE WHICH ACTUALLY SOLVES
C THE EQUATION IS CALLED ROOTS. THIS FINDS ALL THE ROOTS
C IN A GIVEN INTERVAL OR ELSE RETURNS WITH AN ERROR
C INDICATION EITHER THAT THERE ARE TOO MANY ROOTS IN THE GIVEN
C INTERVAL OR THAT THEY COULD NOT BE FOUND
C WITH SUFFICIENT ACCURACY. IN EITHER OF THESE CASES, THE INTERVAL
C IS REPEATEDLY HALVED UNTIL A SUCCESSFUL RETURN IS OBTAINED. WE
C CONTINUE ALONG THE REAL AXIS UNTIL NREQ ROOTS HAVE BEEN
C COLLECTED.
C
OM=OMEGA
N=10
C
C NCOLL WILL HOLD THE NUMBER OF ROOTS COLLECTED SO FAR.
C RGLIM IS THE MAX VALUE THAT IS USED TO FIND THE ROOTS.
C IN AND ID ARE COUNTERS. IN COUNTS THE NUMBER OF PASSES
C WHEN IFAIL=0. ID COUNTS THE NUMBER OF PASSES WHEN IFAIL>0
C AND THE SEARCH FOR ROOTS IS REPEATED WITH A SMALLER INTERVAL.
C DMAX IS THE STANDARD VALUE OF DIFF, SO DIFF CAN BE RESET
C AFTER A SEARCH WITH A SMALLER INTERVAL HAS BEEN COMPLETED
C
CONV=ATAN(1.0D0)/45.0
TEMP=THETA*CONV
SIN THE=SIN(TEMP)
COSTHE=COS(TEMP)
C
NCOLL=0
ALIM=SR
BLIM=FR
RKLIM=TR

```

## Appendix 1: Analytical Analysis Computer Programs

```

IZ=0
IN=0
ID=0
C
C READ(3,*) ALIM,BLIM
C
C PRINT*,ALIM,BLIM,RKCLIM
C WRITE(6,*) ALIM,BLIM,RKCLIM
C
C DIFF=BLIM-ALIM
C DMAX=DIFF
C
C 30 IF (RKLIM .GT. ALIM) THEN
C
C IF (ALIM .GT. 1.0) THEN
C DMAX=1.0
C END IF
C
C IF DIFF HAS BEEN SUBDIVIDED THEN (ID+1) SUCCESSFUL PASSES
C MUST BE MADE TO ENSURE THAT NO ROOTS ARE MISSED, AND
C DIFF CAN BE RESET TO THE MAXIMUM VALUE. THE VALUE OF BLIM IS THEN
C CHANGED TO BE DMAX ABOVE THE CURRENT VALUE OF ALIM.
C
C IF (IN .EQ. (ID+1) .OR. ID .EQ. 0) THEN
C DIFF=DMAX
C BLIM=ALIM+DIFF
C IN=0
C ID=0
C END IF
C WRITE(6,*) DIFF,DMAX,ALIM
C
C DO 40 L=1,50
C
C PRINT*,ROOTS IN
C CALL ROOTS(DET,ALIM,BLIM,N, X,NROOTS,IFAIL)
C PRINT*,IFAIL
C IF (IFAIL .EQ. 0) THEN
C WRITE(6,300) ALIM,BLIM,NROOTS,(X(I),I=1,NROOTS)
C 300 FORMAT(' LIMITS ARE,IP2G14.5/ RETURNED WITH,I4,
C . ROOTS. THEY ARE/(1H,0P5F14.6)
C PRINT*,NROOTS
C IF (NROOTS .GT. 0) THEN
C DO 20 I=1,NROOTS
C NCOLL=NCOLL+1
C ROOT(NCOLL)=X(I)
C IZ=0
C 20 CONTINUE
C END IF
C
C COUNT THE NUMBER OF SUCCESSIVE RETURNS WITH NO ROOTS, AND NO
C SUBDIVIDING, THEN RETURN AFTER 3 TO SAVE CALCULATIONS.
C
C IF ((NROOTS .EQ. 0) .AND. (ID .EQ. 0)) THEN
C IZ=IZ+1
C END IF
C
C IF (IZ .EQ. 10) THEN
C WRITE(6,163) ALIM,OM,NCOLL
C 163 FORMAT(' NO MORE ROOTS TO BE FOUND AFTER 'F7.3,
C . ' FOR OMEGA =,F7.2,' NUMBER OF ROOTS FOUND =,I3)
C RETURN
C
C FINDR PROCEDURE STOPED AS NO MORE ROOTS
C
C END IF
C
C IF ALL THE ROOTS FOR THE CURRENT LIMITS ARE FOUND THEN NEW
C LIMITS ARE SELECTED AND THE PROCESS CONTINUES.
C
C ALIM=BLIM
C BLIM=ALIM+DIFF
C IN=IN+1
C GO TO 30
C
C BACK TO START OF FIND R PROCEDURE
C
C ELSE
C
C ERROR RETURN. HALVE INTERVAL AND TRY AGAIN.
C
C WRITE(6,301) ALIM,BLIM,IFAIL
C 301 FORMAT(' LIMITS ARE,IP2G14.5/ RETURNED WITH IFAIL =,I4)
C DIFF=0.5*DIFF
C BLIM=ALIM+DIFF
C ID=ID+1
C END IF
C 40 CONTINUE
C WRITE(6,304) OMEGA,ALIM
C 304 FORMAT(' IN SUBROUTINE FINDR, INTERVAL HAS BEEN HALVED TOO',
C 1 ' MANY TIMES FOR OMEGA =,F12.4/ SEARCHING FOR ROOTS IN THE',
C 2 ' INTERVAL STARTING AT,F12.4/, ABANDONED FOR THIS OMEGA,')
C DO 45 I=1,NCOLL

```

## Appendix 1: Analytical Analysis Computer Programs

```

ROOT(I)=0.0
45 CONTINUE
RETURN
C 50 GO TO 30
END IF
C WRITE(6,305) OMEGA
C 305 FORMAT(' IN SUBROUTINE FINDR, PROGRAM HAS SEARCHED THE ',
C 1 ' MAXIMUM NUMBER OF', I, ' INTERVALS AND FOUND ALL THE ',
C 2 ' POSSIBLE ROOTS. OMEGA =', F12.4, ' STOPPED FOR ',
C 3 ' THIS OMEGA. ')
DO 55 I=NCOLL+1,NREQ
ROOT(I)=0.0
55 CONTINUE
RETURN
END
SUBROUTINE ROOTS(FUN,ALIM,BLIM,N, X,NROOTS,IFAIL)
C THIS SUBROUTINE FINDS AN UNKNOWN NUMBER OF ROOTS OF THE EQUATION
C
C FUN(X) = 0
C
C BETWEEN THE LIMITS X = ALIM AND X = BLIM. THE ROOTS, NROOTS IN
C NUMBER, ARE RETURNED IN THE FIRST NROOTS ELEMENTS OF THE
C ARRAY X, DECLARED AS BEING OF LENGTH N. THE RETURNED VALUE OF
C INTEGER IFAIL INDICATES WHETHER THE ROUTINE HAS BEEN SUCCESSFUL
C (IFAIL = 0) OR NOT (IFAIL = 1 MEANS MORE THAN N ROOTS, IFAIL = 2
C MEANS THE ROUTINE COULD NOT DETERMINE HOW MANY ROOTS THERE ARE
C IN THE GIVEN INTERVAL. IFAIL = 3 MEANS THE NEWTON SECTION TO
C FIND THE ROOTS ACCURATELY DID NOT CONVERGE.) FOR ANY OF
C THESE ERROR RETURNS, IT IS SUGGESTED THE ROUTINE IS
C CALLED AGAIN WITH A SMALLER INTERVAL.
C
C THE WAY THE SUBROUTINE WORKS IS AS FOLLOWS. THE INTERVAL
C X = ALIM TO BLIM IS SPLIT INTO 2**L EQUAL SUB-INTERVALS AND
C THE FUNCTION IS EVALUATED AT THE 2**L+1 ENDPOINTS OF THESE
C SUB-INTERVALS. THESE FUNCTION VALUES ARE STORED IN THE
C ARRAY WORK. WE THEN LOOK FOR SIGN CHANGES BETWEEN SUCCESSIVE
C POINTS. IF THE SIGN OF THE FUNCTION CHANGES AND IF THE FUNCTION
C IS CONTINUOUS, THERE IS A ROOT BETWEEN THE POINTS. A CHECK IS
C MADE THAT THE FUNCTION DOES NOT HAVE A SINGULARITY BY USING
C THE VALUE OF THE FUNCTION'S DERIVATIVE. IF THERE IS NO
C SINGULARITY, IT IS ASSUMED THAT THE FUNCTION IS CONTINUOUS.
C THE ROOT IS APPROXIMATED BY THE SECANT METHOD AND THE NUMBER
C OF ROOTS FOUND IN THE INTERVAL (ALIM,BLIM) STORED IN NR(L).
C THIS PROCESS IS REPEATED FOR INCREASING L, THE LENGTH OF
C THE SUB-INTERVAL BEING HALVED EACH TIME.
C
C IF THE SUPPLIED FUNCTION DOES HAVE A SINGULARITY IN THE RANGE,
C IT IS ASSUMED THAT FUN IS DEFINED SO THAT THE PROGRAM DOES
C NOT ACTUALLY OVERFLOW AND END IN ERROR.
C
C IF, FOR 4 SUCCESSIVE VALUES OF L, THE NUMBER OF SIGN CHANGES
C REMAINS THE SAME, IT IS CONSIDERED THAT THE INTERVAL
C (ALIM,BLIM) HAS BEEN SUB-DIVIDED SUFFICIENTLY FINELY THAT
C ALL THE ROOTS HAVE BEEN OBTAINED. IF THE NUMBER OF SIGN
C CHANGES HAS NOT BECOME CONSTANT WHEN L REACHES ITS MAXIMUM
C ALLOWED VALUE (10), THE ROUTINE RETURNS WITH AN ERROR
C INDICATOR. IN THIS CASE, THE FUNCTION IS SEVERELY
C OSCILLATING AND IN ORDER TO FIND THE ROOTS, THE ROUTINE SHOULD BE
C CALLED AGAIN WITH A SMALLER INTERVAL.
C
IMPLICIT DOUBLE PRECISION(A-H,K,O-Z)
DIMENSION X(N),WORK(0:1024),NR(10)
ITOP=1024
DIFF=BLIM-ALIM
H=DIFF/ITOP
WORK(0)=FUN(ALIM)
C
C INITIALISE WORK ARRAY SO THAT LATER WE CAN CHECK WHETHER THE
C FUNCTION AT POINT I HAS ALREADY BEEN CALCULATED. THIS IS TO SAVE
C UNNECESSARY COMPUTATION.
C
DO 10 I=1,ITOP
WORK(I)=0.0
10 CONTINUE
DO 15 I=1,10
NR(I)=0
15 CONTINUE
DO 50 L=3,10
NR(L)=0
NSTEPS=2**L
INTRVL=ITOP/NSTEPS
STEP=INTRVL*H
DO 20 I=INTRVL,ITOP,INTRVL
XX=ALIM+I*H
C WRITE(6,*) XX
IF(WORK(I).EQ.0.0) WORK(I)=FUN(XX)
C WRITE(6,*) XX,WORK(I)
20 CONTINUE
DO 30 I=0,ITOP-1,INTRVL
IF(SIGN(1.0D0,WORK(I))*SIGN(1.0D0,WORK(I+INTRVL)) .LE. 0.0) THEN
C
C THERE HAS BEEN A SIGN CHANGE BETWEEN SUCCESSIVE POINTS CURRENTLY
C UNDER CONSIDERATION. NOW APPROXIMATE THE DERIVATIVE AT POINT I

```

## Appendix 1: Analytical Analysis Computer Programs

```

C BY ITS BACKWARD DIVIDED DIFFERENCE ...
C
C IF (.NE. 0) THEN
C   WRITE(6,*) WORK(I),WORK(I-INTRVL),STEP
C   DERIV=(WORK(I)-WORK(I-INTRVL))/STEP
C ELSE
C
C ... OR IN THE SPECIAL CASE OF I=0 WHERE THE BACKWARD DIFFERENCE
C IS NOT AVAILABLE, USE THE FORWARD DIFFERENCE INSTEAD.
C
C   DERIV=(WORK(INTRVL)-WORK(0))/STEP
C END IF
C IF(SIGN(1.0D0,WORK(I))*SIGN(1.0D0,DERIV) .LT. 0.0) THEN
C
C THERE HAS BEEN A CHANGE OF SIGN IN THE FUNCTION AND THE SIGN
C OF THE DERIVATIVE EXCLUDES A SINGULARITY. APPROXIMATE THE
C ROOT BY THE SECANT METHOD AND STORE IT IN THE X ARRAY.
C IF THERE IS ROOM.
C
C   NR(L)=NR(L)+1
C   IF(NR(L) .GT. N) THEN
C
C THIS ERROR RETURN MEANS THERE ARE MORE ROOTS THAN ARRAY X
C HAS ROOM FOR.
C
C   IFAIL=1
C   RETURN
C END IF
C   X(NR(L))=ALIM+I*H
C END IF
C END IF
30 CONTINUE
C   WRITE(6,300) L,ALIM,BLIM,NR(L),X(I),I=1,NR(L)
C300 FORMAT('L',I3,' INT (' ,F2G14.6,') SIGN CHANGES',I3,
C 1 ' AP ROOTS',(I1 ,0F5P13.6)/(I1 ,10F13.6)
C
C WE ARE LOOKING FOR 4 CONSECUTIVE EQUAL NR VALUES. IF L HAS
C ATTAINED THE VALUE OF 8 OR 9 AND NR(L-1) IS DIFFERENT FROM NR(L),
C THERE IS NO POINT IN CONTINUING TO LARGER L VALUES. SAVE WORK
C AND SKIP OUT EARLY WITH ERROR SETTING.
C
C IF(L .EQ. 8 .OR. L .EQ. 9) .AND. NR(L-1) .NE. NR(L) GO TO 60
C IF(L .GE. 9) THEN
C   IF(NR(L) .EQ. NR(L-3) .AND. NR(L) .EQ. NR(L-2) .AND.
C 1 NR(L) .EQ. NR(L-1)) THEN
C     IFAIL=0
C     NROOTS=NR(L)
C     GO TO 100
C   END IF
C END IF
50 CONTINUE
C
C IF WE DROP OUT THE BOTTOM OF DO-LOOP 50, IT MEANS THAT THE
C INTERVAL HAS BEEN SUB-DIVIDED AS FINELY AS POSSIBLE AND THAT
C THE NUMBER OF SIGN CHANGES HAS NOT YET SETTLED DOWN. RETURN
C WITH ERROR.
C
C 60 IFAIL=2
C   RETURN
100 CONTINUE
C
C WE CAN NOW FIND THE ROOTS MORE ACCURATELY BY THE SECANT METHOD
C WITH THE CONFIDENCE THAT WE HAVE GOOD ENOUGH STARTING POINTS
C FOR FAST CONVERGENCE TO THE CORRECT ROOT. WE KNOW THAT
C THE FUNCTION CHANGES SIGN BETWEEN X(I) AND X(I)+STEP, WHERE
C THE X ARRAY WAS SET IN THE FIRST HALF OF THIS SUBROUTINE.
C
C   TOL=DIFF**1.0E-10
C   IO=0
C
C IO IS A COUNTER FOR THE ROOT ARRAY X()
C
C DO 150 I=1,NROOTS
C   SP=STEP
155 XLEFT=X(I)
C   WRITE(6,*) SP
C   XRIGHT=XLEFT+SP
C   FLEFT=FUN(XLEFT)
C   FRIGHT=FUN(XRIGHT)
C
C TEST THAT FLEFT AND FRIGHT ARE OF DIFFERENT SIGNS AND THEREFOR
C EITHER SIDE OF THE ROOT
C
C   JL=0
C   JR=0
C   JLR=0
C   IF (FLEFT.GT.0.0) JL=1
C   IF (FRIGHT.GT.0.0) JR=1
C   JLR=(JL+JR)
C   IF (JLR.EQ.0.OR.JLR.EQ.2) THEN
C     GO TO 150
C   END IF
C

```

## Appendix 1: Analytical Analysis Computer Programs

```

C IF SIGNS ARE THE SAME THEN STOP SEARING FOR THIS ROOT
C AS ROOT IS IS NOT CORRECTLY EVALUATED AND THEREFOR WILL
C BE INCORRECT
C
C OLD C=XLEFT
C WRITE(6,351) XLEFT,FLEFT,XRIGHT,FRIGHT
C 351 FORMAT('ROOT BRACKETED BY,F14.8,(F=,G14.6) AND,0PF14.8,
C 1 (F=,1PG14.6)')
C FLR=FLEFT-FRIGHT
C WRITE(6,*) FLR
DO 110 K=1,20
C=XLEFT+(XRIGHT-XLEFT)*FLEFT/(FLEFT-FRIGHT)
IR=(ABS(C-OLD C),L.T.TOL) GO TO 120
FC=FUN(C)
C
C TEST TO FIND THE FUNCTION AT NEW C IS SAME AR LEFT OR RIGHT POINT
C
C IC=0
C IR=0
C IS=0
C IF (FC.GT.0.0) IC=1
C IF (FRIGHT.GT.0.0) IR=1
C IS=IC+IR
C
C IF FC AND FRIGHT ARE THE SAME SIGN THEN IS=2 OR 0
C IF FC AND FLEFT ARE THE SAME SIGN THEN IS=1
C
C IF (IS.EQ.1) THEN
C
C FUNCTION AT NEW C IS SAME SIGN AS AT LEFT POINT. REPLACE
C LEFT POINT.
C
C XLEFT=C
C FLEFT=FC
C ELSE
C
C FUNCTION AT NEW C IS SAME SIGN AS AT RIGHT POINT. REPLACE
C RIGHT POINT.
C
C XRIGHT=C
C FRIGHT=FC
C END IF
C OLD C=C
C WRITE(6,351) XLEFT,FLEFT,XRIGHT,FRIGHT
110 CONTINUE
C
C IF WE DROP OUT THE BOTTOM OF LOOP 110, IT MEANS THE ROOT
C HAS NOT BEEN FOUND ACCURATELY IN 20 ITERATIONS. WE
C SUPPOSE THIS WAS BECAUSE THE STARTING VALUE WAS NOT SUFFICIENTLY
C ACCURATE AND THAT THE NUMBER OF ROOTS IN THE INTERVAL WAS
C NOT AFTER ALL CORRECT. WE MUST HAVE HAD ACCIDENTAL AGREEMENT.
C RETURN WITH IFAIL = 3.
C
C IFAIL=3
C WRITE(6,*) IFAIL
C RETURN
120 JO=JO+1
C X(JO)=C
C WRITE(6,*) JO,X(JO)
C
C JO IS ONLY INCREMENTED IF A ROOT IS WRITTEN BACK TO X()
C
C 150 CONTINUE
C NROOTS=JO
C RETURN
C END
C DOUBLE PRECISION FUNCTION DET(RK)
C IMPLICIT DOUBLE PRECISION(A-H,K,O-Z)
C DIMENSION WKSPEC(12),Y(12,12)
C COMMON C2,C3,C4,C5,DM,SIN THE,COSTHE,X(11,12,12)
C COMMON Q1,Q2,Q3,LQ1,LQ2,LQ3,XQ1,XQ2,XQ3,K1,K2,GB,DB
C
C IF BLIM IS LESS THAN 1.0 THEN THE
C MATRIX COMPONENTS ARE DIVIDED BY RK (BY RV=1.0)
C OTHERWISE RV = RK, TO AVOID OVERFLOWS
C
C IF (RK.LT.1.0) THEN
C RV=1.0
C RS=RK
C ELSE
C RV=RK
C RS=1.0
C END IF
C
C VELCTY=OM/RV
C V=VELCTY**2
C K1=SIN THE*RS
C K2=COSTHE*RS
C SP2=K1*K1+(C3*K2*K2-V)/C2
C SQ2=K2*K2+(C3*K1*K1-V)/C2
C T1=(C3*K1*K1+C5*K2*K2-V)
C T2=(K1*K1+C3*K2*K2-V)
C T3=(C3+C4)**2*K2*K2
C Z2=T3-T1-T2*C3

```

## Appendix I: Analytical Analysis Computer Programs

```

Z3=TI *T2-T3*K1*K1
DISCR=SQR(Z2*Z2-4.0D0*C3*Z3)
Z1=2.0D0*C3
SP1=(-Z2-DISCR)/Z1
SP3=(-Z2+DISCR)/Z1
U1=(C3*K2*K2+C5*K1*K1-V)
U2=K2*K2+C3*K1*K1-V
U3=(C3+C4)**2*K1*K1
Z2=U3-U1-U2*C3
Z3=U1*U2-U3*K2*K2
DISCR=SQR(Z2*Z2-4.0D0*C3*Z3)
SQ1=(-Z2-DISCR)/Z1
SQ3=(-Z2+DISCR)/Z1
A=((K1*K1-SP1)+C3*K2*K2-V)/(C3+C4)
AB=((K2*K2-SQ1)+C3*K1*K1-V)/(C3+C4)
B=((K1*K1-SP3)+C3*K2*K2-V)/(C3+C4)
BB=((K2*K2-SQ3)+C3*K1*K1-V)/(C3+C4)
G=C3*A/C2-SQ2-K1*K1
GB=C3*AB/C2-SQ2-K2*K2
D=C3*(B-A)/C2+G
DB=C3*(BB-AB)/C2+GB
DO 210 L1=1,12
  DO 210 L2=1,12
    Y(L1,L2)=0
210 CONTINUE
C

IF (SP1.GT.0.0D0) THEN
  P1=SQR(SP1)
  LP1=1
  XP1=EXP(-P1*RV)
  XCP1=1.0D0
  XSP1=1.0D0
ELSE
  P1=SQR(-SP1)
  LP1=0
  XP1=1.0D0
  XCP1=COS(P1*RV)
  XSP1=SIN(P1*RV)
END IF
IF (SP2.GT.0.0D0) THEN
  P2=SQR(SP2)
  LP2=1
  XP2=EXP(-P2*RV)
  XSP2=1.0D0
  XCP2=1.0D0
ELSE
  P2=SQR(-SP2)
  LP2=0
  XP2=1.0D0
  XCP2=COS(P2*RV)
  XSP2=SIN(P2*RV)
END IF
IF (SP3.GT.0.0D0) THEN
  P3=SQR(SP3)
  LP3=1
  XP3=EXP(-P3*RV)
  XCP3=1.0D0
  XSP3=1.0D0
ELSE
  P3=SQR(-SP3)
  LP3=0
  XP3=1.0D0
  XCP3=COS(P3*RV)
  XSP3=SIN(P3*RV)
END IF
IF (SQ1.GT.0.0D0) THEN
  Q1=SQR(SQ1)
  LQ1=1
  XQ1=EXP(-Q1*RV)
  XCQ1=1.0D0
  XSQ1=1.0D0
ELSE
  Q1=SQR(-SQ1)
  LQ1=0
  XQ1=1.0D0
  XCQ1=COS(Q1*RV)
  XSQ1=SIN(Q1*RV)
END IF
IF (SQ2.GT.0.0D0) THEN
  Q2=SQR(SQ2)
  LQ2=1
  XQ2=EXP(-Q2*RV)
  XCQ2=1.0D0
  XSQ2=1.0D0
ELSE
  Q2=SQR(-SQ2)
  LQ2=0
  XQ2=1.0D0
  XCQ2=COS(Q2*RV)
  XSQ2=SIN(Q2*RV)
END IF
IF (SQ3.GT.0.0D0) THEN
  Q3=SQR(SQ3)

```

## Appendix 1: Analytical Analysis Computer Programs

```

LQ3=1
XQ3=EXP(-Q3*RV)
XSQ3=1.0D0
XCQ3=1.0D0

ELSE
Q3=SQRT(-SQ3)
LQ3=0
XQ3=1.6D0
XCQ3=COS(Q3*RV)
XSQ3=SIN(Q3*RV)

END IF
Y(1,1)=GB*K1
Y(1,2)=2.0D0*Q2*K2*LQ2
Y(1,3)=DB*K1
Y(1,4)=GB*K1*XQ1*LQ1
Y(1,5)=2.0D0*Q2*K2*XQ2
Y(1,6)=DB*K1*XQ3*LQ3
Y(3,1)=2.0D0*K1*K2*Q1*LQ1
Y(3,2)=(SQ2+K2*K2)
Y(3,3)=2.0D0*K1*K2*Q3*LQ3
Y(3,4)=2.0D0*K1*K2*Q1*XQ1
Y(3,5)=(SQ2+K2*K2)*XQ2*LQ2
Y(3,6)=2.0D0*K1*K2*Q3*XQ3
Y(2,1)=(K1*K1-AB)*Q1*LQ1*C3/C2
Y(2,2)=K1*K2*C3/C2
Y(2,3)=(K1*K1-BB)*Q3*LQ3*C3/C2
Y(2,4)=(AB-K1*K1)*Q1*XQ1*C3/C2
Y(2,5)=K1*K2*XQ2*LQ2*C3/C2
Y(2,6)=(BB-K1*K1)*Q3*XQ3*C3/C2
Y(4,1)=Q1*K1*XQ1*XSQ1
Y(4,2)=K2*XQ2*XCQ2
Y(4,3)=Q3*K1*XQ3*XSQ3
Y(4,4)=Q1*K1*XCQ1
Y(4,5)=K2*XSQ2
Y(4,6)=Q3*K1*XCQ3
Y(4,7)=P1*K2*LP1
Y(4,8)=K1
Y(4,9)=P3*K2*LP3
Y(4,10)=P1*K2*XP1
Y(4,11)=K1*XP2*LP2
Y(4,12)=P3*K2*XP3
Y(6,1)=K1*K2*XQ1*XCQ1
Y(6,2)=Q2*XQ2*XSQ2
Y(6,3)=K1*K2*XQ3*XCQ3
Y(6,4)=K1*K2*XSQ1
Y(6,5)=Q2*XCQ2
Y(6,6)=K1*K2*XSQ3
Y(5,7)=K1*K2
Y(5,8)=P2*LP2
Y(5,9)=K1*K2
Y(5,10)=K1*K2*XP1*LP1
Y(5,11)=P2*XP2
Y(5,12)=K1*K2*XP3*LP3
Y(5,1)=AB*XQ1*XCQ1
Y(5,3)=BB*XQ3*XCQ3
Y(5,4)=AB*XSQ1
Y(5,6)=BB*XSQ3
Y(6,7)=A
Y(6,9)=B
Y(6,10)=A*XP1*LP1
Y(6,12)=B*XP3*LP3
Y(7,1)=GB*K1*XQ1*XCQ1
Y(7,2)=2.0D0*Q2*K2*XQ2*XSQ2
Y(7,3)=DB*K1*XQ3*XCQ3
Y(9,1)=2.0D0*K1*K2*Q1*XQ1*XSQ1
Y(9,2)=(SQ2+K2*K2)*XQ2*XCQ2
Y(9,3)=2.0D0*K1*K2*Q3*XQ3*XSQ3
Y(8,1)=(AB-K1*K1)*Q1*XQ1*XCQ1*C3/C2
Y(8,2)=K1*K2*XQ2*XCQ2*C3/C2
Y(8,3)=(BB-K1*K1)*Q3*XQ3*XCQ3*C3/C2
Y(7,4)=GB*K1*XSQ1
Y(7,5)=2.0D0*Q2*K2*XCQ2
Y(7,6)=DB*K1*XSQ3
Y(9,4)=2.0D0*K1*K2*Q1*XQ1*XCQ1
Y(9,5)=(SQ2+K2*K2)*XSQ2
Y(9,6)=2.0D0*K1*K2*Q3*XQ3*XCQ3
Y(8,4)=(K1*K1-AB)*Q1*XQ1*C3/C2
Y(8,5)=K1*K2*XSQ2*C3/C2
Y(8,6)=(K1*K1-BB)*Q3*XQ3*C3/C2
Y(7,7)=G*K2
Y(7,8)=2.0D0*P2*K1*LP2
Y(7,9)=D*K2
Y(8,7)=2.0D0*K1*K2*P1*LP1
Y(8,8)=(SP2+K1*K1)
Y(8,9)=2.0D0*K1*K2*P3*LP3
Y(9,7)=(K2*K2-A)*P1*LP1*C3/C2
Y(9,8)=K1*K2*C3/C2
Y(9,9)=(K2*K2-B)*P3*LP3*C3/C2
Y(7,10)=G*K2*XP1*LP1
Y(7,11)=2.0D0*P2*K1*XP2
Y(7,12)=D*K2*XP3*LP3
Y(8,10)=2.0D0*K1*K2*P1*XP1
Y(8,11)=(SP2+K1*K1)*XP2*LP2
Y(8,12)=2.0D0*K1*K2*P3*XP3

```

## Appendix 1: Analytical Analysis Computer Programs

```

Y(9,10)=P1*(K2*K2-A)*XP1*C3/C2
Y(9,11)=-K1*K2*XP2*LP2*C3/C2
Y(9,12)=-P3*(K2*K2-B)*XP3*C3/C2
Y(10,7)=-XP1*K1*K2*XCP1
Y(10,8)=-XP2*P2*XSP2
Y(10,9)=-K1*K2*XP3*XCP3
Y(10,10)=-K1*K2*XSP1
Y(10,11)=-P2*XCP2
Y(10,12)=-K1*K2*XSP3
Y(11,7)=-A*XP1*XCP1
Y(11,9)=-B*XP3*XCP3
Y(11,10)=-A*XSP1
Y(11,12)=-B*XSP3
Y(12,7)=-G*K2*XP1*XCP1
Y(12,8)=-2.0D0*P2*K1*XP2*XSP2
Y(12,9)=-D*K2*XP3*XCP3
Y(12,10)=-G*K2*XSP1
Y(12,11)=-2.0D0*P2*K1*XCP2
Y(12,12)=-D*K2*XSP3
DO 500 I=1,12
DO 600 J=1,12
X1(I,J)=Y(I,J)
600 CONTINUE
500 CONTINUE
N=12
L=12
IFAIL=1
CALL F03AAR(Y,IA,N,DET,WKSPCE,IFAIL)
IF(IFAIL.EQ.0) GOTO 1000
1000 RETURN
END

```

### 1.2 Dispersion Equation, Symmetric Motion

Since the procedure for the solution to the dispersion equation was the same for the antisymmetric and the symmetric motion, only the subroutine concerned with the symmetric motion matrix is presented here.

```

DOUBLE PRECISION FUNCTION DET(RK)
IMPLICIT DOUBLE PRECISION(A-H,K,O-Z)
DIMENSION WKSPCE(12),Y(1,2,12)
COMMON C2,C3,C4,C5,OM,SIN THE,COSTHE,X1(12,12)
COMMON Q1,Q2,Q3,LQ1,LQ2,LQ3,XQ1,XQ2,XQ3,K1,K2,GB,DB
C
C IF BLIM IS LESS THAN 1.0 THEN THE
C MATRIX COMPONENTS ARE DIVIDED BY RK (BY RV=1.0)
C OTHERWISE RV = RK, TO AVOID OVERFLOWS
C
IF (RK.LT.1.0) THEN
RV=1.0
RS=RK
ELSE
RV=RK
RS=1.0
END IF
C
VELCTY=OM/RV
V=VELCTY**2
K1=SIN THE*RS
K2=COSTHE*RS
SP2=K1*K1+(C3*K2*(2-V)/C2
SQ2=-K2*K2+(C3*K1*K1-V)/C2
T1=(C3*K1*K1+C5*K2*(2-V)
T2=(K1*K1+C3*K2*(2-V)
T3=(C3+C4)**2*K2*K2
Z2=T1-T2-T3*C3
Z3=T1*T2-T3*K1*K1
DISCR=SQRT(Z2*Z2-4.0D0*C3*Z3)
Z1=-2.0D0*C3
SP1=(-Z2-DISCR)/Z1
SP3=(-Z2+DISCR)/Z1
U1=(C3*K2*(2-V)+C5*K1*(1-V)
U2=-K2*(2+C3)*K1*(1-V)
U3=(C3+C4)**2*K1*K1
Z2=U3-U1-U2*C3
Z3=U1*U2-U3*K2*K2
DISCR=SQRT(Z2*Z2-4.0D0*C3*Z3)
SQ1=(-Z2-DISCR)/Z1
SQ3=(-Z2+DISCR)/Z1
A=(K1*K1-SP1)*C3*K2*(2-V)/(C3+C4)
AB=((K2*(2-SQ1)+C3*K1*(1-V)/(C3+C4)
B=((K1*(1-SP3)+C3*(K2*(2-V)/(C3+C4)
BB=((K2*(2-SQ3)+C3*K1*(1-V)/(C3+C4)
G=C3*A/C2-SP2-K1*K1
GB=C3*AB/C2-SQ2-K2*K2
D=C3*(B-A)/C2+G
DB=C3*(BB-AB)/C2+GB
DO 210 L1=1,12
DO 210 L2=1,12

```

## Appendix I: Analytical Analysis Computer Programs

```

Y(L1,L2)=0
210 CONTINUE
C
IF (SP1.GT.0.0D0) THEN
    P1=SQRT(SP1)
    LP1=1
    XP1=EXP(-P1*RV)
    XCP1=1.0D0
    XSP1=1.0D0
ELSE
    P1=SQRT(-SP1)
    LP1=0
    XP1=1.0D0
    XCP1=COS(P1*RV)
    XSP1=SIN(P1*RV)
END IF
IF (SP2.GT.0.0D0) THEN
    P2=SQRT(SP2)
    LP2=1
    XP2=EXP(-P2*RV)
    XCP2=1.0D0
    XSP2=1.0D0
ELSE
    P2=SQRT(-SP2)
    LP2=0
    XP2=1.0D0
    XCP2=COS(P2*RV)
    XSP2=SIN(P2*RV)
END IF
IF (SP3.GT.0.0D0) THEN
    P3=SQRT(SP3)
    LP3=1
    XP3=EXP(-P3*RV)
    XCP3=1.0D0
    XSP3=1.0D0
ELSE
    P3=SQRT(-SP3)
    LP3=0
    XP3=1.0D0
    XCP3=COS(P3*RV)
    XSP3=SIN(P3*RV)
END IF
IF (SQ1.GT.0.0D0) THEN
    Q1=SQRT(SQ1)
    LQ1=1
    XQ1=EXP(-Q1*RV)
    XCQ1=1.0D0
    XSQ1=1.0D0
ELSE
    Q1=SQRT(-SQ1)
    LQ1=0
    XQ1=1.0D0
    XCQ1=COS(Q1*RV)
    XSQ1=SIN(Q1*RV)
END IF
IF (SQ2.GT.0.0D0) THEN
    Q2=SQRT(SQ2)
    LQ2=1
    XQ2=EXP(-Q2*RV)
    XCQ2=1.0D0
    XSQ2=1.0D0
ELSE
    Q2=SQRT(-SQ2)
    LQ2=0
    XQ2=1.0D0
    XCQ2=COS(Q2*RV)
    XSQ2=SIN(Q2*RV)
END IF
IF (SQ3.GT.0.0D0) THEN
    Q3=SQRT(SQ3)
    LQ3=1
    XQ3=EXP(-Q3*RV)
    XCQ3=1.0D0
    XSQ3=1.0D0
ELSE
    Q3=SQRT(-SQ3)
    LQ3=0
    XQ3=1.0D0
    XCQ3=COS(Q3*RV)
    XSQ3=SIN(Q3*RV)
END IF
Y(1,1)=GB*K1
Y(1,2)=2.0D0*Q2*K2*LQ2
Y(1,3)=DB*K1
Y(1,4)=GB*K1*XQ1*LQ1
Y(1,5)=2.0D0*Q2*K2*XQ2
Y(1,6)=DB*K1*XQ3*LQ3
Y(3,1)=2.0D0*K1*K2*Q1*LQ1
Y(3,2)=(SQ2+K2*K2)
Y(3,3)=2.0D0*K1*K2*Q3*LQ3
Y(3,4)=2.0D0*K1*K2*Q1*XQ1
Y(3,5)=(SQ2+K2*K2)*XQ2*LQ2
Y(3,6)=2.0D0*K1*K2*Q3*XQ3

```

Appendix 1: Analytical Analysis Computer Programs

$Y(2,1)=(K1*K1-AB)*Q1*LQ1*C3/C2$   
 $Y(2,2)=K1*K2*C3/C2$   
 $Y(2,3)=(K1*K1-BB)*Q3*LQ3*C3/C2$   
 $Y(2,4)=(AB-K1*K1)*Q1*XQ1*C3/C2$   
 $Y(2,5)=K1*K2*XQ2*LQ2*C3/C2$   
 $Y(2,6)=(BB-K1*K1)*Q3*XQ3*C3/C2$   
 $Y(4,1)=Q1*K1*XSQ1$   
 $Y(4,2)=K2*XQ2*XCQ2$   
 $Y(4,3)=Q3*K1*XQ3*XSQ3$   
 $Y(4,4)=Q1*K1*XCQ1$   
 $Y(4,5)=K2*XSQ2$   
 $Y(4,6)=Q3*K1*XCQ3$   
 $Y(4,7)=P1*K2*LP1$   
 $Y(4,8)=K1$   
 $Y(4,9)=P3*K2*LP3$   
 $Y(4,10)=P1*K2*XP1$   
 $Y(4,11)=K1*XP2*LP2$   
 $Y(4,12)=P3*K2*XP3$   
 $Y(6,1)=K1*K2*XQ1*XCQ1$   
 $Y(6,2)=Q2*XQ2*XSQ2$   
 $Y(6,3)=K1*K2*XQ3*XCQ3$   
 $Y(6,4)=K1*K2*XSQ1$   
 $Y(6,5)=Q2*XCQ2$   
 $Y(6,6)=K1*K2*XSQ3$   
 $Y(5,7)=K1*K2$   
 $Y(5,8)=P2*LP2$   
 $Y(5,9)=K1*K2$   
 $Y(5,10)=K1*K2*XP1*LP1$   
 $Y(5,11)=P2*XP2$   
 $Y(5,12)=K1*K2*XP3*LP3$   
 $Y(5,1)=AB*Q1*XCQ1$   
 $Y(5,3)=BB*XQ3*XCQ3$   
 $Y(5,4)=AB*XSQ1$   
 $Y(5,6)=BB*XSQ3$   
 $Y(6,7)=A$   
 $Y(6,9)=B$   
 $Y(6,10)=A*XP1*LP1$   
 $Y(6,12)=B*XP3*LP3$   
 $Y(7,1)=GB*K1*XQ1*XCQ1$   
 $Y(7,2)=2.0D0*Q2*K2*XQ2*XSQ2$   
 $Y(7,3)=DB*K1*XQ3*XCQ3$   
 $Y(9,1)=2.0D0*K1*K2*Q1*XQ1*XSQ1$   
 $Y(9,2)=(SQ2+K2*K2)*XQ2*XCQ2$   
 $Y(9,3)=2.0D0*K1*K2*Q3*XQ3*XSQ3$   
 $Y(8,1)=(AB-K1*K1)*Q1*XQ1*XSQ1*C3/C2$   
 $Y(8,2)=K1*K2*XQ2*XCQ2*C3/C2$   
 $Y(8,3)=(BB-K1*K1)*Q3*XQ3*XSQ3*C3/C2$   
 $Y(7,4)=GB*K1*XSQ1$   
 $Y(7,5)=2.0D0*Q2*K2*XCQ2$   
 $Y(7,6)=DB*K1*XSQ3$   
 $Y(9,4)=2.0D0*K1*K2*Q1*XCQ1$   
 $Y(9,5)=(SQ2+K2*K2)*XSQ2$   
 $Y(9,6)=2.0D0*K1*K2*Q3*XCQ3$   
 $Y(8,4)=(K1*K1-AB)*Q1*XCQ1*C3/C2$   
 $Y(8,5)=K1*K2*XSQ2*C3/C2$   
 $Y(8,6)=(K1*K1-BB)*Q3*XQ3*XCQ3*C3/C2$   
 $Y(7,7)=D*K2$   
 $Y(7,8)=2.0D0*P2*K1*LP2$   
 $Y(7,9)=D*K2$   
 $Y(8,7)=2.0D0*K1*K2*P1*LP1$   
 $Y(8,8)=(SP2+K1*K1)$   
 $Y(8,9)=2.0D0*K1*K2*P3*LP3$   
 $Y(9,7)=(K2*K2-A)*P1*LP1*C3/C2$   
 $Y(9,8)=K1*K2*C3/C2$   
 $Y(9,9)=(K2*K2-B)*P3*LP3*C3/C2$   
 $Y(7,10)=G*K2*XP1*LP1$   
 $Y(7,11)=2.0D0*P2*K1*XP2$   
 $Y(7,12)=D*K2*XP3*LP3$   
 $Y(8,10)=2.0D0*K1*K2*P1*XP1$   
 $Y(8,11)=(SP2+K1*K1)*XP2*LP2$   
 $Y(8,12)=2.0D0*K1*K2*P3*XP3$   
 $Y(9,10)=P1*(K2*K2-A)*XP1*C3/C2$   
 $Y(9,11)=K1*K2*XP2*LP2*C3/C2$   
 $Y(9,12)=P3*(K2*K2-B)*XP3*C3/C2$   
 $Y(10,7)=XP1*P1*K2*XSQ1$   
 $Y(10,8)=XP2*K1*XCQ2$   
 $Y(10,9)=XP3*P3*K2*XSQ3$   
 $Y(10,10)=P1*K2*XCQ1$   
 $Y(10,11)=K1*XSQ2$   
 $Y(10,12)=P3*K2*XCQ3$   
 $Y(11,7)=2.0D0*K1*K2*P1*XP1*XSQ1$   
 $Y(11,8)=(SP2+K1*K1)*XP2*XCQ2$   
 $Y(11,9)=2.0D0*K1*K2*P3*XP3*XSQ3$   
 $Y(11,10)=2.0D0*K1*K2*P1*XCQ1$   
 $Y(11,11)=(SP2+K1*K1)*XSQ2$   
 $Y(11,12)=2.0D0*K1*K2*P3*XCQ3$   
 $Y(12,7)=(K2*K2-A)*P1*XP1*XSQ1*C3/C2$   
 $Y(12,8)=K1*K2*XCQ2*XP2*C3/C2$   
 $Y(12,9)=(K2*K2-B)*P3*XP3*XSQ3*C3/C2$   
 $Y(12,10)=(A-K2*K2)*P1*XCQ1*C3/C2$   
 $Y(12,11)=K1*K2*XSQ2*C3/C2$   
 $Y(12,12)=(B-K2*K2)*P3*XCQ3*C3/C2$   
 DO 500 I=1,12  
 DO 600 J=1,12

## Appendix 1: Analytical Analysis Computer Programs

```
X1(IJ)=Y(IJ)
600 CONTINUE
500 CONTINUE
  N=12
  IA=12
  IFAIL=1
  CALL F03AARY,IA,N,DET,WKSPCE,IFAIL)
  IF(FAIL.EQ.0) GOTO 1000
1000 RETURN
  END
```

### 1.3 Surface Strains in the Direction of Wave Propagation

```
PROGRAM STCOD
IMPLICIT DOUBLE PRECISION(A-H,O-Z)
DIMENSION WA(30000),WS(30000),VA(30000),VS(30000)
DIMENSION FWA(1000),FWS(1000),FVA(1000),FVS(1000)
DIMENSION RKAY(65),AC(12),OM(2000),G(1),NAS(800),NSS(800)
COMMON C2,C3,C4,C5,NAS,NSS
C
C CALCULATING STRAIN V TIME FROM COFACTORS
C UPPER AND LOWER SURFACE STRAIN IN X DIRECTION FOR A DISTANCE XL
C FROM THE DISPLACEMENTS IN THE X2 AND X3 DIRECTION
C
  READ(3,*) X,LIM,TM,THETA,H
  READ(3,*) C2,C3,C4,C5,C1R
  CONV=ATAN(1.0D0)/45.0
  TEMP=THETA*CONV
  AK1=SIN(TEMP)
  AK2=COS(TEMP)
  WRITE(6,*) THETA,CONV,TEMP,AK1,AK2
  TS=TM
C
C CALCULATING TIME CONSTANT
C TC=(H/C1R)*1E6
  TC=1.0
C CALCULATED CONSTANTS
  PI=4.0D0*ATAN(1.0D0)
  HF1=PI/2.0D0
  XL=X+1.25
C
C CONSTANT FOR CALCULATING G1
C ZC=SIN(0.138D0*X)/(X*0.14D0)
C
  DO 47 K=1,700
    FWA(K)=0.0
    FWS(K)=0.0
    FVA(K)=0.0
    FVS(K)=0.0
  47 CONTINUE
  CALL NROGT(NAS,NSS)
  DO 50 KW=1,700
    e WRITE(6,*) NAS(KW)
  c
  c SUM FOR ANTISYMMETRIC WAVE
  C
  NC=NAS(KW)
  DO 40 J=1,NC
  C UL=0.0
  C LL=0.0
  DO 20 I=1,12
    AC(I)=0
  20 CONTINUE
  READ(1,*,END=1) OM(KW),RKAY(J),(AC(I),I=1,12)
  OG=OM(KW)
  RKI=RKAY(J)
  e IF (OGLT.0.05) GOTO 50
  e WRITE(6,*) OM(KW),RKAY(J),(AC(I),I=1,12)
  C
  CALL RESD(RK,AC,OG,THETA,RV,RW)
  C WRITE (6,*) OG,RK,RU
  C
  C FOR EACH VALUE OF K=0.02 TO 20 IN STEPS OF 0.02
  C FIND THE SUM OF RES*SIN(K*X), X IS 40 OR 200,
  C LIM IS ROUGHLY 10*X/PI AND TM IS PI/20
  C
  FWA(KW)=FWA(KW)+RW*(SIN(RK*XL)-SIN(RK*X))
  FVA(KW)=FVA(KW)+RV*(SIN(RK*XL)-SIN(RK*X))
  e WRITE(6,*) FWA(KW),FVA(KW)
  C
  40 CONTINUE
  C
  C SUM FOR SYMMETRIC WAVE
  C
  C IF (KW.NE.1) THEN
  C READ(7,*) NSW
  NC=NSS(KW)
  41 DO 45 J=1,NC
    RKAY(J)=0
    DO 30 I=1,12
```

## Appendix 1: Analytical Analysis Computer Programs

```

ACI)=0
30 CONTINUE
C   UL=0.0
C   LL=0.0
READ(2,*)END=50 OM(KW),RKAY(J),(AC(I),I=1,12)
C   WRITE(6,*) OM(KW)
C
C CHECK THAT THE OMEGA VALUE USED FOR ANTISYMMETRIC AND
C SYMMETRIC ARE THE SAME
C
IF (OG.NE.OM(KW)) THEN
  WRITE(6,*) OG,OM(KW)
  STOP
C IF (OG.GT.OM(KW)) THEN
C   BACKSPACE(1)
C   BACKSPACE(4)
C   ELSE
C   BACKSPACE(2)
C   BACKSPACE(7)
C   END IF
C   GOTO 50
END IF
RK=RKAY(J)
C
CALL RESD(RK,AC,OG,THETA,RV,RW)
C
WRITE(14,*) OG,RK,RV,RW
420 FWS(KW)=FWS(KW)+RW*(SIN(RK*XL)-SIN(RK*X))
FVS(KW)=FVS(KW)+RV*(SIN(RK*XL)-SIN(RK*X))
C
45 CONTINUE
C
C   ELSE
C   FWS(KW)=0.0
C   END IF
C   WINDOWING
C48 C=0.54+0.46*COS(KW*0.00314159)
C   FWA(KW)=FWA(KW)*C
C   FWS(KW)=FWS(KW)*C
C   FVA(KW)=FVA(KW)*C
C   FVS(KW)=FVS(KW)*C
C
C CALCULATION FOR FREQUENCY PLOTS
C
C   OGR=(OM(KW)*CIR)/(H*2.0D0*PI)
C   FU=DABS(FWA(KW))+FWS(KW)
C   FL=DABS(FVA(KW))+FVS(KW)
C
C   OUTPUT FOR FREQUENCY PLOTS
C
WRITE(10,310) OGR,FU
WRITE(11,310) OGR,FL
C
310 FORMAT(2(G15.6))
C   WRITE(12,*) OG,FWA(KW),FWS(KW)
C
50 CONTINUE
C
C NOW FIND THE CORRESPONDING VALUES AT K=0.
C AT K=0, THE RESIDUES ARE NEGLIGIBLE BUT FOR THE
C FUNDAMENTAL MODE OF THE ANTISYMMETRIC MOTION.
C HERE, THE RES=-T*C2/(4*C1) WHERE T=C1*PI/H.
C TO USE THE TRAPEZIUM RULE NEED THE FIRST TERM HALVED.
C
C THE FACTOR WAS WRONG AND SHOULD BE -.C2SQ/(4*C1SQ)
C AND THEN HALVED
C
C
C   G(1)=-0.02909*TM
C
C SINCE U IS EVEN IN K, FIND THE SUM OF FA(K)*COS(K*X)
C FOR EACH VALUE OF T FROM 0 TO T IN STEPS OF 2*PI/20.
CC
C FIND THE SUM OF FWA(KW)*(1-COS(OM(KW)*TM))
C FOR EACH VALUE OF X FROM 0 TO T IN STEPS OF 2*PI/20.
C
C
DO 70 L=1,LIM
  WA(L)=0.0
  WS(L)=0.0
  VA(L)=0.0
  VS(L)=0.0
  DO 60 KW=1,700
    CY=(1-COS(OM(KW)*TM))
    SY=SIN(OM(KW)*TM)
    WA(L)=WA(L)+(FWA(KW)*SY)
    WS(L)=WS(L)+(FWS(KW)*SY)
    VA(L)=VA(L)+(FVA(KW)*SY)
    VS(L)=VS(L)+(FVS(KW)*SY)
  C
  C
60 CONTINUE
C

```

## Appendix 1: Analytical Analysis Computer Programs

```

C FOR U.S. NEED WA+WS. FOR L.S. NEED UA-US.
C MULT BY DELTA K = 0.02. TO BE CONSISTENT WITH
C PREVIOUS GRAPHS, SCALE FURTHER BY 2*C1SQ/C2SQ
C 0.02**2*C1SQ/C2SQ = 0.14
C
TP=(AK1*(VA(L)+VS(L))+AK2*(WA(L)+WS(L)))*0.17187
BS=(AK1*(VA(L)-VS(L))+AK2*(WA(L)-WS(L)))*0.17187
C WRITE(6,*) US,BS
WRITE(8,300) TM*TC,TP
WRITE(9,300) TM*TC,BS
TM=TM*TS
300 FORMAT(2(G15.6))
70 CONTINUE
STOP
END
SUBROUTINE RESD(RK,AC,OG,THETA,RV,RW)
IMPLICIT DOUBLE PRECISION(A-H,O-Z)
DIMENSION AC(12)
COMMON C2,C3,C4,C5
OM=OG
CONV=ATAN(1.0D0)/45.0
TEMP=THETA*CONV
AK1=SIN(TEMP)
AK2=COS(TEMP)
C WRITE(6,*) AK1,AK2
SAK1=AK1*AK1
SAK2=AK2*AK2
VELCTV=OM/RK
V=VELCTV**2
Z1=2.0D0*C3
U3=(C3+C4)**2*SAK1
SQ2=SAK2+(C3*SAK1-V)/C2
U1=(C3*SAK2+C5*SAK1-V)
U2=SAK2+C3*SAK1-V
Z2=U3-U1-U2*C3
Z3=U1*U2-U3*SAK2
DISCR=SQRT(Z2**2-4.0D0*C3*Z3)
SQ1=(-Z2-DISCR)/Z1
SQ3=(-Z2+DISCR)/Z1
AB=(SAK2-SQ1)+C3*SAK1-V/(C3+C4)
BB=(SAK2-SQ3)+C3*SAK1-V/(C3+C4)
GB=C3*AB/C2-SQ2*SAK2
DB=C3*(BB-AB)/C2+GB
IF (SQ1.GT.0.0D0) THEN
    Q1=SQRT(SQ1)
    LQ1=1
    XQ1=EXP(-Q1 *RK)
    XCQ1=1.0D0
    XSQ1=1.0D0
ELSE
    Q1=SQRT(-SQ1)
    LQ1=0
    XQ1=1.0D0
    XCQ1=COS(Q1 *RK)
    XSQ1=SIN(Q1 *RK)
END IF
IF (SQ2.GT.0.0D0) THEN
    Q2=SQRT(SQ2)
    LQ2=1
    XQ2=EXP(-Q2 *RK)
    XCQ2=1.0D0
    XSQ2=1.0D0
ELSE
    Q2=SQRT(-SQ2)
    LQ2=0
    XQ2=1.0D0
    XCQ2=COS(Q2 *RK)
    XSQ2=SIN(Q2 *RK)
END IF
IF (SQ3.GT.0.0D0) THEN
    Q3=SQRT(SQ3)
    LQ3=1
    XQ3=EXP(-Q3 *RK)
    XCQ3=1.0D0
    XSQ3=1.0D0
ELSE
    Q3=SQRT(-SQ3)
    LQ3=0
    XQ3=1.0D0
    XCQ3=COS(Q3 *RK)
    XSQ3=SIN(Q3 *RK)
END IF
C
C WRITING OUT THE RESIDUES CORRESPONDING TO U
C WRITE(6,*) AC(2),AK2,XQ2,LQ2,AC(5)
C
C SURFACE STRAIN
C
RW=AK1*AK2*AC(1)-Q2*LQ2*AC(2)+AK1*AK2*AC(3)
+AK1*AK2*XQ1*LQ1*AC(4)+Q2*XQ2*AC(5)+AK1*AK2*XQ3*LQ3*AC(6)
C
RV=AB*AC(1)-BB*AC(3)-AB*XQ1*AC(4)-BB*XQ3*LQ3*AC(6)
C
C

```

## Appendix 1: Analytical Analysis Computer Programs

```
1000 RETURN
END
c
c SUBROUTINE NROOT(NAS,NSS)
C
C SUB TO COUNT THE NUMBER OF ROOTS IN THE COFACTOR
C DATA FILES
C DATE STARTED 1/6/92
C
DIMENSION NAS(800),NSS(800)
NR=1
ON=0.0
OM=0.0
MT=1
K=1
READ(1,*) ON
DO 20 I=1,30000
READ(1,*,END=40) OM
IF (OM.EQ.ON) THEN
NR=NR+1
ON=OM
ELSE
NAS(K)=NR
NR=1
ON=OM
K=K+1
END IF
20 CONTINUE
40 NAS(K)=NR
c
c REPEATE FOR SECOND FILE
C
NR=1
ON=0.0
OM=0.0
MT=1
K=1
READ(2,*) ON
DO 30 I=1,30000
READ(2,*,END=60) OM
IF (OM.EQ.ON) THEN
NR=NR+1
ON=OM
ELSE
NSS(K)=NR
NR=1
ON=OM
K=K+1
END IF
30 CONTINUE
60 NSS(K)=NR
C
REWIND(1)
REWIND(2)
100 RETURN
END
```

### 1.4 Mid Plane Strains in the Direction of Wave Propagation

```
PROGRAM STCOD
IMPLICIT DOUBLE PRECISION(A-H,O-Z)
DIMENSION WS(30000),VS(30000)
DIMENSION FWS(1000),FVS(1000)
DIMENSION RUC(A)(65),AC(12),OM(2000),G(1),NSS(800)
COMMON C2,C3,C4,C5,NSS
C
C CALCULATING STRAIN V TIME FROM COFACTORS
C MIDPLANE STRAIN IN X DIRECTION
C FROM DISPLACEMENTS OF V AND W
C
READ(3,*) X,LIM,TM,THETA,H
READ(3,*) C2,C3,C4,C5,C1R
CONV=ATAN(1.0D0)/45.0
TEMP=THETA*CONV
AK1=SIN(TEMP)
AK2=COS(TEMP)
WRITE(6,*) THETA,CONV,TEMP,AK1,AK2
TS=TM
XL=X+1.25
C
C CALCULATING TIME CONSTANT
c TC=(H/C1R)*1E6
TC=1.0
C CALCULATED CONSTANTS
PI=4.0D0*ATAN(1.0D0)
HPI=PI/2.0D0
C
C CONSTANT FOR CALCULATING G1
C ZC=SIN(0.138D0*X)(X*0.14D0)
C
DO 47 K=1,700
```

## Appendix 1: Analytical Analysis Computer Programs

```

FWS(K)=0.0
FVS(K)=0.0
47 CONTINUE
CALL NROOT(NSS)
DO 50 KW=1,700
e WRITE(6,*) NAS(KW)
C
C
C SUM FOR SYMMETRIC WAVE
C
C IF (KW.NE.1) THEN
NC=NSS(KW)
41 DO 45 J=1,NC
RKAY(J)=0
DO 30 I=1,12
AC(I)=0
30 CONTINUE
C UL=0.0
C LL=0.0
READ(2,*,END=50) OM(KW),RKAY(I),(AC(I),I=1,12)
C WRITE (6,*) OM(KW)
C
RK=RKAY(I)
OG=OM(KW)
C
CALL RESD(RK,AC,OG,THETA,RV,RW)
C
C WRITE(14,*) OG,RK,RV,RW
420 FWS(KW)=FWS(KW)+RW*RK*COS(RK*X)
FVS(KW)=FVS(KW)+RV*RK*COS(RK*X)
e420 FWS(KW)=FWS(KW)+RW*(SIN(RK*XL)-SIN(RK*X))
e FVS(KW)=FVS(KW)+RV*(SIN(RK*XL)-SIN(RK*X))C
45 CONTINUE
C
C WINDOWING
C
48 C=0.54+0.46*COS(KW*0.004487989)
C FWA(KW)=FWA(KW)*C
FWS(KW)=FWS(KW)*C
C FVA(KW)=FVA(KW)*C
FVS(KW)=FVS(KW)*C
C
50 CONTINUE
C
C NOW FIND THE CORRESPONDING VALUES AT K=0.
C AT K=0, THE RESIDUES ARE NEGLIGIBLE BUT FOR THE
C FUNDAMENTAL MODE OF THE ANTISYMMETRIC MOTION.
C HERE, THE RES=T^2C/(4*C1) WHERE T=C1*U/H.
C TO USE THE TRAPEZIUM RULE NEED THE FIRST TERM HALVED.
C
C THE FACTOR WAS WRONG AND SHOULD BE -C2SQ/(4*C1SQ)
C AND THEN HALVED
C
C
C G(1)=0.02909*TM
C
C SINCE U IS EVEN IN K, FIND THE SUM OF FA(K)*COS(K*X)
C FOR EACH VALUE OF T FROM 0 TO ? IN STEPS OF 2*PI/20.
CC
C FIND THE SUM OF FWA(KW)*(1-COS(OM(KW)*TM)
C FOR EACH VALUE OF X FROM 0 TO T IN STEPS OF 2*PI/20.
C
C
DO 70 L=1,LLIM
WS(L)=0.0
VS(L)=0.0
DO 60 KW=1,700
e CY=(COS(OM(KW)*TM))
SY=SIN(OM(KW)*TM)
WS(L)=WS(L)+(FWA(KW)*SY)
VS(L)=VS(L)+(FVS(KW)*SY)
C
C
60 CONTINUE
C
C FOR U.S. NEED WA+WS, FOR L.S. NEED UA-US.
C MULT BY DELTA K = 0.02. TO BE CONSISTENT WITH
C PREVIOUS GRAPHS, SCALE FURTHER BY 2*C1SQ/C2SQ
C 0.02*2*C1SQ/C2SQ
SC=(1/C2)*0.02*2
C
TP=(AK2*VS(L)+AK1*WS(L))*SC
C WRITE(6,*) US,BS
WRITE(8,300) TM*TC,TP
WRITE(9,300) VS(L)
WRITE(10,300) WS(L)
TM=TM*TS
300 FORMAT(2(G15.6))
70 CONTINUE
STOP
END
SUBROUTINE RESD(RK,AC,OG,THETA,RV,RW)
IMPLICIT DOUBLE PRECISION(A-H,O-Z)
DIMENSION AC(12)

```

Appendix 1: Analytical Analysis Computer Programs

```

COMMON C2,C3,C4,C5
OM=OG
CONV=ATAN(1.0D0)/45.0
TEMP=THETA*CONV
AK1=SIN(TEMP)
AK2=COS(TEMP)
C WRITE(6,*)AK1,AK2
SAK1=AK1*AK1
SAK2=AK2*AK2
VELCTY=OM/RK
V=VELCTY**2
Z1=2.0D0*C3
T3=(C3+C4)**2*SAK2
SP2=SAK1+(C3*SAK2-V)/C2
T1=(C3*SAK1+C5*SAK2-V)
T2=SAK1+C3*SAK2-V
Z2=T3-T1-T2*C3
Z3=T1-T2-T3*SAK1
DISCR=SQRT(Z2*Z2-4.0D0*C3*Z3)
SP1=(-Z2-DISCR)/Z1
SP3=(-Z2+DISCR)/Z1
A=(SAK1-SP1)+C3*SAK2-V/(C3+C4)
B=(SAK1-SP3)+C3*SAK2-V/(C3+C4)
G=C3*A/C2-SP2*SAK1
D=C3*B-A/C2+G
IF (SP1.GT.0.0D0) THEN
    P1=SQRT(SP1)
    LP1=1
    XP1=EXP(-P1*RK)
    XCP1=1.0D0
    XSP1=1.0D0
ELSE
    P1=SQRT(-SP1)
    LP1=0
    XP1=1.0D0
    XCP1=COS(P1*RK)
    XSP1=SIN(P1*RK)
END IF
IF (SP2.GT.0.0D0) THEN
    P2=SQRT(SP2)
    LP2=1
    XP2=EXP(-P2*RK)
    XCP2=1.0D0
    XSP2=1.0D0
ELSE
    P2=SQRT(-SP2)
    LP2=0
    XP2=1.0D0
    XCP2=COS(P2*RK)
    XSP2=SIN(P2*RK)
END IF
IF (SP3.GT.0.0D0) THEN
    P3=SQRT(SP3)
    LP3=1
    XP3=EXP(-P3*RK)
    XCP3=1.0D0
    XSP3=1.0D0
ELSE
    P3=SQRT(-SP3)
    LP3=0
    XP3=1.0D0
    XCP3=COS(P3*RK)
    XSP3=SIN(P3*RK)
END IF
C
C WRITING OUT THE RESIDUES CORRESPONDING TO U
C WRITE(6,*) AC(2),AK2,XQ2,LQ2,AC(5)
C
C SURFACE STRAIN
C
RV=AK1*AK2*XCP1*XP1*AC(7)-P2*XSP2*XP2*AC(8)
+AK1*AK2*XCP3*XP3*AC(9)+AK1*AK2*XSP1*AC(10)
+P2*XCP2*AC(11)+AK1*AK2*XSP3*AC(12)
C
RW=-A*XCP1*XP1*AC(7)-B*XCP3*XP3*AC(9)
-A*XSP1*AC(10)-B*XSP3*AC(12)
C
c write(6,*) RV,RW
c stop
c
1000 RETURN
END
c
SUBROUTINE NROOT(NSS)
C
C SUB TO COUNT THE NUMBER OF ROOTS IN THE COFACTOR
C DATA FILES
C DATE STARTED 1/6/92
C
DIMENSION NSS(800)
C
NR=1
ON=0.0

```

## Appendix 1: Analytical Analysis Computer Programs

---

```
OM=0.0
MT=1
K=1
READ(2,*) ON
DO 50 J=1,30000
READ(2,*,END=60) OM
c write(6,*) OM
IF(OM.EQ.ON) THEN
  NR=NR+1
  ON=OM
ELSE
  NSS(K)=NR
  NR=1
  ON=OM
  K=K+1
END IF
50 CONTINUE
60 NSS(K)=NR
c
REWIND(2)
100 RETURN
END
```

Appendix 2: PVDF Piezo Electric Film Properties

Appendix 2: PVDF Piezo Electric Film Properties

Data from Penwalt [64]

Typical Properties of Piezo Film

Property	Symbols	Values	Units	Conditions
Thickness	t	9,16,28,52 110,220,800	μm	
Piezo Strain Constant	$d_{31}$ $d_{32}$ $d_{33}$ $d_t$ $e_{33}$	$23 \times 10^{-12}$ $3 \times 10^{-12}$ $-33 \times 10^{-12}$ $-22 \times 10^{-12}$ 0.16	(m/m)/(V/m) or (C/m <sup>2</sup> )/(N/m <sup>2</sup> ) (C/m <sup>2</sup> )/(m/m) or (N/m <sup>2</sup> )/(V/m)	laterally clamped  laterally clamped
Piezo Stress Constant	$g_{31}$ $g_{32}$ $g_{33}$ $g_t$	$216 \times 10^{-3}$ $19 \times 10^{-3}$ $-339 \times 10^{-3}$ $-207 \times 10^{-3}$	(V/m)/(N/m <sup>2</sup> ) or (m/m)/(C/m <sup>2</sup> )	laterally clamped
Electro-mechanical Coupling Constant	$k_{31}$ $k_t$	12 29	%	@ 100 Hz ( $V_{f_2}$ ) @ 100 MHz ( $\sqrt{V_{f_2}/V_{f_3}}$ )
Permittivity	$\epsilon$	$106 \times 10^{-12}$	F/m	@ 10 KHz
Relative Permittivity	$\epsilon/\epsilon_0$	12		@ 10 KHz
Capacitance	C	$379 \times 10^{-12}$	F/cm <sup>2</sup>	28 μm Film @ 10 KHz
Acoustic Impedance	$Z_a$ " "	$3.9 \times 10^6$ $2.7 \times 10^6$	kg/m <sup>2</sup> -sec. " "	3 Direction 1 Direction
Electrical Impedance	$Z_e$	1350	ohms	100 cm <sup>2</sup> for 9μm film @ 1 KHz
Speed of Sound	$v_s$ $v_s$	$2.2 \times 10^3$ $1.5 \times 10^3$	m/sec. "	3 Direction 1 Direction
Pyroelectric Coefficient	p	$-30 \times 10^{-6}$	C/(m <sup>2</sup> °K)	@ 20°C
Volume Resistivity	$\rho_v$	$1.5 \times 10^{13}$	ohm-m.	@ 20°C
Surface Resistivity of Electrodes	$R_{\square}$	< 2.0 < 0.5	ohms/square " "	Aluminum Silver
Dissipation Factor	$\tan-\delta_e$	0.015 - 0.02		@ 10 KHz
Mechanical Loss Tangent	$\tan-\delta_m$	0.10		
Dielectric Strength	$E_B$	75	V/μm	
Max. Operating Field	$E_o$	10 30	V/μm V/μm	@ d.c. @ a.c.
Density	$\rho$	$1.78 \times 10^{-3}$	kg/m <sup>3</sup>	
Water Absorption	0.02	%		By Weight
Tensile Strength at Break	$T_B$ $T_B$	$140-210 \times 10^6$ $30-55 \times 10^6$	N/m <sup>2</sup> N/m <sup>2</sup>	1 Direction 2 Direction
Elongation at Break	$S_B$ $S_B$	2.5-4.0 380-430	% %	1 Direction 2 Direction
Elongation at Yield	$S_Y$	2-5	%	
Young's Modulus	Y	$2 \times 10^9$	N/m <sup>2</sup>	

### Appendix 3: Material Tests of AGC LTM22/T700 Material

To evaluate material properties of the Advanced Composite Group LTM22/T700 material a series of elastic tests were completed. The properties required were the Young's moduli  $E_{11}$  and  $E_{22}$ , the Poisson's ratios  $\nu_{12}$  and  $\nu_{23}$ , and the shear modulus  $G_{12}$ , where the fibre direction is in the 1-axis. The data for the Young's moduli and the Poisson's ratios was collected from tensile testing of uni-directional specimens using strain gauges to measure the elastic strain. The shear moduli was calculated from data collected from a V notched beam test. The results of these tests are presented in the following plots.

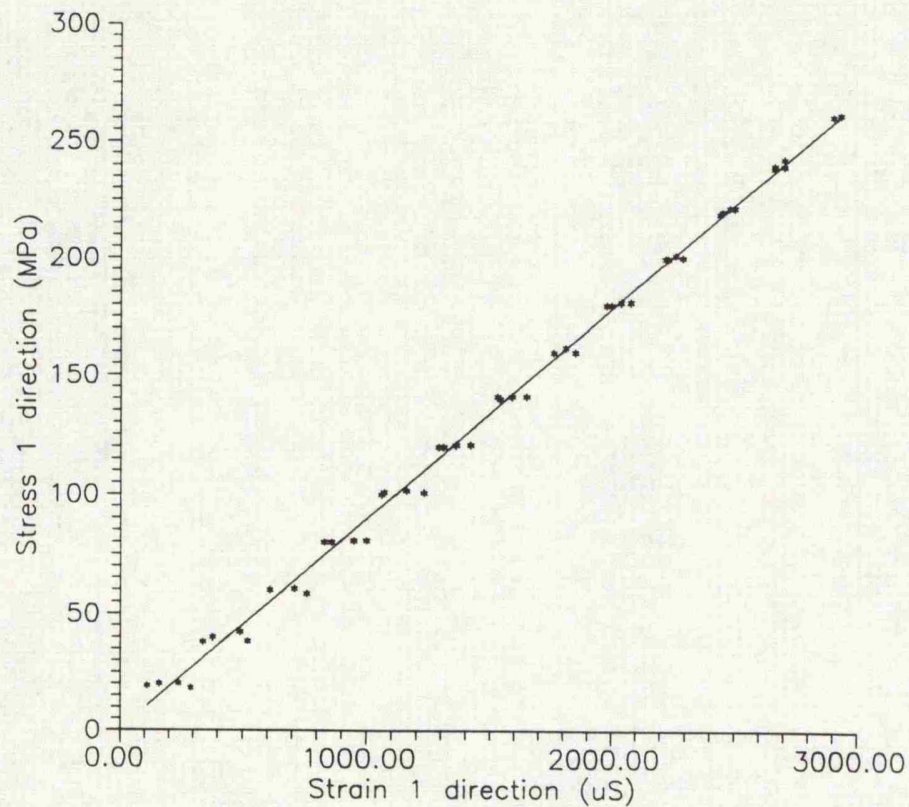


Figure A3.1: Young's Modulus  $E_{11} = 88.9$  GPa

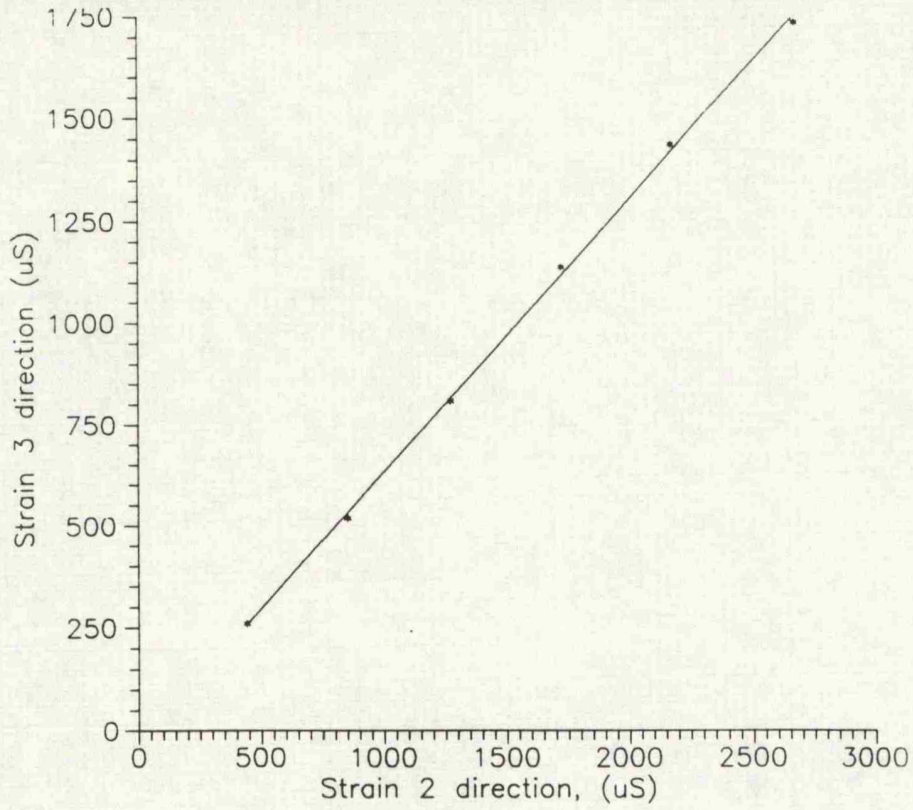


Figure A3.4: Poisson's Ratio  $\nu_{23} = 0.67$

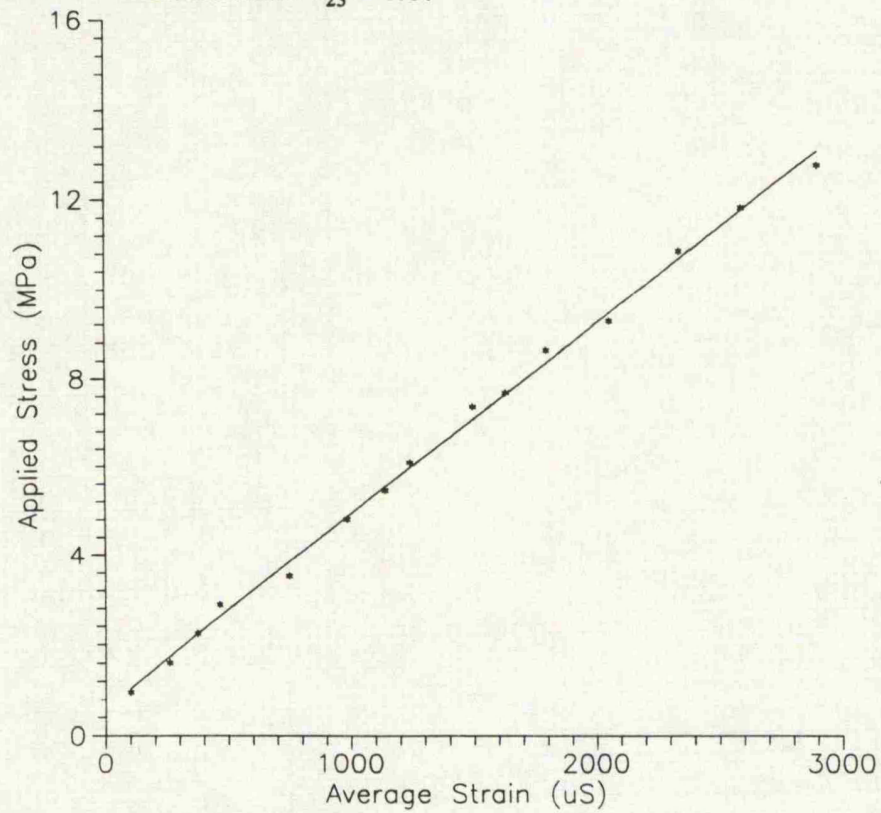


Figure A3.5: Shear Modulus  $G_{12} = 4.32 \text{ GPa}$

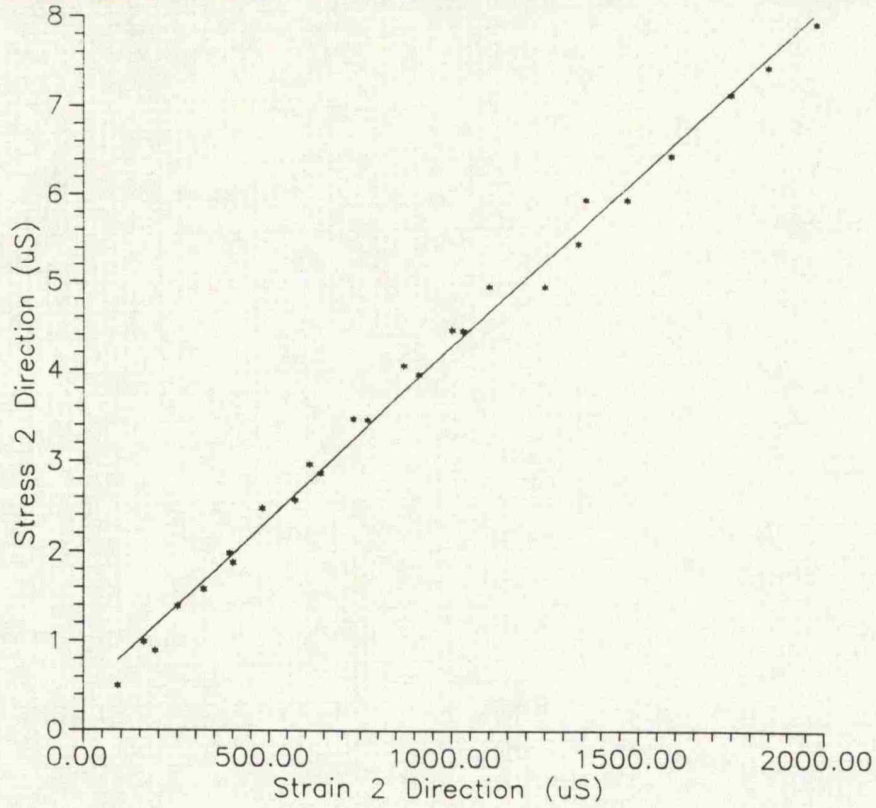


Figure A3.2: Young's Modulus  $E_{22} = 3.84\text{GPa}$

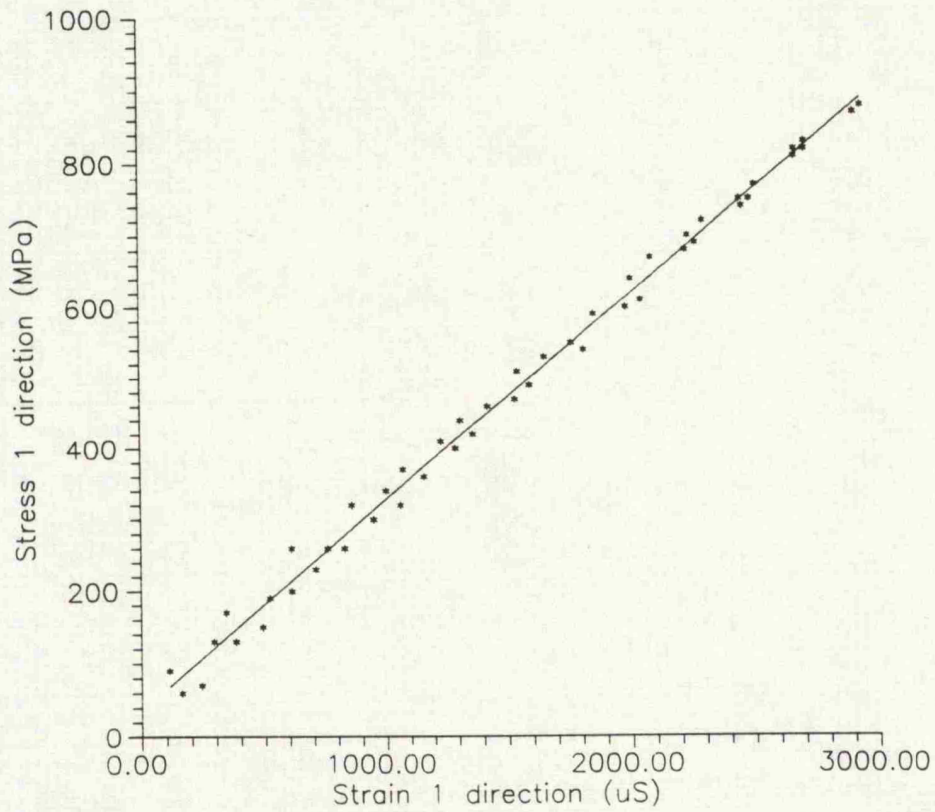


Figure A3.3: Poisson's Ratio  $\nu_{12} = 0.29$

**Appendix 4:      Published Work**

- 1)     Walters, M.B.J, Green E.R., '*Surface Wave Propagation due to Impact in Cross Ply Composite Plates*', Structures Under Shock and Impact II, Eds. P.S. Bulson, Computational Mechanics Publications, ISBN 1 85312 1703, pp393-404.
  
- 2)     Walters, M.B.J., Green E.R., and Morrison C.J., '*Wave Propagation due to Impact in Cross Ply Composite Plates*', Poster Presentation, SERC Polymer Engineering Conf., Loughborough, 1992.

## Surface Wave Propagation due to Impact in Cross Ply Composite Plates

M.B.J. Walters and E.R. Green

*Department of Engineering, University of Leicester, Leicester LE1 7RH, UK.*

### ABSTRACT

To gain further insight into the problem of surface impact on composite materials we have examined the wave propagation resulting from a surface impact on a laminated plate. Theoretical and numerical techniques have been developed for the case of an impulsive line load acting on the upper surface of a plate. The results that are reported are for both analytical and experimental work, and they show the responses for the upper and lower surfaces of a plate subjected to a line load impact. The angle of the line load is varied relative to the ply directions. These results consist of graphs which show the strain on the surfaces of the laminate as a function of time. The experimental procedure for obtaining the data will be described in full, as will a comparison of the analytical and experimental results.

### INTRODUCTION

The increasing use of advanced fibre reinforced materials on the outer skin of structures has led to a need for a better understanding of the response of such materials under impact. Examined in this paper are the surface effects of the elastic waves propagated from a surface impact. Theoretical investigations have been carried out by Green [1], who reports analytical predictions of the response of a symmetric cross ply laminated plate consisting of four layers of a uni-directional fibre reinforced composite to a surface impact. The procedure involves the solving of the full three dimensional equations of elasticity in each layer, matching the solutions across the interfaces and satisfying the appropriate boundary conditions.

Experimental work that has been reported which is of relevance here has been conducted by Daniel et al [2,3], Sachse et al [4], and Gorman [5]. Daniel [2,3] has recorded signals received from surface and embedded strain gauges in order to analyse a variety of characteristics of the propagating wave

resulting from a surface impact on a laminated plate. Sachse [4] has employed a pulse laser technique to produce a short duration impact to measure wave speeds in plates. Also he monitors the effect of damage on the elastic wave transmission. Gorman [5] has monitored the acoustic emissions from the waves travelling through the plate propagated from a lead break.

The current paper is the first report of experimental work undertaken to examine the verification of the analytical procedure developed by Green [1]. An impact system has been established and initial tests examining the surface response of a four layer symmetric cross ply laminated plate are reported. Also included are the analytical results for the same plate, and a comparison between the two is presented. The experimental results do show some evidence for the theoretical predictions reported in Green [1]. Further experimental work has commenced to examine the waves propagated within a laminated plate, and will be reported in due course.

## THEORY

This is described in some detail in Green [1], thus only an outline of the method will be given here. The plate consists of a symmetric cross-ply assembly of four layers of an uni-directional fibre composite material. This material comprises of a single family of straight, parallel, strong fibres embedded in an isotropic matrix and is modelled as a homogeneous continuum of transversely isotropic elastic material with the axis of transverse isotropy parallel to the fibre direction.

A Cartesian co-ordinate system of axes is set-up with the origin in the mid-plane, the  $x_1$  axis being normal to the plate and the  $x_2$  and  $x_3$  axes being parallel to the fibres in the two outer and two inner layers respectively. The line source is taken to be a delta function impulse acting on the upper surface in the negative  $x_1$  direction at an angle  $\pi/2 - \gamma$  to the  $x_3$  axis. The consequent plane wave propagation will be at an angle  $\gamma$  to the  $x_3$  - axis and parallel to the layers, figure 1. Hence, each strain and displacement component at any point  $x$  may be expressed as functions of  $x_1, x$  and  $t$  only, where  $x = x_2 \sin \gamma + x_3 \cos \gamma$  and  $t$  is the time. It is convenient to take the Laplace transform with respect to  $t$  and the Fourier transform with respect to  $x$  for each of these components. Utilising the appropriate constitutive equations, the full three-dimensional equations of elasticity are solved for each layer. The ensuing solutions are subjected to the traction free conditions appropriate to the two outer surfaces, apart from the stress discontinuity at the upper surface due to the impulsive loading. The perfect bonding conditions imply continuity of strain and displacement at each interface.

Once all these conditions have been implemented it is possible to express the transformed strain and displacement components at any point on or within the plate in terms of the material constants, the propagation angle and

the transform parameters. To derive the full solution to the problem the transforms are inverted in order to recover the strain and displacement components as functions of  $x$  and  $t$ . This inversion is carried out numerically using residue theory for the spatial inversion followed by integration with respect to frequency using standard techniques. Due to the symmetry of the plate, any disturbance separates into two distinct motions, flexural (antisymmetric) and longitudinal (symmetric). The numerical techniques are applied to the two motions separately and the full solutions are obtained upon using an appropriate combination of the two partial solutions. The limits of integration are chosen to be consistent with the continuum theory and the summation is restricted to a frequency upper limit of  $\omega = 14c_1 / h$  where  $c_1$  is a typical body wave speed, and  $h$  is the ply thickness.

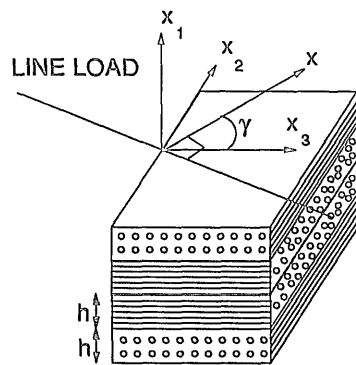


Figure 1, Geometry of plate

## EXPERIMENTAL WORK

The main objective of the experimental work was to produce experimental data that could be realistically compared with the theoretical solutions. This involved the setting up of an experimental system that could reproduce the theoretical conditions as closely as physically possible. The main constraints the theoretical solution presented were firstly that the elastic response was to be studied, so all deformations were to be in the elastic region. The second constraint was that the impact had to be a line load. It has been reported by Cantwell et al [6] and others that initial impact damage can start as low as 1J. Therefore it was decided that the maximum impact energy should be 0.5J, to ensure that all deformations were of an elastic nature. Another consideration was the effect of the impactor acting as a damper onto the plate. Taking both these constraints into consideration the best form of impact would be of low energy, but high velocity. To achieve this style of impact a gas gun was used with a low mass projectile of 1g. The gas gun had an air reservoir which was

demonstrated these effects have been obtained using idealised impact conditions of a delta function impulse on an infinite plate.

The examination of the experimental results was assisted with the use of digital filters. The aim of this filtering was to remove the low frequency impact response of the plate so it would not dominate the high frequency signals. The filters used were 10th order Butterworth band pass filters. The lower limit of the filter was set to avoid the dominance of the low frequency response, the upper limit determined by the frequency limits used in the theoretical integration. The limits used are presented in table 1. To ensure compatibility between the numerical and experimental data the same filter was applied to both sets of data.

Material	Lower frequency limit	Upper frequency limit
Steel	400KHz	4MHz
ICI Plytron	200KHz	3MHz

Table 1: Filter frequency limits

There were two criteria applied for the assessment of the presence of surface waves in the experimental and numerical data. The first was that Rayleigh type surface waves are only present on the impact surface, whereas propagated shear waves would be present throughout the material. The second criteria was that when the Rayleigh type surface wave was present its measured speed from both the numerical and experimental results was consistent with that calculated from the material constants.

## RESULTS AND DISCUSSION

Presented here are three sets of results all of which show the surface strain in the direction of propagation. Figures 4 and 5 refer to an evaluation test for a steel plate. The numerical results in figure 4 show the upper and lower surface strains in the  $x_3$  direction, and the experimental results in figure 5 show the output of the piezo electric transducers in volts. Both sets of results are for a position 15mm away from the line of impact. Figure 4a shows quite clearly a high frequency wave travelling on the upper surface at a speed of  $2.9 \times 10^3 \text{ MS}^{-1}$  which is absent from the lower surface figure 4b. The theoretical Rayleigh wave speed for steel calculated from the material constants is  $2.95 \times 10^3 \text{ MS}^{-1}$ . Comparing figures 5a and 5b (the upper and lower surfaces respectively) It can be seen that there is more disturbance on the upper surface which is consistent with the presence of the Rayleigh wave.

It has been shown by Green [1] that the limiting wave velocity for a laminated 4-ply plate is the smaller of two wave speeds, the Rayleigh type surface wave in the upper layer  $V_R$ , or the shear wave speed in the inner layer

$V_S$ . For the Plytron material these waves are equal when the angle of propagation  $\gamma$  is  $46.14^\circ$ .

For  $\gamma < 46.14^\circ$   $V_R < V_S$

and for  $\gamma > 46.14^\circ$   $V_R > V_S$

Therefore a surface wave effect would be expected when  $\gamma = 0^\circ$  and absent when  $\gamma = 90^\circ$  as  $V_S$  would be the slower wave speed. From the elastic constants of Plytron when  $\gamma = 0^\circ$  then  $V_R = 0.792 \cdot 10^3 \text{MS}^{-1}$ .

Figures 6a and 7a show the upper surface analytical and experimental results respectively for plytron when  $\gamma = 0^\circ$ . They both show large amplitude waves which are not transmitted to the lower surface (figs 6b,7b), which indicates the presence of a Rayleigh type surface wave. The velocity of the wave in fig.6a is  $0.79 \cdot 10^3 \text{MS}^{-1}$  and the velocity of the experimental wave is  $0.8 \cdot 10^3 \text{MS}^{-1}$ , both of which are in good agreement with the calculated value of  $V_R$ . The corresponding figures for  $\gamma = 90^\circ$ , figures 8 and 9 for  $\gamma = 90^\circ$  show a complete absence of any large surface waves which is consistent with the theory above.

In conclusion, it has been shown that the theoretical predictions for the presence and speed of surface waves on a laminated plate have been validated by both the numerical and experimental results. Work is in hand to monitor the response at the interfaces in order to examine the validity of the prediction that in the absence of a surface wave, the high frequency response is channelled in the inner layers.

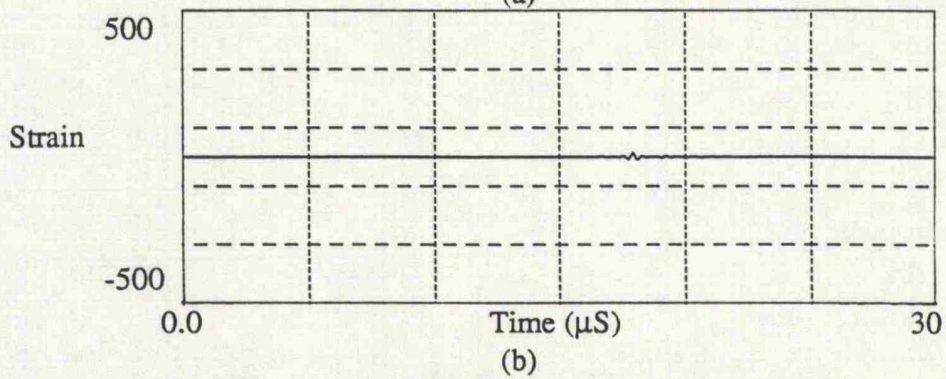
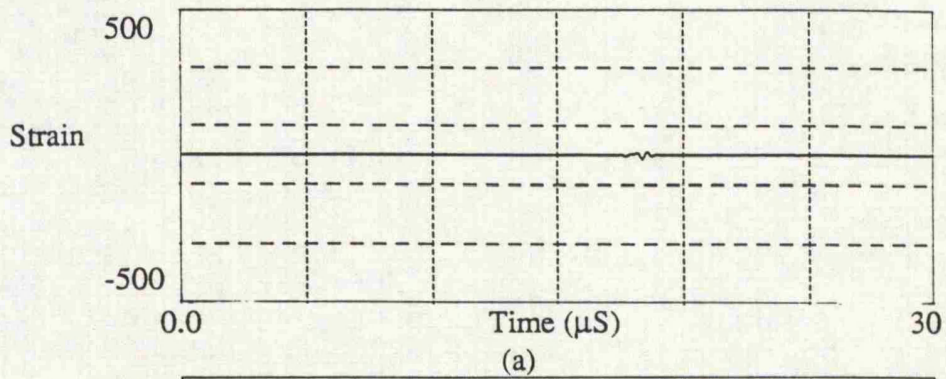


Figure 8, Analytical surface waves for Plytron,  $g = 90^\circ$   
 a) upper surface, b) lower surface.

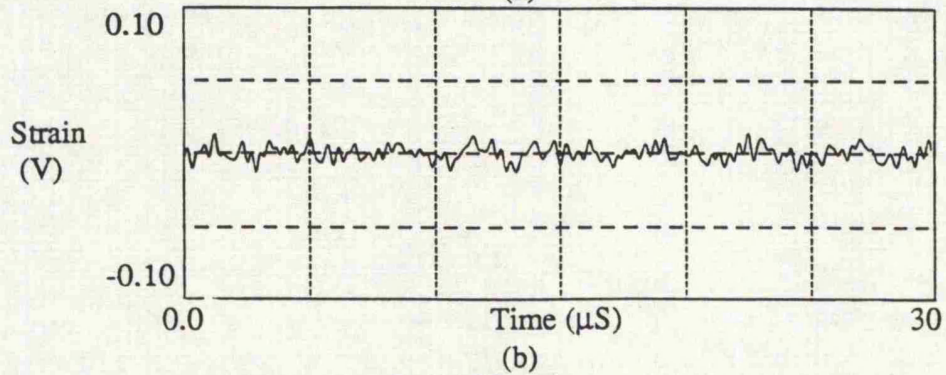
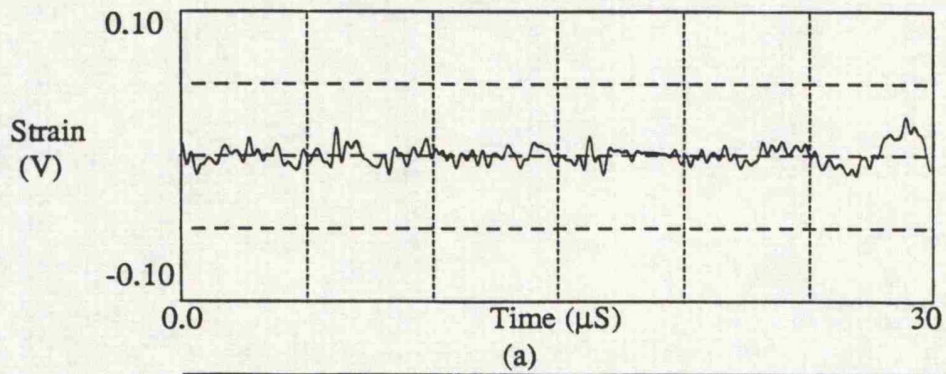


Figure 9, Experimental surface waves for Plytron,  $\gamma = 90^\circ$   
 a) upper surface, b) lower surface.

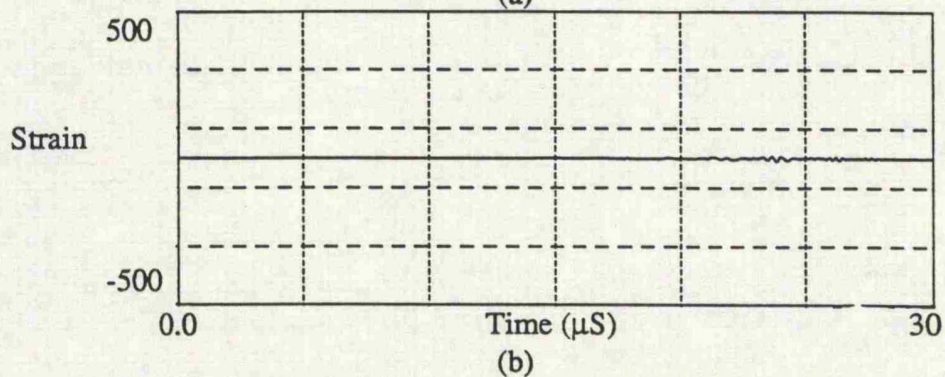
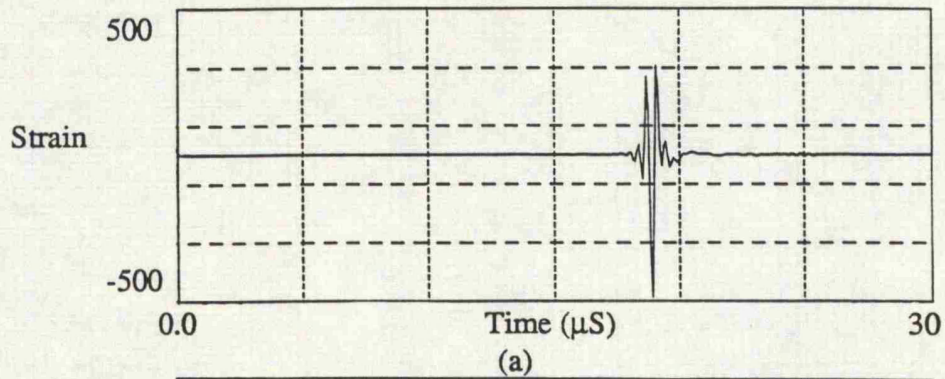


Figure 6, Analytical surface waves of Plytron,  $\gamma = 0^\circ$   
 a) upper surface, b) lower surface.

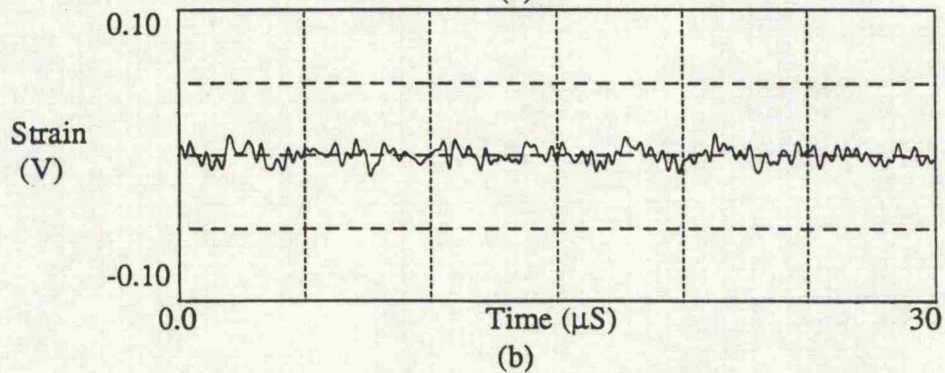
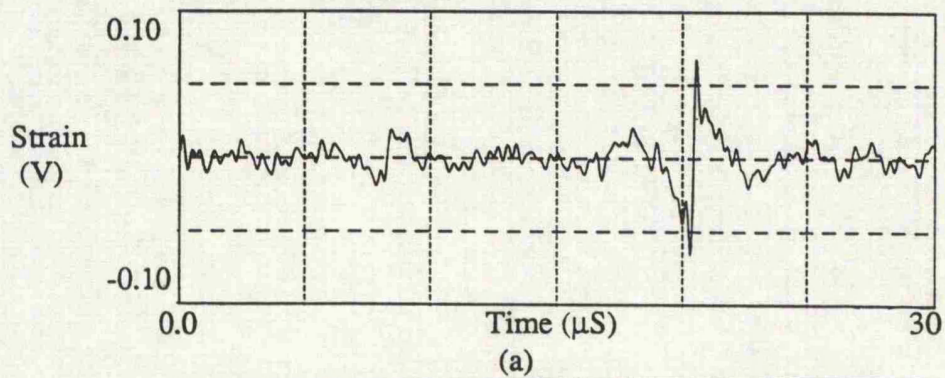


Figure 7, Experimental surface waves for Plytron,  $\gamma = 0^\circ$   
 a) upper surface, b) lower surface.

#### ACKNOWLEDGEMENTS

We would like to express our appreciation for the financial support given to this work by SERC, (Grant No. GR/F/74448), to Dr W A Green for his many helpful discussions, and to Mr C J Morrison for his invaluable help with the experimental work.

#### REFERENCES

1. Green, E.R. Transient Impact Response of a Fibre Composite Laminate. *Acta Mech*, Vol.86, pp.153- 165, 1991
2. Daniel, I.M., Liber, T., and Labeledz, R.H. Wave Propagation in Transversely Impacted Composite Laminates. *Expt. Mech.*, Vol.19, pp.9-16, 1979
3. Daniel, I.M., and Wooh, S.C., Deformation and Damage of Composite Laminates Under Impact Loading. *Impact Response and Elastodynamics of Composites*, ASME AMD Vol 116, pp. 107-134, 1990
4. Sachse, W., Every, A.G., and Thompson, M.O. Impact of Laser Pulses on Composite Materials. *Impact Response and Elastodynamics of Composites*. ASME AMD Vol 116, pp. 51-62, 1990.
5. Gorman, M.R. Plate Wave Acoustic Emission in Composites, *Impact Response and Elastodynamics of Composites.*, ASME AMD Vol 116, pp. 107-134, 1990.
6. Cantwell, W.J., and Morton, J. Comparison of the Low and High Velocity Impact Response of CFRP. *Composites*, Vol 20, No. 6, pp. 545-551,1989.

## WAVE PROPAGATION DUE TO IMPACT IN CROSS PLY COMPOSITE PLATES

M.B.J. WALTERS, E.R. GREEN, C.J. MORRISON

*Department of Engineering, University of Leicester, Leicester, LE1 7RH, UK*

### ABSTRACT

To gain further insight into the problem of surface impact on composite materials we have examined the wave propagation resulting from a surface impact on a laminated plate. Theoretical and numerical techniques have been developed for the case of an impulsive line load acting on the upper surface of a plate. The results that are reported are for experimental work, and they show the through thickness response for a 4-ply (0/90)<sub>s</sub> plate subjected to a line load impact. The angle of the line load is varied relative to the ply directions. These results consist of graphs which show the strain on the surfaces and at the mid plane of the plate as a function of time.

### INTRODUCTION

The increasing use of advanced fibre reinforced materials on the outer skin of structures has led to a need for a better understanding of the response of such materials under impact. Examined in this paper are the through thickness effects of the elastic waves propagated from a surface impact. Theoretical investigations have been carried out by Green [1], who reports analytical predictions of the response of a symmetric cross ply laminated plate to a surface impact.

The current paper reports on experimental work that was undertaken to examine the verification of the analytical results presented in [1]. An impact system has been established and tests examining the through thickness response of a four layer symmetric cross ply laminated plate are reported. The experimental results do show evidence to support the theoretical predictions reported in [1].

### BACKGROUND

The analytical model that has been developed predicts the stress levels at any point on or within the plate following a line load impulse on the top of the plate. The plate consists of four perfectly bonded layers of a uni directional fibre reinforced composite, each of finite depth  $h$  but of infinite lateral extent, (figure 1). This fibre reinforced material is modelled as a homogeneous transversely isotropic, elastic continuum, with the axis of transverse isotropy lying in the plane of the lamina and parallel to the fibre direction. The procedure involves solving the full three dimension equations of elasticity in each layer and subjecting the solutions to the appropriate interfacial and boundary conditions. It is then possible to evaluate any component of stress, strain or displacement at any point in the plate.

The results have shown that there is a relationship between the direction of the wave propagation  $\gamma$  (see fig1) and the stresses developed in the plate. When  $\gamma$  is less than some critical angle,  $\gamma_c$ , the short wave limiting response is a Rayleigh type surface wave

travelling on the impacted surface. When  $\gamma$  is greater than  $\gamma_c$ , however, this behaviour is a shear wave, channelled in the inner layers.

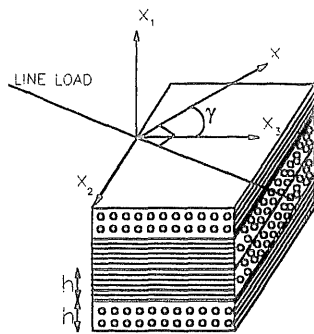


Figure 1, Geometry of plate

### EXPERIMENTAL WORK

The main objective of the experimental work was to produce experimental data that could be realistically compared with the theoretical solutions. This involved the setting up of an experimental system that could propagate elastic waves with a plane wave front. The experimental system is described in detail in [2] so only an outline is presented here. A gas gun was used to fire a low mass projectile of 1g. The projectile then impacted a striker which in turn after a small displacement, impacted the plate. This impact produced a surface line loading on to the plate with an impact energy of 0.5J. The impact initiated the required plane elastic waves propagating through the plate. The whole experimental system is shown in figure 2.

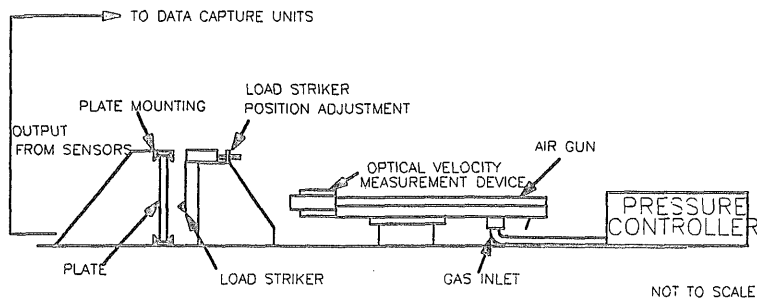


Figure 2, Complete experimental impact system

The elastic response produced by the impact was detected using piezo electric transducers. These transducers were made from a thin Piezo-electric polymer film which was screen printed with silver ink on both sides to produce electrical contacts. The transducers were of a custom design and had an active area of 1mm by 0.5mm. Although the size of the active region meant that there was an integration of the waves as they passed the active area they were the smallest physical size possible to manufacture. The design of the gauges can be seen in figure 3. This size of gauge has a frequency response of 2KHz -1GHz, and can produce large outputs for a small applied strain, so no further amplification was required. The output of the transducers was recorded on data capture units sampling at 20Mhz, and then down loaded to a computer where post processing of the signals took place.

Tests were carried out on cross ply laminated plates. The plates were manufactured using the Advanced Composite Group material LTM22/T700 which was an epoxy resin reinforced with unidirectional carbon fibres. The transducers were embedded into the plate during manufacture and were located on the upper and lower surfaces and at the mid plane of the plate. Two cases are presented here, one where the wave direction is parallel to the fibres in the inner layers,  $\gamma = 0^\circ$ , and the second where the wave direction is perpendicular to the fibres in the inner core,  $\gamma = 90^\circ$ .

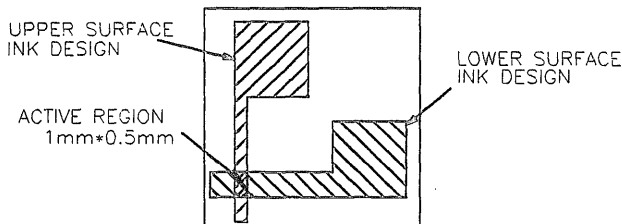


Figure 3, Piezo-electric transducer design

## RESULTS AND DISCUSSION

It has been shown in [1] that the limiting short wave velocity for a laminated 4-ply plate is the smaller of two wave speeds, the Rayleigh type surface wave in the upper layer  $V_R$ , or the shear wave speed in the inner layers  $V_S$ . The occurrence of which is dependent on the angle  $\gamma$ . For the LTM22/T700 material these wave speeds are equal when  $\gamma = 46.3^\circ$

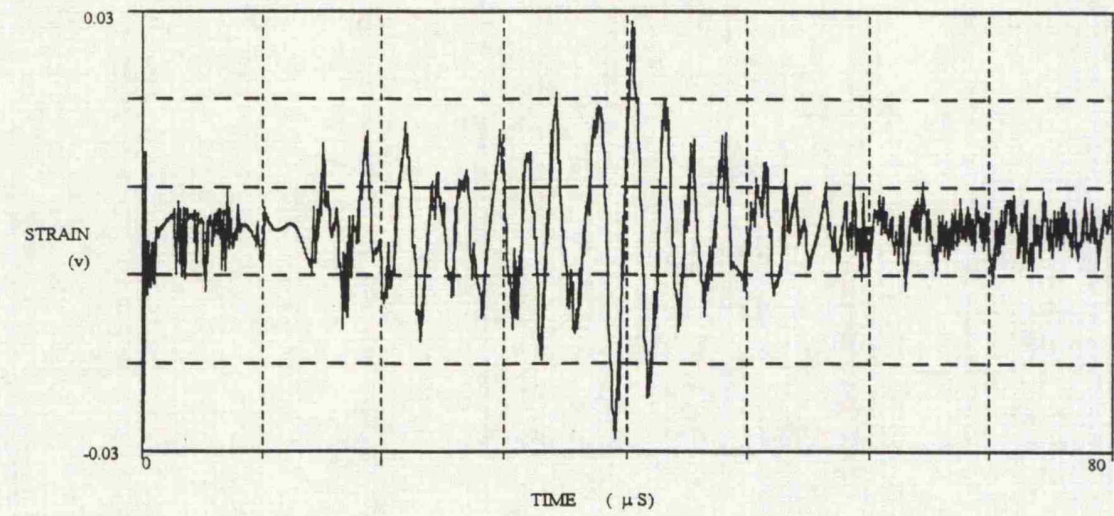
For  $\gamma < 46.3^\circ$   $V_R < V_S$

and for  $\gamma > 46.3^\circ$   $V_R > V_S$

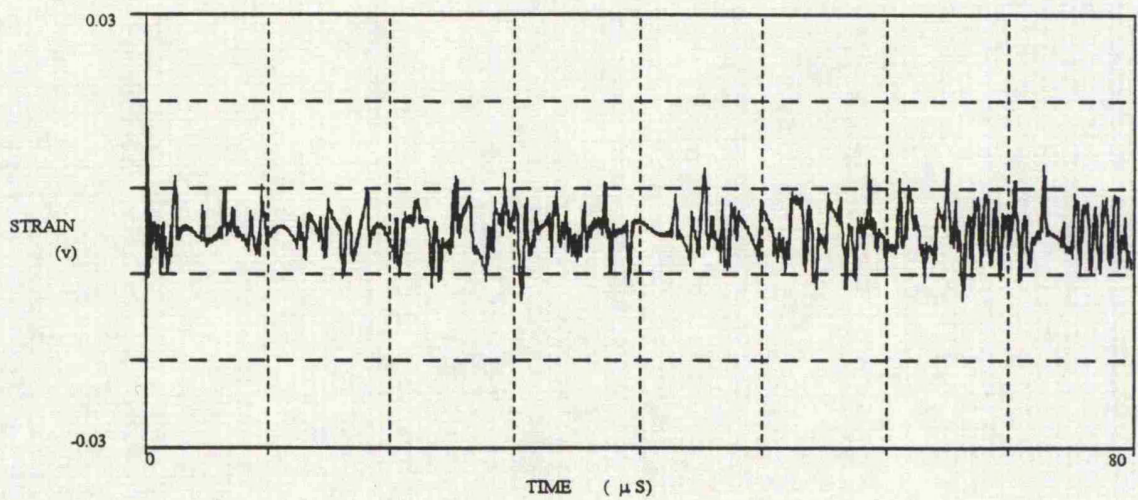
Figures 4 and 5 show the response of the plate at a distance of 32mm from the line of impact. In each case, the time duration is  $80\mu\text{s}$  measured from the point of impact. Curves (a), (b), and (c) refer to the upper surface, mid plane and lower surface respectively. In figure 4 where  $\gamma = 0^\circ$ , the upper surface response shows a larger amplitude disturbance travelling at  $840\text{ms}^{-1}$ . This disturbance is noticeably absent from the mid plane and the lower surface. This behaviour is characteristic of a Rayleigh type surface wave which decays rapidly with depth from the impacted surface. Further the speed,  $V_R$  of a Rayleigh type surface wave may be calculated from the elastic constants for the material. In this case,  $V_R$  is  $838\text{ms}^{-1}$ .

In figure 5, when the angle of propagation  $\gamma$  is  $90^\circ$ , there is no evidence of a surface wave present. However, comparing figures 4b and 5b, the response when  $\gamma = 0^\circ$  is of smaller amplitude than when  $\gamma = 90^\circ$ . This again is consistent with the predicted limiting short wave behaviour which at  $\gamma = 0^\circ$  is confined to the outer layer and at  $\gamma = 90^\circ$  is a shear disturbance in the core.

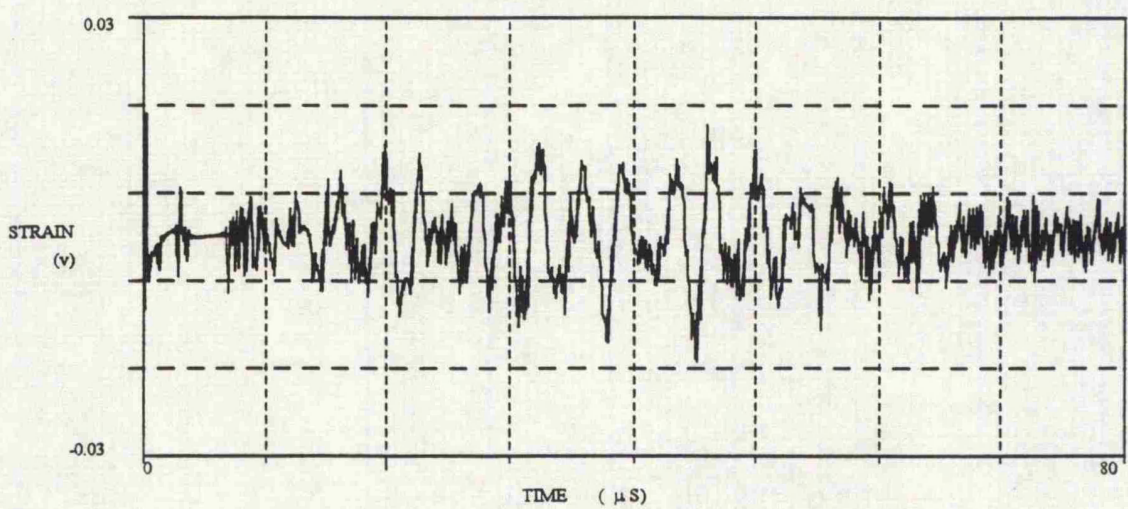
In conclusion the experimental results show good agreement with the analytical predictions on the effect of the angle of propagation  $\gamma$  on the response of a cross ply plate due to impact.



(a)



(b)



(c)

Figure 4

Response of (0/90), plate subjected to a line load 32mm away when  $\gamma = 0^\circ$ .  
 a) Upper surface, b) Midplane, c) Lower surface

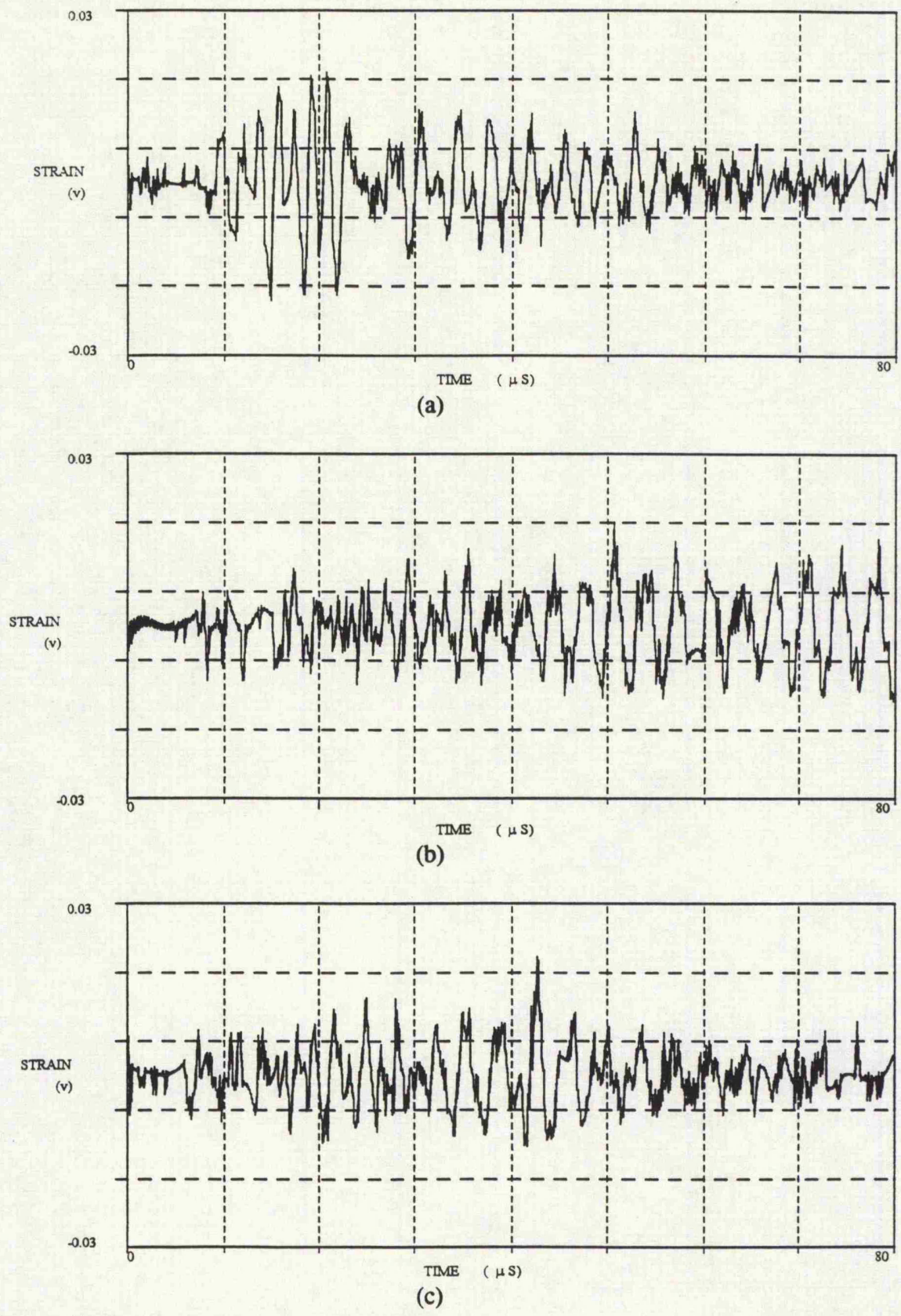


Figure 5  
 Response of (0/90), plate subjected to a line load 32mm away when  $\gamma = 90^\circ$ .  
 a) Upper surface, b) Midplane, c) Lower surface